



University of Strathclyde
Renewable Energy Marine Structures Centre for Doctoral Training
Department of Naval Architecture, Ocean & Marine Engineering

Reliability-constrained design optimisation of extra-large offshore wind turbine
support structures

Mohammad Rezvanipour

A thesis submitted in partial fulfilment of the requirement for the degree of
Doctor of Engineering

2023

Supervisor: Professor Athanasios Kolios

Declaration of authenticity and author's rights

This thesis is the result of the author's original research. It has been composed by the author and has not been previously submitted for examination which has led to the award of a degree.

The copyright of this thesis belongs to the author under the terms of the United Kingdom Copyright Acts as qualified by University of Strathclyde Regulation 3.50. Due acknowledgement must always be made of the use of any material contained in, or derived from, this thesis.

Mohammad Rezvanipour

September 2023

Statement on previously published work

In the course of this thesis, a number of papers are published in scientific conferences or still under review at the time of writing. The author of this thesis was and is in all these publications - even if the paper is co-authored - the main responsible person. The author's contributions to the publications, thus, comprise conceiving the works, administering the studies, realizing the works, performing literature studies, developing the methodologies, performing the researches, developing and applying the approaches, working with and extending the software, curating the data, verifying and validating the methods and results, analysing and investigating the data and results, post-processing and visualizing the results and findings, writing the papers and preparing the original drafts, interacting with the journals' editors and reviewers, as well as reviewing and editing the papers for the final publications.

Mohammad Rezvanipour

September 2023

Abstract

The offshore wind industry has evolved significantly over the last decade, contributing considerably to Europe's energy mix. For further penetration of this technology, it is essential to reduce its costs to make it competitive with conventional power generation technologies. To this end, optimising the design of components while simultaneously fulfilling design criteria is a crucial requirement for producing more cost-effective strategies. Traditional design optimisation techniques rely on the optimisation of design variables against constraints such as stresses or deformation in the form of limit states and to minimise an objective function such as the total mass of a component. Although this approach leads to more optimal designs, the presence of uncertainties, for instance, in material properties, manufacturing tolerances and environmental loads, requires more systematic consideration of these uncertainties. A combination of optimisation methods with concepts of structural reliability can be a suitable approach if challenges such as the approximation of the load effect concerning global input loads and computational requirements are addressed accordingly.

In this study, a reliability-constrained optimisation framework for offshore wind turbine (OWT) support structures is developed, applied, and documented for the first time. First, a parametric finite element analysis (FEA) model of OWT support structures is developed, considering stochastic material properties and environmental loads. The parametric FEA model is then combined with response surface and Monte Carlo (MC) to create an assessment model in the Six Sigma module in ANSYS, which is then further integrated with an optimisation algorithm to develop a fully coupled reliability-constrained optimisation framework. The framework is applied to the NREL 5MW OWT and OC3 sub-structure. Results indicate that the proposed optimisation framework can effectively reduce the mass of OWT support structures meeting target reliability levels focusing on realistic limit states. At the end of the optimisation loop, an LCOE comparison is done to see the effect of mass reduction on the wind turbine cost.

The study expanded with a scaling-up approach and investigated the technical feasibility of increasing the system's power and size in deeper water depth for bottom-fixed support structures. Additionally, parametric equations have been developed to estimate the wind turbine rating and weight considering water depth in the conceptual design stage.

Furthermore, the sensitivity analysis was performed on the latest reference support structure of the IEA 15MW turbine to see the effect of water depth between 30m to 60m. The results showed the influences of water depth on the current structural response of the monopile. It revealed that utilising the proposed support structure is not feasible for water-depth above 50m as the analysis did not fulfil design criteria.

Keywords: Optimisation, Extra-Large Monopiles, Offshore Wind Turbines, Water-depth Sensitivity, 3D FE Analysis

Contents

Declaration of authenticity and author’s rights.....	2
Statement on previously published work.....	3
Abstract.....	4
Contents	6
List of Figures:.....	11
List of Tables:.....	14
Abbreviations.....	16
1. Introduction.....	19
1.1. Background	19
1.1.1. History.....	19
1.1.2. Development of offshore wind energy	21
1.2. Problem statement.....	21
1.3. Aim and objectives.....	22
1.4. Technology Readiness Level (TRL)	25
1.5. Thesis structure	26
2. Literature Review.....	28
2.1. Introduction.....	28
2.1.1. Offshore wind foundations	29
2.1.2. Pros and cons of offshore wind farms.....	30
2.1.3. Types of foundation	31
2.1.4. Discussion and comparative analysis.....	34
2.2. Support structure design problem	35
2.2.1. Design rules	35
2.2.2. Limit states.....	36
2.2.3. Types of loads.....	36
2.2.4. Structural modelling and soil-pile interactions	37

2.3.	Optimisation strategies.....	39
2.3.1.	Optimisation under static loads.....	40
2.3.2.	Optimisation under transient loads	41
2.3.3.	Time series and Fatigue-constrained optimisation	41
2.3.4.	Optimisation based on simulation.....	42
2.3.5.	Probabilistic Optimisation	43
2.4.	Optimisation algorithms.....	44
2.4.1.	Genetic algorithm (GA)	44
2.4.2.	Gradient-based approach (GBA)	47
2.4.3.	Sequential Quadratic Programming (SQP).....	48
2.4.4.	Other algorithms	49
2.5.	Discussion of optimisation models	49
2.6.	Reliability-based methods review	51
2.6.1.	Reliability method classifications	51
2.6.2.	Structural reliability assessment concept in offshore applications	54
2.6.3.	Reliability assessment levels.....	56
2.6.4.	Structural reliability analysis using deterministic values.....	57
2.6.5.	Reliability-based calibration of standards in offshore wind	58
2.7.	Extra-large support structures in deeper sea	62
2.7.1.	Scaling up.....	63
2.7.2.	The importance of water depth	64
2.8.	Cost analysis terminology	65
2.8.1.	Cost breakdown and definitions.....	66
2.9.	Summary	67
3.	Numerical Methods of Structural Reliability Analysis.....	69
3.1.	Introduction	69
3.2.	Numerical methods	69

3.2.1.	Deterministic Methods.....	69
3.2.2.	Simulation methods	79
3.3.	Response surface method.....	84
3.4.	Regression methods.....	86
3.4.1.	Linear Regression	86
3.4.2.	Multivariate Regression	88
3.5.	Parametric FE model design basis	88
3.5.1.	Reference Model and met-ocean	88
3.5.2.	Applied Loads.....	90
3.5.3.	Limit States and DLCs.....	94
3.5.4.	Parametric FEA Model	95
3.6.	Summary	100
4.	Reliability-Constrained Design Optimisation Framework	102
4.1.	Introduction.....	102
4.2.	Optimisation framework development.....	102
4.2.1.	Structural Optimisation of Support Structure	102
4.2.2.	Design Variables.....	103
4.2.3.	Design Constraints and Criteria	105
4.2.4.	Genetic algorithm utilisation.....	114
4.2.5.	FEA geometry model validation.....	115
4.3.	Reliability-Constrained Optimisation (RCO).....	116
4.3.2.	Structural Reliability Assessment	119
4.4.	RCO Framework validation	120
4.5.	Cost analysis of optimised design	124
4.5.1.	Wind farm specification.....	125
4.5.2.	Cost breakdown	125
4.5.3.	Production process	127

4.5.4.	Levelized Cost of Energy (LCOE)	127
4.5.5.	Manufacturing and Installation	128
4.5.6.	CAPEX and OPEX Breakdown	132
4.6.	Summary	132
5.	Scaling up and water-depth sensitivity	133
5.1.	Introduction	133
5.2.	Scale up factor	134
5.3.	Reference turbines for up-scaled foundations	136
5.4.	Met Ocean Condition	138
5.5.	The design procedure and FEA	139
5.5.1.	ULS Loads	141
5.6.	Estimation of monopile mass using preliminary parametric equation	142
5.7.	Water depth sensitivity	145
5.8.	Summary	146
6.	Results and Discussion	147
6.1.	RCO and LCOE Results on 5MW NREL	147
6.1.1.	Design Constraints	147
6.1.2.	Design Variables	147
6.1.3.	Reliability Assessment Results	148
6.1.4.	Structural Response of FEA for DO and RCO	152
6.1.5.	Fatigue assessment of RCO design using S-N curve	156
6.1.6.	Cost analysis result	158
6.2.	Scaling up approach	160
6.2.1.	FEA Analysis Results	160
6.3.	Water depth sensitivity of IEA 15MW	161
6.3.1.	FE Analysis Results of IEA 15MW	161
6.3.2.	Water-depth sensitivity results	163

6.4. Design Limitations	165
7. Conclusions.....	167
7.1. Summary	167
7.2. Statement of contributions	169
7.3. Future work	171
References.....	173
Appendix A:.....	192
Appendix B	193
Appendix C.....	196

List of Figures:

Figure 1-1 The oldest windmills existing in Nashtifan village, Iran	20
Figure 1-2 Proposed framework for reliability-constrained optimisation	25
Figure 1-3 Technology Readiness Levels.....	25
Figure 1-4 The project outline	27
Figure 2-1 The yearly average usage of different sources of energy in Europe (Walsh, 2019)	29
Figure 2-2 Typical fixed bottom support structure options at different water depths (Arshad & O’Kelly, 2013).....	31
Figure 2-3 Number of foundations grid-connected by substructure type in Europe in 2020 (OREC, 2018).....	32
Figure 2-4 Summary of common types of foundations in offshore wind.....	34
Figure 2-5 Comparison of manual and computer-aided optimisation	40
Figure 2-6 Schematic of genetic algorithm optimisation (Diveux et al., 2001a).....	45
Figure 2-7 Classification of the reliability methods	52
Figure 2-8 Reliability analysis of a structure with random parameters	58
Figure 2-9 The yearly average of installed OWT rated capacity in MW (Walsh, 2019)	63
Figure 3-1 First and second order estimations (Kolios, 2010).....	70
Figure 3-2 HL reliability index algorithm	77
Figure 3-3 Normalized tail approximation method (Choi at al.,2006)	78
Figure 3-4 Monte Carlo simulation on reliability analysis (Weiss et al., 2006).....	81
Figure 3-5 Latin Hypercube method for two variables (Kolios, 2010)	83
Figure 3-6 Various Sampling approaches (Gavin & Yau, 2008).....	86
Figure 3-7 Reference model geometry and dimensions	89
Figure 3-8 Hindcast data extraction point in the NL-1 (DHI, 2020)	89
Figure 3-9 Applied loads on OWT support structure (Gentils et al., 2017)	94
Figure 3-10 Parametric FEA model flowchart.....	96
Figure 3-11 NREL 5MW wind turbine and OC3 platform geometry	97
Figure 3-12 Isometric view of geometry and applied loads	97
Figure 3-13 Soil Profile (Passon et al., 2007).....	98
Figure 3-14 Final generated mesh with the cross-section.....	100
Figure 4-1 Flowchart of the structural optimisation model (Gentils et al., 2017)	103
Figure 4-2 Design variables of OWT support structure.....	104

Figure 4-3 Illustration of typical excitation ranges of a modern OWT (Kallehave et al., 2015)	105
Figure 4-4 Probability over design load cases (All Directions) in [%]	109
Figure 4-5 Probability over wind speed (All Directions) in [%]	110
Figure 4-6 Wind Rose (All Directions, All DLCs) in [%]	110
Figure 4-7 Wave Rose (wind-sea) (wind-sea, All Directions, All DLCs) in [%]	111
Figure 4-8 Wind and Wave Rose (wind-sea, All Directions, All DLCs) in [%]	111
Figure 4-9 Wind-Wave Misalignment in 0-30-60-90 degrees (wind-sea, All Directions, All DLCs) in [%]	112
Figure 4-10 Flowchart of Reliability-Constrained Design optimisation framework	117
Figure 4-11 Methodology flow chart	124
Figure 4-12 CapEx cost breakdown for a fix-bottom offshore wind turbine (Stehly & Duffy, 2020)	126
Figure 4-13 Production process of a monopile	127
Figure 4-14 Annual average weather windows based on four North Sea sites (Sarkar & Gudmestad, 2013)	131
Figure 5-1 Schematic of tower scaling up linearly	135
Figure 5-2 Representation of the adapted Reference turbine geometry with details of the TP	136
Figure 5-3 Rated Power vs Support Structure mass of different wind turbine sizes	137
Figure 5-4 Rated Power vs Wind Speed curves for all reference turbines	138
Figure 5-5 Mesh convergence result for all sizes of Turbines	140
Figure 5-6 Final generated mesh for 7.5MW turbine size	140
Figure 5-7 Aero-Hydro dynamic, wind and wave loads of an OWT monopile support structure	141
Figure 5-8 Flow chart of the complete initial design procedure	142
Figure 5-9 Regression analysis for the ‘weight vs Turbine rating’ and ‘weight vs water depth’ equations	144
Figure 5-10 Representation of the adapted reference turbine for water depth sensitivity	146
Figure 6-1 Comparison of reference and optimised design from RCO framework in Thickness and Diameter	148
Figure 6-2 Cumulative density function and probability density function RCO design for (a) Fatigue minimum safety factor; (b) Equivalent stress maximum; (c) First natural frequency; (d) Buckling load multiplier; (e) Total deflection	151

Figure 6-3 FEA results for RCO design, a) Von Mises equivalent stress, b) Buckling deformation, c) mudline displacement, d) Total deformation, e) 1 st mode frequency and displacement, f) Fatigue minimum safety factor	154
Figure 6-4 Local sensitivity analysis for each parameter	156
Figure 6-5 Parameter sensitivity analysis in cost analysis.....	159
Figure 6-6 FE Analysis results for up-scaled design 7.5MW Wind Turbine b) Von Mises equivalent stress, c) Buckling deformation, d) Total deformation, e) first mode frequency and displacement	161
Figure 6-7 FE Analysis results for IEA 15MW a) Fatigue minimum safety factor, b) Von Mises equivalent stress, c) Buckling deformation, d) Total deformation, e) first mode frequency and displacement	163
Figure 6-8 Water depth sensitivity of 15MW OWT monopile support structure in Buckling, Maximum global stress, and Global fatigue damage.....	164
Figure 6-9 Water depth effects on first natural frequency and support structure weight of 15MW OWT	164

List of Tables:

Table 2-1 Comparison of reliability assessment methods (Wang & Kolios, 2017b)	57
Table 2-2 Safety level and failure classifications	59
Table 3-1 The 50-year extreme met ocean data of NL-1 (DHI, 2020)	90
Table 3-2 NREL 5 MW baseline wind turbine (Jonkman et al., 2009)	90
Table 3-3 Wave load assumption and values in ULS	92
Table 3-4 Wind turbine aerodynamic loads (LaNier, 2005)	95
Table 3-5 Design Load Cases in ULS (IEC, 2005)	95
Table 3-6 Sand Properties in different levels (Jung et al., 2015)	98
Table 3-7 Support structure material properties	99
Table 3-8 Mesh sensitivity	99
Table 4-1 Upper and lower bound of the design variables	104
Table 4-2 An overview of the individual DLCs in the load case	108
Table 4-3 Damage Equivalent Moments (Combined Wave/Wind) in compass directions for optimised monopile	112
Table 4-4 Damage Equivalent Load (Combined Wave/Wind) in compass directions at Interface of optimised monopile	112
Table 4-5 Upper and Lower bound of the constraints	114
Table 4-6 Settings of GA	115
Table 4-7 Deformation in the reference model and current model	116
Table 4-8 Design Variables (Jonkman & Musial, 2010; LaNier, 2005; Melchers and Beck, 2018)	119
Table 4-9 Summarized results of FORM and Six Sigma method	123
Table 4-10 Wind farm characteristics	125
Table 4-11 Typical pile transportation vessels and their costs	130
Table 4-12 Typical pile transportation vessels and their costs	131
Table 4-13 CAPEX and OPEX Cost Breakdown (Catapult ORE, 2021)	132
Table 5-1 Scaled-Up turbines dimension	135
Table 5-2 Key Parameters of Reference Wind Turbines	138
Table 5-3 Thrust and Moment applied on the wind turbines	141
Table 5-4 Dataset of the offshore wind turbines in Europe with a monopile support structure (C4Offshore)	142
Table 5-5 Comparison of monopile weight between function value and 3D model value	144

Table 6-1 Reliability assessment comparison	149
Table 6-2 The comparison of DO and RCO framework mass reduction results	154
Table 6-3 Fatigue life assessment for Optimised Turbine	156
Table 6-4 Mass and volume estimation of steel in reference and optimised design of 5MW NREL	158
Table 6-5 Final LCOE results comparison	160
Table 6-6 Summarized results for all developed and reference wind turbine support structures	160

Abbreviations

OWT	Offshore Wind Turbine
DNV-GL	Det Norske Veritas - Germanischer Lloyd
LCOE	Levelized Cost of Energy
FEA	Finite Element Analysis
GA	Genetic Algorithm
ULS	Ultimate Limit State
FLS	Fatigue Limit State
DEL	Damage Equivalent Load
DLC	Design Load Cases
RCD	Reliability-Constrained Design
RCO	Reliability-Constrained Optimisation
FORM	First Order Reliability Method
SORM	Second Order Reliability Method
SLS	Serviceability Limit States
ALS	Accidental Limit State
3D	Three Dimensional
PISA	Pile Soil Analysis
ESL	Equivalent Static Loads
BEM	Blade Element Momentum
FOWT	Floating Offshore Wind Turbine
TLP	Tension-Legged platform
GBA	Gradient-Based Approach
SGD	Stochastic Gradient Descent
SQP	Sequential Quadratic Programming
PSA	Particle Swarm Algorithm
ACO	Ant Colony Optimisation
FDA	Frequency Domain Analysis
TDA	Time Domain Analysis
HAZOP	Hazard and Operability Analysis
HAZID	Hazard Identification

FMEA	Failure Mode and Effects Analysis
ETA	Event Tree Analysis
FTA	Fault Tree Analysis
SRSMs	Stochastic Response Surface Methods
SSA	Six Sigma Analysis
PoF	Probability of Failure
MCS	Monte Carlo Sampling
MCDA	Multi-criteria Decision Analysis
MADM	Multi-attribute Decision Making
FST	Fuzzy Set Theory
PSF	Partial Safety Factor
FOSM	First-Order Second-Moment
GE	General Electric
CF	Capacity Factor
DCF	Discount Factor
RBDO	Reliability-based Design Optimisation
MPP	Most Probable Failure Point
MVFOSM	Mean Value FOSM
LSF	Limit State Function
LHM	Latin Hypercube Method
LHS	Latin Hypercube Sampling
RSM	Response Surface Method
CCD	Central Composite Designs
EWM	Extreme Wind Model
CDF	Cumulative Distribution Function
OD	Outer Diameter
PDF	Probability Density Function
NTM	Normal Turbulence Model
NWM	Normal Wind Model
RNA	Rotor-Nacelle Assembly
CoV	Coefficient of Variation
EWM	Extreme Wind Model

Acknowledgements

I would like to thank my supervisors, Professor Athanasios Kolios and Professor Feargal Brennan, for the support, resources, and opportunities he has provided to me over the years.

I would like to thank my parents, my wife and my siblings for their love and supports.

I would like to thank my friends and all countless individuals I met along at University of Strathclyde and my colleagues in Seaway7 for the knowledge and thoughts shared.

1. Introduction

1.1. Background

During the last decade, renewable energy has grown significantly to achieve global targets for reduced greenhouse gas emissions while ensuring energy security. As a result, wind energy has emerged as one of the most attractive clean and renewable energy sources. Europe and North America significantly contribute to offshore wind farms, with more than two-third of the world's wind power capacity located in these locations. By 2050, it is predicted that wind energy will supply between 15% to 20% of the world's electricity demands (Nghiem & Pineda, 2017; UK ETO, 2024).

1.1.1. History

The Persians and Chinese used the earliest recognized wind-powered grain mills and water pumps in 500–800 A.D (Sahin, 2004). The oldest human construction that still exists and was used for energy production from wind is located in Nashtifan village, Iran, dating back over a thousand years (Figure 1-1). The modern era of using wind energy started in the 16th century in Europe. Historiographers believe that at the peak of the windmill era, 18th century, over 1000 mills were operating in the Netherlands. This used wind power on an industrial scale, especially considering that the Holland province has a land area of only 1,030 mi².

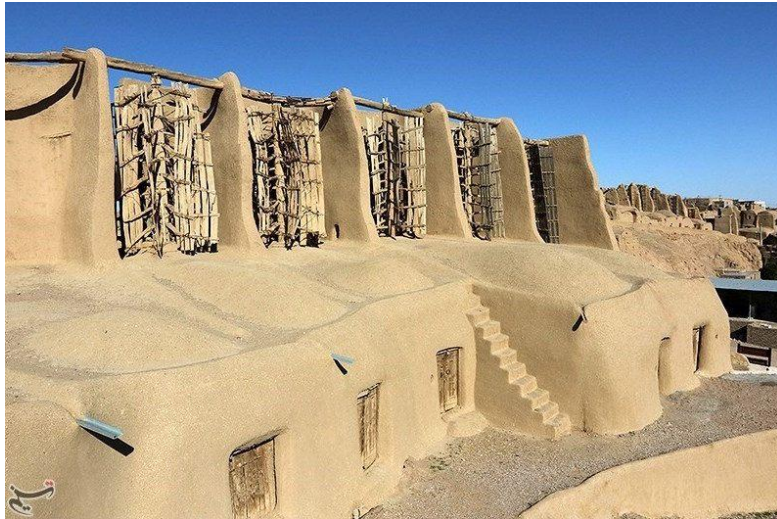


Figure 1-1 The oldest windmills existing in Nashtifan village, Iran

The first time wind energy was used for electricity production was in 1885 in Denmark at the high school of Askov. However, the idea of locating wind turbines offshore emerged shortly after 1930 when it was proposed that wind turbines be attached to towers. Although these ideas were never implemented, they were a brilliant start. William E Heronemus, a professor at M.I.T University, introduced the concept of large offshore wind turbine platforms to produce electrical energy in 1972, approximately 40 years after the original idea (Sahin, 2004).

In 1990, 18 years after the initial concept, a company called 'World Wind' developed and installed the first offshore wind turbine at sea. This OWT was in Nogersund, 250 metres offshore in 7 metres of water depth in the north part of Sweden, and it had a rated power of 220 KW³.

The United Kingdom joined the leading group of countries testing offshore wind energy, and by the year 2000, the first wind park with a rated power of 4 MW had been built in Blyth, east of England. This park includes two Vestas wind turbines of 2 MW each, located 800 metres offshore in water depths ranging from 6 to 11 metres.

As offshore wind energy technology matures, offshore wind farms gradually begin to flourish. By 2030, the EU will invest nearly 20 billion Euros in the wind power market, with 60 per cent allocated for offshore wind (Nghiem & Pineda, 2017; UK ETO, 2024).

1.1.2. Development of offshore wind energy

Foundations supporting fixed and floating offshore wind turbine structures have become a subject of interest to the offshore wind industry as offshore wind energy exploration has accelerated in waters and, more recently, deeper waters, owing to their importance in offshore wind turbine structure stability. Offshore wind farm foundations are exposed to complex loadings, including axial force from the turbine support structure and cyclic loads from extreme sea states. Therefore, such foundations must be designed to withstand a large number of wind and hydrodynamic load cycles of varying direction, amplitude, and frequency that occur over the typical design life of a project, which is about 25 years (Sahin, 2004).

The design of OWTs is challenging since the required accuracy of the reliability estimations and structural response is brutal to achieve. In addition, the combination of aerodynamic effects, hydrodynamic loading, and structural dynamics complicates the design and analysis process. However, the high target reliability levels required for OWT support structures are specified by standards to withstand the nonlinear ocean load effect and harsh environmental conditions.

Currently, DNVGL-ST-0126 (DNV GL, 2016) provides guidelines on offshore wind turbine support structures and design requirements. The design procedures in this study are primarily based on the DNVGL guidelines and the most recent related studies. However, as we know, references are developed following other industry-recommended codes and standards as required. Because the offshore wind industry's pace of innovations and technology is so fast, the updates are critical in keeping up with the enhancements in technology and understanding the system's structural simulations, interpretation, and response. Since the initial publication of DNVGL guidance on offshore wind turbine structures in 2004, DNV has released updated revisions in 2007, 2009, 2010, 2011, 2013, 2014, 2016 (DNV GL, 2016) and the most recent one in 2022. Following the 2013 merger of Germanischer Lloyd (GL) and Det Norske Veritas (DNV), all standards are currently undergoing co - ordination.

1.2. Problem statement

The design of OWTs is challenging since the required accuracy of the reliability estimations and structural response is difficult to achieve (Wang & Kolios, 2017a). In addition, the combination of aerodynamic effects, hydrodynamic loading, and structural dynamics

complicates the design and analysis process. One of the main obstacles to the mass deployment of wind farms is the cost, which should be feasible in construction and maintenance (Kuhn, 2001). However, the high target reliability levels required for OWT support structures are specified by standards to withstand the nonlinearity of the open sea load effect and the challenging environmental conditions. Therefore, target reliability is a crucial factor that helps designers devise a balance between material utilisation and failure risk.

In addition to the higher costs brought on by the offshore location, support structures need to be specifically designed for the site to guarantee a 20-year or more operational lifetime. As a result, the Levelized Cost of Energy (LCOE) for OWT in 2013, for example, was 215 \$/MWh, two times higher than the energy cost for a land-based turbine (Wilkes et al., 2016). On the other hand, the contribution of support structures for OWT accounts for 20-25% of the capital cost (Arshad & O'Kelly, 2013). Therefore, lowering the cost of the support structure through optimisation is a beneficial way to reduce the LCOE of offshore wind and make this solution less reliant on subsidy programmes. The amount of material that could be saved for a monopile support structure might be between 15 and 25 per cent (OREC, 2018).

Then again, offshore wind turbines (OWTs) are becoming larger and more efficient in recent years. Since 2014, the average annual increase in turbine capacity has been 16 per cent, and turbines installed in 2019 had an average rated capacity of 7.8 MW, which is 1 MW higher than the previous year (Walsh, 2019). The industry is thirsty for larger platforms and wind turbines, and their designs are continuously optimised to make them feasible in the market. In the last decade, the applicability for monopiles was just in water depths around 30m or less (Al-Sanad et al., 2021). Currently, it is becoming more frequent to hear about extra-large monopiles (diameters up to 9.5 m and piece weights up to 1,500 tonnes) as viable alternatives to jacket substructures.

1.3. Aim and objectives

This package of study covers three different sections in field of offshore wind support structure. All of them are trying to find a solution to push the technology of monopiles into larger, optimised in weight and applicable in deep water depths. In following categorised section, the aim and objectives of each part is explained, and it is recommended to be read before following chapters.

Study	Aim	Objectives
1. Reliability-Constrained Optimisation Framework	This section aims to develop a framework that uses a parametric Finite Element Analysis (FEA) model of a bottom fixed OWT support structure and integrates this with Genetic Algorithm (GA) and reliability assessment techniques to optimise and reduce the support structure's overall mass while satisfying multiple criteria imposed by design standards. (Please see Figure 1-2)	<ul style="list-style-type: none"> • Combining FEA, GA and reliability assessment of the candidate design models. • Finding an OWT's optimum support structure considering the target reliability constraints. • The cost analysis and comparisons are carried out between the reference OWT design and the optimised design. • The levelized cost of energy (LCOE) is estimated for both initial and optimised designs to see how a lighter structure can affect the LCOE for an offshore wind farm
2. Scale-up approach and weight estimation formula	Furthermore, a scaling-up approach will be proposed as the industry compass for the future is for larger structures in deep water.	<ul style="list-style-type: none"> • Upscale the 5MW NREL and OC3. • Considering different reference turbines, comparing them and using them on top of developed support structures. • Build FE Model and evaluate in ULS and FLS to see if they can fulfil the standard criteria.

		<ul style="list-style-type: none"> • Prepare a wind turbine dataset in different sizes and capacities and add currently-developed monopiles to create a data set to find a preliminary equation to estimate the weight of support structures.
3. Deep water depth sensitivity of large monopiles	Sensitivity analysis needs to be performed on a reference monopile support structure.	<ul style="list-style-type: none"> • The largest reference turbine is adopted (IEA 15MW). The FE parametric model must be created to evaluate the structural response in different water depths in fatigue and ultimate limit states.

These aim and objectives are the hot subjects in the current offshore wind industry to push the technology.

The flow chart of proposed framework for reliability-constrained optimisation is presented in Figure 1-2. It starts with defining the system and limit states following the stochastic variables. After performing optimisation using FEA and GA, the candidate designs are assessed with reliability constraints, comparing the resulted reliability indexes with DNV's target reliability, the final optimum design is generated.

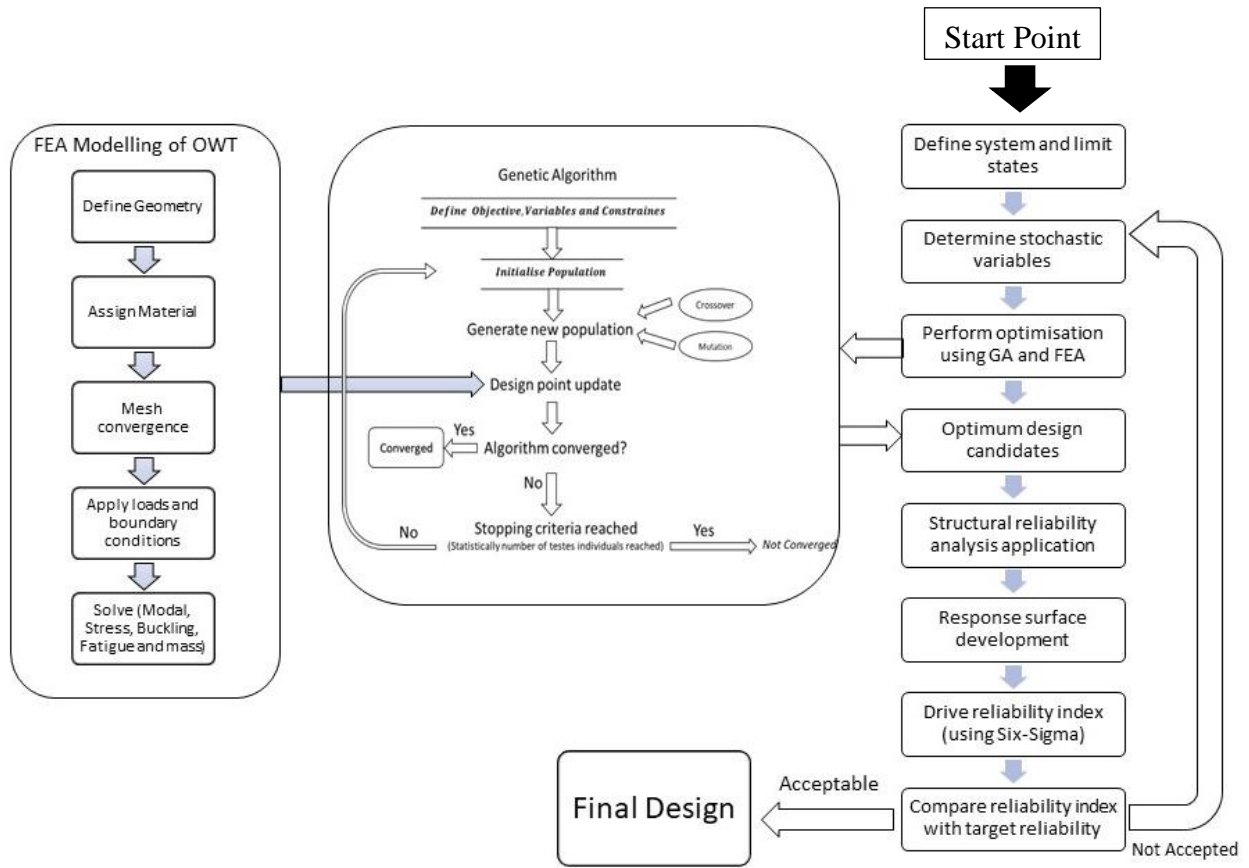


Figure 1-2 Proposed framework for reliability-constrained optimisation

1.4. Technology Readiness Level (TRL)

Technology readiness level (TRL) is a good measuring structure developed by NASA in the 60s in order to identify the required steps to get technology operational. It is a scale from 0 to 7, measuring the distance from an idea (0) to the business (7). However, there are other classifications, for example 1-9 levels, from other certification institutions as well. Figure 1-3 shows the details of this measuring structure. The framework proposed in this thesis and approach can be categorized in level 1 in the conceptual design study stage.

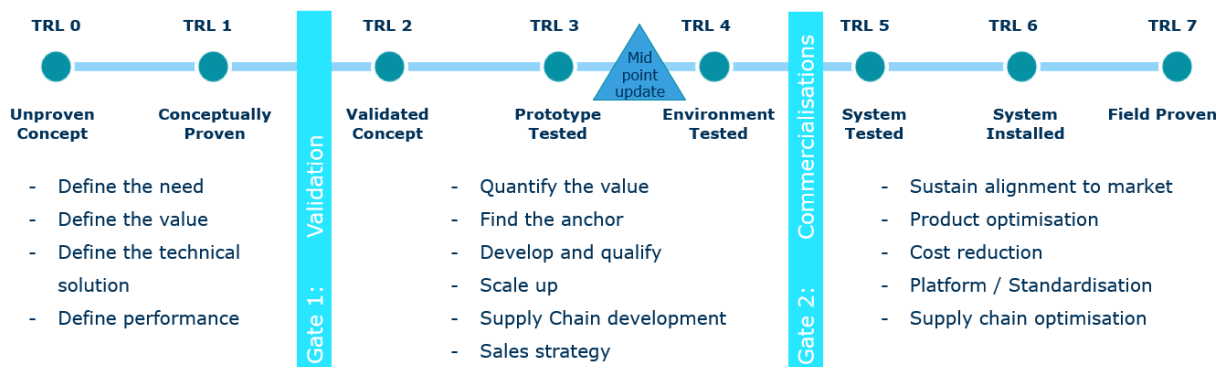


Figure 1-3 Technology Readiness Levels

1.5. Thesis structure

The research objectives are defined in the previous section. According to the aims and objectives of the thesis, an overview of the research is as follows:

- Literature review
 - Fixed-bottom support structures
 - Optimisation strategies
 - Reliability-based methods
 - Extra-large support structures and scaling up
 - Cost analysis and LCOE
- Modelling, finite element analysis and deterministic optimisation
 - Geometry, a numerical model of OWT support structure
 - Load calculations, DLCs and FE analysis
 - Verification through the codes and validation of the FE model
 - Definition of optimisation strategy
 - Design variables, objective function and constraints
 - Deterministic optimisation approach regarding FLS and ULS
- Reliability-constrained design optimisation framework
 - Stochastic variables as uncertainties
 - Safety levels and reliability criteria
 - Defining the RCD framework using reliability assessment, regression, response surface and Monte Carlo simulation
 - Validation of reliability assessment with FORM
 - Fatigue assessment of the optimised design using the DNV approach and DEL
- Scaling up and water depth sensitivity
 - Scale up factor
 - 3D Geometry, the numerical model of extra-large OWT
 - Estimation of monopile mass using preliminary parametric equation
 - Water depth sensitivity
- Results and Discussion
- Conclusions
 - Summary
 - Statement of contributions
 - Future work

Figure 1-4 shows a flow chart describing the sections that have been done in this study. According to the aims and objectives of the thesis, an overview of the research is as follows:

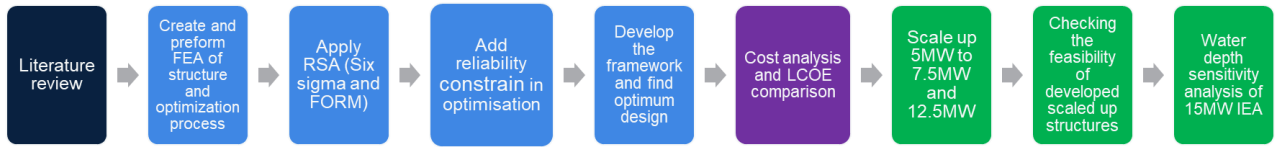


Figure 1-4 The project outline

2. Literature Review

2.1. Introduction

According to climate change policies, international protocols focus on minimizing greenhouse gas emissions, especially in the last decade. The world has realized that the challenges generated by oil reliance and rising carbon emissions must be addressed. The reduction of fossil fuel reserves and the ever-increasing demand for energy worldwide have caused fast growth in renewable energy sources. As a result, we live in an era of energy policy reversal, with intense political and industrial debates to implement renewable energy as the primary energy source.

With the start-up of the first offshore wind farm in 1991, new opportunities and challenges have arisen in this sector. Wind turbines' rated power, size and efficiency are increasing while their Levelized Cost of Energy (LCOE) decreases. According to WindEurope's Central Forecast, the EU will have deployed 323 GW of cumulative wind energy capacity by 2030, including 253 GW onshore and 70 GW offshore (Borkow & Gabbay, 2018). Figure 2-1 shows the yearly average usage of different energy sources in Europe up to 2019, indicating the increase in wind energy contribution in the last decade.

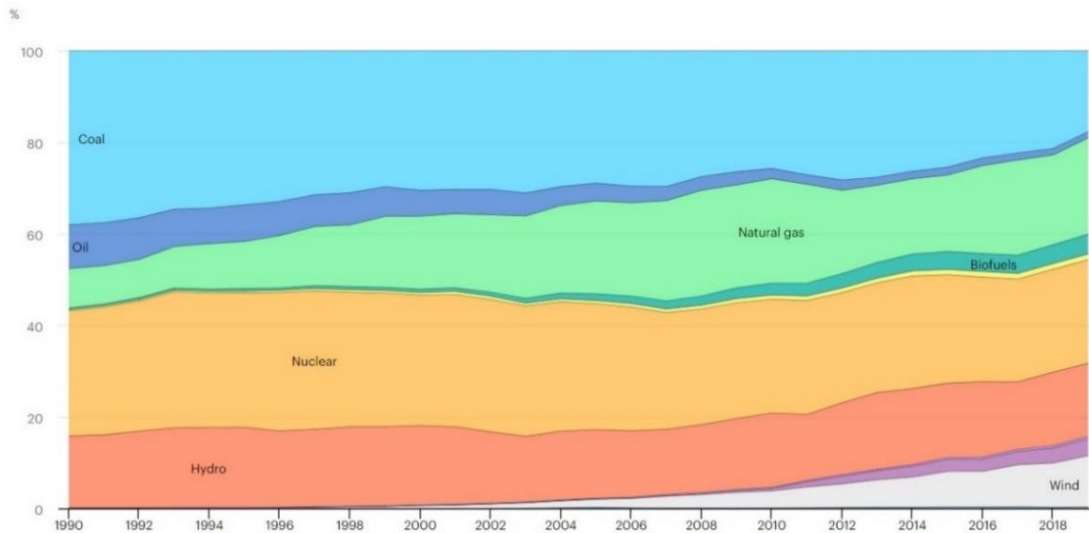


Figure 2-1 The yearly average usage of different sources of energy in Europe (Walsh, 2019)

Most wind farms are currently in-land, but the vast area, higher wind shear, and lower social impact on the marine environment have directed the wind industry to move offshore (Shittu et al., 2020). For this reason, offshore wind energy presents a considerable capacity.

2.1.1. Offshore wind foundations

Most offshore wind farms are situated in water about 10 metres deep on the continental shelf, about 10 kilometres off the coast. Regarding the design of the wind turbine system and the wind farm construction, offshore wind production is significantly more complex than onshore. Offshore wind turbines must be above the highest wave crests and have strong support structures connected to the seabed by foundations. In addition, complicated installation processes and maintenance, submarine cable and other electricity transmission systems are required. This is the main reason that offshore structure costs double or more than an onshore one (Muskulus & Schafhirt, 2014). Offshore wind turbines with fixed foundations are primarily found in depths less than 50 metres.

Over the last decade, there has been a surge of attention to floating offshore wind turbines since the wind resource is significant for water depths greater than 50 m. Yet, floating support structures are not as mature as fixed-bottom structures. At the moment, bottom-fixed offshore wind turbines are not an economically feasible option for resource exploitation in deep seas. But, many coastal countries, including Japan, the United States, and western European countries with an Atlantic seaboard, have limited coastal maritime borders to water depths of less than 50 metres (Al-Sanad et al., 2021). Therefore, optimising bottom fixed structures is still one of the favourite research subjects in the offshore wind industry.

2.1.2. Pros and cons of offshore wind farms

Many countries, mainly in Europe, cannot establish onshore wind farms due to geographical constraints and population concentration. This is evident in Denmark and Netherlands, which are nearly flat, low ground elevation, and densely populated. These conditions are not met offshore because of large continuous areas with no barriers to high wind speeds.

Another key reason for the construction of offshore wind farms is the higher wind velocity in an open sea. Wind velocity typically increases by about 20% in areas 10 kilometres or more from land (Parveen et al., 2021). Offered that wind energy increases in proportion to the cube of the velocity factor, wind energy can be up to 70% greater than wind speed onshore. Economically optimised offshore wind turbines are calculated to produce approximately 50% more power than onshore wind turbines (Wu et al., 2019). The water surface is relatively rigid in low and stable intensity winds. Still, as wind speed increases, a large percentage of wind energy is consumed to create waves, increasing the roughness of the water's surface. When the wave cycle is finished, the roughness of the water gradually decreases. We can see that the roughness of the water surface changes with wind velocity, but when offshore roughness is compared to onshore roughness, it is evident that offshore roughness is lower than onshore, meaning higher wind speed.

In contrast to onshore, where sunlight heats the upper part of the land surface, which becomes much warmer, sunlight penetrates below the water's surface. On land, particularly in comparison to offshore, this causes a temperature difference between the air and the surface, which is much greater, potentially causing the wind to flow more irregularly. As a result, the fatigue load caused by the wind load profile will be much lower, and the wind turbine life will be much longer with a less turbulent flow. Although exact calculations are still unavailable, a wind turbine designed for an onshore installation with a 20-year life cycle could be utilised for an offshore structure with a 25 to 30-year life cycle (Wu et al., 2019).

Although the acquisition cost of offshore wind turbines has dropped over previous years still, the high cost of construction is the primary factor behind the slow development of offshore wind energy usage. The cost of the foundation and the cost of the electrical connection to the shore are the two main factors resulting in the high price. In addition, complex environmental loads make the design process expensive.

2.1.3.Types of foundation

As discussed, the cost of foundations in an offshore wind farm is about 25—50% depending on the foundation type (Wu et al., 2019). This can hint at how selecting the type of foundation can ultimately affect the LCOE. Figure 2-2 depicts typical bottom-fixed support structures for offshore wind turbines in various water depths. This section reviews different types of bottom-fixed OWT support structures.

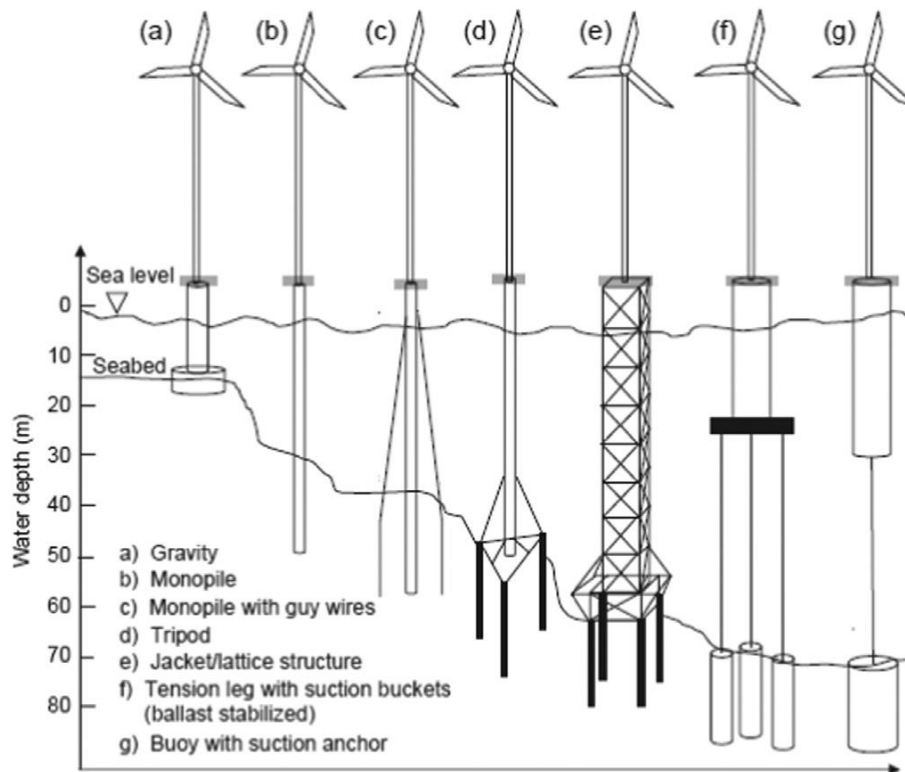


Figure 2-2 Typical fixed bottom support structure options at different water depths (Arshad & O’Kelly, 2013)

2.1.3.1. Gravity base

The gravity base foundations of offshore wind turbines are primarily designed based on their weight. Therefore, they must be sturdy enough to withstand extreme moments while leaving support structures standing upright on the seabed. The gravity base is a reinforced concrete coffer structure that is simpler to build than other types and has a low load-bearing capacity. Thus, this foundation is more appropriate for seabed composed of dense clay, sandy soil, and rock because they require a sufficient load-bearing capacity to support the self-weight, operational and environmental loads acting on the foundation structures. Gravity base foundations are typically located in water depths less than 10m. Most offshore wind turbines implemented gravity base foundations throughout the early days of offshore wind development, such as the Tunø Knob wind farm in Denmark. However, the gravity-based

foundation has recently become more popular after strict regulations about the installation process noise. An excellent example is the Fecamp wind farm on French coasts with more than 25m water depth. However, the rock and hard clay soil composition on wind farm sites is a primary driver in choosing this type of foundation.

2.1.3.2. Monopile

A monopile foundation comprises a single steel tube pile penetrating the seabed by giant hammers. It is still the most common type of offshore wind turbine support structure installed today, owing to its simplicity of fabrication and installation. The general characteristics of OWT monopile are $D = 6 - 9 \text{ m}$, $L = 20 - 30 \text{ m}$, and $L/D = 4 - 5$, where D and L are the diameter and length of the monopile, respectively (Al-Sanad et al., 2021; Shittu, Mehmanparast, Shafiee, et al., 2020). The monopile accounts for over 80% of all OWT foundations currently used in Europe (Figure 2-3). The cost of foundations for most offshore systems is about a quarter of the entire cost (OREC, 2018).

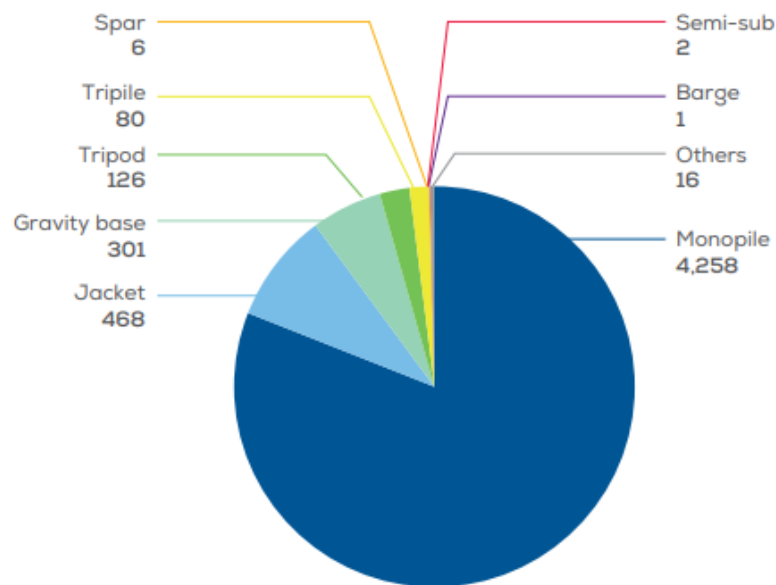


Figure 2-3 Number of foundations grid-connected by substructure type in Europe in 2020 (OREC, 2018)

Both horizontal and vertical loads are applied to a monopile support structure. Horizontal loads are transferred to the soil by mobilising the soil's lateral resistance through bending, whereas vertical loads are carried by pile wall friction and tip resistance. The pile diameter must be large enough to tolerate these loads. The monopile concept has some limitations. As the depth of the water increases, the diameter required to provide adequate stiffness must be more prominent (Kallehave et al., 2015). Due to steel plate sizes, pile driving capacity, and

fabrication limitations, the installation of extra large-diameter piles can be difficult (Trojnar, 2020).

2.1.3.3. Jacket structure

The jacket (or lattice) foundation is a frame structure made of steel tubular members typically prefabricated on land by welding. The structure is then transported to the location and piled into the seabed. Jacket foundations are relatively cost-effective in terms of steel utilisation, but fabrication, storage and installation can be expensive, significantly increasing the overall cost (Gualtieri et al., 2019). Furthermore, even though jacket foundations have been used in intermediate water depths of 25-60m recently, complex force distribution, easy fatigue and high maintenance costs make a severe challenge to the type of structure.

2.1.3.4. Tripod

Tripod foundations consist of three medium-diameter steel pipe piles positioned at an equal distance, the notch supporting the upper tripod truss structure. As a unit, a tripod truss can bear upper loads applied to the tower and deliver stresses and moments to the three steel piles. The tripod foundation is steady but a bit heavy comparing the monopile and suitable for 20 to 45 metres of water depths. However, the high manufacturing and installation cost are the barriers compared to the other types of foundations.

2.1.3.5. Suction bucket

Suction pile or bucket foundations are classified as single-bucket caisson foundations and multi-bucket caisson foundations. This type suits soft and medium clay seabed and wind turbines in varying depths. The installation cost of a suction bucket foundation is less than that of an equivalent offshore pile foundation due to the unique installation method used. In addition, suction bucket foundations have a silent installation process and are easier to manufacture and transport to the sea. As a result, suction bucket foundations have become more attractive in offshore wind turbines in recent years (Gao et al., 2021). However, the main disadvantage of a suction bucket foundation is the installation process's complexity and applicability limitation in soil type.

2.1.3.6. Floating foundation

Better wind conditions can be found in deeper water zones, typically at depths of more than 70 metres (Guo et al., 2022). Therefore, designing a new concept of foundation support structures, such as floating solutions, became necessary to reach deeper seas. Compared to the typical support structures still in use today, the floating idea for a foundation reduces the amount of

material required to make the entire substructure (compared to some concepts), reduces the complicated installation process on the seabed, and helps decommission much simpler. Three floating types developed recently in this sector are Spar buoy, Tension leg and Barge. The floating turbine base is kept in place by anchors installed into the seabed. Offshore floating foundations will probably be the most in demand in the future because of the capacity to produce energy far from the shore. Yet, it is still quite expensive because of the new technology, and some issues remain regarding the maintenance of the structure during its lifetime. Therefore, more research is required to investigate the technology and reduce the costs associated with its substructures. However, the stability of the turbine is a huge concern, either. Figure 2-4 summarises all common types of foundations in the offshore wind industry.

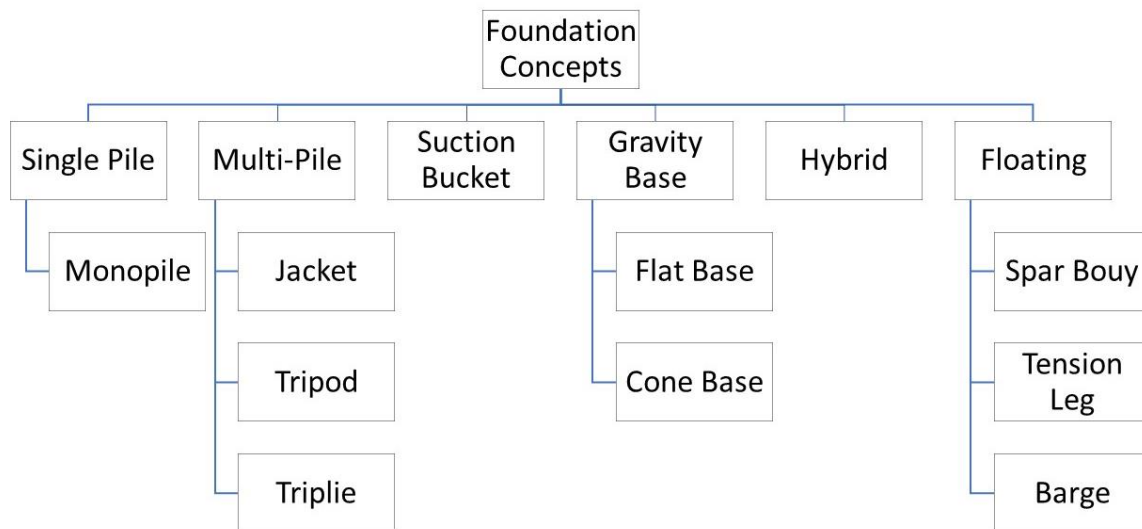


Figure 2-4 Summary of common types of foundations in offshore wind

2.1.4. Discussion and comparative analysis

After explaining all existing foundations for offshore wind energy, it is hard to find the best substructure due to the necessary knowledge of the local conditions in which it would be installed and the project's budget. So, no specific foundation type is equally suitable for all locations (Guo et al., 2022). Because of the massive costs involved in designing and manufacturing such structures, foundation design is the main topic in offshore wind turbines. Because the foundation can account for around 25% of the total cost of an offshore wind farm, evaluating the design could lead to a significant cost reduction (Ishtiyak et al., 2021). Although not a unified solution, the monopile is the best, cheapest, most dependable, and most flexible

option compared to the other alternatives. With the extra-large monopiles concept, such advantages take on a new and improved scale.

This study focuses on the monopile foundation due to its advantages and popularity compared to other types of foundations. The following section explains the design problem of an offshore wind support structure, particularly a monopile.

2.2. Support structure design problem

Offshore wind turbines are complex and strictly coupled systems, and their design presents specific challenges (P. Schaumann, C. Böker, A. Bechtel, 2011; Petrini et al., 2010; Quarton, 1998). The force vectors continuously rotate due to the blades' rotation, causing periodic fluctuations, primarily at the 1P (single blade passage) and 3P (rotor) frequencies. The aerodynamic forces are substantially influenced by the wind speed experienced by the blades, which is an irregular environmental state characterised by turbulence and spatiotemporal correlations at different scales. Hydrodynamic loads are a second source of irregular excitations for offshore turbines that must be considered while studying structural response. The stochastic, unstable nature of environmental loads, combined with the wide range of conceivable environmental conditions encountered during the turbine's lifecycle, creates different problems for estimating both ultimate and fatigue loads. It is commonly thought that a stationary stochastic process may characterise the environment on short timescales. This is based on observing a spectral gap for wind speed (Isaac Van der Hoven, 1957), while for offshore wind, it is a bit different (Heggem et al., 1998). The long-term distribution of environmental loads is extremely site-dependent and must be analysed using long-term data or climate model simulations. Load analysis for wind turbine constructions is currently strictly regulated (e.g., (DNV GL, 2014; IEC, 2005)).

2.2.1. Design rules

The structural design of an OWT can be accomplished using the following significant approaches, according to the DNV standard (DNV GL, 2014):

- Partial Safety Factor (PSF) approach with a linear combination of loads.
- PSF approach with a direct simulation of load effects at the same time.
- Design aided by testing.
- Probability-based approach.

Based on a separate assessment of the load effects in the structure due to the applied loads, the PSF technique is used in the DNV standard. As a result, the PSFs utilised in various activities ensure structural reliability by guaranteeing that the limit states are not exceeded when the partial coefficients are implemented. In this study, the DNV method has been used, and since the load effects are not independent, direct simulation of combined load effects at the same time has been utilised for design.

It should be noted that structural components shall be designed to (DNV GL, 2014):

- Sustain loads likely to occur during all temporary, operating and damaged circumstances if necessary;
- Maintain adequate structural safety throughout the structure's design life;
- Maintain a sufficient level of protection for both employees and the environment;
- Hold enough ductile resistance;
- Minimizing stress concentration;
- Durability during design life.

2.2.2.Limit states

The limit states that can be considered when designing offshore wind turbines are listed:

- Fatigue Limit State (FLS) corresponds to the failure of the structure because of cyclic loading;
- Ultimate Limit State (ULS) corresponds to the structure's maximum load-carrying capacity for supporting actions and impacts that may occur during its deployment and lifecycle;
- Serviceability Limit States (SLS) correspond to the maximum criteria or the capacity of the structure to continue to be able of the required use. The SLS for offshore steel structures is related to the structure's deflections and vibrations, which can cause deformations;
- Accidental Limit State (ALS) is the maximum load-carrying capacity for (uncommon) accidental loads such as fire, explosions, and collisions.

2.2.3.Types of loads

Based on the standards mentioned in section 1.1.2, the following will present the loads typically considered in the design of offshore wind turbines, depending on the case study, conditions and assumptions (DNV GL, 2010a).

Permanent loads: this type of load refers to loads that will not change in magnitude or direction during a time. The mass of the turbine and the hydrostatic pressure acting on the monopile are considered permanent loads.

Environmental loads: Environmental phenomena can be a source of loads which damage the structure installed in the sea. Unlike permanent loads, these loads may vary in direction and value during the time under consideration. The site location in the study determines the definition of these loads. The main environmental loads such as waves, current, wind and soil conditions will be studied during this study.

Accidental loads: Collision impact, large breaking wave, fire, or explosion can cause technical failures, accidents, or unusual operations. These loads are infrequent but dangerous. In this study, accidental loads are not considered because the number of accidental events that should be considered to provide accurate and reasonable analysis is unavailable.

Deformation loads are generated by unfavourable events to which the structure is subjected, such as the settlement of the support structure due to soil deformations or changing temperature loads. Once again, data availability concerning temperatures and soil conditions is challenging. It must be noted that the analysis of the inconsistent settlements of the structure depends on the soils' structure and condition, i.e. if it is well compact in sedimentary layers or as a mixture of different sediments. Even with the data used in further analysis of the soils' stiffness, the study of the structure settlement is not the primary purpose of this research. However, if such analysis is required, particularly for complex soil configurations, there are interesting works on soil-structure interaction in the literature, such as (Porter et al., 2012).

Dynamic loads: Considering the cyclic excitation effect in offshore structures is vital. These loads generate a dynamic structural response, resulting in vibrations that can cause serviceability damage or total collapse. In addition, waves, wind, earthquake or rotor frequency modes could cause dynamic structure response.

Variable function loads: Caused by the installation process, maintenance, or personnel weights are another type of load not considered in this study due to the lack of information.

2.2.4. Structural modelling and soil-pile interactions

A structural structure model is required to estimate the structural behaviours of OWT support structures when subjected to complicated loading and soil-structure interaction, which is necessary for evaluating the structural reliability of OWT support structures.

There are two main categories for the structural designs employed in OWT 1) the 1D beam model and 2) the 3D FEA model, which typically models OWT support structures as shell elements and, in some cases, solid elements.

Global responses, including frequencies and deflections, can be calculated with relative accuracy using the 1D beam model, which also increases efficiency in the computing process. However, it cannot accurately capture local behaviour, such as the local stress concentrations. Although the 3D FEA model is more computationally complex than the 1D beam model, it gives more precise results. With advanced processors, the 3D FEA model has recently seen broad applicability to wind turbine structures, including blades (Wang et al., 2016) and support structures (Gentils et al. 2017), because of its high fidelity.

The soil-structure interaction can significantly impact the structural behaviour of OWT support structures because the foundation of the OWT support structure is embedded in the soil. Consequently, soil-pile interaction must be considered precisely to have accurate structural response results.

Soil modelling techniques can be divided into two broad categories: (i) the p-y method and (ii) the finite element method. The p-y approach uses a soil model composed of distributed equivalent springs, the stiffness of which is calculated using the p-y curve. As a result of its processing efficiency, the p-y method has been widely adopted for modelling the soil in OWT support structure reliability analyses (Carswell et al., 2015; G. Kim et al., 2015). Nevertheless, this method was designed for oil and gas industry pipes and is therefore inadequate for modelling the soil behaviour of OWT support structures, which diameters are substantially larger. Thus, the FEA model of the soil is recommended to capture the soil's behaviour with precision. Soil is usually presented in FEA models employing three-dimensional brick elements. The material model for soil is generally based on one of the Drucker-Prager model (Drucker and Prager, 2016) or the Mohr-Coulomb model (Labuz & Zang, 2012). Soil interaction using the p-y method and FEA model is compared and studied in the PISA (Pile Soil Analysis) project (Byrne B & RA McAdam, 2017; Byrne et al., 2020; Zdravkovic et al., 2020) led by the University of Oxford researchers. The PISA design technique takes into account wind turbine loading conditions and larger diameter monopile geometries to facilitate location-specific optimisation of turbine substructures. The steel used for the monopile may be reduced by as much as 30 percent in the embedded portion of the pile. The results showed

that the FEA model matches well with experimental data, but at a fraction of the computational cost. Because of its accuracy, the FEA model is increasingly used for soil modelling.

It is essential that scouring phenomena around the foundation be taken into account while modelling soil-structure interaction. A scour is a region of eroded soil around the base of a structure induced by waves and currents. The scour can be controlled in p-y curve soil models by eliminating the appropriate springs (Abhinav & Saha, 2017). However, using FEA to simulate the soil, scour can be accounted for by changing the soil's shape close to the foundation (Porter et al., 2012). The stiffness, natural frequency, and fatigue reliability of OWT support systems have all been impacted by scouring (Van der Tempel et al., 2004).

2.3. Optimisation strategies

Like any complex project, the modelling, simulating, and optimizing of an OWT are prerequisites. Structural optimisation has progressed almost in lockstep with the improvement of structural analysis. Developing a design problem with a reliable analytical approach allows for discovering optimal solutions and implementing semi-automated and algorithmic solutions (Arora et al., 2012). The application of these methods has grown significantly as the cost of computational resources has decreased, expanding possibilities for designing structures and systems. Unlike a human designer and manual optimisation, which is frequently restricted to a short number of design iterations, computer-aided optimisation can search through a considerable number of different cases and will investigate non-clear solutions. Figure 2-5 shows the difference between manual and computer-aided optimisation strategies.

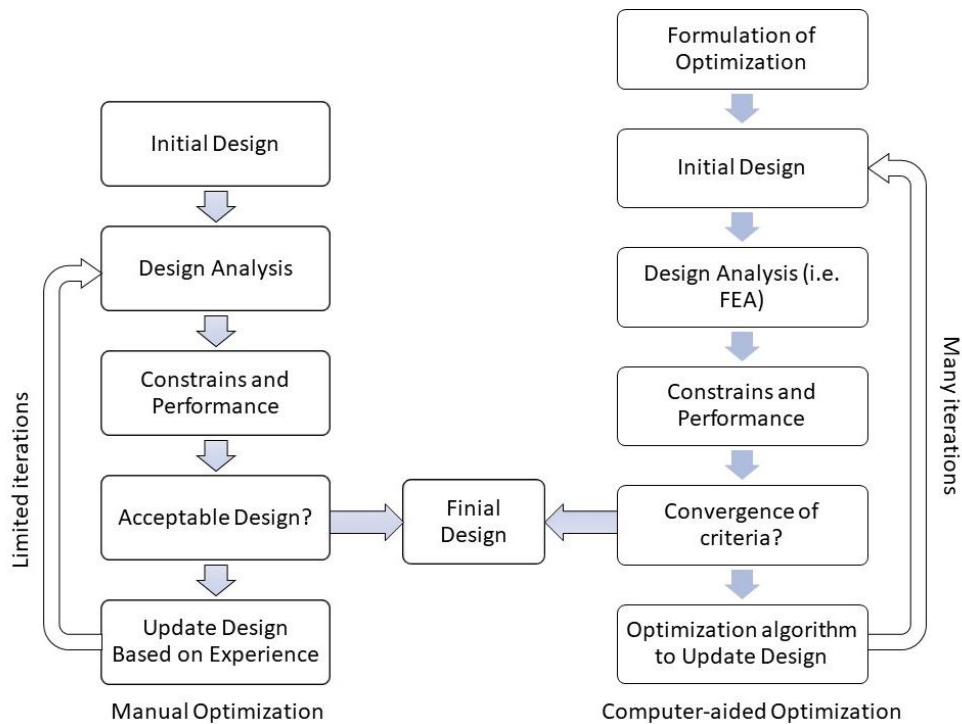


Figure 2-5 Comparison of manual and computer-aided optimisation

In the review by (Muskulus & Schafhirt, 2014), six characteristic challenges in designing a wind turbine structure were discussed: nonlinearities, complex environment, fatigue as a design driver, technical analysis software, tightly coupled and interrelated systems, and multiple influencing variables and constraints. Although OWT analysis has been rigorously regulated, many studies have developed a framework to design and optimise large offshore structures (Gentils et al., 2017; Stieng & Muskulus, 2020). These analyses should be built on a numerical wind turbine model, which is (1) as accurate as possible and (2) subject to an understanding of the stochastic methods characterizing the environmental loads. These complexities lead to a multidisciplinary design optimisation problem. In the following sections, optimisation under various conditions will be discussed.

2.3.1. Optimisation under static loads

In recent years, structural optimisation has concentrated heavily on identifying the best solution(s) to static problems using finite element methods. The common application is to reduce the weight of a structure by modifying the parameters that define its geometry, such as the diameters and thicknesses of structural parts. In parallel, the rigidity and stiffness of a design shall be considered by doing a modal analysis. The objective function describes the level to which the structure succeeds in achieving this aim as a single numerical value (e.g., the global weight of the structure). This value is fixed and predetermined concerning the

geometrical characteristics of the construction. Optimizing under static loads simplified the loads applied to the structure. Overall, the nonlinear mathematical structures are challenging to address, and estimates and reductions to simpler issues are used as much as possible. However, when both the objective function and the constraint equations are linear, the problem can be addressed using linear programming optimisation methods respectively (J Nocedal & SJ Wright, 2006).

2.3.2. Optimisation under transient loads

This type of optimisation is less established than static optimisation. The standard method is restraint-based, and unlike the static condition, the constraints must be followed at every interval, i.e., the problem consists of an infinite amount of constraint equations (Muskulus & Schafhirt, 2015). In order to create the applicable method, the time dependence is frequently removed by taking into account an integrated constraint (e.g., the integral sum of constraint violation across time), which must be zero for a feasible solution. Instead, the constraint is assessed at all critical points, which are the local minima of the constraint function that reflect the instants in time when the constraint is most likely to be broken (Nagendra et al., 1991). The Equivalent Static Loads (ESL) approach simplifies the problem by breaking it down into a series of static optimisation problems for which analytical gradients are easily produced, and then merged to approximate the actual sensitivities (Park et al., 2007). Other advantages of this method include that it can be implemented with most structural analysis software packages and that static response optimisation may be conducted with the ESL.

2.3.3. Time series and Fatigue-constrained optimisation

Until this section, the constraints have been considered general, consisting of limits determined by material yield stress (ULS), buckling, manufacturing methods, etc. However, the need to analyse and limit fatigue damage to the structure is a significant class of restrictions. Time domain analysis refers to evaluating the structural response and fatigue damage accumulation over time in the context of fatigue analysis for offshore wind turbines. Fatigue is a major concern in the design and operation of offshore wind turbines due to the dynamic and harsh environmental conditions they are subjected to. Damage Equivalent Loads (DEL) is a concept used in time domain analysis to assess the cumulative fatigue damage caused by dynamic loads on the turbine structure. DEL is a simplified representation of the complex load history, condensing the fatigue damage contribution into a single equivalent load level (Rychlik, 1987). Time domain analysis for DEL involves the following steps:

- **Load Data Acquisition:** Similar to the previous explanation, relevant environmental and operational data are collected over a specified period. This includes wind speed, wave height, tidal conditions, turbine operational states, and control parameters.
- **Load Reconstruction:** The acquired data is used to reconstruct the time-varying loads acting on the turbine structure. This includes the aerodynamic loads on the rotor blades, gravitational and inertial loads, wave-induced loads on the support structure, and other dynamic loads.
- **Load Combination:** Different load components are combined according to the DLCs. For example, extreme wind, turbulence, or loads during specific operational states can be considered separately.
- **Fatigue Analysis:** The reconstructed load time series is applied to a detailed structural model of the wind turbine. Through numerical simulations, the response of the structure, such as bending moments, stresses, or strains, is computed for each load case.
- **Rainflow Counting:** Rainflow counting is performed on the response time series to identify the fatigue-dominant load cycles. Rainflow counting extracts the stress or strain ranges from the response data, considering both the amplitude and direction of the cyclic loading.
- **DEL Calculation:** The fatigue damage contribution of each load cycle is evaluated using a fatigue damage model, typically based on Palmgren-Miner's rule method. DEL is then determined as the equivalent constant-amplitude load that would cause the same cumulative damage as the original load history.

Finally, it is typically analysed for specific spots (e.g., welded joints) using numerical formulas that estimate the hotspot stresses based on several nodal stress histories and geometry (DNV GL, 1987). However, since many structures behave linearly for minor displacements, frequency domain analysis and semi-empirical fatigue damage assessment can be performed as an alternative to time-domain simulation, often by employing a model established by fitting an extensive set of computer simulations (Dirlik, 1985).

2.3.4. Optimisation based on simulation

Optimization based on simulation for offshore wind structures concerns using computational models and simulations to improve the design and performance of offshore wind turbines and their supporting structures. This approach allows designers to evaluate different design options,

assess system behaviour under various operating conditions, and identify optimal solutions that meet performance criteria and minimize costs. The steps that outline this process are:

1. Define Objectives and Constraints
2. Create Simulation Models
3. Design Variable Selection
4. Define Design Constraints
5. Define Objective Functions
6. Optimization Algorithm Selection
7. Perform Simulation-Based Optimization
8. Evaluate and Validate Results
9. Iterative Improvement
10. Final Design Candidate

Optimization based on simulation allows for systematically exploring design options, enabling designers to find solutions that evaluate performance, cost, and other relevant factors for offshore wind structures. As a result, it can lead to improved efficiency, reduced costs or weight, and enhanced overall performance of offshore wind turbines and their supporting systems.

Various simulation-based optimisation methods can be used in such scenarios where the objective function or issue constraints are not accessible for efficient assessment (Murray et al., 2010). Approaches are based on meta-models, such as general response-surface methods (Cheng & Li, 2009). In addition, neuronal networks, genetic algorithms, and stochastic search and optimisation approaches are prominent methodologies (Kolios, 2010).

2.3.5. Probabilistic Optimisation

The optimisation approaches described above assume a deterministic, objective function. A probabilistic explanation of variability, uncertainty, and error causes (both from external effects and internal faults) is often a more natural approach. The two complimentary methodologies of reliability-based and robust design optimisations allow for incorporating uncertainty and unpredictability in the design process (Psarropoulos & Tsompanakis, 2008). Because they involve structural analyses, these methods are at least an order of magnitude more complicated than "classic" structural optimisation methods. They are linked to the frequent practice of grouping environmental situations into a discrete set of load cases (Kuhn, 2001) as well as the subject of how partial safety factors are calibrated (Veldkamp, 2006).

2.4. Optimisation algorithms

In engineering optimisation, the selection of the optimisation algorithm is an essential element that depends on the nature of the problem and the characteristics of its design space. In wind turbine performance optimisation, choosing the optimisation algorithm is crucial since the results depend on the algorithm's accuracy and sensitivity to local minima. Consequently, the methods used to address optimisation problems in wind turbine design have evolved. Initially, the majority of approaches were derived directly from the Blade Element Momentum (BEM) theory, mainly from the BEM theory of (Wilson et al., 1976). However, in the 1990s, (Selig MS & Coverstone-Carroll VL, 1996) were among the first to propose a GA-based wind turbine blade design technique. Furthermore, meta-heuristic algorithms are preferred in optimising wind turbine support structures because of their robustness and consistency (Gentils et al., 2017).

(Rodrigues et al., 2017) classify optimisation algorithms into two categories: Calculus-based approaches and meta-heuristic algorithms. The following sections describe the common types of algorithms researchers in the offshore wind industry have used.

2.4.1. Genetic algorithm (GA)

The genetic algorithm (GA) was most explored among the various meta-heuristic algorithms. The following section discusses the use of GA and why it is preferable among other algorithms in our case study. Because of its consistency and durability, genetic algorithms have become the most preferred evolutionary algorithm. However, evolutionary algorithms are time-consuming and require adding a regularization term for constraints to the objective function, which might reduce their sensitivity to local minima.

A genetic algorithm uses natural selection to favour the best solutions among a population (set) of individuals (individuals) through time (generations). Figure 2-6 shows the schematic of the GA optimisation process. Populations consisting of individuals with high "fitness" values, as measured by the objective function chosen for the optimisation process, have a higher chance of "reproducing" and hence of producing a new generation than do populations consisting of individuals with low "fitness" values. A single string represents each individual, and the search is guided through the generations by operators representing reproduction, crossing, and mutation, just like in a DNA chain.

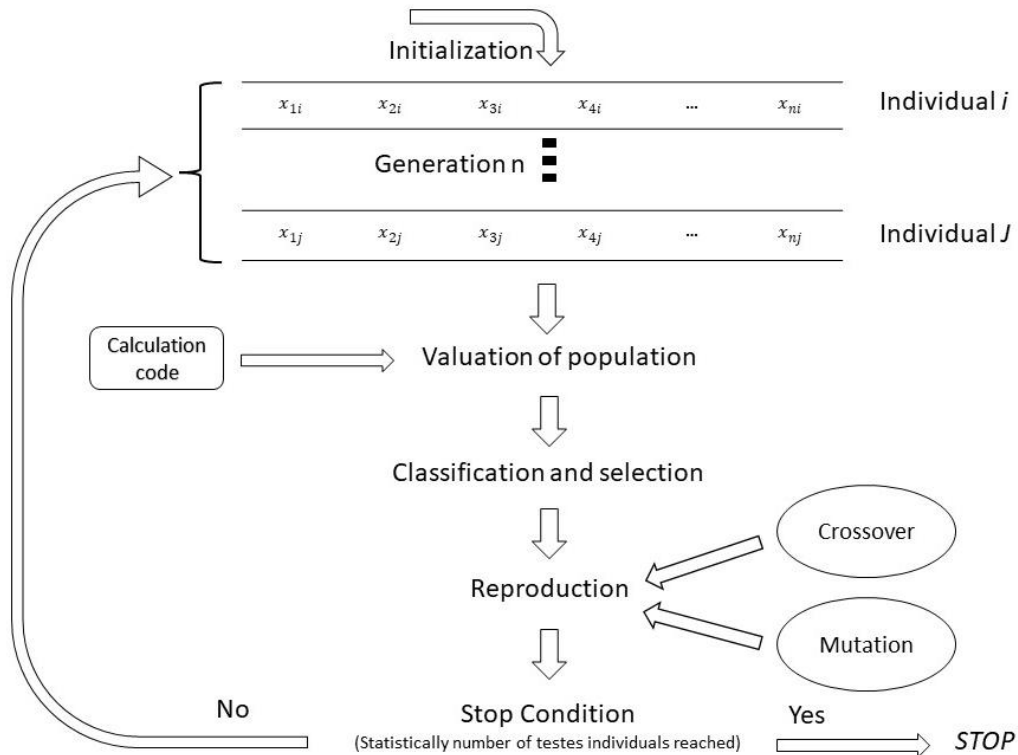


Figure 2-6 Schematic of genetic algorithm optimisation (Diveux et al., 2001a)

A GA's primary characteristic is its ability to operate directly on structural objects directly without derivation and function continuity limitations (Sineglazov et al., 2016). It has inherent, implicit parallelism and enhanced global optimisation capabilities that employ probabilistic optimisation methods and do not require specific rules. It can automatically obtain and guide the optimum search space and adaptively alter the search direction. When applied to a group of individuals, the genetic algorithm uses randomization technology to explore a coded parameter space efficiently.

Genetic algorithms are extensively used for the design optimisation of OWTs. (Hall, 2012) provided an optimisation framework based on evolutionary algorithms for FOWT substructures. First, a frequency-domain model assessed the performance of the FOWT in terms of six-degree-of-freedom motions. The evolutionary algorithm was then used to investigate the design space and identify local optimums that minimise root-mean-square (RMS) nacelle acceleration and cost. (Banzo & Ramos, 2011) utilised geometric programming to solve an optimisation model based on cost, loss, and reliability for a single main substation and validated this strategy with a small wind farm. (Gentils et al., 2017) developed a structural optimisation model for an offshore wind turbine substructure based on coupled parametric FE model and genetic algorithms by minimising the mass of the support structure under

multicriteria constraints. Using the proposed model, they optimised the support structure's components (tower, transition piece, grout, and monopile) and reduced the weight of the support structure by deterministic optimisation. (Karimi et al., 2017) introduced a multi-objective design optimisation approach for floating wind turbines with a design space spanning three stability classes of floating wind turbine substructure, spar, TLP, and semisubmersible, employing nine design parameters. The 5MW FOWTs were analysed using FAST and WAMIT. A multi-objective genetic algorithm optimisation strategy was used to evaluate and compare. In the study of (Pasamontes et al., 2014), a genetic algorithm was utilised to optimise the structural design of the Upwind jacket support structures from the OC4 project. Each design was assessed using a comprehensive wind turbine simulation for a load situation in the time domain.

The population-based search of a GA provides a population of optimal solutions, which is crucial if a large portion of the design space yields optimal outcomes without a clear optimum. In addition, GA is superior at exploring non-linear, non-derivable, non-continuous domains and is less sensitive to the initial condition (Fernandes et al., 2014; Grasso & Grasso, 2012; Shahrokhi & Jahangirian, 2007). Other examples of studies that used a genetic algorithm to optimise the performance of wind turbines: (Diveux et al., 2001b; Eke & Onyewudiala, 2010; Giguère & Selig, 2000; Wang & Tang, 2011). In general, GA is unique in its approach and offers several advantages over other optimisation approaches, such as:

- **Global Search Capability:** Genetic algorithms are well-suited for global optimisation problems, where the goal is to find the best solution across an ample search space. GAs use a population-based approach that maintains a diverse set of candidate solutions, allowing them to explore the search space more comprehensively than many other optimisation algorithms that rely on a single solution or a limited set of solutions.
- **Robustness to Local Optima:** Genetic algorithms are less likely to get trapped in local optima, suboptimal solutions in a restricted search space region. Due to their ability to maintain diversity in the population, GAs can escape local optima and continue searching for better solutions in other areas of the search space.
- **Handling Non-differentiable and Discrete Problems:** Genetic algorithms are well-suited for optimising problems involving non-differentiable or discrete variables. Unlike gradient-based approaches, GAs do not require objective function or constraint derivatives, making them suitable for problems with complex or discontinuous fitness landscapes. GAs can also handle problems with discrete variables, as they operate on a

population of solutions that can undergo discrete changes through genetic operators such as mutation and crossover.

- **Flexibility and Adaptability:** Genetic algorithms are highly flexible and adaptable. They can be easily customized to suit specific problem requirements by adjusting population size, mutation rate, and crossover strategy. They can also be combined with other optimisation techniques or problem-specific heuristics to enhance performance.
- **Parallelism:** Genetic algorithms can be parallelized to take advantage of modern computing capabilities, allowing for efficient search space exploration and faster convergence. This makes them well-suited for parallel and distributed computing environments.
- **Exploratory Capability:** Genetic algorithms can experimentally find novel and unexpected solutions. They can generate diverse solutions in the population, allowing for discovering non-obvious and innovative solutions that other optimisation approaches may not discover.
- **Robustness to Noisy Environments:** Genetic algorithms are robust to noisy or uncertain environments, where the objective function evaluations may be loud or subject to uncertainties. The population-based nature of GAs can help mitigate the effects of noise, as the best solutions can still be identified even if some individuals in the population have noisy fitness values.

2.4.2. Gradient-based approach (GBA)

Gradient-based approach (GBA) is a technique used in optimisation algorithms for finding the optimal solution to a mathematical problem, typically an unconstrained or constrained optimisation problem. The key idea behind GBA is to leverage the gradient, the vector of partial derivatives of a function concerning its variables, to guide the search for the optimal solution. In the other word, the calculus-based algorithm relies on the gradient calculation of the objective function to find the sensitivity of each design variable. Regarding computation time and choice of objective functions, gradient-based approach algorithms have been compared to genetic algorithms. However, they are primarily utilised for quicker results but are susceptible to the initial condition and, therefore, not robust (Obayashi, 1996). In GBA, the optimisation algorithm iteratively updates the solution by taking steps toward the negative gradient, as the negative gradient points towards the steepest decrease in the function's value. This process continues until a stopping criterion, such as a certain number of iterations or a slight change in the objective function value, is met.

Several optimisation algorithms use gradient-based approaches, such as gradient descent, conjugate gradient, Newton's, and stochastic gradient descent (SGD). These algorithms may have different variations and adaptations depending on the specific problem and requirements. GBA has several advantages, including its ability to efficiently handle large-scale problems, fast convergence rate, and ease of implementation. However, it also has limitations, such as sensitivity to the initial conditions, getting stuck in local optima, and potential convergence issues in ill-conditioned problems.

Overall, GBA is a powerful and widely used approach in optimisation algorithms, and it plays a crucial role in various fields, including machine learning, computer vision, operations research, and engineering, among others.

2.4.3. Sequential Quadratic Programming (SQP)

The sequential quadratic programming (SQP) algorithm is considered one of the efficient techniques for resolving constrained nonlinear optimisation problems. An iterative method seeks to find the optimal solution by approximating the problem as a sequence of quadratic programming subproblems at each iteration. In comparison to other algorithms, the SQP technique has the benefits of good convergence, high calculation efficiency, and excellent limit and boundary searchability. The SQP approach reformulates the overall problem into a quadratic programme (QP) subproblem and approximates the Hessian matrix using a modified version of the Broyden–Fletcher–Goldfarb–Shanno procedure.

The key idea behind SQP is to iteratively update the solution by solving a sequence of quadratic programming subproblems. These smaller optimisation problems can be solved more efficiently than the original nonlinear constrained optimisation problem. At each iteration, SQP generates a search direction by solving a quadratic programming subproblem and then takes a step in that direction to update the solution. The algorithm continues iteratively until a stopping criterion is met, such as a certain level of accuracy or a maximum number of iterations.

The primary advantage of SQP approaches is their ability to handle complex nonlinear problems with rapid ultimate convergence. The major downside of the SQP approach is that it can only accomplish fast convergence in the case of accurate gradients and typically requires a substantial amount of storage space. Furthermore, the necessity of obtaining these gradients analytically before iterating to a solution, a technique employing SQP for case studies with

many variables and constraints might involve highly complex calculations, and its sensitivity to the initial conditions will cause a convergence issue in ill-conditioned problems.

2.4.4. Other algorithms

Several algorithms, such as Particle Swarm Algorithm (PSA) and Ant Colony Optimisation (ACO), are widely used to optimise offshore wind turbines.

The particle swarm algorithm (PSA) was inspired by studying the predatory behaviour of bird flocks and schools of fish. It simulates the behaviour of flocks of birds flying for food. A collective effort among birds guarantees that the group achieves its objective. A bird represents each solution to the optimisation issue, referred to as a particle. All particles employ a fitness function to decide if their current position is favourable or unfavourable. PSO is utilised for offshore wind turbine blade design. (Liao et al., 2012) optimised wind turbine blades using PSO and comparing optimised blades with reference design showed that this strategy is feasible for OWT.

Ant Colony Optimisation (ACO) algorithm is developed to solve discrete optimisation problems. Furthermore, the programme simulates the behaviour of an actual ant colony as it looks for food (Eroğlu & Seçkiner, 2012). These methodologies are commonly utilised in wind farm layout design instead of the optimal design of the offshore wind turbine supports (Salcedo-Sanz et al., 2014).

2.5. Discussion of optimisation models

As discussed, the wind turbine's complexity and environmental characteristics require a comprehensive design optimisation issue for the structural design and optimisation of the turbine (Martins & Lambe, 2013; Rodon et al., 2003). In addition, the system is strongly coupled, so optimising specific elements of the turbine separately would result in inefficient or infeasible solutions. For example, in the early stages of offshore wind turbine deployment, it was attempted to isolate the impacts of wind and waves on turbines. However, it has been demonstrated that this results in unacceptably significant inaccuracies in fatigue damage estimations (Kuhn, 2001).

In design optimisation for large wind turbines, static analysis is still prominent. A solitary static load case Enhancing the investigation, (Lavassas et al., 2003) employed 18 different static load

cases, indexed by wind velocity and defined by the wind turbine producer, to validate their design for a 1 MW tower. (Uys et al., 2007) employed a similar procedure and load to improve the tower concerning diameters and the number of stiffeners for a 1.3-megawatt wind turbine. The optimal design was accomplished using the fewest resources, reducing costs. (Perelmuter & Yurchenko, 2013) present the optimisation of a circular tower with a more refined approach that uses dynamic sensitivity factors and accounts for turbulence-induced load changes. Their optimal tower for a 5-MW onshore turbine is 140 metres and weighs 340 tonnes, nearly the same as the 87.6-meter tower of the NREL model 5-MW offshore wind turbine (Jonkman et al., 2009). (Gentils et al., 2017) also studied the deterministic optimisation approach to make the lighter 5MW monopile support structure and reduce 20% weight using finite element analysis tools.

Several researchers have used frequency-domain analysis for wind turbines. (Häfele, 2019) studied monopile design and optimisation with a genetic algorithm and a semi-analytical wind turbine model, assuming a stiff rotor and no aerodynamic damping. (Long & Moe, 2012) explored the construction of lattice towers in the frequency domain, utilising the (Dirlik, 1985) approach to quantify fatigue damage. Linear dashpots provided aerodynamic damping. The main advantage of frequency domain analysis is its performance, despite nonlinearities and approximate fatigue calculations. It can check several thousand load cases in minutes, making it ideal for early design.

Simulation in the time domain provides a realistic examination of wind turbines. Standards approve this method for certification analysis (DNV GL, 2016; IEC, 2019). The European Opti-OWECS study found that integrating wind turbine design improves cost efficiency. All wind turbine components must be designed together, and installation, operation, and maintenance must be considered (Kuhn, 2001). (Yoshida, 2006) employed customised dynamics to test the tower design's structural integrity using time-domain simulations and a genetic algorithm. However, for complex support structures like jackets or 3D monopiles, the number of load scenarios is limited, and with less-than-real-time simulation ratios, this strategy is quite time-consuming.

(De Morais et al., 2021) proposed a comparison model to simulate the structural response of wind turbine towers subjected to high winds created as a spatially correlated field, utilizing the MATLAB codes for frequency-domain (FDA) and time-domain (TDA) analysis. The FDA implemented the approach performed as well as the standard direct TDA integration method in

the tested case in terms of performance and computational processing time. However, the performance of the analysis was not predicted with the existence of a 3D model and optimisation algorithms.

Overall, the mathematical expression of structural optimisation is that of a non-linear programming issue (Arora et al., 2012) and therefore needs a simpler structural model to solve the difficulties. Moreover, optimisation problems for offshore structures are mostly non-convex and multi-modal (Clauss & Birk, 1996), making them less robust and more likely to end in local optimum (Saka et al., 2016). Thus, a meta-heuristic algorithm (MHA) such as GA should be chosen.

2.6. Reliability-based methods review

In this section, reliability methods used in the offshore and marine renewable energy industry are categorised and analysed in terms of how they can be used for offshore wind turbine systems, their advantages and disadvantages, and their ability to be improved. Trends and new ways to overcome problems that have not yet been solved are also discussed.

2.6.1. Reliability method classifications

Several forms of Reliability Assessments (RA), such as mechanical, electrical, and software, can be conducted at various points in the engineering process, including during the design and manufacturing phases. For instance, Stapelberg (2009) concentrates on reliability in engineering design, placing a boundary between conceptual, preliminary/schematic, and detailed design stages for reliability prediction, assessment, and evaluation. In addition, two levels, component and system, are specified for applying reliability.

Depending on the quantity and quality of data availability, there are two primary classes into which the various dependability approaches can be arranged: qualitative and quantitative (Stapelberg 2009). Figure 2-7 is a chart that illustrates both classifications. Some qualitative reliability methods can be extended with some quantitative approximate methods and, therefore, can be used for quantitative reliability assessment.

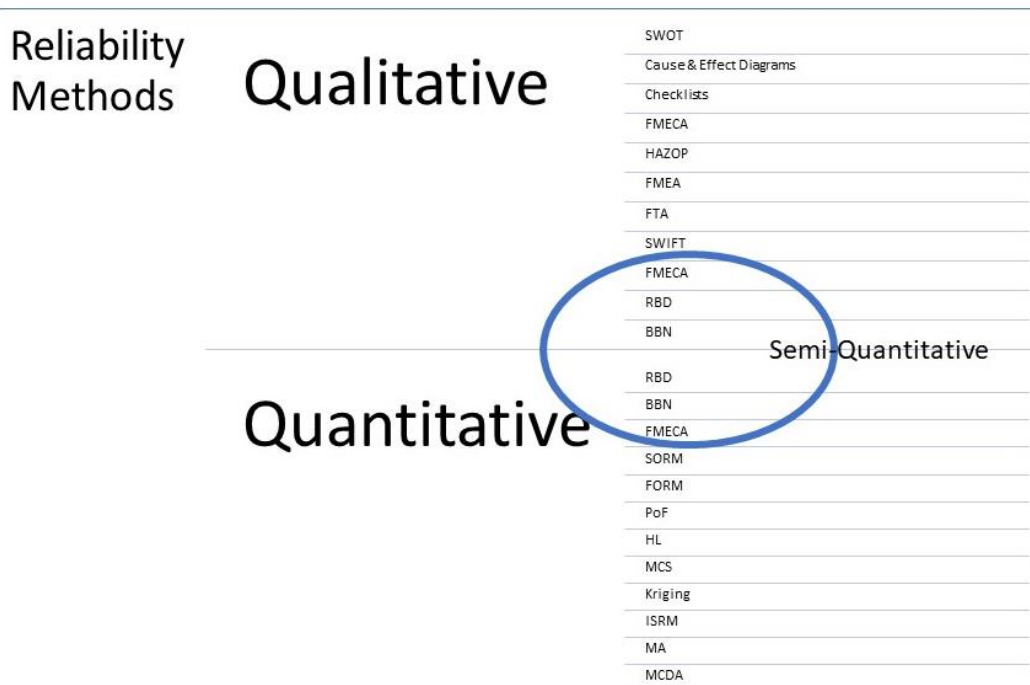


Figure 2-7 Classification of the reliability methods

2.6.1.1. Qualitative reliability approaches

Data that is missing or insufficient prevents a quantitative assessment of reliability. However, relationships within the system are possible, including hazards, failure causes, events, failure modes, faults, effects, and consequences, and an estimate of reliability, failure probability, and consequence can still be obtained using qualitative methods.

Prior to conducting any qualitative RA, the system structure and functions must be identified and classified (Rausand & Hyland 1994). A qualitative reliability assessment can be performed on this basis. The following briefly explains some of the most common methods, divided into sheet-based, table-based, and diagrammatic techniques.

- Sheet-based qualitative approach: Engineers utilise them to assess potential threats to the design's operability, serviceability, reliability, safety, and availability (Rausand & Hyland, 1994). This method can investigate the relevant parameters based on distinct question sets at each stage. An example of this type is the checklist method.
- Table-based qualitative approach: Focuses on hazards and failure modes (FM) can lead us to table-based qualitative methods. The goal is to recognise the potential hazards (HAZID) as well as their causes and effects. The typical examples in this type of study are SWIFT, HAZOP and FMEA.

- Diagrammatic qualitative approach: This method can be organised upward or downward in a diagram. The cause-and-effect diagram (often called a fishbone diagram) visually represents this form of top-down analysis. The right side of the fish represents an incident or failure at the top. Then, fish-bones representing several cause categories, including numerous components, are added to the design to facilitate a systematic evaluation of potential dangers (Rausand & Hyland, 1994). An Event Tree Analysis (ETA) or Fault Tree Analysis (FTA) are examples of this classification.

2.6.1.2. *Quantitative reliability approaches*

Quantitative methods are required in order to carry out an in-depth analysis of the reliability, which should include a rating of the risks and a prioritisation of where attention should be focused to incorporate necessary corrections or safety measures. These approaches will be categorised as analytical, stochastic and sophisticated (Rausand & Høyland 1994).

- Analytical quantitative approach: Analytical methods for assessing reliability are based on interference between load and strength. The difference between the system's resistance and the operating load is called performance or limit state function (LSF). Some parameters utilised in these formulations are unpredictable and must thus be represented as stochastic or random variables. The performance function is used to illustrate the region of failure, which is the case when negative results are obtained. The LSF must be solved in a variety of methods in order to evaluate its reliability. The first-order reliability method (FORM) and the second order reliability method (SORM) are frequently used to simplify the analytical expression when computing the reliability under the condition that the LSF must be positive. These methods use a first or second order Taylor expansion, respectively (Sundrarajan 1995). In further sections, these methods will be discussed in more detail.
- Stochastic quantitative approach: Surrogate modelling methods, such as kriging or stochastic response surface methods (SRSMs), on the other hand, only use an approximated LSF rather than the true one. Surrogate modelling methods meet all initial data points. They are thus a more accurate method for approximating the LSF, which is then solved for the PoF and reliability using FORM, SORM, or MCS. In contrast, SRSM only uses some sample points for interpolating and approximating the response surface. Aside from the benefit of reducing the computational effort for solving iterations by simplifying the simulation expressions, SRSMs can also link input and output variables (Chopra et al. 2013).

- Quantitative reliability methods can handle even more complex system conditions. For example, when there are multiple criteria within an analysis process, multi-attribute decision making (MADM), also known as multi-criteria decision analysis (MCDA), can assist in selecting the best option. In contrast, fuzzy set theory (FST) can deal with incomplete information or fuzzy data.

2.6.2. Structural reliability assessment concept in offshore applications

After understanding onshore and offshore conditions in previous sections, when it refers to wind turbines, offshore locations provide a better supply of steady and robust wind, as well as more available space, than onshore (Kaldellis & Kapsali, 2013). Support structures for offshore wind turbines are designed differently than those for onshore wind turbines. There are additional hydrodynamic loads on OWT support structures, which are absent in the onshore wind turbines. As different types of foundations were described, it was realized that significant uncertainties exist in the soil properties and environmental loads on the OWT support structures exposed to the harsh ocean environment. A Partial Safety Factor (PSF) is applied to loads and material properties in order to account for uncertainties. When the design process is simplified, it almost always results in excessively large or inadequately designed designs. An alternate approach to dealing with uncertainty is stochastic modelling, which uses appropriate distributions (e.g. normal, lognormal, Weibull, etc.) to model variables stochastically.

Calibration of codes and standards based on reliability provides an efficient method for adjusting PSFs to account for specific load regimes and deployment locations, providing adequate safety and avoiding unnecessary generalisation of generic PSFs. This method has been widely adopted over the last decade and is based on publications such as Eurocode recommended guidelines (Eurocode 3, 2005) and background documentation (Mazzolani & Piluso, 1997) that explain the basic steps of the calibration process. Structural reliability analysis is an important component of the probabilistic design approach, as is PSF calibration. Structural reliability analysis predicts the likelihood of a structure's limit state being violated. The first principles, also known as failure modes with physics behind them, are used to formulate limit states.

To mention a few typical failure modes, the main OWT support structures are vulnerable to fatigue failures such as buckling and scouring (Martinez-Luengo & Shafiee, 2019; Scheu et al., 2019).

Wind and wave loads cause considerable cyclic loads on OWT support structures. As a result, fatigue reliability is often dominant in their design (Yeter et al., 2015). The fatigue analysis methods used in fatigue reliability assessment are roughly divided into two groups:

- 1) S-N curve method (Dong et al., 2012), which is based on typical S-N data obtained through fatigue testing;
- 2) The fracture mechanics method (Anderson, 2017) uses crack growth data from an initial defect.

It is essential to create effective fatigue reliability evaluation models to improve the fatigue reliability of OWT support structures.

So far, only a few review papers on wind turbine reliability have been published. (Greco et al., 2013) conducted a database survey on wind turbine subsystem dependability. The poll offered a brief overview of each database and emphasised major findings that were judged useful.

(Wen et al., 2020) evaluated probabilistic approaches for assessing wind power reliability and discussed the factors influencing wind power system reliability. (Pfaffel et al., 2017) conducted a review of wind turbine performance and dependability. The failure rates of various wind turbine components (subsystems) were reviewed and discussed, including the rotor, drive train system, yaw system, central hydraulic system, control system, power generation system, transmission, nacelle, and cooling system, meteorological measurement, and tower system. (Guo et al., 2022) address the reliability of OWT support structures and evaluations to facilitate the development of more cost-effective OWT support structures.

The reliability index is widely used in reliability analysis to measure risks and thus assess the consequences of failure (Manuel et al., 2008). The problem's governing parameters are typically represented as random variables that can be gathered into a random vector X . The space D of random variables can be split into two sections for reliability analysis:

- D_f as failure region

$$D_f = \{x | g(x) \leq 0\} \quad (2.1)$$

- D_s as safety region

$$D_s = \{x | g(x) > 0\} \quad (2.2)$$

where g is the performance function; the limit state surface, denoted by $g(X) = 0$, is defined as the boundary between the failure and safe zones. In its most basic form, the performance function g is provided by:

$$g = R - E \quad (2.3)$$

In the performance function, R is resistance, and E is load effect, and the function is expressed in terms of stress, strain, modal frequency and displacement.

2.6.3. Reliability assessment levels

Structured reliability analysis approaches are classified into four levels based on the level of sophistication used to solve specific problems: Levels I, II, III, and IV (DNV GL, 2011).

- Level I methods

The level I approach, which always uses one characteristic value to define each uncertain variable, is the deterministic reliability method. The probability of failure is not explicitly computed in such practices, and variables' uncertainties are considered by applying a set of PSFs derived from design standards.

- Level II methods

In the Level II reliability analysis methodologies, each uncertain variable is often described by two values (i.e. mean and variance). Level II methods include the reliability index method, such as the First-Order Second-Moment (FOSM) (Wong, 1984).

- Level III methods

The joint probability distribution of unknown variables is used in Level III reliability analysis approaches. These methods use the probability of failure as a reliability index. FORM (First Order Reliability Method) (Gollwitzer & Rackwitz, 1988) and SORM (Second Order Reliability Method) (Kiureghian et al., 1987) and simulation methods, such as directional sampling and Monte Carlo Sampling (MCS) (Kukol et al., 2006), are examples of approximatively analytical techniques. DNV standards (DNV GL, 2016) have recommended using this reliability analysis as it achieves a satisfactory result.

- Level IV methods

Level IV reliability methodologies compare an engineering economics prospect uncertainty analysis in parallel. Beyond Level III, it considers target reliability, maintenance, and costs in the failure's effects to maximise a structure's lifetime cost-benefits.

Table 2-1 compares four reliability analysis methodologies based on whether to employ PSFs, some characteristic values for each stochastic variable, joint probability, and extra elements (goal reliability, costs, advantages of building, etc.)

Level III methods are the most extensively utilised reliability analysis methodologies for OWT support structures (Lee et al., 2014a; Peeringa & Bedon, 2017). However, it is predicted that level IV methods will be used a lot in future as they can include the cost aspects in parallel with target reliability and maintenance.

Table 2-1 Comparison of reliability assessment methods (Wang & Kolios, 2017b)

SRA level	PSFs used	No. of characteristic values used for each stochastic variable	Joint probability distributions used	Examples
I	Yes	One	No	PSF
II	No	Two	No	FOSM
III	No	Two or more	Yes	FORM, SORM, MCS
IV	No	Two or more	Yes	Combination of FORM with the optimiser to achieve target reliability

2.6.4. Structural reliability analysis using deterministic values

The finite element solution effectively solves the engineering problem's mathematical model. However, a practical issue solution involves a physical (behavioural) model, a failure model, parameter selection, and safety coefficient selection.

The requirement for safety coefficients is also widely accepted due to engineering's multiple sources of uncertainty. For example, natural randomness of problem characteristics like material resistance and environmental loads, modelling uncertainty (difference between failure models and failure tests), statistical uncertainty, decision uncertainty, and a human mistake can be the source of uncertainties (Maymon, 1993).

Structural reliability theory quantifies and analyses various uncertainties. Based on these uncertainties, structural reliability analysis calculates the failure probability. Figure 2-8 SRA approaches can help determine a project's characteristic values and safety coefficients. This is especially significant and vital in the construction of novel structures.

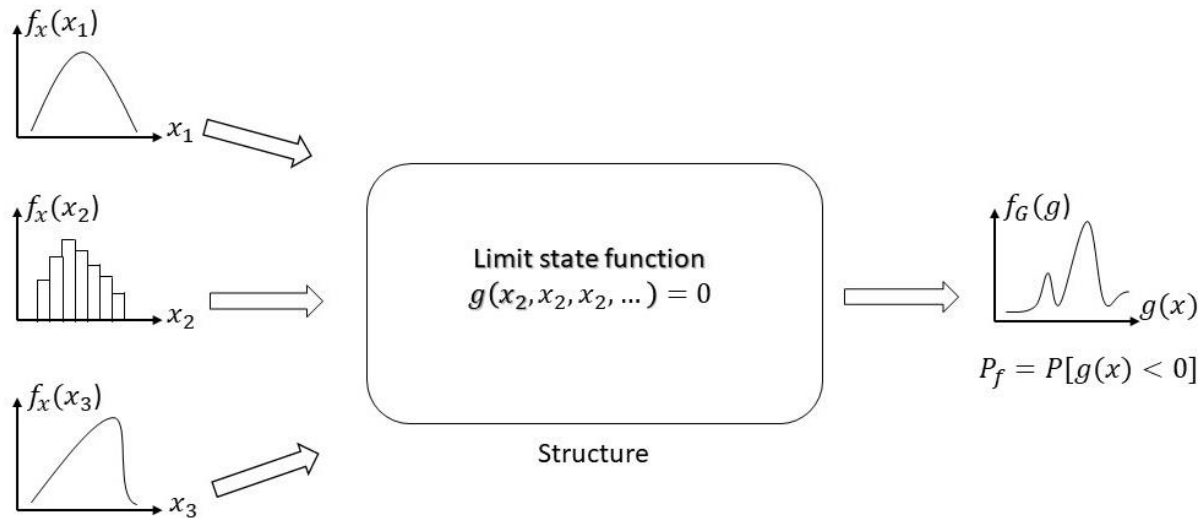


Figure 2-8 Reliability analysis of a structure with random parameters

P_f can be solved directly by sampling the problem's random variables according to the density $f_x(x)$ and evaluating the limit state function at each sampled position using a crude Monte Carlo simulation or First or Second Order Reliability Methods (FORM and SORM).

2.6.5. Reliability-based calibration of standards in offshore wind

Empirical and experimental expertise in probabilistic principles has been developed through historical evolution. The systematic recording of this knowledge is advantageous for developing a technique that enables the design of novel structures to reach a desired level of reliability and for formulating applicable design codes and standards.

This section starts with a study of offshore structure design standards. Following the presentation of the design safety level and reliability-based calibration of PSFs, the limitations of existing design standards are discussed.

2.6.5.1. Offshore structures standards

DNV-GL offshore: DNVGL-ST-0126 is provided for designing OWT support structures and covers the design, manufacture, installation, and inspection. It is consistent with IEC61400-3 (IEC, 2019). DNV also published the standards for the design of floating wind turbines, DNVGL-ST-0119, the design of offshore substations, DNVGL-ST-0145.

IEC standard: IEC 61400-3 (IEC, 2019), which intends to provide an acceptable level of safety for OWTs against all hazards for the duration of their designed life. Generally, it is used in conjunction with the relevant ISO and IEC standards, particularly IEC 61400-1. For fixed and floating installations, IEC 61400-3-1 and IEC 61400-3-2 are referred to accordingly.

BS EN 1993-1-1:2005 + A1:2014 Eurocodes 3: The European Commission developed the Eurocodes as a set of standards (Eurocode 3, 2005). These standards permit using probabilistic techniques in design, allowing additional design optimisation. In addition, the steel structure design standard BS EN 1993-1-1:2005 + A1:2014 is suited to the design of offshore structures.

API RP-2A: In 1969, the API (American Petroleum Industry) established a recommended practice for planning, designing, and constructing fixed offshore platforms. In 1989, a revised version was produced in a Load Resistance Factor Design (LRFD) format and made publicly available in 1993. This standard is currently in its 22nd edition, published in November 2014.

ABS guides: The ABS onshore guide includes design, fabrication, installation, and inspection standards for fixed-bottom OWT installations, whereas the ABS offshore guide provides the criteria for floating OWT installations. ABS (American Bureau of Shipping) has created both guides sources of classification and design guides for the offshore industry.

2.6.5.2. Safety levels in design

Different standards (such as ISO, IEC, and DNV GL) use a safety class system to ensure structural safety. The structures are assigned a safety class based on the consequences of failure. A nominal annual probability of failure is typically used to set the target safety level for each safety class.

According to DNV GL (DNV GL, 2016), there are two safety classes for OWTs: 1) normal safety class, which concerns when a failure poses a risk of personal injury and/or environmental, economic, or social consequences, and 2) special safety class, which applies when the safety requirements are agreed upon by the customer and the designer and/or are determined by local guidelines.

Table 2-2 Safety level and failure classifications

Failure classification	Failure consequence	
	Minor	Major
I – Redundant structure	$P_f = 10^{-3} (\beta = 3.09)$	$P_f = 10^{-4} (\beta = 3.71)$

II – Significant warning before failure occurrence in a non-redundant structure	$P_f = 10^{-4}(\beta = 3.71)$	$P_f = 10^{-5}(\beta = 4.26)$
III – No warning before failure occurrence in a non- redundant structure	$P_f = 10^{-5}(\beta = 4.26)$	$P_f = 10^{-6}(\beta = 4.75)$

Table 2-2 overviews permissible annual failure probabilities based on DNV Classification Note 30.6 (DNV GL, 1992). For the design of OWT support structures, DNVGL-ST-0126 (DNV GL, 2016) recommends that a nominal annual probability of failure of 10^{-4} should be used as the target safety level. This goal safety level reflects that OWT support structures are unmanned and designed to meet regular safety standards.

2.6.5.3. Calibration of PSFs using reliability assessment

Several methods can achieve reliability-based calibration. The adjustment of design values is one of those methods. In this approach, all fundamental variables must be assigned by design values. The structure is supposed to be safe if the limit states are not reached when the design values are introduced into the analysis model. According to the performance function, this matter can be stated as:

$$R_d \geq E_d \quad (2.4)$$

that means the design load effects, E_d should not exceed the corresponding resistance, R_d . Load effect and resistance can be defined as (Eurocode 3, 2005):

$$R_d = R\{X_{d1}, X_{d2}, \dots, b_{d1}, b_{d2}, \dots, \theta_{d1}, \theta_{d2}, \dots\} \quad (2.5)$$

$$E_d = E\{F_{d1}, F_{d2}, \dots, b_{d1}, b_{d2}, \dots, \theta_{d1}, \theta_{d2}, \dots\} \quad (2.6)$$

where F_{di} is design value for load i and X_{dj} is design value for material strength j . Geometrical properties and model uncertainties are denoted by b and θ in expressions. The design values of resistance R_d and load effects E_d should be defined such that the following equations are fulfilled:

$$P(R < R_d) = \Phi(-\beta_t \alpha_R) \quad (2.7)$$

$$P(E > E_d) = \Phi(+\beta_t \alpha_E) \quad (2.8)$$

where t is the target reliability index and α_R and α_E are the FORM sensitivity factors. Equations (2.7) and (2.8) could be used to calculate the design values (such as X_{d1} and F_{d1}). Finally, the relevant PSF is obtained by dividing a variable's design value by its characteristic or representative value.

An alternative method of reliability-based calibration of PSFs defined in (Wang & Kolios, 2017c) commences with some unconstrained partial factor format. It requires that the partial factors be chosen so that the structure's reliability is as close to some qualified value as possible.

According to (ISO, 1998), partial factor format can be expressed as:

$$g\left(\frac{f_{k1}}{\gamma_{m1}}, \frac{f_{k2}}{\gamma_{m2}}, \dots, \gamma_{f1} F_{k1}, \gamma_{f2} F_{k2}, \dots\right) \geq 0 \quad (2.9)$$

where f_{ki} and γ_{mi} are the characteristic strength and partial factor of material i , respectively and F_{kj} and γ_{fj} are the representative value and partial factor for load j , respectively. The next stage is to establish a representative set of j test elements that address 1) different types of actions, 2) different types of structural dimensions, 3) various types of materials, and 4) various kinds of limit states.

The set of representative structural elements can be designed for a given set of partial factors ($\gamma_{m1}, \gamma_{m2}, \dots, \gamma_{f1}, \gamma_{f2}, \dots$). Each element will thus have a level of reliability that differs more or less from the target level. The average deviation D_A can be stated using the reliability index as:

$$D_A = \sum_{k=1}^n [\beta_k(\gamma_{mi}, \gamma_{fj}) - \beta_t]^2 \quad (2.10)$$

where β_k is the reliability index for element k in the result of a design using a set of partial factors ($\gamma_{m1}, \gamma_{m2}, \dots, \gamma_{f1}, \gamma_{f2}, \dots$). The optimal choice of partial factors is achieved by minimising the aggregated deviation D_A provided in Eq. (2.10). Weighted factors may be utilized if not all elements are considered equally important.

Several research papers have been published on the reliability-based calibration of PSFs for OWT support structures. (Tarp-Johansen & Sørensen, 2006) calibrated the fatigue safety factors for OWT support structures based on their reliability. If wave loads dominate the fatigue loads on the support structure instead of wind loads, then slightly larger fatigue safety factors are required. (Velarde et al., 2020) provided a system for reliability-based calibration of fatigue safety factors for OWT concrete support structures and applied it to a standard gravity-based foundation. The results suggested that the reliability-based calibration of PSFs has the potential to reduce offshore wind energy costs. (Morató et al., 2017) conducted a reliability analysis and then calibrated PSFs based on the results. The calibrated PSFs were applied to a standard turbine and its supporting structures. Reliability based on calibrated PSFs reduced failure probabilities for most difficult design situations to relatively low levels.

Even though the suitable reliability of OWT support structures can typically be obtained using design standards, the applicability of these standards to unique and innovative structures presents challenges. This results from the fact that design guidelines primarily apply to specific structures and are typically described at a high level, providing limited background information on the methodologies employed (Kolios & Brennan, 2009). In this respect, the reliability-based design method can produce enough results for designing innovative and specialised OWT support structures. Furthermore, the estimation of PSFs independently is possible by reliability-based adjustment methods (Morató et al., 2017) that can eliminate the unintended conservatism.

Stochastic wind and wave variation development needs statistical models, specifically statistical distributions and proper methods. Weibull, Rayleigh, Lognormal and Poisson are commonly used for wind modelling, while Lognormal, Weibull, and Gumbel are used for waves. The findings from the research are that the best distribution choice depends on the site, so it is important to conduct fit testing and handbook recommendations.

2.7. Extra-large support structures in deeper sea

Since the first commercial wind turbine's introduction in the 1980s, wind turbine capacity ratings and dimensions have increased rapidly. The primary motivation for this development is to have a view on future of big turbines in deep seas. In contrast to onshore turbines, which may be limited in size owing to operational and capacity restrictions, the design of offshore

wind turbines will expand as long as it is technically feasible and economically viable (Wiser & Bolinger, 2010). As a result, wind turbines' rated power, size, and efficiency increase while their Levelized Cost of Energy decreases. Only in 2019, Europe connected 3,623 MW of net offshore wind generating capacity, breaking the previous year's record (Walsh, 2019). In recent years, offshore wind turbines (OWTs) are becoming increasingly robust and reliable. Since 2014, the average annual increase in turbine capacity has been 16 per cent. As illustrated in Figure 2-9, turbines installed in 2019 had an average rated capacity of 7.8 MW, which is 1 MW higher than the previous year.

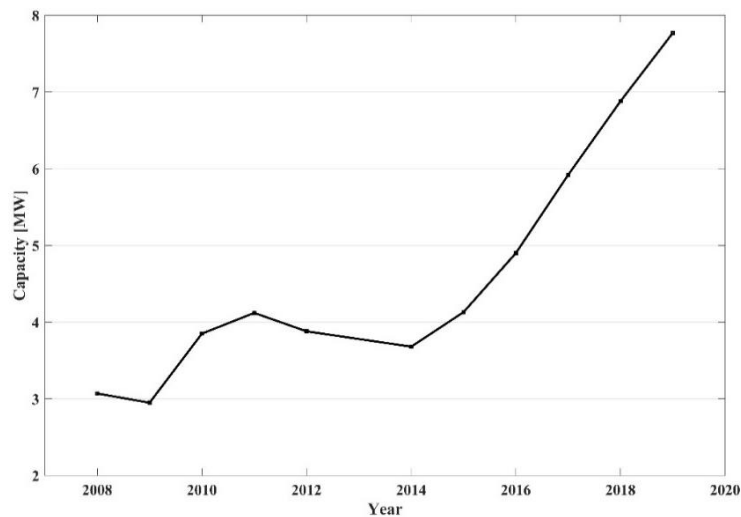


Figure 2-9 The yearly average of installed OWT rated capacity in MW (Walsh, 2019)

2.7.1. Scaling up

As discussed in previous sections, onshore wind turbines generally employ concrete foundations, but OWT foundation types vary significantly depending on sea depth. Far off the shore, where ocean depths exceed 30 metres, favourable wind conditions can often be encountered. In 2021, Siemens Gamesa launched the largest OWT, with a rated power of 14MW and a rotor diameter of 222m (Gamesa et al., 2020). General Electric (GE) is supposed to install a 12MW Haliade-X platform in parallel, and they have some prototypes in 14MW OWTs under development. The industry is thirsty for larger platforms and wind turbines, and their designs are continuously optimised to make them feasible in the market. There are always new technologies to allow for larger sizes, but there is no control over the market demand and state regulations. For instance, Siemens Gamesa optimises the rotor blade diameter of the "Quantum Leap" turbine by 10% to produce more rated power from the same platform technology (Gamesa et al., 2020). Despite some belief that larger wind turbines are not always

better, the market proves that extra-large turbines have been demanded in the industry every year (Aldersey-Williams et al., 2020).

Multiple studies have already investigated wind turbines and substructure scaling. Linear scaling equations for wind turbines established as part of the Upwind project (Sieros et al., 2012) are frequently employed as a starting point, such as in the work of (Leimeister et al., 2016; Leimeister & Kolios, 2021), among others, which upscaled the 5 MW OC4 semi-submersible to 7.5 MW by scaling the floater dimensions with the square root of the power rating ratio between turbines. They discovered that the scaled-up systems had greater pitch stability and longer natural periods than the original design. (George et al., 2014) adopted a similar strategy, enlarging the 5 MW OC4 to 7.5 MW and 10 MW by increasing the mass-to-cubic-root-of-mass ratio between turbines while maintaining a consistent platform height to support assembly in European drydocks. (Kikuchi & Ishihara, 2019) scaled up a 2 MW wind turbine used in the Fukushima FORWARD project to 5 MW and 10 MW by scaling the support structure with the cube root of the mass ratio between turbines and then scaling the column distance to maintain the static balance between overturning moment and pitch restoring moment.

2.7.2. The importance of water depth

In the last decade, the applicability for monopiles was just in water depths around 40m or less (Al-Sanad et al., 2021). Currently, it is becoming more frequent to hear about extra-large monopiles (diameters up to 9 m and piece weights up to 1,500 tonnes) as viable alternatives to jacket substructures. On the other hand, larger turbines and deeper water will put a monopile's technological feasibility to the test, especially as wave loads significantly interfere with the turbine structure's dynamics. In addition, their diameter influences the hydrodynamic performance of bottom-fixed monopile OWTs. Using fewer conservative solutions for the OWT support structure will decrease the capital cost by 6–8% (Gilbert et al., 2015; Ivanhoe et al., 2020; Rezvanipour et al., 2020; Wang & Kolios, 2017c).

The design of offshore wind turbine support structures has received much research attention. Muskulus and Schafhirt (Muskulus & Schafhirt, 2014) have reviewed the design problem's different aspects and challenges and the various methods demonstrated within the literature. They emphasize the importance of integrating fatigue and the high computational costs due to the numerous simulations required to deal with wind and wave conditions. (Morató et al., 2017) investigated the Design Load Cases (DLCs) mainly responsible for driving design loads to

lower overall analysis loads in iterative design processes. The primary factors for designing OWTs are water depth, the aerodynamic and hydrodynamic loadings, and loads due to controller and soil conditions. (Velarde & Bachynski, 2017) studied the utilization of DTU 10MW monopiles in deeper waters using numerical methods. They noticed that the sea-states act an increasing role in fatigue damage with increasing sea depths. The hydrodynamic load is relatively small for shallow water sites (assuming the structure does not meet wave-breaking load); hence the design is mainly governed by the aerodynamic load. The hydrodynamic load's effect proliferates by increasing water depth. Wind-generated waves in the open ocean typically have a frequency range of 0.05–0.25 Hz e.g., (DNV GL, 2016).

Along with the ocean currents, these waves are the primary contributors to the hydrodynamic loads. Generally, a single low-frequency wave governs the extreme load case, whereas high-frequency waves affect the structure's fatigue design. (Ishtiyak et al., 2021) proposed a new concept of the support structure named 'bottom supported tension leg tower' (BSTLT) for utilizing in water depth of 50m. In this design, an OWT's tower is positioned over a transition piece hinged to a monopile and supported by tethers. There are some developments around this concept, but the main issue is the maintenance and applicability of the hinge itself in such a massive structure in salty water still exists.

The bottom-fixed support structures are on-demand in the market (despite being expensive in manufacturing and installation). They also have to meet the natural frequency conditions and resist the forces on their body for water depths more than 30m. Then again, the floating OWT concepts with the spar-type Hywind and semisubmersible-type WindFloat are other options. However, the hull structure and ballast become bulky and pricy, although they are suitable for water depths above 60m. This matter made us investigate water depth sensitivity between 30m-60m of the latest IEA 15MW reference turbine (Gaertner et al., 2020) to cover the demand in the current offshore wind industry.

2.8. Cost analysis terminology

Another factor influencing the effectiveness of structural optimisation for wind turbine constructions is the fact that its levelized cost of energy must be considered. This is generally true that many unknown (for example, market commodity fluctuations) costs and competition from other businesses are existed in these types of studies. The cost study aims to clarify the

benefits of the new offshore wind turbine design and identify potential design differences between the reference structure and the optimised one. The outcomes will provide design recommendations for future large offshore wind turbine generation.

For a detailed study and understanding of the costs of the OWT support structure design, all variables affecting it must be simplified. A simplification of all the variables influencing the design of the OWT support structure is required for straightforward analysis and understanding of its costs. Water depth, manufacturing, transportation, weather downtime and steel price are the key criteria in this study which affect the design and, as a result, the cost of an OWT support structure. Water depth is vital as a deeper sea means larger and heavier substructures and foundations (Arshad & O'Kelly, 2013). Therefore, more costly manufacturing and installation costs. Distance to land may affect installation costs since the transport time will increase, but it is not a critical factor because it will only account for a small portion of the total cost.

2.8.1. Cost breakdown and definitions

The first step in this study is to break down the cost of the structure. In order to understand the breakdown of the system, it is necessary to know the offshore wind farm operation and financing terminology.

Capital expenditure or CapEx is the amount of money spent on procuring, buying wind turbines, cables, and other key wind farm components, and sometimes also including the cost of constructing a project, for example, paying for installation vessels & additional installation costs.

Operational expenditure or OpEx is the amount of money spent operating the project. As well as the obvious direct costs of running the site, some definitions include seabed leasing, transmission, and port facility costs.

Capacity factor or CF is a key performance metric for any site. It is a factor which indicates how much of the total wind farm capacity we expect the wind farm to generate. For example, a 500MW wind farm with a capacity factor of 40% (0.4) will have an annual energy yield of $(500 \times 0.4 \times 8760) = 1,752,000$ MWh. This is before any electrical, wake, or other performance losses are applied.

Discount factor or DCF is a company-specific factor used to weigh the value of future net revenue from investments. The higher the discount factor, the lower the value we allocate to future reserves in today's judgments.

Availability in the offshore wind can be defined in two ways. Time-based availability is the time that the wind farm is available to generate electricity, and it can be expressed as a factor, $1.0 = 100\%$ for a perfectly functioning wind farm. Yield-based availability is the same metric but for energy rather than time. If a wind farm captures all the potential energy in each period, its yield-based availability is 100% (or 1.0).

2.9. Summary

The chapter has presented various topics regarding modelling and optimising methods for offshore wind turbine support structures. Additionally, a list of optimisation algorithms and structural reliability assessments was stated. These topics are discussed to provide a viewpoint on which approaches and models to choose for a given task and gaps in the topic.

Some of the gaps in previous research are as follows. First, offshore wind turbine modelling and designing procedures involved many uncertainties, and most optimisation studies were based on the deterministic process. Including reliability constraints with stochastic variables can fill this issue. However, some reflections on reliability-based optimisation utilized 1D models of monopile and simplified them. Developing a 3D geometry to simulate the actual condition can cover this problem. The lack of investigations regarding the soil interaction and feasibility of structures in the water depth between 30m to 60m is also noticeable for extra-large monopiles. Much less work has been done concerning modifying PSFs of fixed-bottom OWT support structures using numerical methods. However, reliability-constrained optimisation (RCO) design is one of the complementary approaches and frameworks that integrate uncertainty and randomness in the design process without the complexity of RBDO and the hybrid method (Psarropoulos & Tsompanakis, 2008) in order to optimise the geometry and check the PSF in parallel contemplating target value of reliability.

This study focuses on a framework that uses a parametric model of finite element analysis of OWT support structures and integrates this with the Genetic Algorithm (GA) to optimise and reduce the support structure's overall mass while satisfying multiple criteria imposed by the design standards. This framework strategy in combining FEA, GA and reliability assessment of the candidate design models allows us to achieve OWT's optimum reliable support structure considering the target reliability constraints. The study is completed with the cost analysis and comparison of LCOE of initial and optimised models.

Follow up with the 3D model of the most recent reference wind turbine (IEA 15MW) in the water depth sensitivity section. The simulations in water depths of 30m, 40m, 45m, 50m and 60m are performed, and numerical results in different water depths are studied and discussed in maximum equivalent stress, fatigue damage, 1st natural frequency and global buckling capacities. The study concludes with the feasibility of structure and water depth sensitivity. A brief discussion about the manufacturing limitations and installation challenges of extra-large monopiles is presented at the end of that section.

In this chapter, offshore wind foundations, support structure design principles, optimisation strategies, reliability assessment methods and extra-large structures have been presented and discussed. Even though these subjects are broad in their terms, this chapter intends to provide a concise description of relevant findings. The following is a summary of each section's primary inferences:

- Selecting the best support structure is mainly determined by the local conditions and project budget, and there is no particular foundation ideal type for all locations. Yet, in contrast to the other options, the monopile is the cheapest, more reliable, and most adaptable. Statistics demonstrated that more than 80% of current substructures are monopile worldwide.
- The structural design of OWT support structures is complicated due to harsh environmental conditions. Therefore, the relevant standards recommend several design principles by considering different limit states and design load cases. In addition, selecting appropriate DLCs, applied load types, and soil interaction methods can maximise the accuracy of the design approach.
- Optimisation under various conditions is discussed. Genetic algorithms are extensively used for the design optimisation of OWTs. Probabilistic optimisation based on reliability is one of the best methodologies in case studies for considerable uncertainties in material properties and environmental loads.
- As well as optimisation, focusing on scale-up and water depth sensitivity is essential in the current situation of the offshore wind industry as the demand for renewable energy is rising every day. In parallel with the market demands, the manufacturing technology, installation and transportation facilities are changed with more capacities, leading us to reduce the LCOE of offshore wind turbines.

3. Numerical Methods of Structural Reliability Analysis

3.1. Introduction

This chapter will explain the numerical methodologies for structural and reliability evaluations. Calculating the probability of failure equation is complex by the integral solution of the joint probability distribution function. Consequently, limit state function approximations can be utilised to overcome this challenge. Methods for Level III reliability analysis will be discussed analytically in the following parts, which will be implemented later in this thesis. There will be a discussion of both deterministic and probabilistic formulations. Then, the Stochastic Response Surface Method (SRSM) and multivariate regression approaches will be presented. Then again, the finite element model will be developed, including applying the corresponding loads in the proposed optimisation framework. Finally, the validation of the FEA model will be performed.

3.2. Numerical methods

3.2.1. Deterministic Methods

The approaches and algorithms addressed in this section concern the deterministic processing of limit state functions using a geometrical approximation of the stochastic variables. The moments of random variables define them. The First-order Second Moment Reliability Method

(FOSM) will be introduced as the basis for the First Order Reliability Method (FORM). The reference (Wong, 1984) provides an analytical description of these methods.

The multiple variables contributing to the probability of failure estimation have generated several methods to simplify this procedure. First and second-order employment of Taylor series expansion is a typical method for linearizing the limit state equations using the First and Second Order Moment techniques, respectively. However, FOSM, also known as the mean value, first-order second-moment method (MVFOSM), is a simple method that cannot yield accurate findings for very low failure probability or nonlinear limit state functions (Lee et al., 2014b).

To overcome the above challenge, The safety index approach, a geometrical solution, converts the problem to a mathematical optimisation problem of finding the point of the limit state surface with the shortest distance to the origin of the standard normal space. The Hasofer and Lind (HL) algorithm is proposed in (Hasofer et al., 1974), which converts the vector of design stochastic variables X into a vector of standardised independent variables U . The design point in U -space shows the place with the highest probability density and is referred to as the Most Probable Failure Point (MPP). The converted limit state surface $g(U)=0$ can be reached with first or second order estimations, and thus First and Second Order Reliability Methods (FORM/SORM) are appropriately considered. The interpretation of the preceding approach is that in FORM, the limit state surface is approximated by a tangent plane at the MPP. In contrast, in SORM, the MPP is reached by a curve, as shown in Figure 3-1.

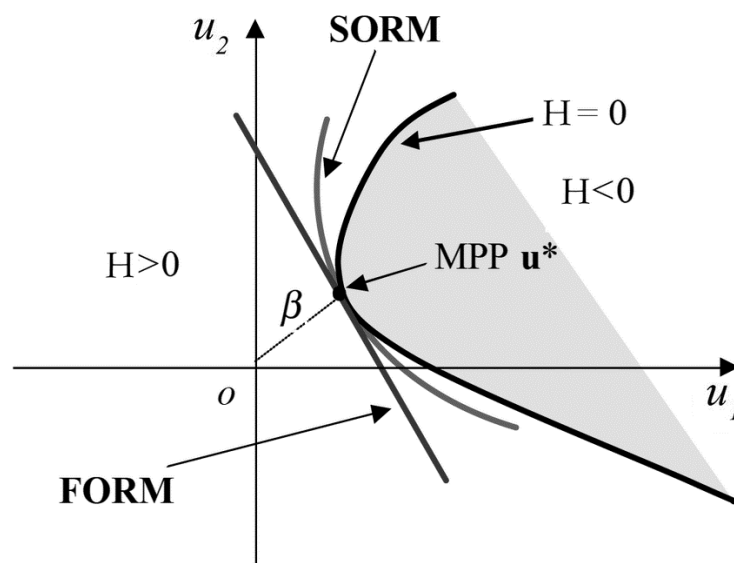


Figure 3-1 First and second order estimations (Kolios, 2010)

3.2.1.1. Mean Value FOSM (MVFOSM)

As mentioned, MVFOSM simplifies the calculation of a limit state function's failure probability. The Mean Value First-Order Second-Moment (MVFOSM) method is a commonly used approach in structural reliability analysis that combines both the first-order and second-order statistical moments of the random variables to estimate the reliability of a structure. The term "first-order" refers to using first order expansions to linearise the initial function, with inputs and outputs represented as mean and standard deviation. This basic approximation excludes higher moments, increasing the following model uncertainty. MVFOSM is an approximation technique that provides an efficient and accurate estimate of the failure probability by considering both the mean value and variance of the random variables. The basic formulation of the MVFOSM method can be described as five steps:

1. Limit State Function (LSF):

The limit state function (LSF) is a mathematical expression that defines the failure condition of the structure in terms of the random variables. It is denoted as $g(\mathbf{U})$, where \mathbf{X} represents the vector of random variables, and $g(\mathbf{U}) = 0$ defines the failure region.

2. Taylor Series Expansion:

The LSF is approximated using a Taylor series expansion up to the second-order terms around the mean values of the random variables. This method approximates the limit-state function by the first-order Taylor series expansion at the mean value point. Assuming \mathbf{X} as a vector of statistically independent variables, the approximate limit-state function at the mean is as follows:

$$\tilde{g}(\mathbf{X}) \approx g(\boldsymbol{\mu}_X) + \nabla g(\boldsymbol{\mu}_X)^T \cdot (\mathbf{X}_i - \mu_{xi}) \quad (3.1)$$

Where $\boldsymbol{\mu}_X = \{\mu_{x_1}, \mu_{x_2}, \dots, \mu_{x_n}\}^T$ is the mean values vector and gradient and g evaluated at $\boldsymbol{\mu}_X$ as:

$$\nabla g(\boldsymbol{\mu}_X) = \left\{ \frac{\partial g(\boldsymbol{\mu}_X)}{\partial x_1}, \frac{\partial g(\boldsymbol{\mu}_X)}{\partial x_2}, \dots, \frac{\partial g(\boldsymbol{\mu}_X)}{\partial x_n} \right\}^T \quad (3.2)$$

Also, the expected mean value of approximated limit state function $\tilde{g}(\mathbf{X})$ is:

$$\mu_{\tilde{g}} \approx E[g(\mu_X)] = g(\mu_X) \quad (3.3)$$

The standard deviation of the approximate limit state function is calculated using fundamental statistics transformations:

$$\sigma_{\tilde{g}} = \sqrt{Var[\tilde{g}(X)]} = \sqrt{[\nabla g(\mu_X)^T]^2 \cdot Var(X)} = \left[\sum_{i=1}^n \left(\frac{\partial g(\mu_X)}{\partial x_i} \right)^2 \cdot \sigma_{x_i}^2 \right]^{\frac{1}{2}} \quad (3.4)$$

3. Reliability Index:

The reliability index (β) is defined as the distance between the origin and the design point, which is the point on the LSF where $g(X) = 0$. The reliability index is given by:

$$\beta = \frac{\mu_{\tilde{g}}}{\sigma_{\tilde{g}}} \approx \frac{g(\mu_X)}{\left[\sum_{i=1}^n \left(\frac{\partial g(\mu_X)}{\partial x_i} \right)^2 \cdot \sigma_{x_i}^2 \right]^{\frac{1}{2}}} \quad (3.5)$$

The above reliability expression can be applied to cases of linear limit state functions. The index can be calculated analytically by expressing the safety margin between a system's resistance R and loading S .

$$g(X) = R(X) - S(X) \quad (3.6)$$

Then mean value and standard deviation resulting from Equation 3.6 are:

$$\mu_g = \mu_R - \mu_S \quad (3.7)$$

$$\sigma_g = \sqrt{\sigma_R^2 + \sigma_S^2 - 2 \cdot \rho_{RS} \cdot \sigma_R \cdot \sigma_S} \quad (3.8)$$

The correlation coefficient between R and S is indicated by ρ_{RS} and also μ_R , μ_S , σ_R and σ_S the mean values and standard deviations of variables R and S . Then, the reliability index can be calculated by:

$$\beta = \frac{\mu_g}{\sigma_g} = \frac{\mu_R - \mu_S}{\sqrt{\sigma_R^2 + \sigma_S^2 - 2 \cdot \rho_{RS} \cdot \sigma_R \cdot \sigma_S}} \quad (3.9)$$

In case of $\rho_{RS} = 0$ (uncorrelated variables), β can be calculated as:

$$\beta = \frac{\mu_g}{\sigma_g} = \frac{\mu_R - \mu_S}{\sqrt{\sigma_R^2 + \sigma_S^2}} \quad (3.10)$$

The approximate limit-state surface of a nonlinear limit-state function can be determined by linearizing the original limit-state function at the mean value point. A hyperplane defined as a linear-failure function represents the failure surface in the generalised scenario with multiple independent variables.

4. Failure Probability (Pf)

The failure probability (Pf) is estimated using the MVFOSM method by considering the mean value (first-order) and variance (second-order) of the random variables. The failure probability is $P_f \approx \Phi(-\beta)$.

5. Sensitivity Factors:

The sensitivity factors, also known as importance factors, are derived from the gradient vector and Hessian matrix of the LSF, and provide information about the contribution of each random variable to the failure probability. The sensitivity factors can be used to identify the most influential random variables in the structural reliability analysis and guide further analysis or design improvements.

The MVFOSM technique is a simple approach for calculating the reliability index that uses the minimum possible representation of basic variables and provides a good balance between accuracy and computational efficiency in structural reliability analysis. However, this fact restricts the method's range of applicability because linearization of the limit-state function about the mean values can lead to inaccurate results. Therefore, the process cannot deal with nonlinearity or significant variations efficiently.

3.2.1.2. Hasofer and Lind method

The Hasofer-Lind (HL) method, also known as the First-Order Reliability Method (FORM), is widely used for estimating structures' reliability in structural reliability analysis. A first-order approximation method utilizes the random variables' first-order statistical moments to evaluate a structure's failure probability. The HL method provides an efficient and accurate estimate of the failure probability by iteratively updating the design point along the most probable failure direction. As defined, the geometrical distance measured from the origin of a u-dimensional space to the Most Probable Failure Point (MPP) on the failure surface can be interpreted as the

reliability index. The Hasofer and Lind reliability index method improves the MVFOSM approach by transforming the expanding point from the mean value point to the MPP. Hasofer and Lind (Hasofer and Lind, 1974) presented a linear transformation of the essential variables x_i into a set of normalised and independent variables u_i to expand this method to issues with multiple variables.

For the basic case with two independent, normally distributed variables of strength R and stress, S , Hasofer and Lind transformed the initial variables to standard normalized variables:

$$\hat{R} = \frac{R - \mu_R}{\sigma_R} \quad \text{and} \quad \hat{S} = \frac{S - \mu_S}{\sigma_S} \quad (3.11)$$

Where μ_R , μ_S , σ_R and σ_S the mean values and standard deviations of R and S , respectively. Now, the limit state surface must be transformed from $g(R, S) = R - S = 0$ in the original coordinate system into the standard normalised system (\hat{R}, \hat{S}) as follow:

$$g(R(\hat{R}), S(\hat{S})) = \hat{g}(\hat{R}, \hat{S}) = \hat{R} \cdot \sigma_R + (\mu_R - \mu_S) = 0 \quad (3.12)$$

The distance from $\hat{g}(\hat{R}, \hat{S})$ coordinate system to the failure surface, $\hat{g}(\hat{R}, \hat{S}) = 0$ is the safety index:

$$\beta = \widehat{OP}^* = \frac{\mu_R - \mu_S}{\sqrt{\sigma_R^2 + \sigma_S^2}} \quad (3.13)$$

The most possible failure point (MPP) is the point $P^*(\hat{R}^*, \hat{S}^*)$ on $\hat{g}(\hat{R}, \hat{S}) = 0$ and matches to the shortest space. A nonlinear function characterises the failure surface in the general situation of n normally distributed and independent variables.

$$g(X) = g(\{x_1, x_2, \dots, x_n\}^T) = 0 \quad (3.14)$$

The variables must then be transformed into their standard forms.

$$u_i = \frac{x_i - \mu_{x_i}}{\sigma_{x_i}} \quad (3.15)$$

The mean and standard deviation of x_i are μ_{x_i} and σ_{x_i} , respectively and the mean and standard deviation of u_i are zero and unity.

The failure surface $g(X) = 0$ in X-space is represented in the resultant failure surface $g(U) = 0$ in U-space. The geometrical distance from the origin in U-space to any point on $g(U) = 0$ corresponds to the number of standard deviations from the mean value point in X-space to the equivalent point on $g(X) = 0$. This is due to the rotational symmetry of the second-moment representation of U . The safety index is defined as the shortest distance between the origin and the failure surface $g(U) = 0$, as follows:

$$\beta = \min_{U \in g(U)=0} (U^T \cdot U)^{1/2} \quad (3.16)$$

In this case, β is called the ‘‘HL Safety index’’. The design point, $U^*(u_1^*, u_2^*, \dots, u_n^*)$ on $g(U) = 0$ surface in U-space can provide the corresponding vector point in the X-space. Based on the theory, the reliability index β can be calculated as a solution to the optimisation problem in the standard normal U-space.

$$\text{minimizing} \rightarrow \beta(U) = (U^T \cdot U)^{1/2} \text{ with } g(U) = 0 \quad (3.17)$$

In (Freudenthal et al., 1966), To tackle this optimisation problem, numerous constrained optimisation methods were applied, including simple methods (possible directions, gradient, projection, and reduced gradient), penalty methods, dual methods, and Lagrange multiplier methods (Lee et al., 2014b). The applicability of each method is determined by the nature of the problem being researched. HL and HL-RF methods are the most commonly used algorithms in this case.

Hasofer and Lind developed the HL algorithm to study normally distributed random variables. Rackwitz and Fiessler introduced the extended HL-RF approach by expanding the HL method to deal with non-Gaussian statistical distributions. Assuming that the (linear or nonlinear) limit state surface X has n regularly distributed and independent random variables:

$$g(X) = g(\{x_1, x_2, \dots, x_n\}^T) = 0 \quad (3.18)$$

And after transformation of the limit state function:

$$g(U) = g(\{x_1 u_1 + \mu_{x1}, \sigma_{x2} u_2 + \mu_{x2}, \dots, \sigma_{xn} u_n + \mu_{xn}\}^T) = 0 \quad (3.19)$$

The intersection point P^* is generated by the normal vector from the origin \hat{O} to the limit-state surface $g(U)$. The safety index β is the distance between the origin and the MPP. The first-order Taylor series expansion of $g(U)$ at MPP P^* is as follows:

$$\tilde{g}(X) = g(U^*) + \sum_{i=1}^n \frac{\partial g(U^*)}{\partial U_i} \cdot (u_i - u_i^*) \quad (3.20)$$

And from transformation:

$$\frac{\partial \hat{g}(U)}{\partial U_i} = \frac{\partial g(X)}{\partial x_i} \cdot \sigma_{xi} \quad (3.21)$$

The minimum distance from $\hat{g}(U)$ surface to the \hat{O} can be derived by:

$$\hat{O}P^* = \beta = \frac{g(U^*) - \sum_{i=1}^n \frac{\partial g(U^*)}{\partial x_i} \cdot \sigma_{xi} \cdot u_i^*}{\sqrt{\sum_{i=1}^n \left(\frac{\partial g(U^*)}{\partial x_i} \cdot \sigma_{xi} \right)^2}} \quad (3.22)$$

The direction cosine of each transformed variable is provided below, reflecting the relative effect of the corresponding random variable on the total variance.

$$a_i = \cos \theta_{x1} = \cos \theta_{u1} = -\frac{\frac{\partial g(U^*)}{\partial u}}{|\nabla g(U^*)|} = -\frac{\frac{\partial g(X^*)}{\partial x_i} \cdot \sigma_{xi}}{\left[\sum_{i=1}^n \left(\frac{\partial g(U^*)}{\partial x_i} \cdot \sigma_{xi} \right)^2 \right]^{1/2}} \quad (3.23)$$

And P^* coordinates are:

$$u_i^* = \frac{x_i^* - \mu_{x_i}}{\sigma_{x_i}} = \hat{O}P^* \cos \theta_{x1} = \beta \cos \theta_{x1} \quad (3.24)$$

While transforming to the origin space X :

$$x_i^* = \mu_{x_i} + \beta \sigma_{x_i} \cos \theta_{x1} \quad , \quad (i = 1, 2, \dots, n) \quad (3.25)$$

And because P^* is a point on the limit state surface, it must fulfil the term:

$$g(\{x_1^*, x_2^*, \dots, x_n^*\}^T) = 0 \quad (3.26)$$

In situations where the failure surface contains numerous points related to fixed values of the reliability-index function (multiple MPP problem), it could be necessary to use several starting points to find all the values.

$$\min(\beta_1, \beta_2, \dots, \beta_m) = \beta_{HL} \tag{3.27}$$

The algorithm of the HL reliability index is demonstrated in Figure 3-2.

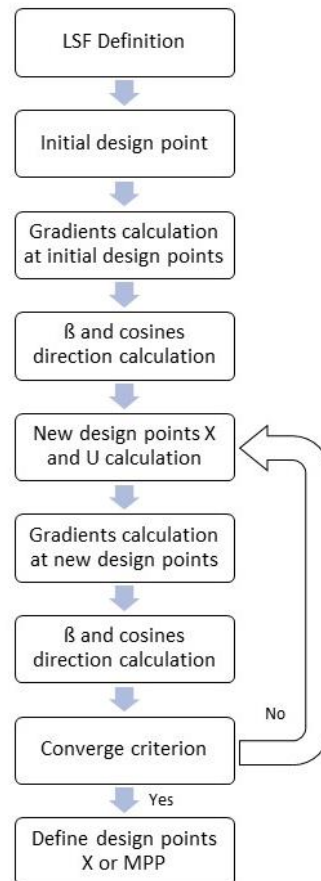


Figure 3-2 HL reliability index algorithm

The HL method, as opposed to the MVFOSM method, approximates the limit-state function using the first-order Taylor expansion at the design point $X(k)$ or $U(k)$ rather than the mean value point μ_x (Lee et al., 2014b). Moreover, the MVFOSM method is simple, whereas the HL method requires multiple converging iterations, particularly for nonlinear situations. For nonlinear problems, the HL technique frequently outperforms the mean-value method. The accuracy of the calculation of the probability of failure P_f will be determined by the quality and accuracy of the linearized limit-state function, $\tilde{g}(U)$. Overall, the Hasofer-Lind (HL) method is a first-order approximation technique that uses the gradient vector of the limit state

function at the design point to estimate the failure probability of a structure. It is widely used in engineering practice to assess structures' safety and performance subject to random variability in material properties, loads, and other design parameters.

3.2.1.3. Other reliability methods

The Hasofer-Lind reliability index approach assumes that the random variables X have a normal distribution. In circumstances of non-Gaussian variables, the described methods for calculating reliability are inefficient. Various structural reliability issues contain non-Gaussian random variables; thus, proposing a solution for such matters is vital. There are multiple techniques for transforming the normalised space, such as those described in (Rosenblatt, 1952) and (Hohenbichler & Rackwitz, 1981). A fundamental approximative transformation is the "equivalent normal distribution" or "the normal tail approximation". This approximation is shown in Figure 3-3 while the change of the random variables from the X -space to the U -space can be achieved, and the performance function $g(U)$ in U -space is approximately obtained.

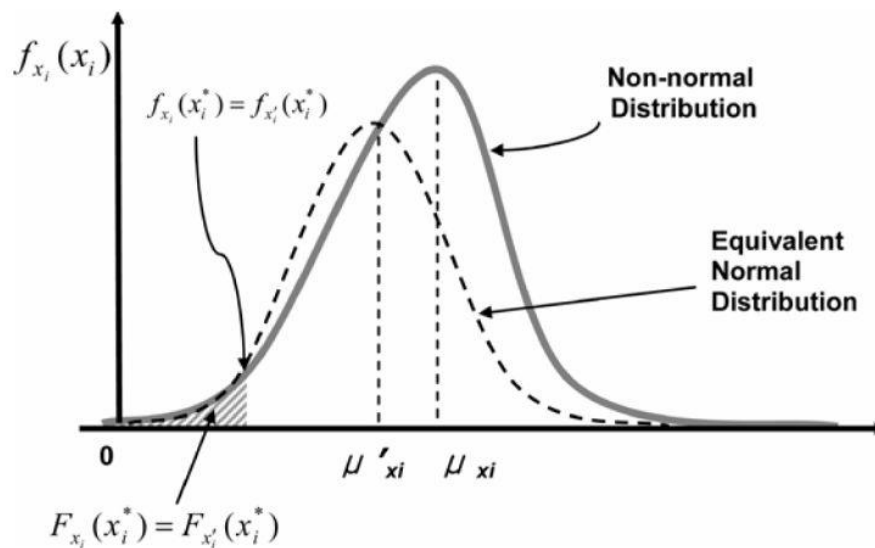


Figure 3-3 Normalized tail approximation method (Choi et al., 2006)

The RF technique is often referred to as the HL-RF method. Hasofer and Lind initially proposed the iteration algorithm and later extended it by Rackwitz and Fiessler to integrate random variable distribution information. The procedures presented in Figure 3-2 should be performed for the expanded RF algorithm, adding one variable transformation block before the initial design point is determined.

FORM approximation offers satisfactory results when the limit-state surface has only one minimal distance point, and the function is nearly linear close to the design point. However,

the failure probability computed by FORM using the safety index may be inaccurate in cases where the failure surface has large or irregular curvatures (high nonlinearity) (Melchers, 2007). This difficulty could be solved by introducing second-order Taylor series expansions (or other polynomials). Various nonlinear approximate methods have been proposed in the literature. For example, in (Altes et al., 1990; Breitung, 1984; Cai & Elishakoff, 1994; Köylüoglu et al., 1994), SORM have been developed using the second-order approximation to simplify the original surfaces.

3.2.2. Simulation methods

Simulation approaches have been developed for both the description of statistical distributions and the solution of the complex integration of the probability of failure directly using the results of multiple computing experiments. Monte Carlo Simulation, including importance sampling, and Latin Hypercube Simulation will be discussed as sampling methods in the following sections.

3.2.2.1. Monte Carlo simulation

Monte Carlo simulation is a numerical method for solving problems involving uncertainty and randomness. According to the literature, the study by (Metropolis & Ulam, 1949) was the basis for Monte Carlo Simulation. It refers to a basic random sampling strategy that provides random sampling sets for various uncertain variables. This technique has evolved considerably during the previous few decades, allowing estimation of the probability of an occurrence resulting from a stochastic process. Following the choice of a distribution type, a sampling set that could be utilized as input in the simulations is generated. The basic idea behind Monte Carlo simulation is to generate a large number of random samples from the uncertain input parameters of a problem and use these samples to compute the desired outputs. By averaging or aggregating the results from many samples, Monte Carlo simulation provides estimates of the mean, variance, and other statistical properties of the outputs, along with confidence intervals.

The steps involved in a typical Monte Carlo simulation are as follows:

1. Define the problem: Identify the problem or system that needs to be analysed and determine the uncertain input parameters (also known as random variables) that affect the system's behaviour.

2. Define probability distributions: Specify the probability distributions for each uncertain input parameter. Common probability distributions used in Monte Carlo simulation include normal (Gaussian), uniform, triangular, and log-normal distributions.
3. Generate random samples: Generate many random samples from the specified probability distributions for each uncertain input parameter. The number of samples should be large enough to achieve accurate results, and the sampling should be done independently for each parameter.
4. Perform simulations: Use the generated random samples as input values in the system or problem model and perform simulations or calculations to compute the outputs of interest. This can involve running numerical simulations, solving mathematical equations, or performing other types of computations.
5. Analyse results: Aggregate the results obtained from the simulations to compute the desired statistics, such as mean, variance, and confidence intervals, for the outputs of interest. This can provide insights into the behaviour and performance of the system or problem under uncertainty.

Once the stochastic variables have been identified in structural reliability issues for structural reliability problems, sampling sets are produced using the relevant probability density functions. Then, simulations are run with the resulting sampling sets to determine the structure's response. The limit state function represents the area's boundaries to be determined in the area calculation example. The failure probability for N trials can be defined as:

$$P_f = \frac{N_f}{N} \quad (3.28)$$

Monte Carlo simulation on reliability analysis is based on a formulation for the probability of success estimation. Assume an indicator function $I(x)$ is x-space:

$$I(x) = \begin{cases} 1 & \text{if } G(x) \leq 0 \\ 0 & \text{if } G(x) > 0 \end{cases} \quad (3.29)$$

Iteratively dividing the number of samples by the proportion of successful implementations yields an estimate of the event's probability.

$$I(x) = \frac{1}{N} \sum_{i=1}^N I(x_i) \quad (3.30)$$

As a result, the computational time and effort needed to analyse a case with a large number of random variables or a very low probability of failure increase dramatically. Important sampling, subset simulation, line sampling, etc., are just a few of the methods employed to solve the ineffectiveness of direct MCS in such cases. Furthermore, computational cost can be decreased while accuracy is maintained with the same number of runs by employing variance reduction approaches (Weiss et al., 2006).

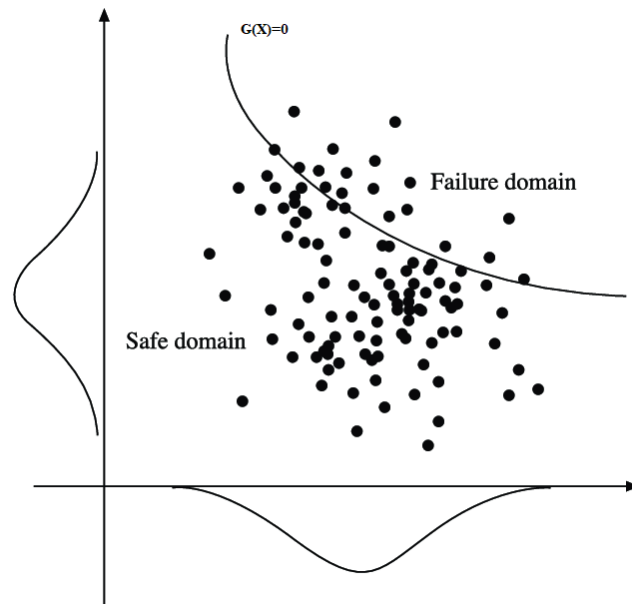


Figure 3-4 Monte Carlo simulation on reliability analysis (Weiss et al., 2006)

3.2.2.2. *Design point simulation*

Design Point simulation is a method used in reliability analysis to evaluate the reliability of a system under different operating conditions or stress levels. This simulation aims to identify the design point, which is the operating condition or stress level at which the system fails or experiences a significant reduction in performance. This method, introduced by (Shinozuka & Asce, 1983), applies to utilise MC sampling around the design point. After approximating the MPP in u -dimensional space, Monte-Carlo simulation is performed at this point rather than doing simulations across the entire range of each distribution. For each simulation, a weighted indicator function is created in the sampled u -space point $u_i = d + v_i$ where d is the design point or alternatively a point moved from the design point, and v_i is the normal independent variable from which the Monte-Carlo simulation method samples. For each simulation, the indicator function $I(u)$ is as follows:

$$I(x) = \begin{cases} 1 & \text{if } g(u) \leq 0 \\ 0 & \text{if } g(u) > 0 \end{cases} \quad (3.31)$$

Then, the probability of success for an event is then approximated as:

$$I(x) = \frac{1}{N} \sum_{i=1}^N I(u_i) \left(\prod_{j=1}^n \sigma_j \right) \frac{\exp(\sum_{j=1}^n u_{i,j}^2)}{\exp\left(-\sum_{j=1}^n \left(\frac{u_{i,j} - d_{i,j}}{\sigma_j}\right)^2\right)} \quad (3.32)$$

In this estimation, the coordinate of the design point is d_i , and σ_i is the standard deviation of sampling density. By replacing $v = u - d$, the success probability becomes:

$$\widehat{P}_E = \varphi(d) \frac{(2\pi)^{n/2}}{N} \sum_{i=1}^N I(u_i) \left(\prod_{j=1}^n \sigma_j \right) \exp\left(-d^T v_i - \sum_{j=1}^n v_{i,j}^2 \left(1 - \frac{1}{\sigma_j^2}\right)\right) \quad (3.33)$$

As the standardised variables have $\sigma_i = 1$ and d as design points:

$$\widehat{P}_E = \varphi(u^*) \frac{(2\pi)^{n/2}}{N} \sum_{i=1}^N I(u_i) \exp(-(u^*)^T v_i) \quad (3.34)$$

In summary, a design point simulation is a powerful tool for reliability analysis that can help engineers to identify and mitigate potential failure modes in a system under different operating conditions or stress levels.

3.2.2.3. Latin Hypercube Sampling method

Latin Hypercube Sampling (LHS) is a statistical technique used in reliability analysis to generate samples of input variables for use in simulation models. The Latin Hypercube Method (LHM) is a variation of LHS designed for computer experiments and commonly used in reliability analysis.

The basic idea behind LHS is to divide the range of each input variable into equal intervals and randomly sample one value from each interval. This ensures that the sample points are spread evenly throughout the input space and that all regions of the space are adequately represented. By generating a set of samples in this way, LHS provides a representative sample of the input space, which can be used to estimate the system's behaviour over a wide range of input values. The LHS Method, first proposed by (Mackay & Ross, 1979), is a method for representing multi variables while preventing overlapping data sets. The strategy is applied by splitting the

distribution of each stochastic variable into n nonoverlapping periods with equal probability. Once generated, one value from each interval should be picked randomly for every variable, and the analysis point should be linked to its respective dataset. Compared to the standard Monte Carlo sampling, the response variance is significantly reduced due to the homogenous allocation of intervals on the probability distribution function. Simultaneously, the computational cost of producing the analysis is reduced considerably. Figure 3-5 shows a specific case of a two-variable sampling problem.

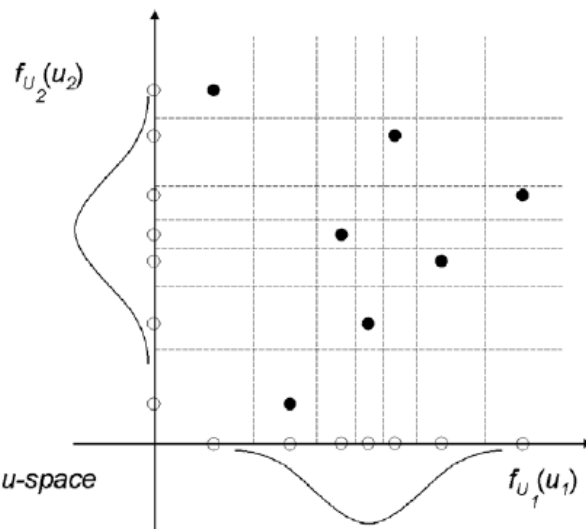


Figure 3-5 Latin Hypercube method for two variables (Kolios, 2010)

To apply LHM in reliability analysis, the following steps are typically followed:

1. Define the input variables: Identify the input variables relevant to the system's reliability analysis under consideration. These variables may include load, stress, temperature, or other environmental factors affecting the system's performance.
2. Divide the range of each variable into intervals: Divide the range of each input variable into a set of equal intervals. The number of intervals for each variable can be selected based on the desired level of accuracy and the number of samples required.
3. Generate a Latin Hypercube sample: Use a random number generator to select one value from each interval for each input variable. The resulting set of values represents a Latin Hypercube sample of the input space.
4. Evaluate the system response: Use the Latin Hypercube sample as input to a simulation model of the system and evaluate the system response. This may involve running the simulation multiple times with different samples to obtain a range of responses.

5. Analyse the results: Analyse the simulation results to determine the system's reliability under different input conditions. This may involve calculating statistics such as mean response, variance, or probability of failure.

In summary, LHM provides a systematic and efficient way to generate samples of input variables representing the input space, essential for accurate reliability analysis. Using LHM, engineers can identify and quantify the effects of input variables on the system's performance and optimise the design to improve reliability.

3.3. Response surface method

Response Surface Methodology (RSM) is a statistical technique used in reliability analysis to build predictive models of a system's behaviour based on input variables. RSM determines the relationship between input variables and system response, such as failure rate or mean time to failure. The models generated by RSM can be used to optimise the design of a system and improve its reliability. However, in complicated 3D structures, such as an OWT support structure, it is challenging to express explicitly the mathematical relationship between the actual loading acting on the entire structure (e.g., wave or wind loads) and the behaviours that each member is subjected to (e.g., axial force and bending moments). In such conditions of sophisticated failure processes, simulation techniques can handle the problem's complexity; nevertheless, they are frequently inefficient for calculating small failure probability values, as many iterations are required until relevant findings are obtained. In such circumstances, where simulation techniques are computationally expensive, the stochastic response surface method (SRFM) (Faravelli, 1989) can accurately predict structural reliability.

Using simple and explicit mathematical functions of the stochastic variables impacting the response of the structural member or system. This method approximates the precise limit state function, which in certain situations may be unknown. These functions may be simple polynomials (e.g., second or higher order) with coefficients that may be computed by fitting the response surface function to a sample of points based on the member's response. The Stochastic Response Surface Method (SRSF) limitations occur when the initial limit state involves nonlinearities or when very low failure probabilities must be precisely estimated. For example, the remarks highlighted in (Cox & Baybutt, 1981) and (S.-H. Kim & Na, 1997) result from an inaccurate representation of the response surface based on random sampling sites that may be considerably far from the MPP.

In (Olivi, 1980), it was mentioned that the accuracy of a highly non-linear limit state depends on the initial selection of sampling points. In most instances, the order of polynomials employed for approximating the response surface function is two. Reaching the function's coefficients requires a few sample points ($2n+1$). In (Olivi, 1980), the application of polynomials of higher order is discussed in detail. The limitation of this method is that it requires more sampling points, which is not always possible due to the complexity of the computing process and the fact that ill-conditioned matrices are formed for the derivation of the coefficients of the polynomials using regression (Gavin & Yau, 2008; Impollonia & Sofi, 2003). Chebyshev polynomials use statistical analysis of the high-order response surface. (Enevoldsen & Sorensen, 1994) introduces an algorithm that utilizes a quadratic response surface achieved from Central Composite Designs (CCD). In this algorithm, once a global search has been done and the possible failure point domain is detected, a revised response surface is fitted locally to apply the reliability calculation procedures.

As discussed, the probability of failure of the system is defined as $P_f = P[g(x) < 0]$, where $g(x)$ is the limit state function that denotes the critical failure surface and $X = [x_1, x_2, \dots, x_n]$ is a vector containing n stochastic variables. The response surface approach presents a new function $\tilde{g}(x)$ that will use enough sample orders to establish the polynomial coefficients (Faravelli, 1989).

$$\tilde{g}(x) = a + \sum_{i=1}^n b_i X_i + \sum_{i=1}^n c_i X_i^2 \quad (3.35)$$

An equal or greater number of sample points is expected to calculate the coefficients ($2n+1$), a , b , and c . It is possible to determine sample points so the measured response is better mapped. Depending on the approach, the number of samples can range from $(2n+1)$ to 3^n , typically combining μ and $\mu \pm f\sigma_i$, where μ and σ_i are the mean value and standard deviation of a stochastic variable X_i respectively, and f is a coefficient equal to 3 typically. For example, Figure 3-6 illustrates various sample combination patterns for a problem with two variables (Gavin & Yau, 2008).

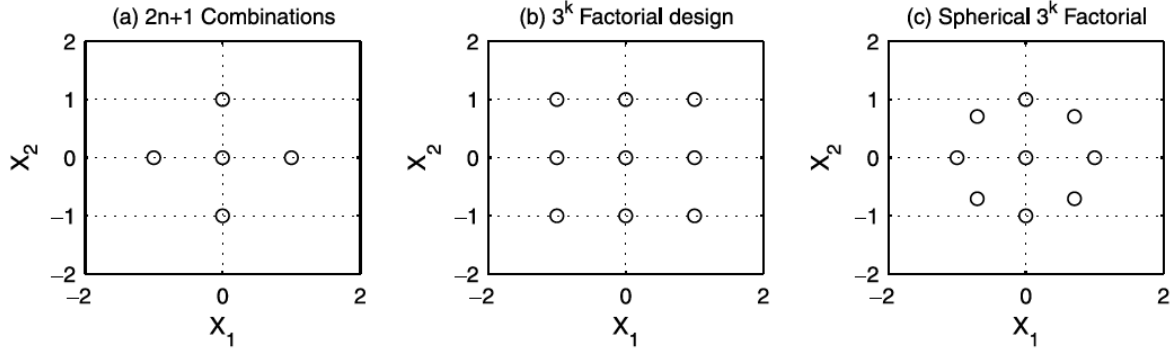


Figure 3-6 Various Sampling approaches (Gavin & Yau, 2008)

In linear limit states, parameter selection is less crucial than nonlinear performance. In subsequent circumstances, the sampling point choice is essential for approximating the initial limit state functions. The study in (Khuri & Cornell, 1996) presents a different expression of the generic polynomial approximation of quadratic limit states that incorporates mixed terms of the stochastic variables. This equation may describe the nonlinearity of a limit state, although it increases the design matrix's complexity for calculating polynomial coefficients. The required number of sample points among the n -dimensional space is between $\left(\frac{n(n-1)}{2} + 2n + 1\right)$ and 3^n . The approximation function $\tilde{g}(x)$, typically a quadratic polynomial with cross-terms is used in the form:

$$\tilde{g}(x) = a + \sum_{i=1}^n b_i X_i + \sum_{i=1}^n c_i \cdot X_i^2 + \sum_{i=1}^{n-1} \sum_{j=i}^n d_{ij} \cdot X_i \cdot X_j \quad (3.36)$$

where, a, b_i, c_i and d_{ij} with $i, j=1, \dots, n$ are the regression coefficients and $X_i, i=1, \dots, n$ are the n input variables. Equation (3.36) is a regression model. The response domain was derived, and an appropriate response surface model was produced. The response surface model interpolates the values in the multiple dimensions characterized by the DoE. Several types of response surfaces are available in the commercial package of ANSYS DesignXplorer.

3.4. Regression methods

3.4.1. Linear Regression

In situations where two (or more) variables must be expressed as a function, linear regression is the underlying principle. This can indicate the challenge of correlating measurements to properties in an experimental method. In non-linear regression, the dependent variable is a

linear function of the parameters (independent variables). This method presupposes that a straight line can conveniently represent the plotted sets of dependent and independent variables.

The previous approach proposed by Gauss and Legendre is known as the Least Squares Method (LSM). It presents a solution by reducing the absolute distance between the given data and the potential function (residuals) to obtain the best match. Considering $a_i, i = 1, 2, 3, \dots, v$ as the regression coefficient vector and using mathematical notation, it can be written as:

$$y(x) = a_0 + a_1 \cdot f_1(x) + a_2 \cdot f_2(x) + \dots + a_v \cdot f_v(x) + e \quad (3.37)$$

Where e is the error of the model, Equation (3.37) can be written in a matrix form:

$$Y = X \cdot a + e \quad (3.38)$$

Where Y, X, a and e are described as:

$$Y = \begin{bmatrix} y_1 \\ y_2 \\ \vdots \\ y_n \end{bmatrix}, X = \begin{bmatrix} 1 & f_1(x_1) & f_2(x_1) & \dots & f_m(x_1) \\ 1 & f_1(x_2) & f_2(x_2) & \dots & f_m(x_2) \\ \vdots & \vdots & \vdots & \ddots & \vdots \\ 1 & f_1(x_n) & f_2(x_n) & \dots & f_m(x_n) \end{bmatrix}, a = \begin{bmatrix} a_1 \\ a_2 \\ \vdots \\ a_n \end{bmatrix}, e = \begin{bmatrix} e_1 \\ e_2 \\ \vdots \\ e_n \end{bmatrix}$$

In order to determine the regression coefficients vector a , the least squares approach is represented in matrix form as follows:

$$a = (X^T \cdot X)^{-1} \cdot X^T \cdot Y \quad (3.39)$$

After calculating the regression coefficients, the dependent variable values for the sampled dependent variables and the error for each are as follows:

$$\bar{Y} = X \cdot a \quad \text{and} \quad e = Y - \bar{Y} \quad (3.40)$$

The total sum of squares (SST), the sum of squares for regression (SSR), and the error sum of squares (SSE) are computed as follows:

$$SST = Y^T \cdot Y \quad \text{and} \quad SSR = \bar{Y}^T \cdot \bar{Y} = a^T \cdot X^T \cdot Y \quad \rightarrow \quad SSE = SST - SSR \quad (3.41)$$

The coefficient of determination can be defined to assess the accuracy of the modelled equation R^2 . It implies that when $SSE = 0, R^2 = 1$ and the absolute regression has been achieved.

$$R^2 = 1 - \frac{SSE}{SST} \quad (3.42)$$

3.4.2. Multivariate Regression

When there are multiple independent or dependent variables, the fundamental equation can be solved if sufficient sets are provided (y, x_i) . The general issue can be defined as:

$$y(x) = \sum_i a_i \cdot p_i(x_1, x_2, \dots, x_n) + e \quad (3.43)$$

In terms of multiplications, this is also described as

$$y(x) = \sum_i a_i \cdot x_1^{\alpha_i} \cdot x_2^{\beta_i} \dots x_n^{\omega_i} + e \quad (3.44)$$

Where a_i is the coefficient of regression and $\alpha_i, \beta_i, \dots, \omega_i$ are the independent variable power coefficients. Consider the following data matrices: Y is a $(n \times q)$ data matrix holding the dependent variables, X is a $(n \times p)$ data matrix carrying the independent variables, A is a $(p \times q)$ data matrix having the regression coefficients, and E is a $(n \times q)$ matrix containing the error terms. It converts the given equation into a matrix. (\tilde{X} indicates a matrix formed from X , having the different powered values of X):

$$Y = \tilde{X} \cdot A + E \quad (3.45)$$

The dimensions of the matrices in Equation 3.42 demonstrate that $(p \times q)$ data sets must be accessible for the system to have a solution. An important observation that can ensure accuracy in the regression coefficients results is the level of how well conditioned the matrix $X^T \cdot X$ is.

3.5. Parametric FE model design basis

3.5.1. Reference Model and met-ocean

The reference turbine used in this study is NREL's OWT, developed based on the Senvion 5MW wind turbines and considered representative of typical utility-scale land- and sea-based multi-megawatt turbines. The characteristics of this turbine are listed in Table 3-1. The substructure is a monopile OC3 (LaNier, 2005; Passon et al., 2007). The tubular pile has a constant

section with 60mm thickness and 6m outer diameter. The embedded part of the monopile is 36m, and the sea depth is 20m. The transition piece is 10m above the mean water level. The adopted NREL 5MW and OC3 Monopile geometry implanted in layered sandy soil is illustrated in Figure 3-7.

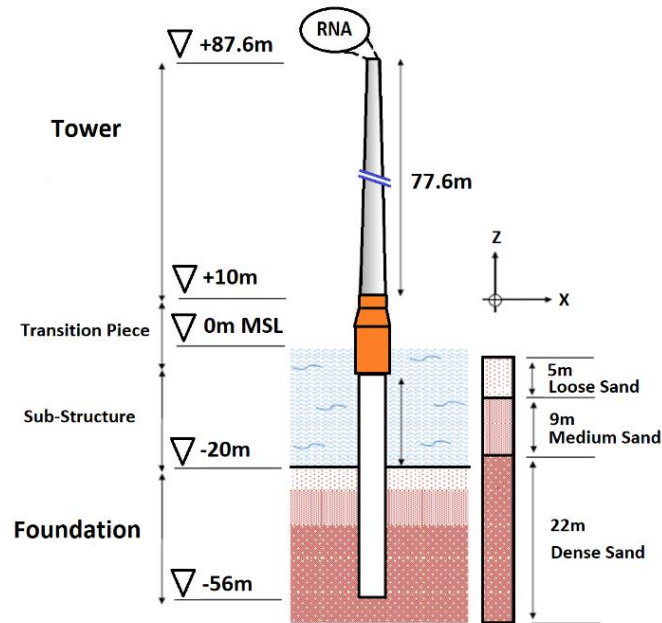


Figure 3-7 Reference model geometry and dimensions

According to the technical reference report for the OC3 pile (LaNier, 2005), the site considered in this study is located in the North Sea, IJmuiden City. It refers to the NL-1 location, approximately 6 miles off Ijmuiden, Holland. The met ocean database for the NL-1 site is extracted from the Netherlands Enterprise Agency (RVO) open-source website.

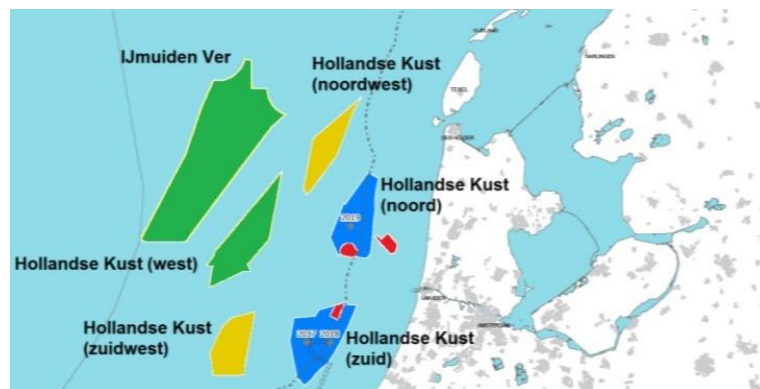


Figure 3-8 Hindcast data extraction point in the NL-1 (DHI, 2020)

The extracted individual wind and wave hindcast data cover approximately 50 years. Joint datasets of wind and waves have been established from the individual hindcast time series. A 50-year extreme met ocean data are summarised in Table 3-1:

Table 3-1 The 50-year extreme met ocean data of NL-1 (DHI, 2020)

Item	Value
Significant wave height H_s [m]	6.9
Peak Period T_p [s]	7.7s
Maximum wave height H_{max} [m]	9.1
Wave period associated with H_{max} [s]	5
High water level [m]	3.5
Low water level [m]	-0.7
Reference Wind speed [m/s]	50
Ave annual Wind speed [m/s]	10

3.5.2. Applied Loads

Various environmental loads are imposed on the OWTs. IEC 61400-3 (IEC, 2019) or DNV-OS-J101 (DNV GL, 2014) have suggested a list of loads that should be applied to the structure, and the formulation of these loads is captured from DNV-RP-C205 (DNV GL, 2010a). The main loads that have been used for our case study are (A) inertia loads; (B) wind turbine rotor load; (C) wind load applied to the tower; (D) wave load; (E) current load and (F) hydrostatic loads applied to the support structure as shown in Figure 3-9.

Table 3-2 NREL 5 MW baseline wind turbine (Jonkman et al., 2009)

Item	Value
Rating	5 MW
Rotor orientation	Upwind
Control	Variable speed, collective pitch
Drivetrain	High speed, multiple stages, gearbox
Rotor diameter	126 m
Hub height	90 m
Cut-in, rated, cut-out wind speed	3 m/s, 11.4 m/s, 25 m/s
Cut-in, rated rotor speed	6.9 rpm, 12.1 rpm
Rated tip speed	80 m/s
Overhang, shaft tilt, precone	5 m, 5°, 2.5°
Rotor diameter	126 m
Tower base diameter	6 m
Tower base thickness	0.027 m
Tower top diameter	3.87 m
Tower top thickness	0.19

3.5.2.1. Inertia Load

Due to the mass of the support structure and the RNA mass at the top of the tower, inertia loads can considerably contribute to the buckling and change of the modal frequencies of the OWT support structure. Therefore, they should be included in the structural analysis of support structures. In addition, the structure's gravitational loads, system weight and applied loads impact the modal analysis (Freebury & Musial, 2000).

3.5.2.2. Rotor Loads

Aerodynamic loads result from the moving parts of the wind turbine and static components. The magnitude of the load is not constant, as it depends directly on wind and air density. The design load values are defined in the WindPACT (Wind Partnership for Advanced Component Technologies) Turbine design study (Malcolm & Hansen, 2006). The fatigue design resistance, developed initially by NREL, was calculated by the Damage Equivalent Load (DEL) method. The DEL method was validated in the study by (Freebury & Musial, 2000).

3.5.2.3. Wave Loads

The calculated wave load, composed of inertia and a drag term, results from the interaction between the wave and the cylindrical shape of the OWT support structure. Morison's equation can be employed according to DNV-OS-J101 (DNV GL, 2014) to estimate the amount of the load when the monopile diameter, D , is smaller than 0.2 of wavelength, λ .

$$D \leq 0.2 \lambda \quad \text{For Shallow water depth: } \lambda = T\sqrt{gh} \quad (3.46)$$

The drag force is written in the form of $\frac{1}{2}\rho C_D D U |U|$. The combination of hydrodynamic mass force and Froude-Krylov force is the inertia force in the equation and leads to the following Morison equation (Clauss & Birk, 1997):

$$F_{hyd} = F_{Drag} + F_{inertia} \quad (3.47)$$

$$F_{hyd} = \frac{1}{2}\rho C_D D U |U| + \rho C_m A \ddot{U} + \rho A \dot{U} \quad (3.48)$$

$$F_{hyd} = \frac{1}{2}\rho C_D D U |U| + \rho C_M A \dot{U} \quad (3.49)$$

$$F_{hyd} = \frac{1}{2}\rho C_D D (U + U_c) |(U + U_c)| \quad (3.50)$$

where ρ is the fluid density; U and \dot{U} are the particle velocity and acceleration of the wave, respectively; A is the area of the cylinder cross-section; C_m is the hydrodynamic mass coefficient; C_D and C_M are drag and inertia coefficients, respectively.

For a slender structure such as a monopile, Morison's equation is usually employed to calculate approximately the wave loads on the structure. However, in this study, the water depth, h , is 20m, and the wave period, T , is 5sec, so the wavelength is 70m, which satisfies the Equation (3.46). Therefore, Morison's equation is considered the appropriate method to calculate the wave load. The final form of Morison's equation can be written as:

$$F_{wave}(z) = \frac{1}{4} \rho_w \cdot \pi \cdot D^2 \cdot C_M \cdot \dot{U}(z, t) + \frac{1}{2} \rho_{water} \cdot D \cdot C_D \cdot U(z, t) \cdot |U(z, t)| \quad (3.51)$$

The descriptions and values for equation (3.48) are listed in Table 3-3. The calculated pressure value from the above equation shows that when the depth increases, the wave pressure is reduced.

Table 3-3 Wave load assumption and values in ULS

Item	Description
Monopole Inertia Coefficient, C_m	1.6 (LaNier, 2005; DNV, 2014)
Monopile Drag Coefficient, C_D	1.0 (LaNier, 2005; DNV, 2014)
Water Density, ρ_{water}	1025 Kg/m ³
Horizontal Velocity of Water Particles, $U(z, t)$	The linear/Airy wave theory (Chakrabarti, 2005)
Acceleration of Water Particles, $\dot{U}(z, t)$	The linear/Airy wave theory (Chakrabarti, 2005)

3.5.2.4. Current loads

Drag loading produced from the current must be included in the hydrodynamic loads. Therefore, an exponential profile for the sub-surface current was used to describe the current velocity $u_c(z)$ from surface to seabed d :

$$u_c(z) = u_{c,sub} \left(\frac{d+z}{d} \right)^{1/7} \quad (3.52)$$

Where $u_{c,sub}$ is the velocity of current at the surface. Current velocity could be added to the wave particle velocity in the drag term of Morison's equation if the current and wave were assumed as aligned loads. The calculated pressure value from the current load equation on the

surface shows that when the depth increases, the current pressure rises to 18m, and because of the seabed surface, the pressure reduces.

3.5.2.5. Wind Loads

Wind loads on the tower are caused by drag force and are defined by equation (3.54). In that equation, the power-law profile represents the wind shear as:

$$\bar{V}(z) = \bar{V}_r \left(\frac{z}{z_r} \right)^\alpha \quad (3.53)$$

where α is the roughness coefficient, its value is taken as 0.115 considering the offshore condition (Jonkman & Musial, 2010). The reference wind speed \bar{V}_r is measured at the nacelle reference height, z_r . Finally, wind loads can be calculated by:

$$F_{tower}(z) = \frac{1}{2} \rho_a C_{D,T} D(z) V_r^2(z) \quad (3.54)$$

The Drag Coefficient, $C_{D,T}$ is 1.0 (Chehouri et al., 2015), $D(z)$ is the external diameter of the tower segment at the height of z , and the outer diameter of the tower narrows at the height of z . Figure 3-9 shows the schematic OWT support structure with all applied loads. The calculated pressure value from the wind load profile on the surface indicates that when the height increases, the wind pressure increase.

3.5.2.6. Hydrostatic Loads

The outer surface of the monopile is subjected to hydrostatic pressure when submerged in water. This is a constant normal load that increases linearly with water depth. Therefore, the hydrostatic force, F_h , can be calculated using the gravitational constant, g , and water depth, h :

$$F_h = \rho_w g h \quad (3.55)$$

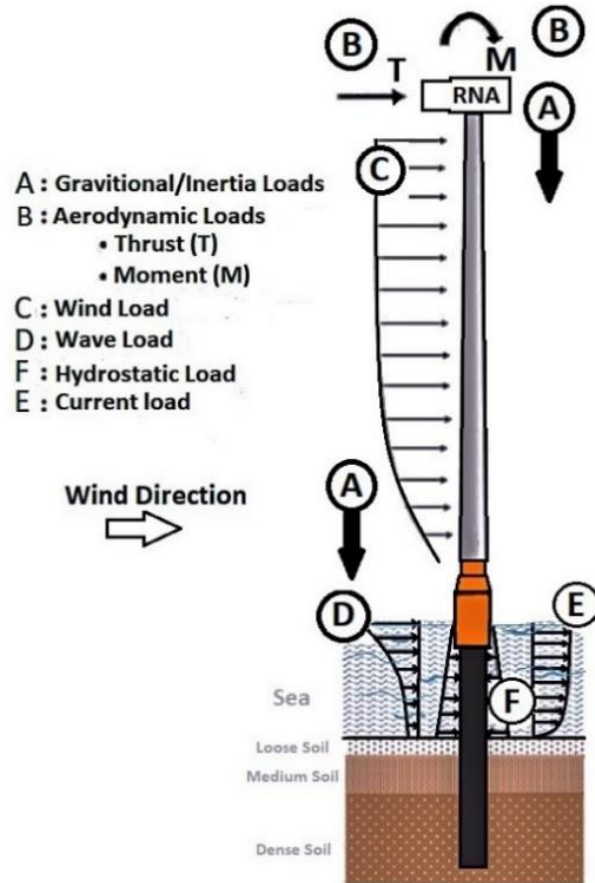


Figure 3-9 Applied loads on OWT support structure (Gentils et al., 2017)

3.5.3. Limit States and DLCs

Several load cases that cover all conditions of OWTs design are defined in (DNV GL, 2016), and (IEC, 2019) as a reference. As suggested by (P. Schaumann, C. Böker, A. Bechtel, 2011), two structurally prominent load cases have been considered. The ultimate limit state (ULS) and fatigue limit state (FLS).

3.5.3.1. ULS

Ultimate limit state (ULS) corresponds to extreme environmental conditions based on a 50-year return period. Under the 50-year Extreme Wind Model (EWM) with the 50-year Reduced Wave Height (RWH) and Extreme Current Model (ECM), defined as the Design Load Case (DLC) 6.1b and 2.1 for IEC (2019) and DNV-GL (2014) standards, the most critical ULS load case is often considered to correspond to the parked wind turbine. According to standards (IEC, 2019), the safety factors for the design loads are 1.1 and 1.35 for gravitational and environmental loads, respectively. Tables 3-4 and 3-5 summarise the load cases and aerodynamic loads applied to the model in ULS and FLS from a conceptual design study of (LaNier, 2005) on 5MW steel tower, respectively.

Table 3-4 Wind turbine aerodynamic loads (LaNier, 2005)

Limit State	Tilting moment (MN.m)	Torsional moment (MN.m)	Thrust force (kN)
ULS	38.567	7.876	781
FLS	3.687	3.483	197

Table 3-5 Design Load Cases in ULS (IEC, 2005)

Load Case	Wind	Wave	Load safety Factor
Ultimate:	EWM:	RWH:	-
DLC 6.1b/2.1 (Parked)	V_{g50}	$1.32 \times H_{s50}, T_{s50}$ ECM: $V_{c,ex}$	1.0
Fatigue:	NTM:	NSS:	Normal N
DLC 1.2/7.2 (Operation)	V_{ave}	H_{ave}, T_{ave} No Current	1.1/1.35

3.5.3.2. FLS

Fatigue limit state (FLS) is another limit state caused by variation in operation and cyclic loads. FLS is an essential source of cyclic loading during the OWT lifetime. In the current case study, a popular load scenario for FLS is an operating state under the Normal Turbulence Model (NTM) and the Normal Sea State (NSS), where wave height and cross zero periods were calculated using the site's joint probability function, assuming no current. According to (IEC, 2005), the safety factor for this load case is equal to 1.0. Fatigue Wind Load Tower Forces values for reference turbine are provided from the reference technical report (LaNier, 2005). Later for optimised model, OWECS software, the in-house tool in Seaway7 company will be used to generate Damage Equivalent Load (DEL) in FLS analysis for optimised model considering time-series analysing.

3.5.4. Parametric FEA Model

A parametric finite element model is performed using the ANSYS workbench. The modelling phase started by defining parameters such as geometry data, material properties and structure thickness. The flow chart is illustrated in Figure 3-10.

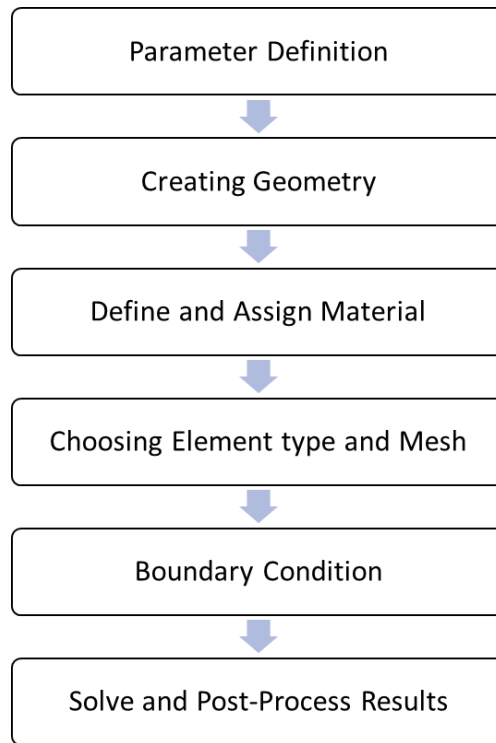


Figure 3-10 Parametric FEA model flowchart

3.5.4.1. *Geometry and applied loads*

A 3D model consisting of five parts was created using the previous section's geometrical parameters, i.e., soil, tower, grout, monopile, and transition piece. The monopile and tower parts were sectioned into 10 and 15 pieces (LaNier, 2005; Passon et al., 2007). The diameter of the soil was considered 20 times the diameter of the monopile support structure. This is large enough to prevent boundary effects from influencing pile-soil behaviour. As the reference documents recommend, this model was created with precise tower dimensions, transition piece, grout, and monopile (Brown & Brown, 2012). Wind, wave, and current load profile data have been calculated and applied as variable loads on the outer area of the structure. The thrust force is located at the tower's designated point at the top. The moment is applied to the whole structure. Gravitational load is located downward on the centre of mass of the support structure. Details are illustrated in Figure 3-11 and Figure 3-12.

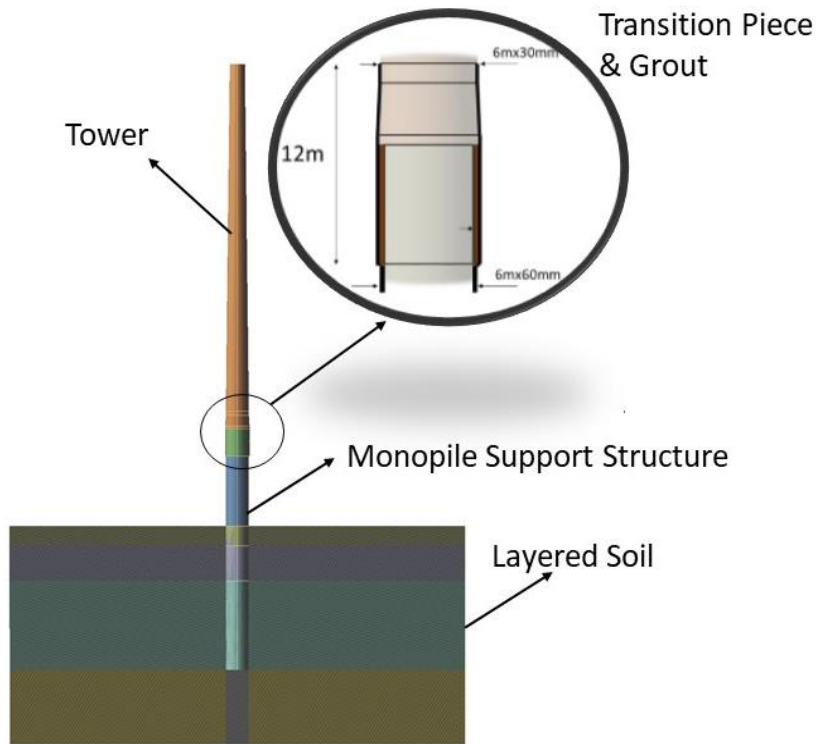


Figure 3-11 NREL 5MW wind turbine and OC3 platform geometry

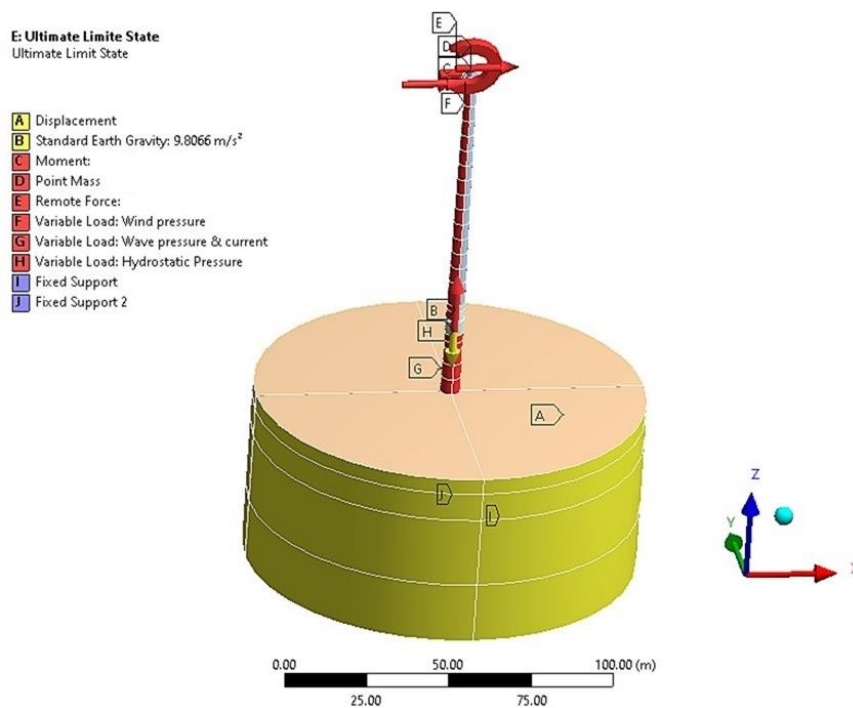


Figure 3-12 Isometric view of geometry and applied loads

3.5.4.2. Material

According to (DNV GL, 2016), the support structure's primary material is S355 Steel. The grout material is Ducorit D4. Sand properties are defined by using the Drucker-Prager model.

According to (Drucker and Prager, 2016), the soil yield strength can be defined in terms of cohesion value and friction angle as in equation (3.56):

$$\sigma_{y,s} = \frac{6c \cos(\phi)}{\sqrt{3}(3 - \sin(\phi))} \quad (3.56)$$

where ϕ is the friction angle, c is the cohesion value. Thus, the friction between pile and soil can be driven by equation (3.57) (Jung et al., 2015):

$$C_f = \tan\left(\frac{2}{3}\phi\right) \quad (3.57)$$

Regarding the above equations and soil properties adopted from (Jung et al., 2015), the soil characteristics and Steel/Grout material used in this study (Theotokoglou & Papaefthimiou, 2017) are summarized in Tables 3-6 and 3-7. In addition, the contacts between the soil and the monopile are defined in ANSYS, considering the friction coefficients.

Table 3-6 Sand Properties in different levels (Jung et al., 2015)

Sand Type	Young's Modulus (MPa)	The angle of friction (deg)	Friction coefficient	Yield stress (kPa)
Loose	30	33	0.40	59.2
Medium	50	35	0.43	58.5
Dense	80	38.5	0.48	57

The soil properties are defined in the OC3 benchmark study (Passon et al., 2007), as shown in Figure 3-13.

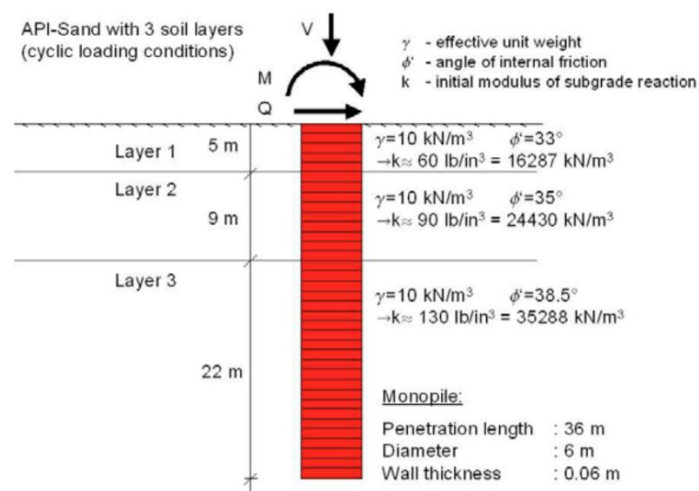


Figure 3-13 Soil Profile (Passon et al., 2007)

Table 3-7 Support structure material properties

Item	Steel	Grout
Young Modulus, E (GPa)	210	70
Density (kg/m ³)	8500	2740
Poisson's ratio	0.38	0.19
Tensile Strength (MPa)	-	10
Yield Strength (MPa)	355	-

3.5.4.3. Meshing

Mesh generation is essential in FEA simulation since it is susceptible to the result's accuracy. This model used the shell element type, Shell281, for the thin-wall structures such as towers and monopile. Shell281 characteristics are suitable for considerable strain nonlinearity and large rotation applications (Thompson & Thompson, 2017); therefore, it is appropriate for this study. Furthermore, the grouting part is meshed by the element SOLID186 to obtain accurate bending stress considering friction. Finally, SOLID185 was used for the soil part.

Table 3-8 Mesh sensitivity

Description	Element size of Steel part	Number of Elements	Max Von Mises (MPa)
Mesh #1	4 m	1780	25.4
Mesh #2	2 m	7584	23.1
Mesh #3	1 m	37356	23.0
Mesh #4	0.5 m	235180	23.0

Mesh convergence is performed to obtain an accurate result. The process starts with applying 100kN Force on top of the tower. The application of 100kN Force is a test force on top of the structure to optimise the mesh in the x-direction. Because the mesh quality check is essential, it could be any value or load in any direction, but a single force is preferred to reduce the calculation run time. The calculated maximum Von Mises value converges after using a mesh type with an element size of 1m (37356 elements) refinements by comparing the result values and the differences. Figure 3-14 illustrates the final optimum mesh, and Table 3-8 presents the optimum number of elements. By comparing the values and the differences, Mesh #3 is selected in order to proceed with the analysis.

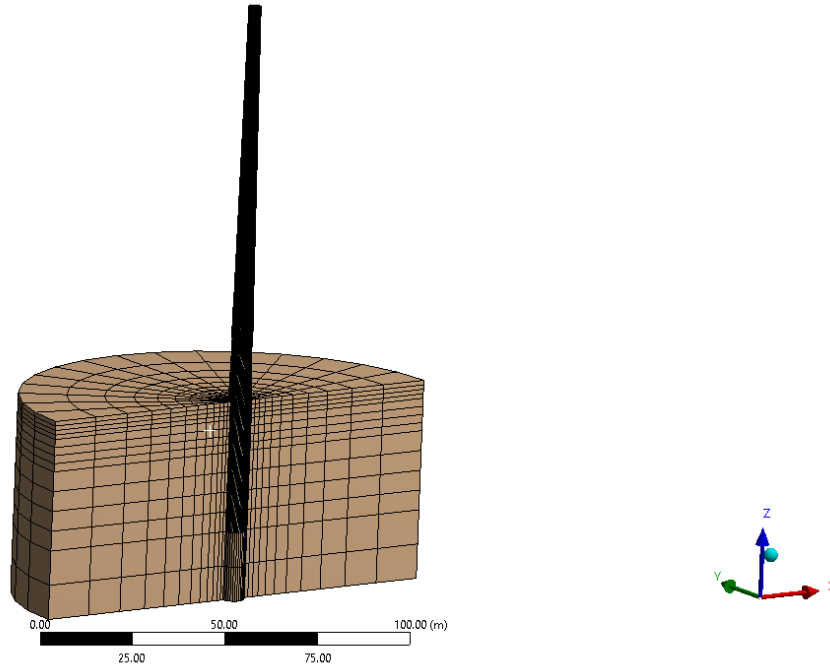


Figure 3-14 Final generated mesh with the cross-section

3.5.4.4. *Boundary Condition*

Boundary conditions are applied to the geometry, as the bottom of the soil model is fixed in all directions. The side boundaries of the soil are fixed against lateral translation. Contact between soil and monopile is set according to the frictional coefficients, and other contacts are assumed as bonded. On top of the tower, wind turbine rotor aerodynamic loads are applied. Other loads (such as wave, current, wind loads, and hydrostatic loads) are applied using pressure formulations, which allow these loads to automatically update with the updated diameters of the support structure during the optimisation process in a more accurate representation. Hydrostatic loads surround the submerged components. The RNA is a concentrated mass applied to the tower top via a multi-point constraint. The interface at the top of the tower is defined as Rigid (CERIG boundary condition) to avoid any unnecessary deformation on top surface (Flanged attachment).

3.6. Summary

In this Chapter, numerical approaches for assessing structural reliability are discussed. Deterministic Methods, including First Order Reliability Methods, have been provided in accordance with the procedure followed in the formulation of developing codes. Simulation

methods such as Monte Carlo (MC) were also briefly discussed. The Stochastic Response Surface Method (SRSM) has been explained in detail, and the processes for the standard SRSM have been deduced. At the end, the parametric FEA model was developed, and they were explained in order to prepare all essentials to create reliability-constrained design optimisation framework.

4. Reliability-Constrained Design Optimisation Framework

4.1. Introduction

As discussed, structural reliability assessment is employed to assess the safety levels of the OWT structure. Safety has a direct relation with failure modes. Several time-dependent failure modes of an OWT support structure can directly affect its resistance to applied loads. However, the predominant phenomenon is fatigue damage due to the marine environment and corrosion, which results in the degradation of the components (Price & Figueira, 2017) and also because of the amplitude of fatigue loads caused by the mixed responses of wind, wave, and other loads. Consequently, fatigue is a design-driving criterion for an OWT as a welded structure, according to (Dong et al., 2012).

4.2. Optimisation framework development

4.2.1. Structural Optimisation of Support Structure

Optimisation in the early stages of the design process can reduce a significant cost. The structural optimisation model merges the parametric FEA model and GA. The result will be a lighter and more robust structure with optimum responses to environmental loads.

$$F_{obj} = \min(M_{global}) \quad (4.1)$$

where F_{obj} is an objective function that is chosen to minimize M_{global} , the global mass of the support structure. As this study aims at developing an integrated optimisation methodology, the minimum global mass of the support structure is chosen as the objective function. The mass reduction in an OWT support structure is to achieve cost reduction goals. Partial safety factors (PSFs) are applied according to DNV standards (DNV GL, 2016). The corresponding flowchart is presented in Figure 4-1.

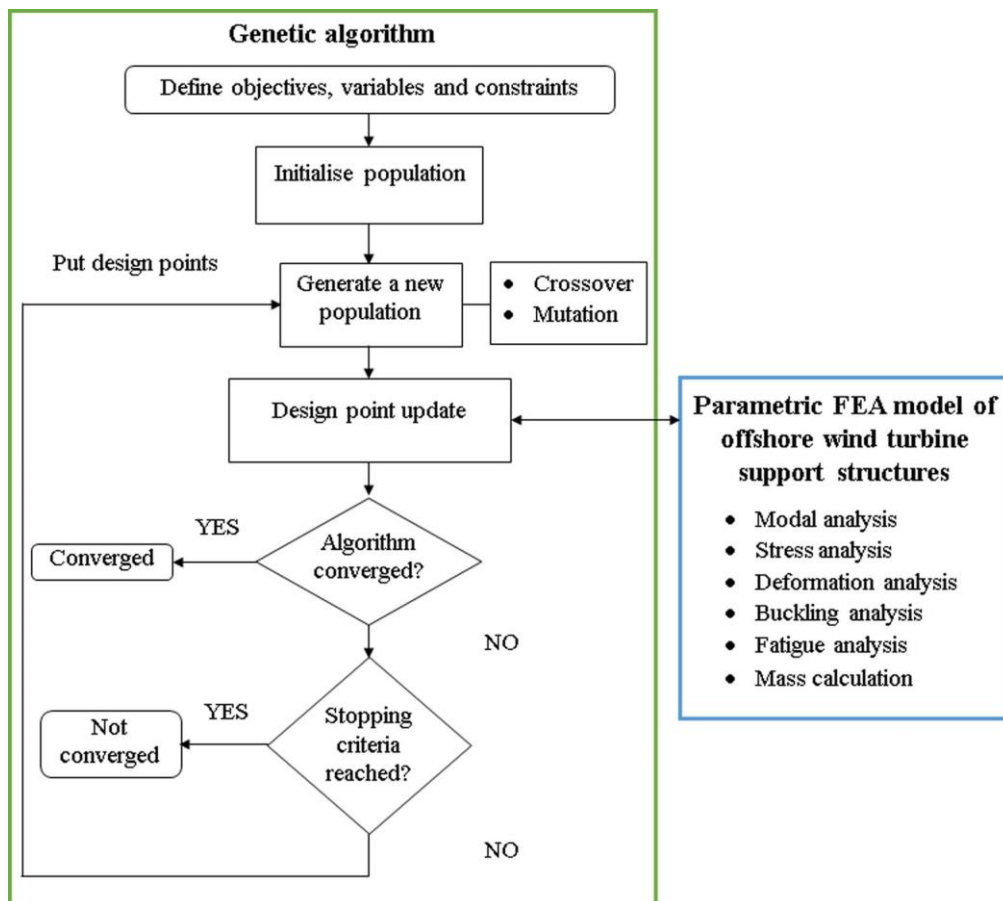


Figure 4-1 Flowchart of the structural optimisation model (Gentils et al., 2017)

4.2.2. Design Variables

According to (Kallehave et al., 2015; Muskulus & Schafhirt, 2014), thickness and diameter dimensions are two types of variables that significantly influence structural response and are individually designed driven by different criteria. Defining several sections on the tower and monopile caused an increase in the number of variables. This issue can be a challenge in the

simulation process and calculation time. A reduction technique has been introduced by (Ashuri, 2012), which uses linear interpolation between the top and bottom ends. This strategy has been adopted and applied to the tower, foundation and monopile. As a result, the number of variables decreased from 30 to 13 in the final process. It should be noted that the diameter of the foundation section stays constant all along the length due to installation limitations. So, design variables for a design point j can be stated in Equation (4.2) as a vector of variables inspired by the chromosome formulation:

$$X_j = [x_1 \ x_2 \ x_3 \ \dots \ x_n]^T \quad \text{with } n = 13 \quad (4.2)$$

where, x_1 and x_2 are the diameters at the base and top of the monopile, and x_3 and x_4 are the diameters at the bottom and top of the tower. x_5 , x_6 , x_7 and x_8 are the thickness at the base and top of the tower; x_9 and x_{10} are the thickness at the bottom and top of the sub-structure and x_{11} , and x_{12} are the thickness along the foundation. Finally, x_{13} is the thickness of the transition piece. In Figure 4-2, the position of all variables is presented. The list of variables with their upper and lower bounds is available in Table 4-1.

Table 4-1 Upper and lower bound of the design variables

Variable	Name	Unit	Lower Bound	Upper Bound
Monopile base diameter	X_1	[m]	5	7
Monopile top diameter	X_2	[m]	5	7
Tower base diameter	X_3	[m]	5	7
Tower top diameter	X_4	[m]	3	4.5
Tower base thickness	X_5	[mm]	20	40
Tower Int1 thickness	X_6	[mm]	20	40
Tower Int2 thickness	X_7	[mm]	15	35
Tower top thickness	X_8	[mm]	10	30
Monopile substructure base thickness	X_9	[mm]	45	70
Monopile substructure top thickness	X_{10}	[mm]	45	70
Monopile foundation base thickness	X_{11}	[mm]	40	70
Monopile foundation top thickness	X_{12}	[mm]	45	70
Transition piece thickness	X_{13}	[mm]	25	40

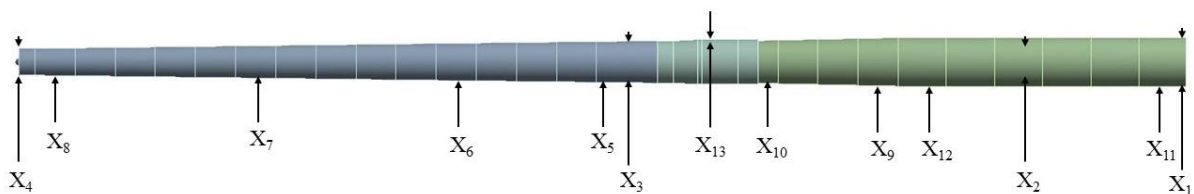


Figure 4-2 Design variables of OWT support structure

4.2.3. Design Constraints and Criteria

Choice of criteria is paramount for the reliability of optimisation solutions. A wrong choice or lack of proper criteria could lead to unexpected structural failure during experimental tests or structure lifetime. This paper defined seven structural constraints based on modal, stress, deformation, buckling, and fatigue requirements. Geometrical constraints on the design variables were also considered and are described below. It's worth noting that the turbine's foundation and tower are both composed of steel. If the turbine's tower is composed of composite material, it should be addressed independently from the monopile base.

4.2.3.1. Resonance Constraint

As seen in Figure 4-3, OWTs are dynamically loaded structures, with loads coming from the wind, waves, and rotor excitations. The fundamental frequency f_0 (the first tower bending frequency) and the dynamic interaction with the external loads have a strong influence on the structure's response. This occurs when f_0 is higher than the rotor's rotational frequency, f_{1P} , which is caused by rotor imbalances, but lower than the blade-passing frequency, f_{3P} , which is caused mainly by aerodynamic impulse loads when the blades pass the tower (Kallehave et al., 2015). To avoid resonance phenomena, the first natural frequency f_{1st} should be sufficiently separated from the turning rotor-induced frequencies f_{1P} and blade-passing frequency f_{3P} . The structure's natural frequency should be between f_{1P} and f_{3P} (Gentils et al., 2017).

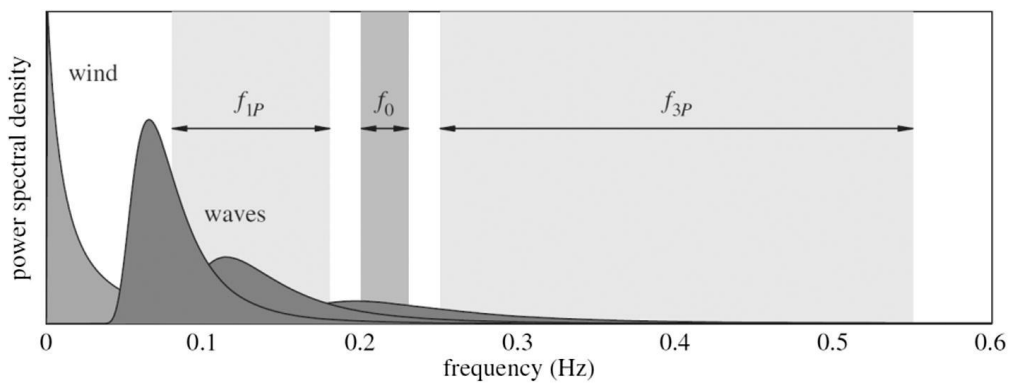


Figure 4-3 Illustration of typical excitation ranges of a modern OWT (Kallehave et al., 2015)

According to (DNV GL, 2010b), the first natural frequency should avoid rotor-induced frequencies with a tolerance of $\pm 5\%$:

$$f_{1P \pm 5\%} \leq f_{1st \pm 5\%} \leq f_{3P \pm 5\%} \quad (4.3)$$

The cut-in and rated rotor speed of the NREL 5MW are 6.9 rpm and 12.1 rpm, respectively. f_0 would be roughly 0.20– 0.23 Hz for a 6–8 MW offshore wind turbine on a monopile constructed for the soft–stiff frequency range of Ducorit Data Sheet. Therefore, resonance constraints are:

$$0.212 \text{ Hz} \leq f_{1st} \leq 0.328 \text{ Hz} \quad (4.4)$$

4.2.3.2. Stress Constraints

In the Ultimate Limit State (ULS), the maximum stress of the support structure $\sigma_{VM,max}$ (Von Mises) should stand below the allowable stress limits $\sigma_{VM,allow}$. The following inequality expresses this.

$$\sigma_{VM,max} \leq \sigma_{VM,allow} \quad (4.5)$$

where the allowable stress value $\sigma_{VM,allow}$ is derived from Equation (4.6):

$$\sigma_{VM,max} = \frac{\sigma_{y,Steel}}{\gamma_m \cdot \gamma_f} \quad (4.6)$$

where, $\sigma_{y,steel}$ is the steel component's yield strength, and γ_m and γ_f are the PSFs for material and consequence of failure, respectively. The yield strength for S355 steel is 355 MPa is adopted from (Arshad & O'Kelly, 2013). Furthermore, the PSFs for material γ_m and failure γ_f are 1.1 and 1.0 (IEC, 2005), respectively. Thus, the allowable stress $\sigma_{VM,allow}$ is 322.7 MPa.

4.2.3.3. Deformation Constraints

The stability of the monopile foundation is a vital factor in ULS. Therefore, rotation and deflection constraints have been defined to ensure that pile-head deflection d_{pile} and seabed rotation θ_{seabed} values are less than allowable values. These constraints could be expressed by:

$$d_{pile} \leq d_{allow} \quad (4.7)$$

$$\theta_{seabed} \leq \theta_{allow} - \theta_{inc} \quad (4.8)$$

where, θ_{inc} is the installation uncertainty and was chosen analytically here at 0.1° . According to (DNV GL, 2010b), the values of d_{allow} and θ_{allow} were fixed at 0.1 m and 0.5° , respectively.

The material safety factor γ_m of 1.0 was applied for the soil strength in this section (DNV GL, 2016).

4.2.3.4. Buckling Constraints

The risk of instability due to buckling is not negligible in a monopile's design and optimisation process due to the slenderness of the tower and sizeable weighted Rotor – nacelle assembly (RNA) at the top. The results of the ULS static analysis are used as pre-stress loads. To avoid this type of failure in ULS mode, the load multiplier L_m , the ratio of the critical load to the current applied load, should be larger than the allowable load multiplier $L_{m,allow}$. If the buckling load multiplier is negative, the model will buckle when the applied loads are reversed (and scaled by the multiplier). For example, A buckling multiplier of -0.75 implies that the part will buckle with a 750 Pa compression load if a pressure of 1000 Pa is applied to the model, which puts it in tension. According to (DNV GL, 2010b), $L_{m,allow}$ value of 1.4 has been chosen. This constraint could be expressed by:

$$L_m \geq L_{m,allow} \quad (4.9)$$

4.2.3.5. Fatigue Constraints and Assessment

As discussed earlier, fatigue is one of the main governing factors for the OWT support structure design process. Therefore, the design life-number of cycles N_{life} could be assessed based on rated rotor speed n_{rated} (12.1 rpm) and availability η_a (98.5%) of the chosen met ocean region (Kuhn, 2001). Thus, considering a lifetime requirement of 20 years (DNV GL, 1987, 2010a), the number of cycles to be expected is 1.25×10^8 : For practical fatigue design, welded joints are divided into several classes, each with a corresponding design S-N curve. Using the design life number, N_{life} , and S-N curve, the design fatigue stress range, $\sigma_{f,Design}$ can be derived. In this case study, global fatigue stress is considered.

$$N_{life} = \eta_a \times n_{rated} \times (60min \times 24hr \times 365day \times 20years) \quad (4.10)$$

The basic design S_N curve is given as:

$$\log N = \log \bar{a} - m \log \Delta \sigma \quad (4.11)$$

where N is the predicted number of cycles to failure for stress range $\Delta\sigma$, m is the negative inverse slope of the S-N curve and $\log\bar{a}$ is the intercept of the design S-N curve with the log N-axis by the S-N curve. However, as the fatigue strength of weld joints is dependent on plate thickness, the thickness of the adjoining plate is essential, and the thickness effect needs to be considered:

$$\log N = \log\bar{a} - m \log \left(\Delta\sigma \left(\frac{t}{t_{ref}} \right)^k \right) \quad (4.12)$$

where t_{ref} is 25mm for plates, t is the thickness of place where the crack is most likely propagated, and k is the thickness exponent (0.1 for tubular girth weld and 0.25 for threaded bolts).

4.2.3.5.1. Damage Equivalent Load approach in fatigue assessment of optimised model

To produce reliable, cost-effective, and safe designs for offshore wind turbines, it is necessary to accurately model the site-specific wind-wave joint distribution in fatigue load calculations. However, the number of design load simulations required to account for every possible combination of wind and wave parameters for every wind direction and wave direction is prohibitively high. This results in equivalent wind-wave correlations for design purposes. Wind-wave correlations can reduce the number of possible wind-wave parameter combinations for design load calculations. Still, they can also present difficulties maintaining the hydrodynamic fatigue distribution regardless of the underlying full-wave climate. The OWECs tool software uses the new method described in (Passon, 2015) based on the preliminary work carried out in (Passon & Branner, 2015). The new approach retains hydrodynamic fatigue damages from the whole wave climate across the structure. It focuses on an adequate consideration of dynamics for the fatigue design of hydrodynamically sensitive offshore wind turbines.

This section presents a summary of contained and processed the met ocean data of the DLC in FLS using OWECs software, the in-house tool in Seaway7 company to generate Damage Equivalent Load (DEL) in FLS analysis considering time-series analysing. At first, 3 different DLCs are defined in Table 4-2.

Table 4-2 An overview of the individual DLCs in the load case

DLC	Total Probability [-]	# Cases in Load Case Table	# Non-zero probability cases
1.2	0.8849529	6336	3776

6.4	0.0550471	1728	700
7.2	0.1400000	8064	4476
ALL	1.0000000	16218	8952

Figure 4-4 shows the (omnidirectional) probability in [%] over design load cases. It was observed that DLC1.2 can represent the most fatigue limit state because it covers more than 80% of the fatigue damage.

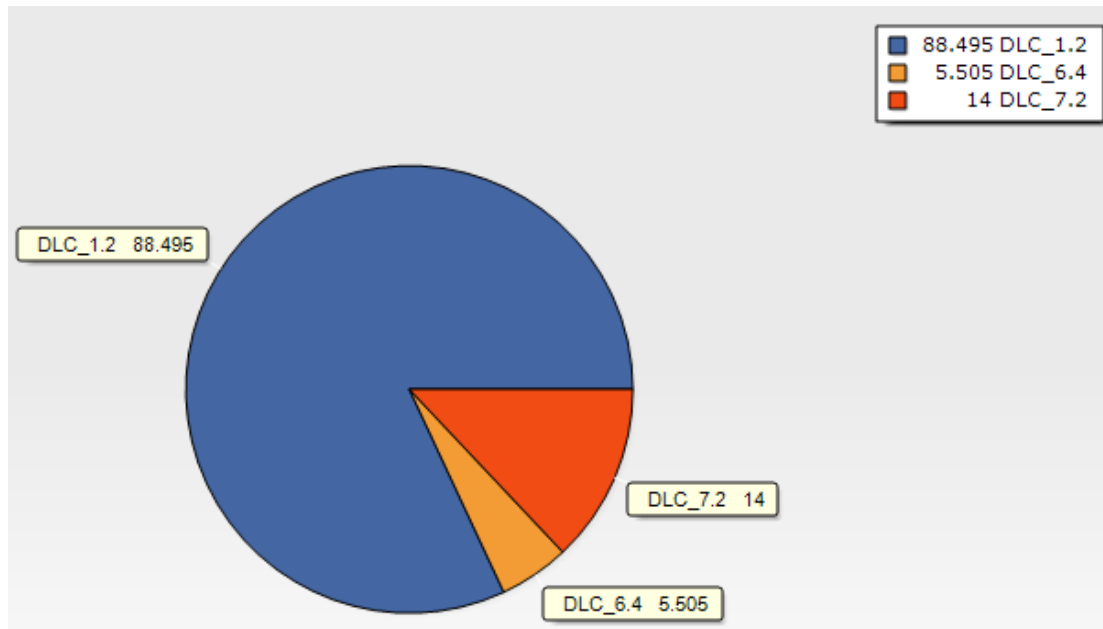


Figure 4-4 Probability over design load cases (All Directions) in [%]

Probabilities over wind/wave speed needs to be consider. Figure 4-5 show the omnidirectional probability in [%] over wind speed for the combined DLCs:

- Design Load Case: 1.2
- Design Load Case: 6.4
- Design Load Case: 7.2

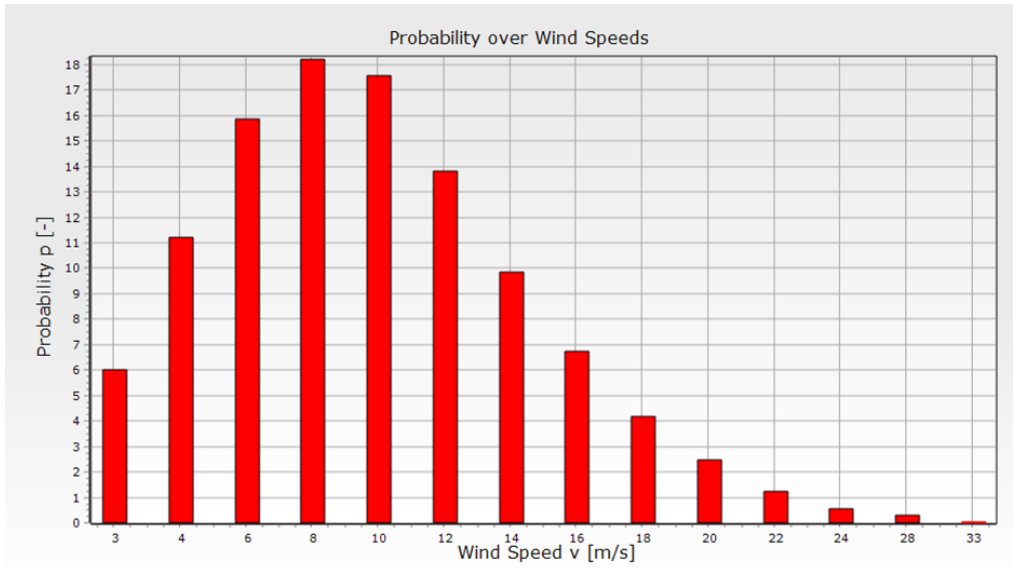


Figure 4-5 Probability over wind speed (All Directions) in [%]

Figure 4-6 shows the probability distribution over wind directions, i.e. wind rose, for all DLCs in the load case table.

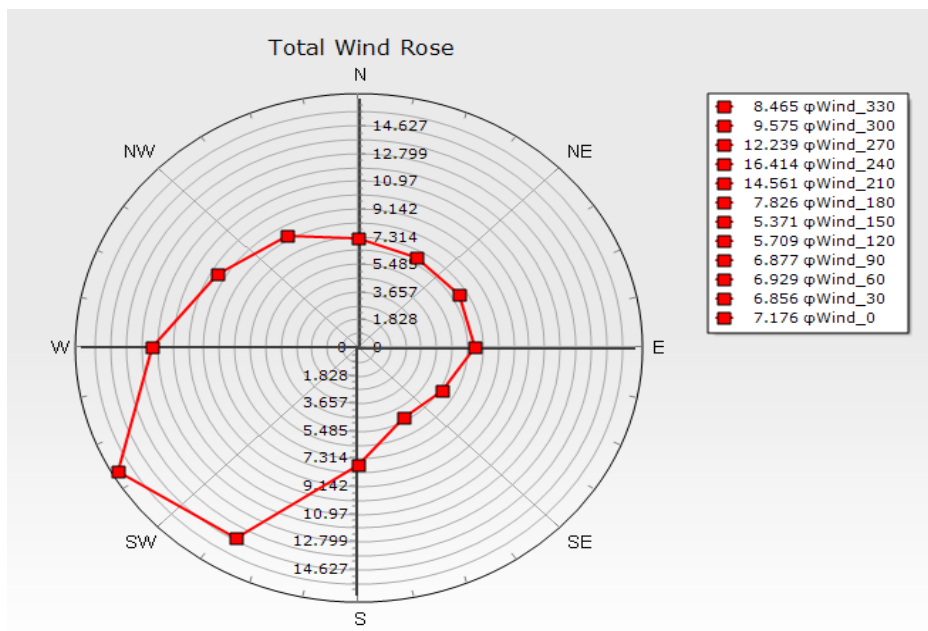


Figure 4-6 Wind Rose (All Directions, All DLCs) in [%]

Figure 4-7 shows the probability distribution over wave directions, i.e. wave rose (wind-sea), for all DLCs in the load case table.

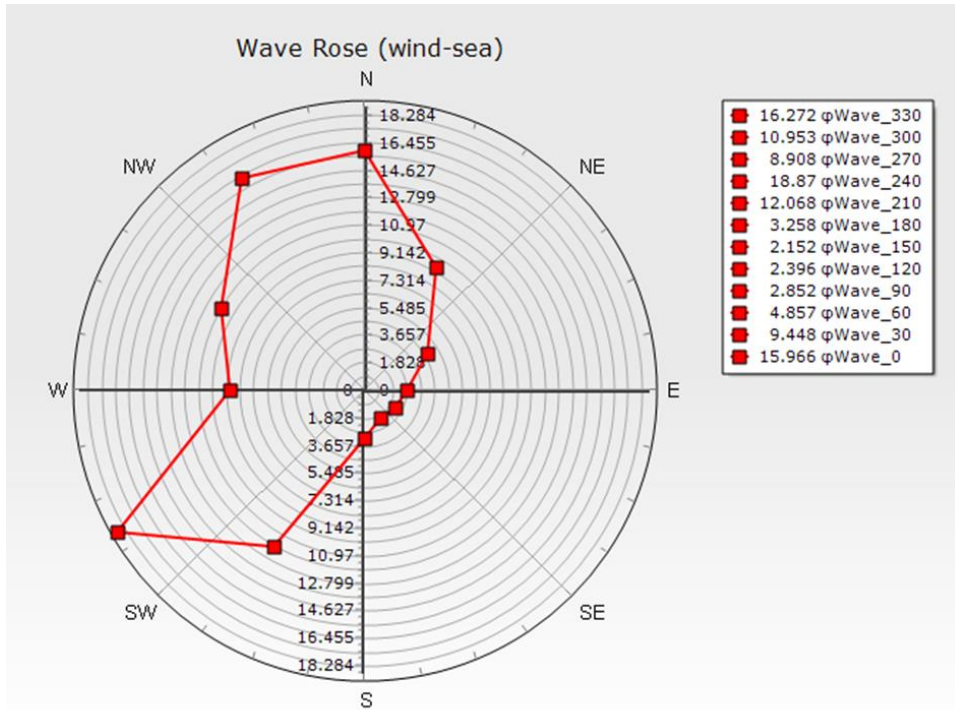


Figure 4-7 Wave Rose (wind-sea) (wind-sea, All Directions, All DLCs) in [%]

Now by having both wave/wind directions (Figure 4-8), the effective misalignment figure can be generated in Figure 4-9 for all DLCs for FLS.

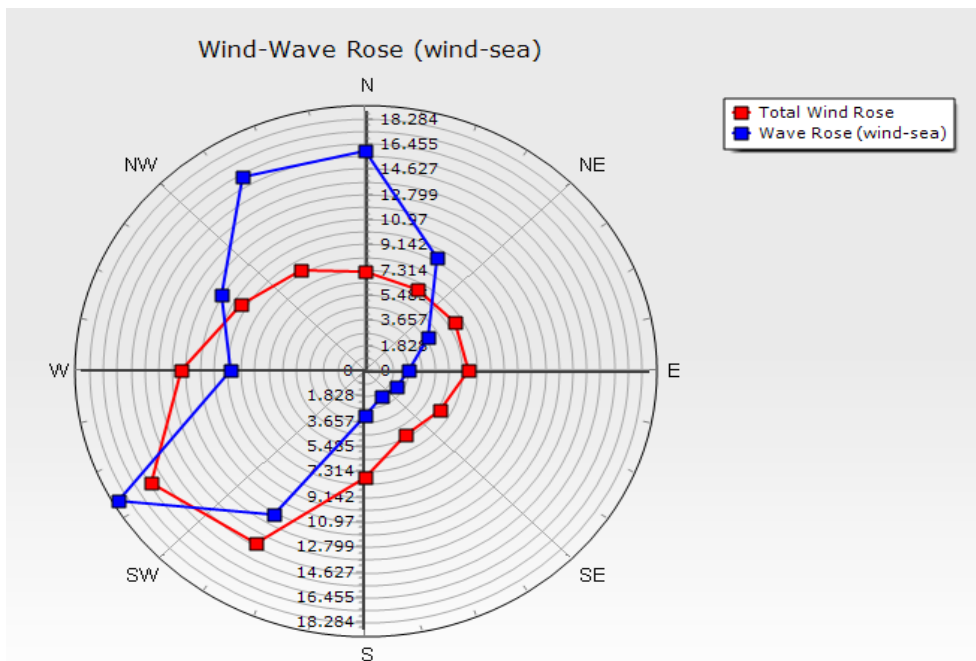


Figure 4-8 Wind and Wave Rose (wind-sea, All Directions, All DLCs) in [%]

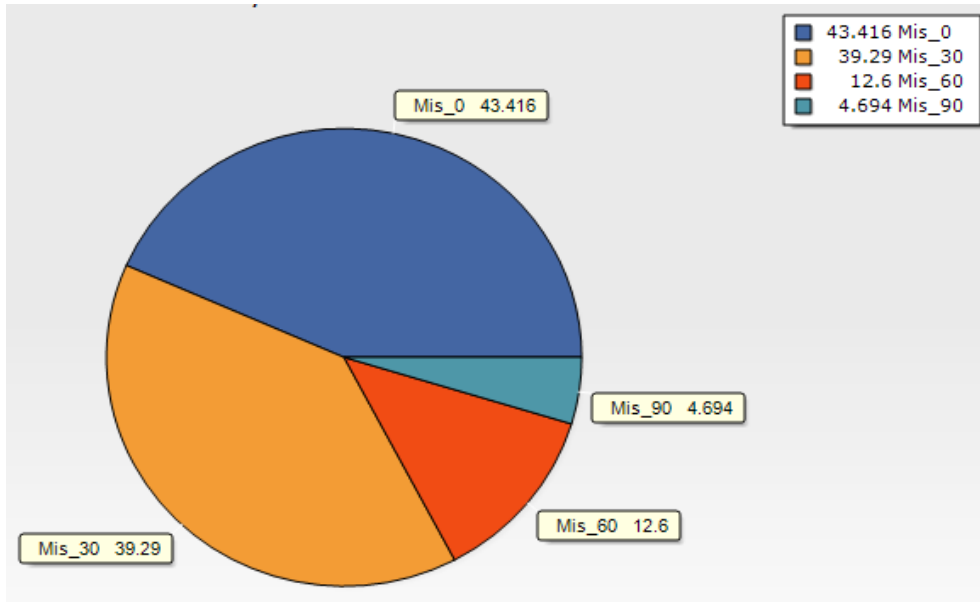


Figure 4-9 Wind-Wave Misalignment in 0-30-60-90 degrees (wind-sea, All Directions, All DLCs) in [%]

Considering Wind-Wave misalignments, the in-house OWECs tool calculated the combined wave/wind directional Moments/Loads for all three DLCs in different altitudes in monopile, presented in Table 4-3 and Table 4-4. In addition, the eigenfrequency of the structure was extracted from the first mode of the modal analysis of the FE Model.

Table 4-3 Damage Equivalent Moments (Combined Wave/Wind) in compass directions for optimised monopile

Mode	m	Lifetime	N _{ref}	0	30	60	90	120	150	Omni	
[-]	[-]	[years]	[kNm]	[kNm]	[kNm]	[kNm]	[kNm]	[kNm]	[kNm]	[kNm]	
INTERFACE	1	5	20+2	1e+7	35496	32347	30116	31503	36789	38442	38442

Table 4-4 Damage Equivalent Load (Combined Wave/Wind) in compass directions at Interface of optimised monopile

Mode	m	Lifetime	N _{ref}	0	30	60	90	120	150	Omni	
[-]	[-]	[years]	[-]	[kN]	[kN]	[kN]	[kN]	[kN]	[kN]	[kN]	
INTERFACE	1	5	20+2	1e+7	163.37	181.95	190.1	182.36	165.72	155.06	190.1

The fatigue assessment on the central column has been performed using the damage equivalent loads (DEL) approach, only assessing the primary circumferential welds. This assessment will be done on an optimised design in order to observe if the optimisation results meet the fatigue assessment criteria or not. The approach has adopted a Category ‘D’ of the S-N curve. Appropriate SCFs have been applied where there is a change in plate thickness and at the conical transitions. “In air” S-N curves have been considered above the splash zone, and “in

water with cathodic protection” curves below the splash zone for the entire field life. The splash zone is coated, and the coating life is 14 years.

Consequently, the splash zone is treated as “in the air” for the first 14 years and then treated as water without corrosion protection after that. The average corrosion allowance is applied after the first 14 years. It is assumed that the length of plates in circumferential welds is between 2.5m to 3.5m for current thicknesses. According to DNV-RP-C203 (DNV GL, 1987), the wall thickness at each weld was checked to achieve the required fatigue life with a Design Fatigue Factor (DFF) of 3 (In this case, $3 \times 20\text{years} = 60\text{years}$).

The stress concentration factor (SCF) for welding between plates with different thicknesses can be derived by:

$$SCF = 1 + \frac{6(\delta_m + \delta_t - \delta_0)}{t \left[1 + \frac{T^{1.5}}{t^{1.5}} \right]} \quad (4.13)$$

where T is the thickness of the thicker plate, t is the thickness of the thinner plate, δ_m is the maximum misalignment, $\delta_t = \frac{1}{2}(T-t)$ is the eccentricity due to change in thickness and $\delta_0 = 0.1$ is misalignment inherent in S-N Data for butt welds. Also, the SCF for the tabular side and cone side can be calculated as:

$$SCF = 1 + \frac{0.6t\sqrt{D_j(t+t_c)}}{t^2} \tan\alpha \rightarrow \text{for Tabular side} \quad (4.14)$$

$$SCF = 1 + \frac{0.6t\sqrt{D_j(t+t_c)}}{t_c^2} \tan\alpha \rightarrow \text{for Cone side} \quad (4.15)$$

where D_j is cylinder diameter at a junction, t plate thickness, t_c is cone thickness, and α is the slope angle of the cone. When the thicknesses are revised and redesigned at the end of the optimisation process, a fatigue assessment shall be performed to check if the structure's lifetime is acceptable considering standard DFF.

In FE Model, an appropriate S-N curve of slope m and $\log \bar{a}$ is provided by DNV-RP-C203. The maximum fatigue stress range $\sigma_{f,max}$ in the OWT support structure subjected to the fatigue loads is calculated from the FEA simulations. The minimum fatigue safety ratio $f_{sr,min}$ could be derived from the design stress σ_{design} over the maximum fatigue stress $\sigma_{f,max}$ in the structure.

This safety ratio should stay above the allowable fatigue safety ratio f_{allow} , which is equal to one time the material PSF γ_m . Fatigue constraint can be written as:

$$f_{allow} \geq f_{sr,min} \quad (4.16)$$

The PSF of material for the Fatigue Limit State is 1.15 (DNV GL, 1987, 2010a); therefore, f_{allow} is equal 1.15. Finally, the fatigue life of the optimised model will be assessed in Section 6.1.3 by the DNV S-N curve method with calculated DEL. This will validate the FE model and approve the structure fatigue design approach.

At this stage, all constraints are described, and Table 4-5 summarises all structural constraints that have been used in this study.

Table 4-5 Upper and Lower bound of the constraints

Constraint	Name	Unit	Lower Bound	Upper Bound
1 st Natural frequency	f_{1st}	[Hz]	0.21	0.328
Maximum equivalent Stress (Von Mises)	$\sigma_{VM,max}$	[MPa]	-	323
Pile head deflection	d_{pile}	[m]	-	0.1
Pile head rotation	θ_{pile}	[°]	-	0.4
Buckling load multiplier	L_m	-	1.4	-
Minimum fatigue safety ratio	$f_{fs,min}$	-	1.15	-

4.2.4. Genetic algorithm utilisation

As the FE Model is parametric, the parameters involved in the optimisation process in the multi-objective GA procedure can be easily chosen and updated. The initial samples are created and individually solved by the respective module during optimisation. After all the initial samples have been solved, the specified optimisation algorithm is automatically run. The optimisation module suggests a candidate design that meet the requirements at the end of the process. A GA is divided into five parts: initialization, fitness assignment, selection, crossover, and mutation (Kharmanda et al., 2014). The number of initial samples should be at least ten times the number of design variables. This value was increased by 200 points in this study to improve the chances of finding a better solution (Haupt et al., 2004). Convergence speed is affected by the number of samples per iteration.

In this study, an empirical value of 50 is chosen. The output parameters' maximum spread, mean, and standard variation calculates the convergence criterion. The optimisation was

assumed to have converged when the criteria value reached 1.5 per cent, implying a homogeneous population. The maximum number of iterations is the blocking criteria of the algorithm. Cross-over probability is a value between 0 to 1. A low value encourages using available design points (parents), whereas a high value encourages the exploration of new designs through offspring generation. A crossover probability of 0.90 (Haupt et al., 2004) is used in this study. The probability of mutation must be between 0 and 1. A higher value increases the algorithm's randomness until it becomes a simple random search for a value of one. This study uses a typical mutation probability of 0.01 (Haupt et al., 2004). The “performance” of a genetic algorithm depends highly on the method of encoding candidate solutions into chromosomes and “the particular criterion for success,” or the fitness function measuring. The probability of crossover, the probability of mutation, the population size, and the number of iterations are all critical details. After a few trial runs, these values can be adjusted based on the algorithm's performance. In Table 4-6, the main characteristics and settings of the GA have been provided.

Table 4-6 Settings of GA

Parameter name	Value
Number of Initial Samples	200
Number of Samples per Iteration	50
Convergence Stability Criteria	1.5%
Maximum Number of Iterations	25
Crossover Probability	0.9
Mutation Probability	0.01

After applying GA settings to the parametric FEA model, the requested “Candidate Points” number under the properties table pane displays. The quantity of gold stars or red crosses next to each objective-driven parameter indicates how well it matches the specified objective. For instance, three red crosses are the worst, and three gold stars represent the best. The user can also add and edit its candidate points, view values of candidate point expressions, and calculate the percentage of variance for each parameter for which a goal has been established in the table panel.

4.2.5.FEA geometry model validation

The geometry is validated by comparing the results of the current and 5MW NREL reference models. This case study was also the opportunity to test the mesh convergence study to ensure reasonable accuracy and an appropriate number of elements in the model. A case study was

defined by (Damiani et al., 2013), in which a 2MN rotor thrust load was applied to the tower's top, and the soil was considered rigid. Considering the weight of the nacelle and blades, the results show good agreement with the reference model. The result values are presented in Table 4-7, confirming the present model's validation.

Table 4-7 Deformation in the reference model and current model

Load case	Deformation		
	Current model	Reference model	%Diff
2MN +Weight	1.676 m	1.644 m	+1.94%

4.3. Reliability-Constrained Optimisation (RCO)

4.3.1. Framework definition

Defining the RCD framework using reliability assessment, regression, response surface and Monte Carlo simulation to find the optimal design for OWT by satisfying the criteria specified by design standards, which correspond to a target reliability level. The model combines OWT deterministic optimised candidate design solutions and a simulation model with the Six Sigma reliability assessment. Figure 4-10 illustrates the flowchart of the reliability-constrained design optimisation framework developed in this work.

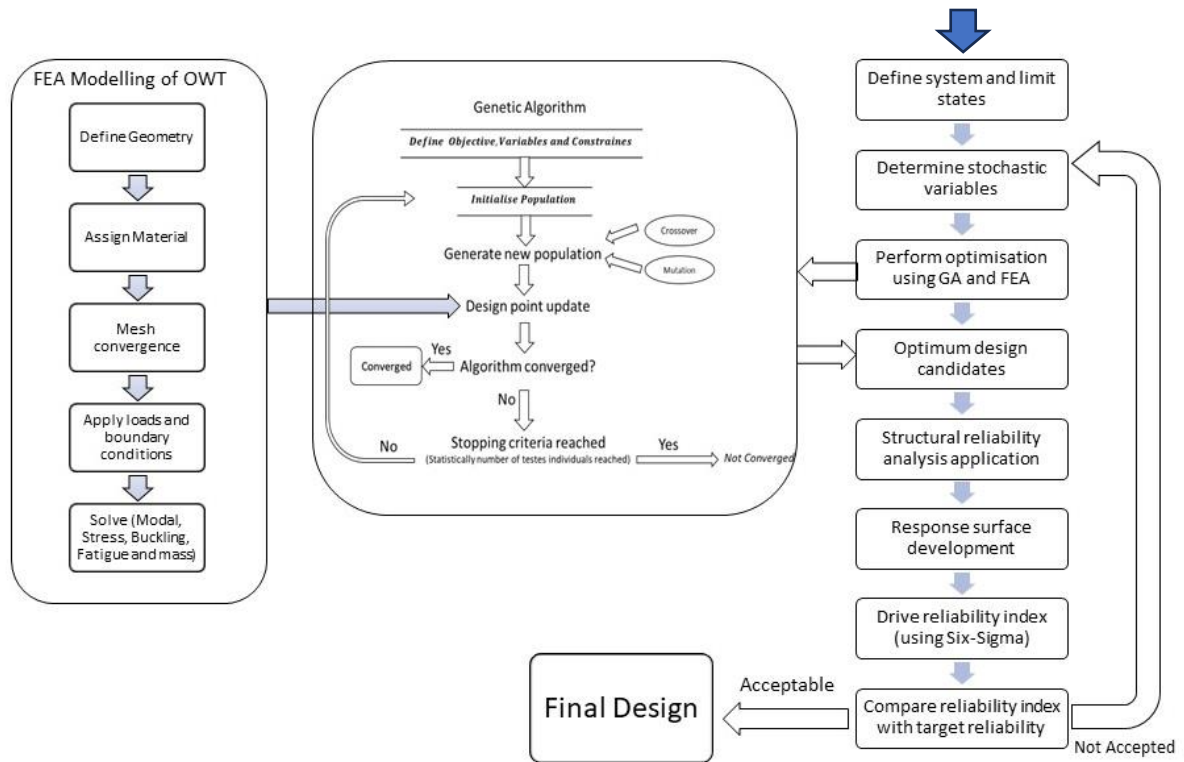


Figure 4-10 Flowchart of Reliability-Constrained Design optimisation framework

To perform the SRA, a parametric FEA model was built in the ANSYS© at the first step. Then, the various input parameters are given using their corresponding distributions. The developed FEA model is then used to run a series of FEA simulations through the Design of Experiment (DoE) module in the DesignXplorer© of ANSYS.

Choosing a proper sampling method is vital in reliability assessment. At first, the Monte Carlo Sampling (MCS) method is used to calculate the probability of failure (P_f). The MCS approach tries to sample each random variable, X_i to provide a value \hat{x}_i . Then the limit state function is checked by those x_i values, and if the function is violated, it is noted as a failed structure.

$$P_f = \frac{n(g(\hat{x}_i) \leq 0)}{N} \quad (4.17)$$

where n is the number of trials in which the limit state function result is more than zero, $g(\hat{x}_i)$ is the limit state function, and N is the number of trials.

MCS can calculate the P_f heuristically but cannot transform the limit state function (Lee et al., 2014b). MCS randomly simulates the samples, depending on the probability density functions of input variables; therefore, P_f accuracy depends on the iterating sampling size. Latin Hypercube Sampling (LHS) by (Loh, 1996) is a variance reduction method that helps the user save time and reduce the number of iterations needed in the MCS method. In this study, LHS

with the number of samples equal to 1×10^7 is selected and applied to all the design constraint cases.

A good design point is typically the outcome of a trade-off between multiple objectives. As a result, optimisation procedures that lead to a single design point during design exploration should be avoided. Enough data on the existing design are required in order to answer "What-if" inquiries regarding how design factors affect product performance. The best judgments can be possibly made based on precise data, even if the design limitations change unexpectedly. DoEs and Response Surfaces (RS) provide all the data needed to develop simulation-driven products. The Response Surface method replaces the original input-output relationship with an approximation function. For the approximation function \hat{y} , typically a quadratic polynomial with cross-terms is used in the form:

$$\hat{y} = C_0 + \sum_{i=1}^n c_i \cdot x_i + \sum_{i=1}^n \sum_{j=i}^n c_{ij} \cdot x_i \cdot x_j \quad (4.18)$$

where, C_0 , c_i and c_{ij} with $i, j=1, \dots, n$ are the regression coefficients and x_i , $i=1, \dots, n$ are the n input variables. Equation (4.18) is also a regression model. The response domain was derived, and an appropriate response surface model was produced. The response surface model is the interpolation of the values in the multiple dimensions characterized by the DoE. Several types of response surfaces are available in the commercial package of ANSYS DesignXplorer© (Thompson & Thompson, 2017), including genetic aggregation, standard response surface full second-order polynomials, kriging algorithms, non-parametric regression, and the sparse grid. In this study, the standard response surface full second-order polynomials, with manual refinements, are adopted. The second-order model is the most common approximating polynomial model in response surface methods (Bezerra et al., 2008). The Central Composite Design (CCD) presented by (Box & Wilson, 1951) is the selected design, as it is the most recommended design for fitting second-order models (Brown & Brown, 2012). The goodness of fit metric is also packaged within the response surface module, calculated for the DoE points and can be assessed for verification points to check how accurately the response surface can predict the design points. The predicted and observed chart must be reviewed to show the goodness of fit of data for outputs in all limit state cases. Moreover, the output values should be checked to determine if most points fall on or near the line. The response surface correctly evaluates the values for most of the design points within its range, including the verification points.

The Six Sigma Analysis (SSA) function of the DesignXplorer© module in ANSYS is employed in this study for the probabilistic assessment. The Six Sigma Expression was created by Motorola initially (Harry & Motorola University Press., 1997). SSA can also determine the extent to which model uncertainties affect analysis results. To do so, SSA uses several statistical distribution functions to define uncertain parameters. In practice, Six Sigma analysis has been employed for robust design approaches in recent years.

In the ANSYS DesignXplorer© module, the parameters defined in the simulation have been recognized automatically. The user assigns design or random variables, and a statistical distribution function can be selected for each of these random variables.

Finally, the cumulative distribution function (CDF) is used to assess the P_f of the component. The resultant CDF value at any given point shows the probability that the relevant parameter value remains below that point. The equivalent reliability index β is evaluated through appropriate statistical transformation (Melchers & Beck, 2018).

4.3.2. Structural Reliability Assessment

Selecting appropriate stochastic variables and assigning appropriate statistical distributions are vital for the systematic consideration of uncertainty through reliability analysis. Even though the stochastic data are characterized in this application by normal distributions, the framework can accommodate any statistical distribution variables through appropriate consideration. In this section, ANSYS converted the input parameters from the DoE function and produced sets of stochastic variables based on the defined statistical distribution. A series of deterministic FEA simulations were performed, and then the results were exported to the Response Surface Module to map the response with those design points. The Six Sigma module uses these results to assess the system's reliability. The corresponding reliability index β is evaluated by appropriate statistical transformation (Melchers & Beck, 2018). Table 4-8 presents the mean values and standard deviation of the stochastic variables.

Table 4-8 Design Variables (Jonkman & Musial, 2010; LaNier, 2005; Melchers and Beck, 2018)

Stochastic Variables	Ultimate Load Case		Fatigue Load Case		CoV	Distribution Type as (DNV GL, 2014)
	Mean value	Standard deviation	Mean value	Standard deviation		
Wind Thrust (kN)	781	78.1	197	19.7	0.1	Normal
Torsional Moment (kN.m)	38,567	3856.7	3686	368.6	0.1	Normal
Tilting Moment (kN.m)	7876	787.6	3483	348.3	0.1	Normal

Steel Young's Modulus (GPa)	210	21	210	21	0.1	Normal
RNA Mass (Tonne)	350	35	350	35	0.1	Normal

When structural reliability analysis is carried out, suitable safety levels must be selected considering failure, applicable rules, access for inspection, and repair; this safety level is called the target safety level. According to DNV guidelines (Ashuri, 2012; DNV GL, 2010a), the designs' target annual failure probability is 1E-4.

It should be noted that, in DO, the methodology contains specified reliability as the PSF is included. Thus, these safety factors must be eliminated in the reliability assessment.

4.4. RCO Framework validation

The validation of an optimisation framework involves testing the performance and accuracy of the optimisation algorithm and the resulting solutions. Validation is essential to ensure that the optimisation framework is reliable and produces high-quality results. The objective of validation of an analytical procedure is to demonstrate that it is suitable for its intended purpose. There are several ways to validate an optimisation framework. In this case, analytical validation is selected. Analytical validation involves comparing the optimisation results with available analytical solutions or benchmarks. This method is useful when analytical solutions exist. The analytical validation can verify the correctness of the optimisation framework and its implementation.

In this study, a reliability-constrained optimisation framework for offshore wind turbine support structures is developed. First, a parametric 3D FEA model of Monopile OWT support structures is developed in ANSYS, taking account of stochastic material properties and environmental loads and optimised in the “Direct Optimisation” module in ANSYS. For details, please read Section 4.2.

Then, the model reliability was assessed in “ANSYS DesignXplorer®”. A six-sigma analysis function has been used to perform a reliability assessment on the FEA parametric model with the variables defined in the previous section. The sampling method is Latin Hypercube Sampling (LHS), with 10^7 samples. In order to find the probability of failure, a cumulative distribution function (CDF) is extracted and utilised. The corresponding reliability index β is evaluated by appropriate statistical transformation (Melchers & Beck, 2018). In the validation process, there is no need to apply all limit states. Comparing the results with just the same

condition is enough to save the calculation time. Therefore, only ULS is considered in this section, as ULS check is always a first check in conceptual design process.

Performing the reliability assessment and finding the reliability index, β , using the H&L method or FORM, described in Section 3.2.1.2, is the primary step in the analytical validation of the RCO optimisation framework. First, a performance function needs to be defined to start FORM. For our monopile design, there is a dependent variable (here, in this case, maximum equivalent stress from ULS) and several independent variables (here, in this case, Thrust load and Bending Moments in ULS and Steel Young Modulus). Then, using multivariate regression analysis explained in Section 3.4.2, the relation between dependent and independent variables is processed.

$$\sigma_{VM,max} = [a_0, a_1, \dots, a_6] \begin{bmatrix} 1 \\ x_1 \\ x_1^2 \\ \vdots \\ x_3 \\ x_3^2 \end{bmatrix} \quad (4.19)$$

where (a_0, a_1, \dots, a_6) are seven regression coefficients. As discussed, the probability of failure of the system is defined as $P_f = P[g(x) < 0]$, where $g(x)$ is the limit state function that implies the critical failure surface and $X = [x_1, x_2, \dots, x_n]$ is a vector containing n stochastic variables. An equal or greater number of sample points is expected to calculate the coefficients $(2n+1)$. Therefore, the number of regression coefficients is chosen as 7. Now we can define the performance function in Eq (4.20) at the first step of FORM Hasofer and Lind algorithm:

$$g(x) = \sigma_{VM,allow} - [a_0, a_1, \dots, a_6] \begin{bmatrix} 1 \\ x_1 \\ x_1^2 \\ \vdots \\ x_3 \\ x_3^2 \end{bmatrix} \quad (4.20)$$

The mean value is set as an initial design point, $x_{i,k} = \mu_{x_i}$ ($i = 1, 2, \dots, n$) and calculation of gradients of performance function is started. Then the initial reliability index starts using mean value method and direction cosine.

$$\beta = \frac{\mu_{\tilde{g}}}{\sigma_{\tilde{g}}} = \frac{g(\mu_x)}{\sqrt{\left[\sum_{i=1}^n \left(\frac{\partial g(\mu_x)}{\partial x_i} \right)^2 \cdot \sigma_{x_i}^2 \right]}} \quad (4.21)$$

$$\alpha_i = - \frac{\left(\frac{\partial g(\mu_x)}{\partial x_i}\right)^2 \cdot \sigma_{xi}}{\sqrt{\left[\sum_{i=1}^n \left(\frac{\partial g X^*}{\partial x_i} \sigma_{xi}\right)^2\right]}} \quad (4.22)$$

Here, $x_{i,k}$ indicates the i -th element in the vector X_k of the k -th iteration, and μ_{xi} is the mean value of the i -th element. Now a new design point is computed, X_k and U_k following by the gradients.

$$x_{i,k} = \mu_{x_i} + \beta \sigma_{xi} \alpha_i \quad (4.23)$$

$$u_{i,k} = \frac{x_{i,k} - \mu_{x_i}}{\sigma_{xi}} \quad (4.24)$$

Using Eq. (4.23) and Eq. (4.24), the reliability index β and direction cosine α_i can be computed. And the iteration needs to be repeated until the convergence of β .

$$\alpha_i = - \frac{\left(\frac{\partial g X^*}{\partial x_i}\right) \cdot \sigma_{xi}}{\sqrt{\left[\sum_{i=1}^n \left(\frac{\partial g X^*}{\partial x_i} \sigma_{xi}\right)^2\right]}} \quad (4.25)$$

$$\beta = \frac{g(U^*) - \sum_{i=1}^n \left(\frac{\partial g(U)}{\partial x_i}\right) \cdot \sigma_{xi} u_i^*}{\sqrt{\left[\sum_{i=1}^n \left(\frac{\partial g(U^*)}{\partial x_i}\right)^2 \sigma_{xi}\right]}} \quad (4.26)$$

The MATLAB code used to calculate the reliability index from above analytical solution is provided in APPENDIX C.

Finally, the estimated reliability index for reference and optimised model from FORM must be compared with the reliability index from the Six Sigma method in ANSYS with the design ULS load analysis and variables.

For the optimised model, the ULS maximum equivalent stress probability of failure, $P_f(f_{sr} \leq 322.7 \text{ MPa})$, is about $5.3E-4$ using the ANSYS six sigma module, while the calculated value by FORM was $8.31E-4$. Then, the corresponding β for the initial model is 3.14 , while the corresponding β for ANSYS six sigma method is 3.27 . The summarized results from both FORM, and Six Sigma methods are in Table 4-9.

Table 4-9 Summarized results of FORM and Six Sigma method

Case	Probability of Failure	
	Six Sigma (ANSYS)	FORM
Initial design	2.81E -14	1.07E -12
Optimise design	5.30E-4	8.31E-4

Case	β	
	Six Sigma (ANSYS)	FORM
Initial design	7.51	7.0245
Optimise design	3.27	3.14

Both reliability assessment tools, i.e. the developed non-intrusive formulation and ANSYS DesignXplorer© module, give reasonably close results in the optimised model. The deviation of reliability calculation in ANSYS results from FORM calculation is due to a limitation in the number of simulations performed with ANSYS. Furthermore, the fact that the computational time required by the non-intrusive formulation of FORM is much less than that required by the six-sigma analysis in ANSYS, which is a great advantage for this method in simple case studies but in full-scaled coupled and more complicated models with different limit states the computational time will be increased. The advantage of the ANSYS DesignXplorer© module over FORM is:

1. DesignXplorer© module allows engineers to model complex systems that involve multiple variables and parameters. In contrast, FORM is limited to analysing systems with only a few variables and parameters.
2. DesignXplorer© module uses advanced algorithms to perform optimisation, sensitivity, and robustness analyses. This allows engineers to quickly identify the most critical design factors and make informed decisions to improve the reliability of the structure.
3. DesignXplorer© module is integrated with other Six Sigma tools, such as Monte Carlo simulation and Design of Experiments (DOE). This enables engineers to perform more comprehensive reliability analyses and identify the root cause of failures.
4. DesignXplorer© module provides a user-friendly interface that makes setting up and running simulations easy. This can save time and reduce the risk of errors in the analysis.

Overall, the DesignXplorer© module in Six Sigma offers several advantages over the FORM approach when finding a structure's reliability in 3D structure in which the correlation between parameters affecting objective function is not clear initially. However, FORM still can give us

a fair result to validate the framework and compare the reference and optimised model reliability index with two different assessing methods.

4.5. Cost analysis of optimised design

The optimisation study combined a numerical optimisation algorithm, reliability assessment and cost analysis with different calculations, as Figure 4-11 sketches. This section focuses on estimating LCOE for reference and optimised models to see the effect of optimisation results.

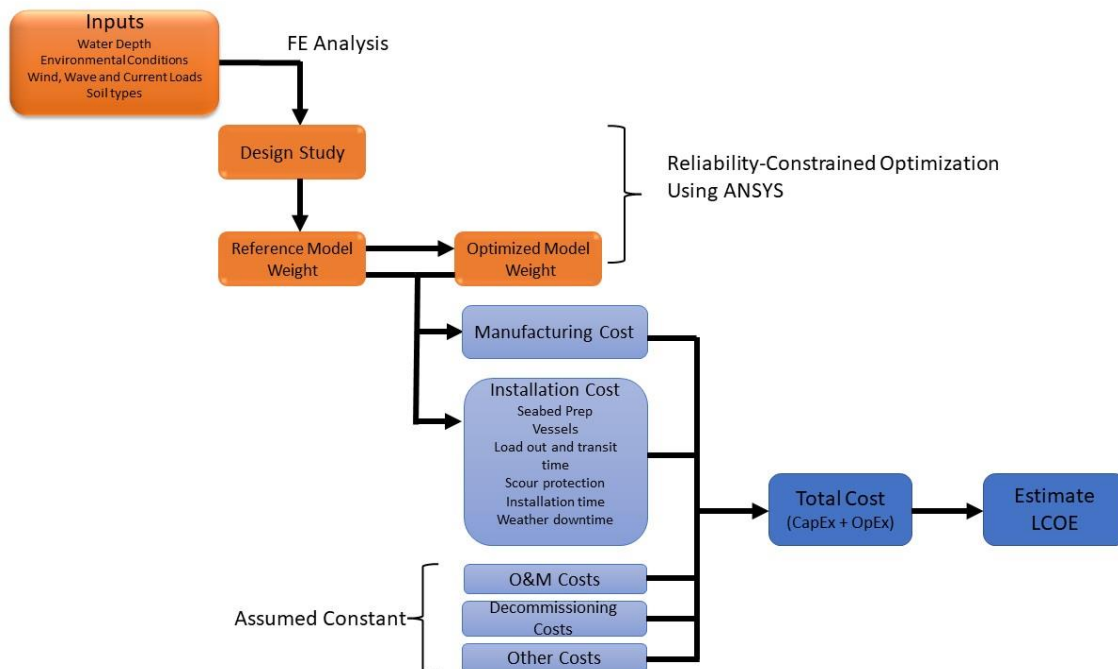


Figure 4-11 Methodology flow chart

To review the study up to this section, the input to the problem is the list of information needed to execute the finite element analysis and optimisation algorithm and the specifications for the essential design tools. The numerical optimisation process needs:

- An objective function: F_{obj} is an objective function that is chosen to minimize M_{global} , the global mass of the support structure.
- Design variables: any parameters that influence the global mass, such as wind turbine overall design, thicknesses and diameters of the pile, tower or transition piece.
- Constraints: low or upper bounds of design variables, but also limits on stresses, strains, or loads. The bound of constraints keeps the design space in a feasible area where the optimum values are found.
- State-of-the-art reliability-constrained optimisation framework takes to involve target reliability in the optimisation process.

The input for the modelling of the reference turbine in ANSYS software, in order to perform the numerical analysis and simulation, includes:

- Environmental conditions
- Wind, wave, and current load profile calculations
- A complete description of turbine aerodynamics, structure, control, and safety strategies regarding the regulations so that the structure's response to the wind inflow shall be determined and relevant extreme and fatigue loads can be obtained.

Finally, the cost analysis has been done to compare the LCOE prices of the reference and optimised models, considering the most influential parameters involved in reducing the weight of the support structure.

4.5.1. Wind farm specification

Regarding the cost analysis and estimation of LCOE, the initial step is to define a wind farm. The wind farm features are assumed to be a fixed bottom site consisting of 100 wind turbines rated at 5.0 MW, yielding a total plant capacity of 500 MW. The turbines are supposed to operate for 20 years without any catastrophic O&M incidents. The farm is also assumed to be 30km far from the shore. The summary of the farm characteristics is presented in Table 4-10.

Table 4-10 Wind farm characteristics

Parameter	Description/Value
Location	North Sea
Turbine-rated power (MW)	5
Number of Turbines	100
Wind plant capacity (MW)	500
Water Depth (m)	20
Substructure	Monopile
Distance from Shore (Km)	30
Project design life (years)	20

4.5.2. Cost breakdown

Cost definitions and terminology were presented in section 2.8.1. In this part, the breakdown of the CapEx for the fixed-bottom offshore reference project is explained and illustrated in Figure 4-12. Again, the shades of green represent the turbine cost, shades of blue represent the balance of system (BOS) costs and shades of purple represent financial costs. This chart's main objective is to find the key factors that affect a monopile's cost by optimising the structure's weight.

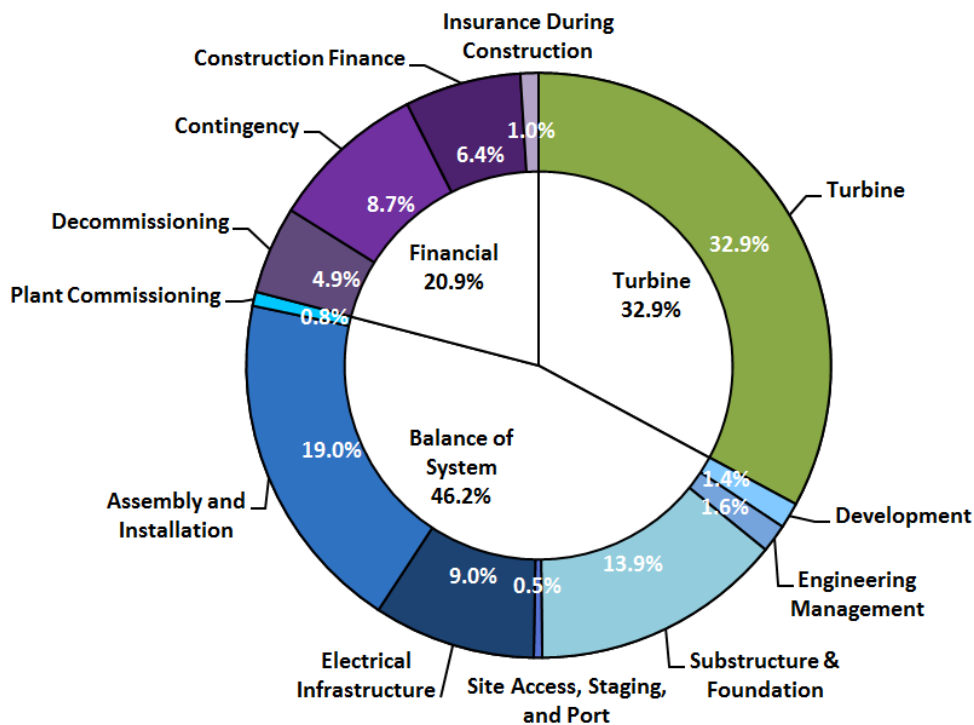


Figure 4-12 CapEx cost breakdown for a fix-bottom offshore wind turbine (Stehly & Duffy, 2020)

Maintenance costs for offshore wind farms are projected to be roughly 25% of the Levelized Production Cost (LPC) (Stehly & Duffy, 2020). The LPC is the average cost of one production (kWh) during the estimated lifetime of a wind power station, stated in £/kWh. With predicted CapEx reductions in the coming years, this ratio might rise to 33 per cent of the total lifetime cost. However, they are just estimations that could drastically change in the future primarily because of the evolutionary strategies in Operating and maintenance (O&M). Additionally, some big projects are still under warranty, preventing us from observing the actual O&M costs. Conversely, as turbine technology improves and becomes more reliable, O&M costs should decrease. In this study, the effects of weight reduction in O&M and decommissioning costs are much less than the “Turbine manufacturing” and “Assembly, Installation” sections, so the values remain constant.

Insurance and contingency expenses for the support structure during the lifetime were projected at 10% and 12%, respectively, according to (Stehly & Duffy, 2020). However, these figures should fall in the future, along with offshore wind industry uncertainties, as more experience is gathered. The study did not include these expenditures due to difficulties calculating them for various foundations and substructures. Furthermore, because they are considered a fixed

percentage value that is the same for all support structures, excluding them from the study provides a more precise cost comparison and more comprehensible outcomes.

4.5.3. Production process

Production of the OWT monopile support structure can be divided into three sections, illustrated in Figure 4-13.

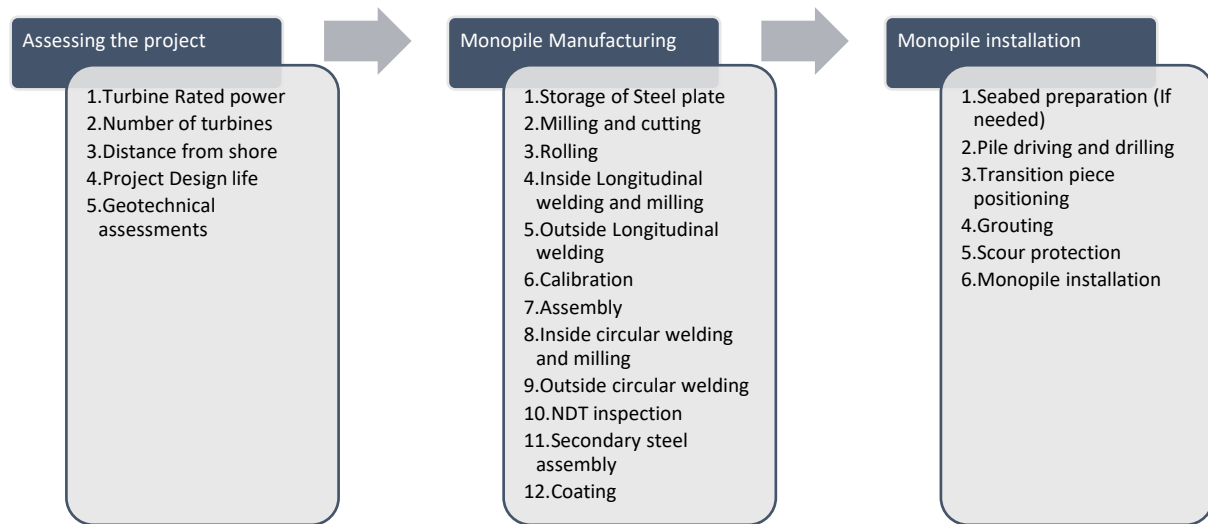


Figure 4-13 Production process of a monopile

Assessing the project is an initial step before manufacturing and installation. Understanding the project size, the farm's distance from shore and geotechnical assessments are vital. Next, a monopile and its transition piece are made using a reasonably easy and automated method. "Cans," cylinders of the rolled plate with a longitudinal seam, are commonly used to construct piles. It entails a number of fabrication steps, which are listed in Figure 4-13.

4.5.4. Levelized Cost of Energy (LCOE)

This section gives a methodology for estimating the levelized cost of energy (LCOE) for both reference and optimised 5MW NREL offshore wind turbine performed in the previous section. LCOE is a metric used to assess the cost of electricity generation and the total power-plant-level impact of technology design changes. It can be used to compare the costs of all types of generation.

In addition, sensitivity analyses have shown the range of effects that essential LCOE variables could have on the cost of wind energy for offshore wind power. Therefore, this report addresses

many assumptions and cost variables but does not include the full spectrum of drivers that affect wind energy prices.

According to NREL documents (Stehly & Duffy, 2020), for wind energy, the following equation is used to calculate LCOE:

$$LCOE = \frac{(CapEx \times FCR) + OpEx}{AEP_{net}} \quad (4.27)$$

The LCOE equation's first three primary inputs, CapEx, OpEx, and net average annual energy production (AEP_{net}), allow it to incorporate system-level consequences from design changes (e.g., larger rotors or taller wind turbine towers). The fourth essential input, fixed charge rate (FCR), shows the revenue required to pay the annual carrying costs on that investment during the estimated project's economic life.

In the other word, LCOE "represents the average revenue per unit of electricity generated that would be required to recover the costs of building and to operate a generating plant during an assumed financial life and duty cycle" and is calculated as the ratio between all the discounted costs over the lifetime of an electricity generating plant divided by a discounted sum of the actual energy amounts delivered (Ioannou et al., 2017).

$$LCOE = \frac{\text{Overall lifetime cost}}{\text{Sum of electrical energy produced in lifetime}} = \frac{\sum_{t=1}^n \frac{I_t + M_t}{(1+r)^t}}{\frac{E_t}{(1+r)^t}} \quad (4.28)$$

I_t : Investment expenditures in the year t

M_t : Operations and maintenance

E_t : Electrical energy generated in year t

r : Discount rate

t : Expected lifetime of system or power station

4.5.5. Manufacturing and Installation

4.5.5.1. Manufacturing of monopile

A monopile and its transition piece are manufactured relatively straightforwardly and automated. The piles often consist of "cans," cylinders of a rolled plate with a longitudinal seam. It consists of numerous fabrication steps, which are summarised below:

1. Storage of Steel plate
2. Milling and cutting
3. Rolling
4. Inside Longitudinal welding and milling
5. Outside Longitudinal welding
6. Calibration
7. Assembly
8. Inside circular welding and milling
9. Outside circular welding
10. NDT inspection
11. Secondary steel assembly
12. Coating

Finally, the components are stored before being delivered to the logistic port, where they will await the start of the installation process. However, the manufacturing costs of the monopile have risen significantly in recent years, owing primarily to increases in steel and commodity prices, which contribute around 45-50% to the monopile's production costs (Stehly & Duffy, 2020).

4.5.5.2. *Installation of a monopile foundation*

The construction of a typical monopile consists of the following phases:

1. Seabed preparation (If needed): A "mattress" of rock and stones are laid around the foundation to prevent erosion. Typically, no seabed preparation is required for driving the pile (except where seabed erosion is a problem). This eliminates the need for this time-consuming underwater procedure.
2. Pile driving and drilling: The pile is hammered to the desired depth through the mattress. Pile driving is recommended when the overburden consists of soils (sands, gravels, clay, and so on). This could be a diesel or hydraulic hammer system or a vibrator or oscillator.
3. Transition Piece (TP) positioning: Transition Piece (TP) is installed, complete with pre-installed features such as boat landing arrangement, cathodic protection, cable ducts for underwater cables, turbine tower flange, and such. TP allows for the absorption of inaccuracies during the pile installation process. As a result, even if the foundation is not perfectly level, it is possible to raise the turbine tower to a completely vertical

position. The transition piece's upper rim is a flange that allows the fastening of the turbine tower. Before grouting, brackets are put inside the TP to provide temporary support.

4. Grouting: Installation Tolerances can be adequately tested for and adjusted within grouted connections. The grouting procedure is straightforward and can be executed above and below the waterline with standard processing equipment. Grouting is the most common connection between the TP and the pile at mean sea level. This is accomplished by pushing grout through flexible hoses into the annuli gaps.
5. Scour protection: There are numerous scour protection methods, ranging from asphalt to concrete beds; however, most of these choices need costly offshore installation. The most economical approach is laying crushed rock, often called "rip-rap." The concept underlying the placement of a layer of rock is that the rock particles are chosen so that they cannot be washed away by the increased current surrounding the construction.
6. Monopile transportation with barge and tug.

The review of the Manufacturing and Installation process of OWT indicates the CapEx is mainly affected by the following sections:

A. Seabed preparation and Scour protection cost

The cost of scour protection is calculated on a rock volume cost basis. Hence, the protection volume is calculated and multiplied by 350£/m³ (UK beis, 2020). Finally, the amount of steel used for reference and the optimised foundation is estimated and presented later in the results section.

B. Pile transportation and installation cost:

The pile and transition pieces are transported from the onshore base to the site by barge and a tug. HLV will accomplish pile driving, Transition Piece (TP) and grouting. The prices are listed in Table 4-11. The vessel cost depends on the lifting weight and varies from 40K£/day for 200Tn to 120K£/day for 1000Tn. The average time and weather window for each operation ($H_s = 1.5$) is shown in the graph as 60%.

Table 4-11 Typical pile transportation vessels and their costs

Vessel	Operational H_s (m)	Cost (£/Day)
Barge	1.5	10000
Tug	3	30000

The weather window and availability of vessels shall be counted. The average duration of each procedure is summarised in Table 4-12, based on information from recent projects. Then, the weather windows for these operations must be considered a function of the vessel's operational Hs. Consideration is given to a minimum weather window of six hours for the start of operations. The results are depicted in Figure 4-14 using data collected from four North Sea sites (Sarkar & Gudmestad, 2013). The overall cost can be estimated after the total required time and the daily rate of each vessel are known. In addition, according to the market information (Meißner, 2020), the cost of a large piling hammer is estimated at 15000£/Day

Table 4-12 Typical pile transportation vessels and their costs

Operation	Time (Day)
Pile Loading and Transportation (Return)	0.5
Tower Loading and Transportation (Return)	0.5
Pile Installation	1
Tower Installation	1

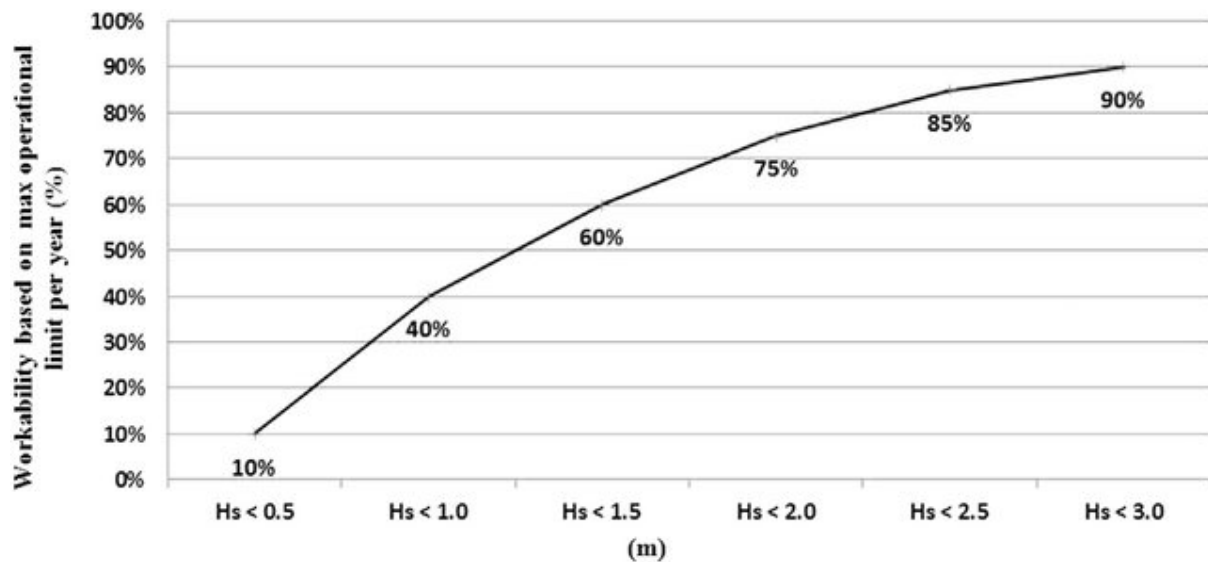


Figure 4-14 Annual average weather windows based on four North Sea sites (Sarkar & Gudmestad, 2013)

C. Mob and Demob Cost

Based on “Electricity Generation Costs Report from UK Government” information (UK beis, 2020), mob and demob fixed cost of 35000£ is considered. For each monopile, the price is divided by 100: 3500£ for each Monopile.

4.5.6. CAPEX and OPEX Breakdown

A summary of Capex and Opex cost breakdown is presented in Table 4-13 according to estimations in sections 4.5.4 and 4.5.5 and also some high-level estimations are according to a study that has been done by UK Catapult ORE in 2021 (Catapult ORE, 2021).

Table 4-13 CAPEX and OPEX Cost Breakdown (Catapult ORE, 2021)

CAPEX Cost Breakdown	
Category	Estimated Cost (£/MW)
Engineering, Development, Engineering Management	£ 130,000.00
Turbine	£ 900,000.00
Foundation Fabrication, Cable and Substation	£ 600,000.00
Transportation & Installation	£ 700,000.00
	£ 2,330,000.00

Total

OPEX Cost Breakdown	
Category	Estimated Cost (£/MW)
Operation, maintenance, and service (per annum)	£ 80,000.00
Decommissioning	£ 350,000.00
Unpredicted events	£ 50,000.00
	£ 480,000.00

Total

4.6. Summary

The objective of this section was to illustrate the benefit of integrating (1) a proper parametric FEA model and (2) a multi-criteria Genetic algorithm to optimise the mass of an OWT support structure. During optimisation, modelling with shell elements for the support structure and solid elements for the soil was used to ensure more reliable and accurate modelling than possible. This FEA model was combined with a genetic algorithm, and it was determined that the global support structure mass would be lowered using an integrated optimisation strategy. Diameters and section thickness were identified as design variables, and an approach to limit the number of variables was devised and implemented. Several constraints were applied based on standard regulations, including modal, stress, deformation, buckling, and fatigue. The model was used to evaluate the performance of the NREL 5 MW reference monopile on OC3. Then, the cost analysis methodology was defined to compare the LCOE of the reference design model and the optimised design model.

5. Scaling up and water-depth sensitivity

5.1. Introduction

Finding a best solution to win in competition of getting project between big companies are always a priority in industry. Early engagements are involved in proposing the best type of support structure considering the cost. In this matter, weight estimation is vital especially for futuristic view of extra-large foundations. Having an efficient approach in scaling up a support structure, and a preliminary equation to estimate the weight is the concern of many companies in their technology teams.

This section starts with developing a scaling-up approach of 7.5MW and 12.5MW wind turbine support structures. These foundations are the scrambled-up version of OC3 on NREL 5MW wind turbine and modified by considering the dimensions and properties of similar available reference turbines such as 8MW Vestas and 10MW DTU, and 15MW IEA. The main objective of this modelling is to propose a simple method to scale up the structure considering the main criteria. Finally, developing a preliminary equation for estimating the weight of these massive structures in conceptual design steps.

In addition, the sensitivity analysis of IEA 15MW is done in this section, which tries to answer the most popular questions of industry these days: How large can we go regarding the monopile support structures?

5.2. Scale up factor

In multi-megawatt wind turbines, upwind, three-bladed, horizontal-axis turbines are the most common design. All wind turbines developed in this section are specially designed for offshore applications. The two OWT foundation sizes of 7.5MW and 12.5MW are examined for the feasibility of the suggested upscaling approach on a bottom-fixed monopile offshore platform, of which 12.5MW is categorized as extra-large monopile. Both 7.5MW and 12.5MW follows current and near-future offshore wind industry norms, but the aim for deep water depth is a futuristic point of view.

The first step is to estimate the initial size and dimension of 7.5MW and 12.5MW support structures and then use this assumption to find the scale factors.

The 7.5MW tower height was mainly derived from linear interpolation between the 5MW and 10MW turbine monopile foundations. The size of the tower is close to 8MW Vestas's wind turbine; therefore, the support structure of the current 8MW Vestas can be used to validate the scale factor of our developed 7.5MW.

The developed 12.5MW dimension is very close to the support structure of the 10MW DTU reference turbine; as we know, DTU has a very conservative design in that size; therefore, the support structure of 10MW Vestas can be used to validate the scale factor of our developed 12.5MW.

The entire tower mass does not increase linearly but instead in a logarithmic trend. The mass per tower length [kg/m] is expressed for the tower mass density, which decreases from bottom to top, as defined in Equation (5.2).

$$m = \rho A \quad (5.1)$$

$$m = \rho \pi [(D/2)^2 - (D/(2-t))^2] \quad (5.2)$$

where ρ is the steel density, A is the cross-section area, D is the outer diameter of the structure, and t is the wall thickness. As shown in Figure 5-1, the values were interpolated based on the relative height fractions of the respective towers.

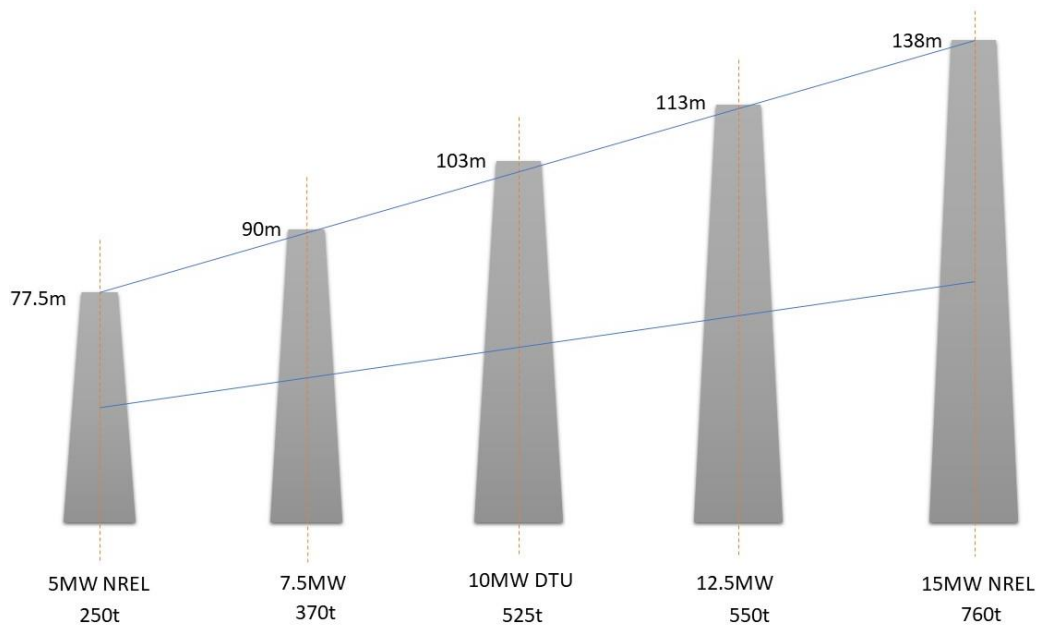


Figure 5-1 Schematic of tower scaling up linearly

The shape of the OC3 platform is not changed in the scaling approach. However, the scaling factor should be used to refine the dimensions to tolerate the larger displacement and mass. The scaling factor is generated by basic geometry rules, which are proportional to the cubic root of the increased mass.

$$S \approx \sqrt[3]{m} \quad (5.3)$$

where S is the scaling factor, and m is the platform mass increase ratio. For instance, according to the DTU reference datasheet (Bak et al., 2013), a 10MW turbine is more than twice as heavy as an NREL 5MW turbine which means:

$$S \text{ for upscaling 5MW to 10MW Platform is : } \sqrt[3]{2.3} = 1.32$$

For 7.5MW and 12.5MW support structures, the initial estimated mass is increased by 1.22 and 2.47, respectively. Therefore, the scale factors, S , are 1.07 and 1.35, respectively. The components are illustrated in Figure 5-2, listed in Table 5-1, which shows the dimensions of scaled turbines according to the scale factor. It should be noted that these dimensions are all approximations, and optimisation procedures can achieve the final and practical dimensions.

Table 5-1 Scaled-Up turbines dimension

Item (See Fig. 5.2)	Description	5MW (reference)	7.5MW	12.5MW
A	Tower Height (m)	77.6	83	104.76
C	Sea level to the top of Transition piece (m)	10	10.7	13.5

B	Water Depth (m)	20	23	28
D	Loose Soil depth (m)	5	5.3	6.75
E	Medium Soil depth (m)	9	9.6	12.2
F	Pile Embedded depth (m)	36	38.5	48.6
H+THK	Monopile Diameter and Thickness (m x mm)	6 X 60	6.9 x 65	8.1 x 80
G+THK	Tower (Bottom) Diameter and Thickness (m x mm)	6 X 30	6.9 x 33	8.1 x 40
N	Grout Thickness (mm)	30	32.1	40.5
K	Cylindrical part of Transition piece(m)	7.5	8	10
J	Conical part of Transition piece (m)	1.5	1.6	2
L	Transition Piece Length (m)	12.5	13.3	16.5

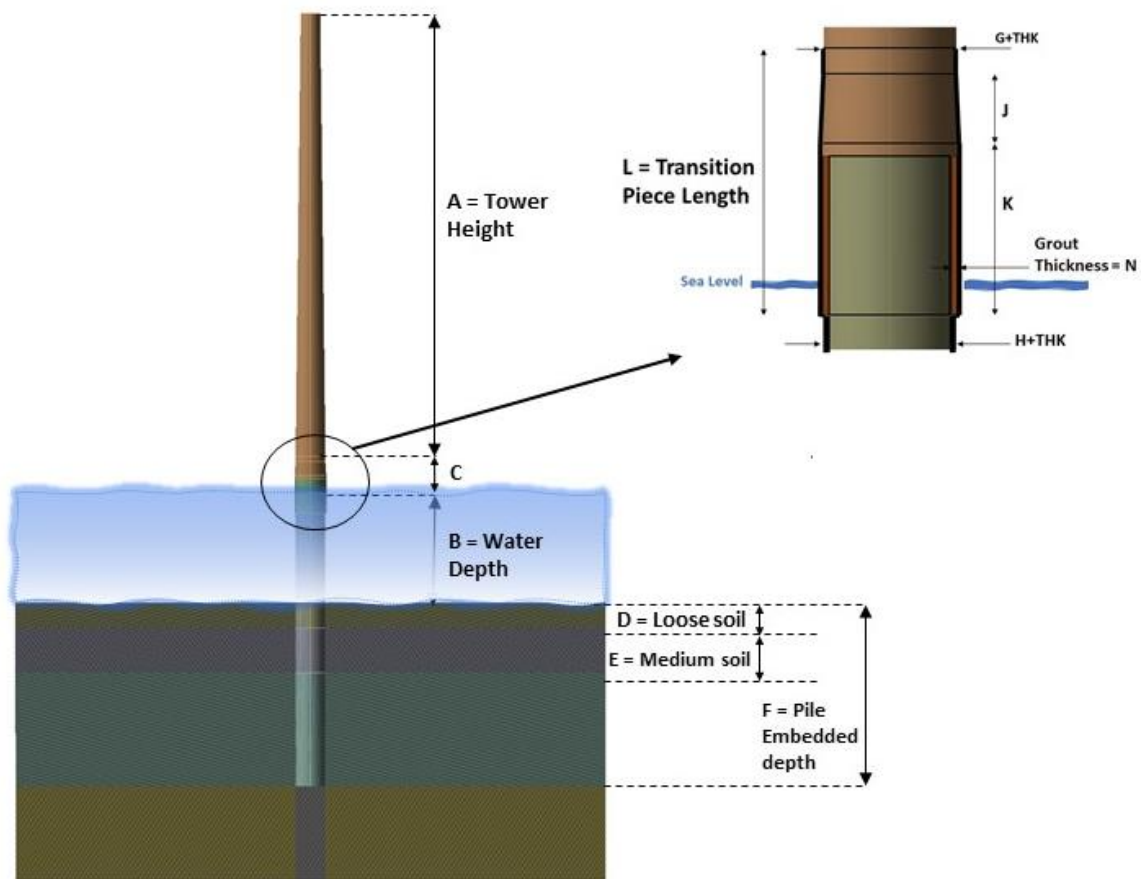


Figure 5-2 Representation of the adapted Reference turbine geometry with details of the TP

5.3. Reference turbines for up-scaled foundations

Reference turbines were implemented for research purposes to facilitate a more straightforward comparison with a standardised design. Furthermore, only reference turbines come with all the detailed information needed for a helpful simulation because most data are kept secret by wind

turbine manufacturers. The NREL 5MW reference wind turbine (Jonkman et al., 2009) with OC3 monopile is modelled in the ANSYS Design Modeler module. In addition, the DTU 10MW (Bak et al., 2013) and IEA 15MW (Gaertner et al., 2020) were also chosen as reference turbines for scaled turbines because they were both published by internationally renowned research institutions and are specially created for offshore cases.

These reference turbines are available to validate our developed turbines and upscaling procedure. The NREL 5MW and V164 8MW (Vestas, 2011) were operated in Class 1A wind, and DTU 10MW and IEA 15MW were operated in Class 1B wind, according to the IEC61400-1 (IEC, 2005).

Table 5-2 specifies the key parameters of reference turbines. Having this information in one table gives us a good overview of how these parameters change by increasing structure size. The first impression from the table is that we can use the 8MW Vestas and 10MW DTU reference loads and data to apply on our developed 7.5MW and 12.5MW support structures and towers as their dimensions are more than 90% similar to each other and then do the FE analysis to see the proposed scale-up approach is applicable for early-stage conceptual design or not.

Figure 5-3 illustrates the rated power vs support structure mass in different turbine sizes that indicate the exponential behaviour of this trend. However, it can be seen in some conservative reference designs; for instance, in DTU 10MW, the thicker plate and wider pile diameter can cause a heavier structure. From Figure 5-4, we can see that most turbines have their maximum power with a rated wind speed in the range of 10-11 m/s. This information is valuable to get started on the process of scaling up and water depth sensitivity.

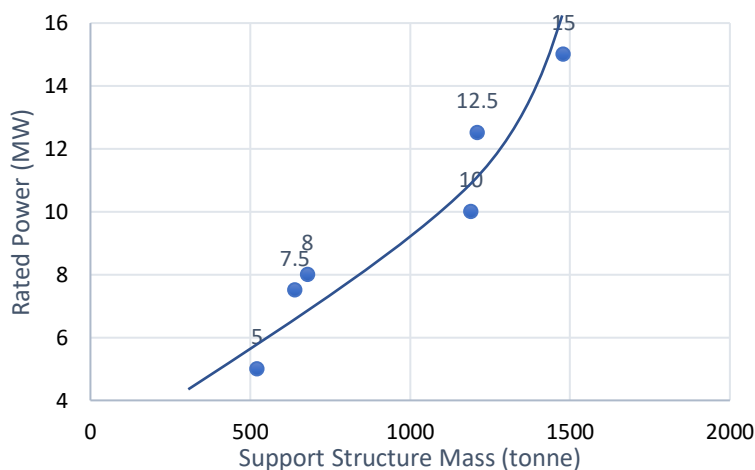


Figure 5-3 Rated Power vs Support Structure mass of different wind turbine sizes

Table 5-2 Key Parameters of Reference Wind Turbines

item	NREL 5MW	7.5MW (Tower)	8MW Vestas	DTU 10MW	12.5MW (Tower)	IEA 15MW
Wind Regime	IEC Class 1A	-	IEC Class 1A	IEC Class 1B	-	IEC Class 1B
Cut in	3 m/s	-	4 m/s	4 m/s	-	3 m/s
Cut out	25 m/s	-	25 m/s	25 m/s	-	25 m/s
Rated Wind Speed	11.4 m/s	-	11.1 m/s	11.4 m/s	-	10.6 m/s
Rated Power	5 MW	-	8 MW	10 MW	-	15 MW
Rotor Diameter	126 m	-	164 m	178.3 m	-	240 m
Hub Height	90 m	105 m	108 m	120 m	134m	150
Tower Height	77.5 m	90 m	92 m	103 m	113 m	138 m
RNA Mass	350 t	-	515 t	674 t	-	1017 t
Tower Mass	250 t	371 t	390 t	525 t	550 t	760 t
Monopile Mass	522 t	630 t	655 t	1190 t	1210 t	1480 t

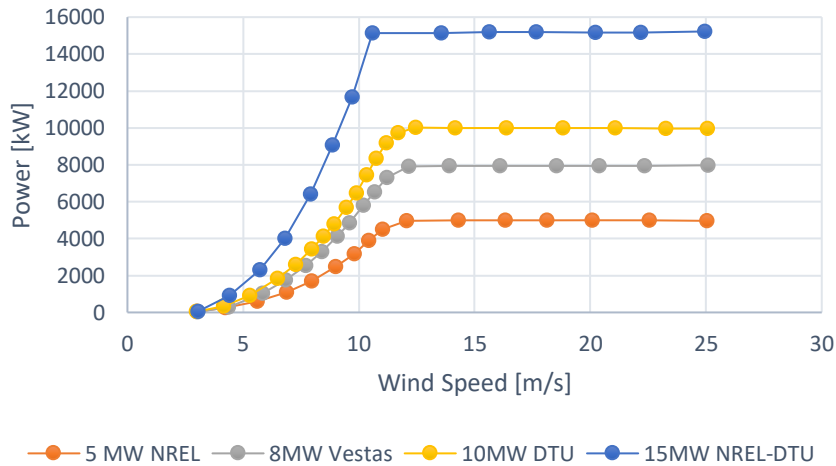


Figure 5-4 Rated Power vs Wind Speed curves for all reference turbines

5.4. Met Ocean Condition

The NL-1 location in the Dutch part of the North Sea was chosen as it is open source. Furthermore, it was recognized as appropriate for deploying monopiles considering the soil

condition, available data and water depth. The site's characteristic is the same as what is described in Section 3.5.1.

5.5. The design procedure and FEA

In general, the procedure of FEA modelling is the same as explained in the RCO framework in Chapter 3. In this section, the overall design strategy is reviewed. The wind turbine foundation geometries were modelled in a widely used software, ANSYS commercial package, to simulate the operational and ultimate load conditions applied to the structures. The progress started with modelling NREL 5MW turbine geometry. Boundary conditions must be applied properly. The bottom of the soil model is fixed in all directions. The side boundaries are secured against lateral translation. The frictional coefficients set the contact between the soil and the monopile, and all other connections are bonded. According to reference reports, wind turbine rotor aerodynamic loads are applied to the top of the tower. Other loads (such as wave, current, wind, and hydrostatic loads) are applied through pressure formulations, which allow these loads to update automatically with the revised diameters of the support structure during the upscale process. Hydrostatic loads surround the submerged component. A multi-point constraint represents the RNA as a concentrated mass applied to the tower top. Using the scale factors explained before, the dimensions of 7.5MW and 12.5MW turbines were calculated and modelled in ANSYS.

As mentioned in Chapter 3, previous studies (Gentils et al., 2017; Kallehave et al., 2015) recommended using shell elements to get more accurate results for thin-wall sections such as tower, transition piece and monopile. Regarding the Ansys Help Documentation (Thompson & Thompson, 2017), the Shell281 element type with eight nodes and six degrees of freedom (DoF) has been used as it has behaviour in linear and considerable strain nonlinear purposes. Furthermore, experiments and standards (DNV GL, 2016) recommend using SOLID 186 for grout to examine bending stress in this section. Finally, SOLID 185 has been used for modelling the soil.

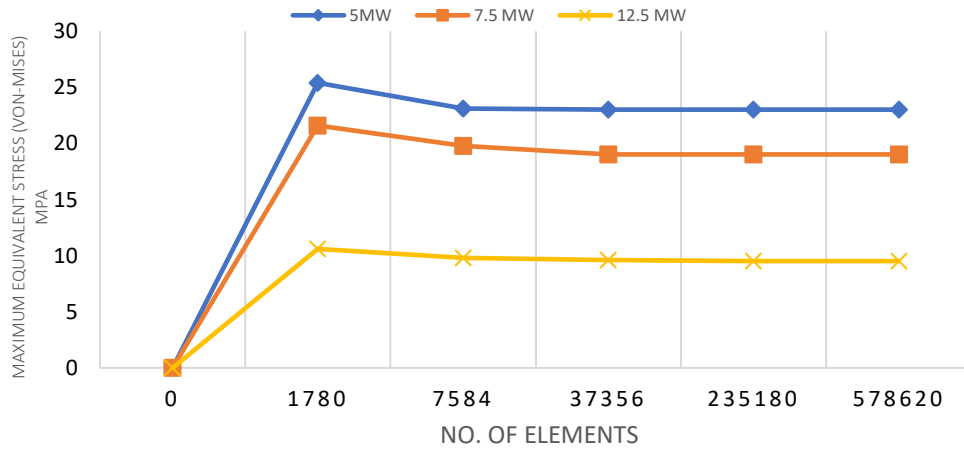


Figure 5-5 Mesh convergence result for all sizes of Turbines

Mesh convergence is accomplished to gain an accurate result with the optimum number of elements to save calculation time. The process starts with applying 100kN Force on top of the tower for each size and gets results with a different number of elements. Figure 5-5 shows the optimum number of elements for each turbine, and Figure 5-6 illustrates the final generated mesh on the 7.5MW wind turbine as an example.

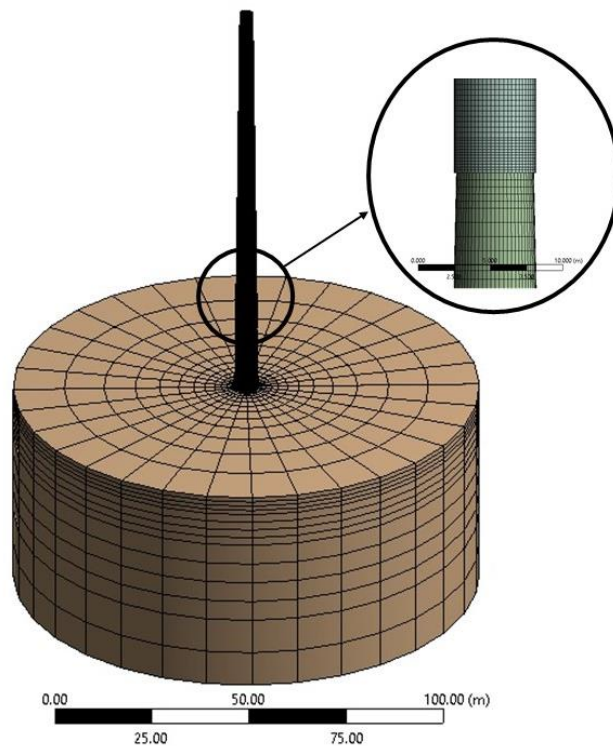


Figure 5-6 Final generated mesh for 7.5MW turbine size

The type of contact between the soil and the monopile is set according to the frictional coefficients presented in Table 3-6.

There are several approaches to validate a model; comparing the deflection of RNA or natural frequency of the developed model with the reference calculated data are the common ways to validate an offshore wind turbine's geometry. As the NREL 5MW reference model is the base of all other developed models, we have validated the 5MW geometry with the reference NREL data. The FEA model validation of 5MW NREL has been explained in Section 4.2.5.

5.5.1. ULS Loads

Ultimate sea state is considered in this part of study, as the loads are available in reference reports. Table 5-3 shows the thrust and tilting moments of developed turbines. The hydrostatic and wind/wave loads are calculated and applied as the way explained in Section 3.5.2 and illustrated in Figure 5-7.

Table 5-3 Thrust and Moment applied on the wind turbines

Load Case	Moment (MNm) on base of tower			
ULS (DLC6.1)	5MW (LaNier, 2005)	7.5MW (Vestas, 2011)	12.5MW (Wang et al., 2021)	15MW (Gaertner et al., 2020)
	38.5	49.5	128	401
	Thrust Force (kN) (Gaertner et al., 2020; LaNier, 2005)			
	781	1052	1650	2580

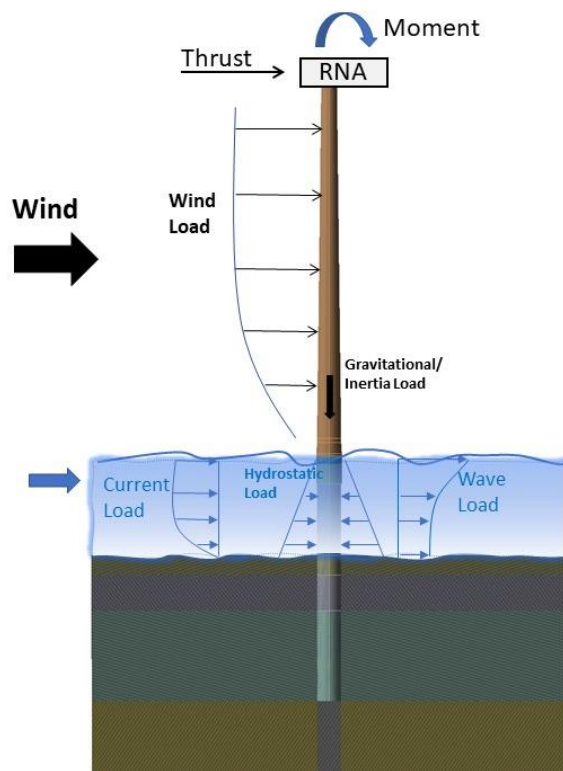


Figure 5-7 Aero-Hydro dynamic, wind and wave loads of an OWT monopile support structure

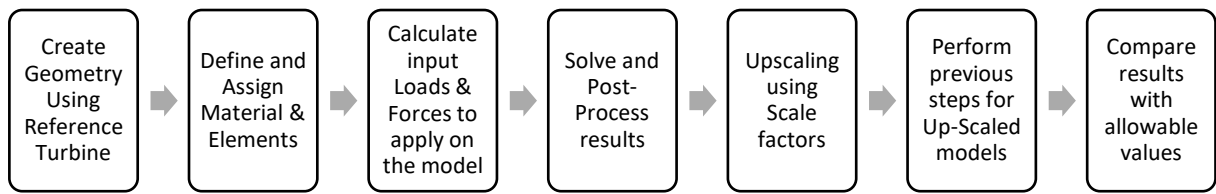


Figure 5-8 Flow chart of the complete initial design procedure

It should be noted that the safety factor is not applied to these values in this table and will be considered in the analysis of the input data into the software. The flow chart of the complete initial design and the upscaling procedure is illustrated in Figure 5-8. Finally, the results will be presented and discussed in Chapter 6.

5.6. Estimation of monopile mass using preliminary parametric equation

The other objective of this section is to obtain an equation to show the relation between the weight and water depth of large steel offshore monopiles. It is a helpful tool for many offshore wind companies in the technology section to estimate and adjust their compass for future projects. The equation is a rough estimation, but it can be verified and optimised in future studies. The methodology in this section consists of the following:

- Finding as many as OW Turbines data to create a dataset (see Table 5-4)
- Plotting the graphs of Weight vs Rating and Weight vs Water depth.
- Finding the relation and equation
- Checking and validating the function with the scaled turbines

Table 5-4 Dataset of the offshore wind turbines in Europe with a monopile support structure (C4Offshore)

Wind Farm/Turbine Name	Turbine (MW)	Max Water depth (m)	Diameter (m)	Length (m)	Weight (t)
Lely	0.5	10	3.7	30	89
Bockstigen	0.5	6	2.1	21	43
Utgrunden 1	1.5	10	3.6	33.7	165
Horns Rev 1	2	14	4	42	230
Prinses Amalia	2	24	4	54	320
North Hoyle	2	11	4	25	250
Scroby Sands	2	10	4.2	42	200

Horns Rev 2	2.3	17	3.9	40	280
Samsø	2.3	13	4.5	45	300
EnBW Baltic 1	2.3	19	4.3	37	215
Teesside	2.3	16.5	5	48	160
Belwind	3	24	5	72	550
Egmond aan Zee	3	18	4.6	60	250
Kentish Flats	3	5	4	38	247
Robin Rigg	3	13	4.3	35	310
Barrow	3	20	4.7	60	530
Vestas V112	3.3	20	6	48	750
Anholt	3.6	19	5	54	630
DanTysk	3.6	31	6	65	730
Riffgat	3.6	23	6	70	720
Rhyl Flats	3.6	12	4.7	40	235
Gunfleet Sands	3.6	15	5	50	423
Burbo Bank	3.6	8	5	52	400
Sheringham Shoal	3.6	22	5.2	61	530
Lincs	3.6	16.3	5.2	48	480
Gwynt Môr	3.6	28	6	70	700
Greater Gabbard	3.6	32	6	60	700
Walney Phase 2	3.6	30	6	68	805
London Array	3.6	25	7	85	650
Amrumbank West	3.8	25	6	70	800
Borkum Riffgrund 1	4	29	5.9	66	700
NREL	5	20	6	56	522
Vestas V164	8	30	8	66	1150
DTU	10	35	8	65	1190
NREL-DTU	15	40	10	80	1480

The relationship between monopile weight vs turbine rating and water depth is shown in Figure 5-9. Equations 5.5 and 5.6 are extracted from these figures, where W is the weight of the monopile in tonnes, B is the water depth in meters, and r is the wind turbine rating in MW.

$$W = 126.04 r^{1.05} \quad (5.5)$$

$$B = \frac{\ln\left(\frac{W}{98.5}\right)}{0.071} \quad (5.6)$$

The weight values from the 3D model and the above equations are compared in Table 5-5, considering the maximum water depth estimation for developed 7.5MW and 12.5MW support structures to validate the formulas. For instance, the weight of the turbine is estimated using Eq. (5.5). Then, the maximum suitable water depth is calculated by Eq. (5.6). The values are then compared, and the deviations are observed.

Table 5-5 Comparison of monopile weight between function value and 3D model value

	Developed up-scaled 7.5 MW in 30m	Developed up-scaled 12.5 MW in 40m
3D model estimation	1020 t	1760 t
Function (W vs r)	1045 t (+2.4% Deviation)	1787.5 t (+1.5% Deviation)
Water-depth estimation according to (Eq.19)	33.26 m (+10% Deviation)	40.82 m (+2% Deviation)

The values in Table 5-5 show a good agreement between the function results and the developed 3D model of these upscaled wind turbines. This confirms the validity of the scale-up methodology proposed in this study. Therefore, these equations can be used in the preliminary design stage to forecast each turbine's material or cost and the maximum considered water depth.

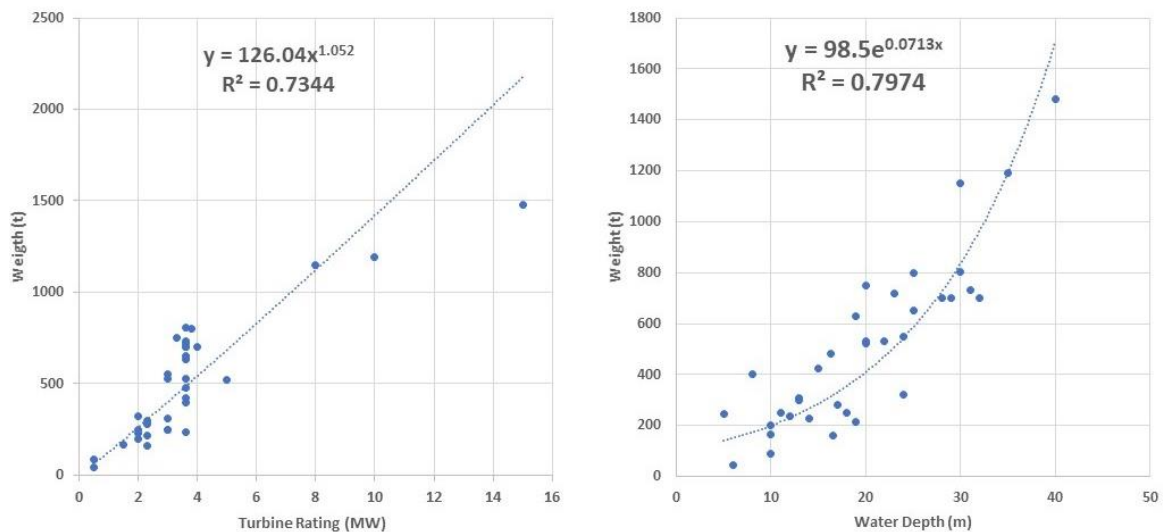


Figure 5-9 Regression analysis for the ‘weight vs Turbine rating’ and ‘weight vs water depth’ equations

5.7. Water depth sensitivity

Water depth sensitivity is performed on the biggest offshore reference wind turbine model, 15MW IEA, with a bottom-fixed monopile support structure. This reference wind turbine is a Class IB direct-drive machine with a rotor diameter of 240 m and a hub height of 150 m.

The monopile diameter, thickness, and length were constant for each water depth. The monopile thickness was calculated using an estimated diameter-thickness ratio (van Wingerde et al., 2006). The pile diameter and penetration depth were chosen to obtain the first mode eigenfrequency derived from the wind turbine blade passing frequency intervals of 1P and 3P. The first mode of the original tower-monopile design was 0.175 Hz which lies within the allowable range. With up to 120-meter blades, the tower height was chosen so that the hub height reached 150 metres. This allows for 30 metres of ground (water surface) clearance beyond the recommended clearance of 20m (Bortolotti et al., 2019) in standards. The monopile foundation has a 10-meter outer diameter, pushing the limits of current manufacturing and installation technology. The initial water depth was 45m. However, in this study, we want to put this structure in different water depths (30-60m) and examine the feasibility and behaviour in the new conditions. It should be noted that the maximum possible embedded depth of the pile in the ground is assumed to be 50m for a water depth of more than 45m, considering current technology barriers.

In this case, the IEA 15MW reference wind turbine (Gaertner et al., 2020) is modelled in the ANSYS Design Modeler. In addition, the support structure of this reference turbine is optimised by (McWilliam et al. 2021) and has been used in this study. Table 5-2 shows the key parameters of the IEA 15MW reference turbine and support structure, and Figure 5-10 illustrates the dimensions.

An IEC design load case (DLC) analysis was performed to determine the worst-case ultimate loading on critical design constraining components. The DLC 1.1 for Normal Turbulence Model (NTM) and DLC 6.1 for Extreme Wind Shear (EWS) were chosen from reference model report (Gaertner et al., 2020). The Tower base Moments are 37 MN.m for DLC 1.1 and 401 MN.m for DLC 6.1. The corresponding wind/wave profile and hydrostatics are calculated as the methodology described in Section 3.5.2.

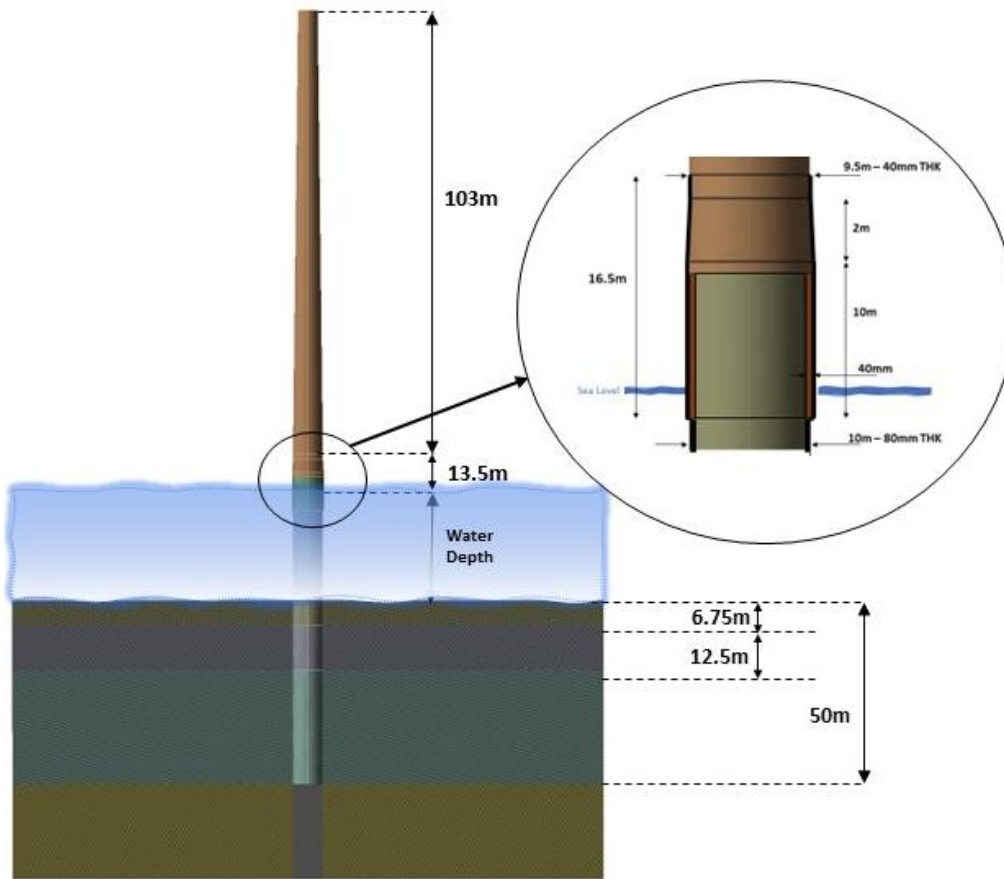


Figure 5-10 Representation of the adapted reference turbine for water depth sensitivity

5.8. Summary

This chapter focuses on developing a scale up approach and parametric equations to estimate the weight and suitable water depth for future extra-large offshore wind turbines was another purpose of this chapter. The methodology of finding a relation between the “weight vs turbine rating” and “weight vs water depth” for preliminary estimation for design was suggested and will be utilized to obtain a function. To achieve the objective, a dataset of several OWTs has been selected.

Also, the feasibility of a scale-up approach for bottom-fix foundations, such as monopile, in the deeper sea was examined by performing FEA (finite element analysis) simulations.

Finally, the sensitivity analysis methodology is proposed for the largest available reference support structure, IEA 15MW, using numerical methods and 3D analysis. The maximum equivalent stress, first natural frequency, global buckling, fatigue damage and safety factor have been studied in water depths between 30-60m.

6. Results and Discussion

6.1. RCO and LCOE Results on 5MW NREL

6.1.1. Design Constraints

The evolution of the design constraints is tracked and shown in Appendix B. As the most populated constraints, the first natural frequency and fatigue drive the design. These findings confirm the recommendations of primary codes and standards (DNV GL, 2016; IEC, 2019). Although buckling and maximum Von Mises stress may appear less contributory, they are highly activated during the selection of first-generation points from the initial population, which is critical for the rest of the optimisation. Therefore, the Tresca stress or pile-head deflection are the constraints for which the choice of constraint conditions is considered irrelevant. This demonstrated the necessity of multi-criteria optimisation. Furthermore, the significant activation and saturation of constraints highlight the importance of using accurate data. In fact, because the final solution is near the farthest edge of the allowable space, even the most minor deviation from reality in the model attributes (such as load estimation, material strength, etc.) could result in failure under real-world conditions.

6.1.2. Design Variables

Comparing the reference and RCO designs in Figure 6-1, thickness and diameter profiles are evaluated. It appears that the monopile's mass is reduced mainly through its thickness, particularly for the base, while its outer diameter is only slightly increased. Considering the combined stiffness of the soil and piling, the outcome of the foundation thickness may be

justified. Because the earth provides more stiffness at deeper soil locations, a thinner pile can obtain the same comparable stiffness. Where the stress is anticipated to be the highest for the remainder of the construction, the material quantity is raised (i.e. junction of tower and transition piece). The section of the support structure that is not buried has a significantly reduced outer diameter. Therefore, it would seem that both categories of design variables are essential for the optimisation result.

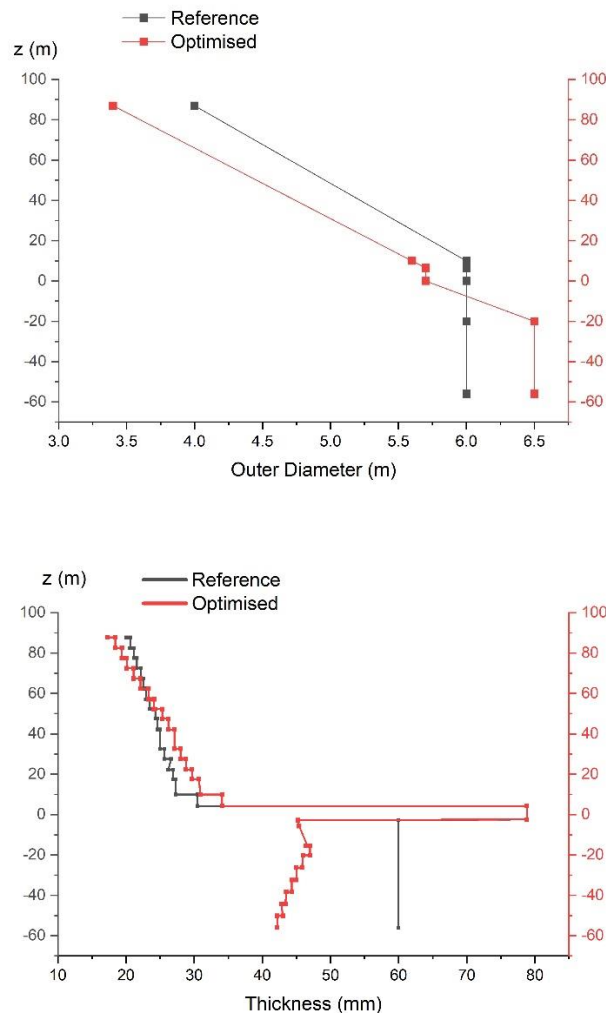


Figure 6-1 Comparison of reference and optimised design from RCO framework in Thickness and Diameter

6.1.3. Reliability Assessment Results

6.1.3.1. Reliability-Constrained Optimisation (RCO) Framework Results

A new framework for optimising an OWT support structure by assessing the reliability of complex support structures in parallel was developed in the previous sections. In this section,

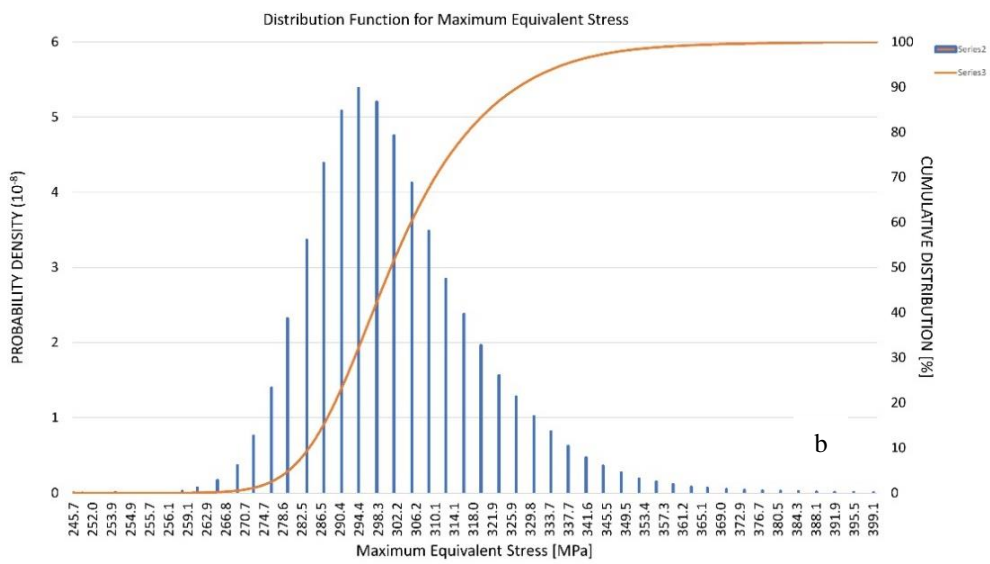
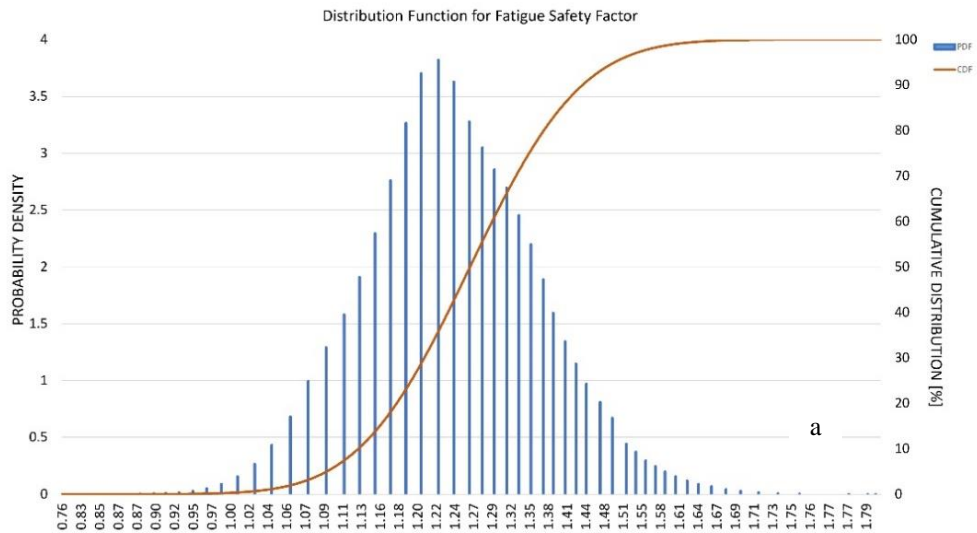
the reliability assessment results of Reference, DO and RCO designs are explained in Table 6-1. The RCO framework and Deterministic Optimisation (DO) were applied to the NREL 5MW OWT monopile structure. The RCO accounts for several stochastic input variables and ultimate and fatigue limit states. The failure probability value was extracted from the design parameters' cumulative density function (CDF) and probability density function (PDF). Figure 6-2 a-e presented the CDF and PDF of design constraints of RCO design as an example.

In this assessment, the target reliability level of $1E-4$ (or Reliability Index of 3.8) should be considered the threshold. The comparisons of design parameters obtained from different models indicate that the P_f in both optimised models decreased significantly in the buckling and eigenfrequency due to the reduction in the tower and monopile diameter and thickness.

As expected, the reference model was designed conservatively, and the reliability index is much higher than the target value. However, as shown in the results, the reliability assessment performed on the optimised structure revealed that the RCO design, in which the stochastic variables are considered, meets the recommended reliability assessment criteria since the reliability value of all of the design constraints considered is within the design thresholds. Nevertheless, the DO design does not fulfil the criteria because it has less probability of failure than the target reliability level of $1E-4$ in resonance capacity.

Table 6-1 Reliability assessment comparison

Ultimate Limit State	5MW NREL on OC3 monopile Reference Design		RCO Design		DO Design	
	P_f	β	P_f	β	P_f	β
Max Stress Capacity	1.3E-06	4.71	3.0E-5	4.01	3.5E-5	3.99
Buckling Capacity	≈ 0	7.01	4.1E-5	3.94	5.3E-5	3.88
Maximum Deflection	≈ 0	7.61	6.0E-8	5.28	9.0E-8	5.21
Resonance Capacity	2.1E-08	5.48	5.9E-5	3.85	2.1E-4	3.53
Fatigue Limit State						
Min Safety Factor	8.0E-06	4.32	6.1E-05	3.84	7.9E-5	3.81



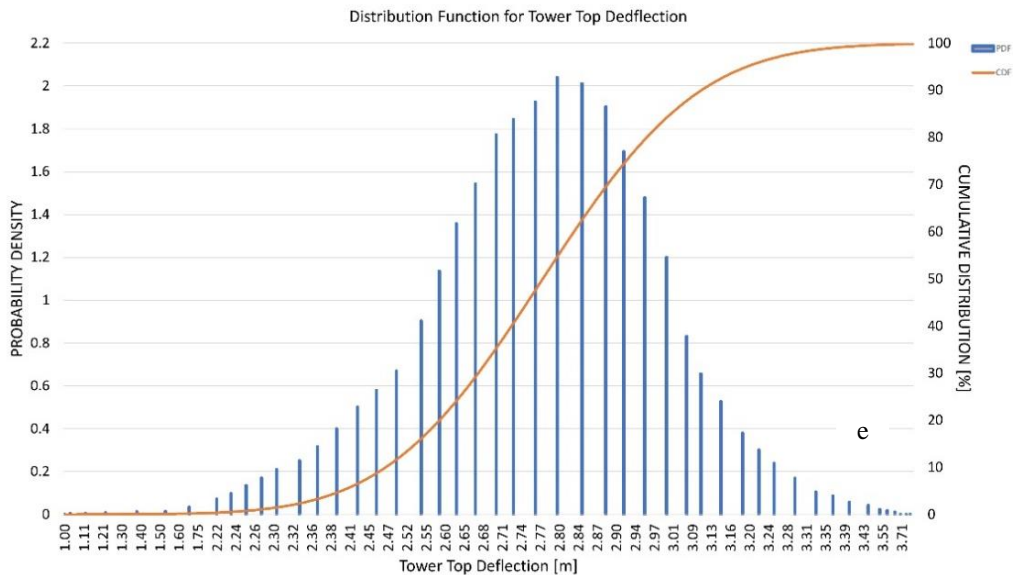
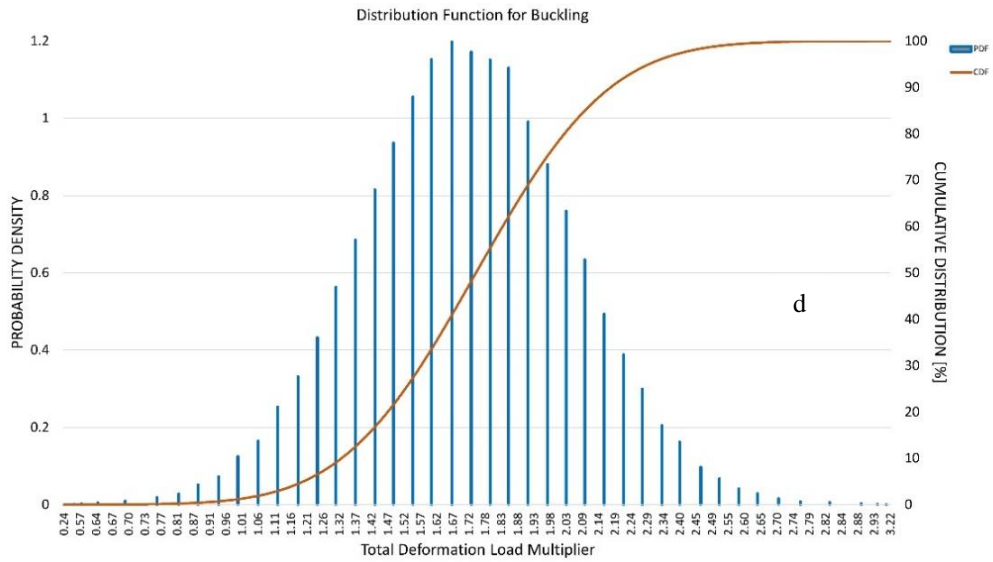
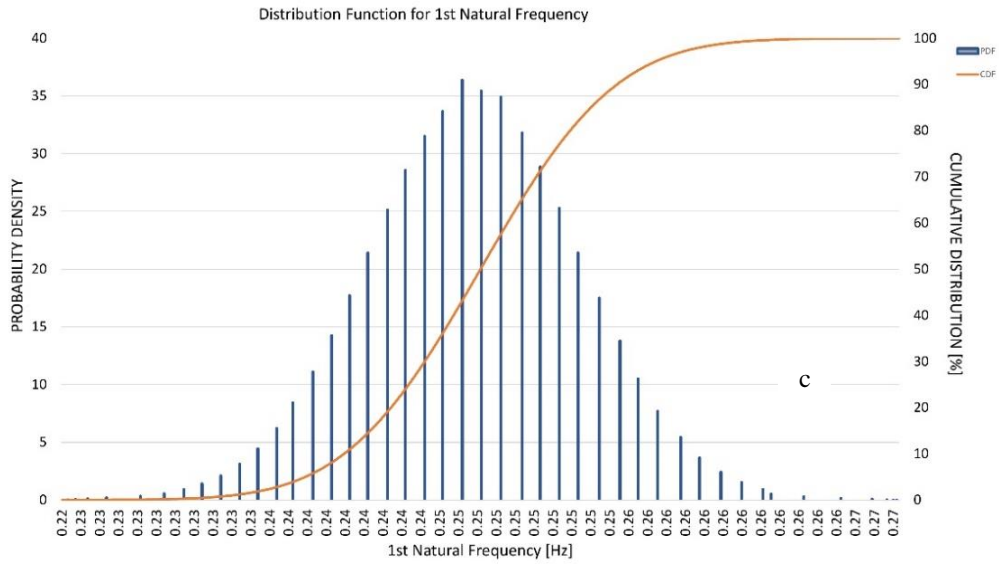


Figure 6-2 Cumulative density function and probability density function RCO design for (a) Fatigue minimum safety factor; (b) Equivalent stress maximum; (c) First natural frequency; (d) Buckling load multiplier; (e) Total deflection

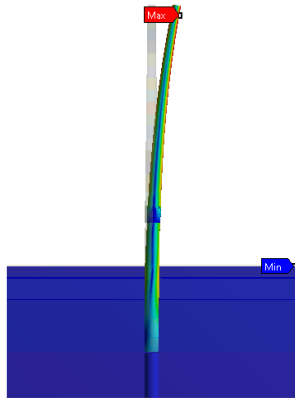
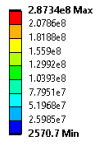
6.1.4. Structural Response of FEA for DO and RCO

This section gives the structural responses of optimised models in ultimate and fatigue limit states. In order to see the importance of considering reliability constraints in the optimisation process, the FEA results of the DO design are compared with the FEA results of the RCO Design in Table 6-3 in more detail.

Prior to comparing the DO and RCO results, it is worth seeing the RCO design FEA figure results in Figure 6-3 (a) for maximum Von Mises equivalent stress, Figure 6-3 (b) for buckling, Figures 6-3 (c) and Figure 6-3 (d) for total deformation and mudline displacement in the ULC, Figure 6-3 (e) for modal analysis, and Figure 6-3 (f) for safety factor in fatigue load condition. The global maximum equivalent stress equals 287MPa , 11% less than the allowable stress of 323MPa . The maximum deformation of the support structure is 2.94m , which shows the considerable deflection experienced by the structure; however, considering the foundation and soil deformation of 0.077m , which is 23% lower than the allowable 0.1m . Also, 0.351 degrees rotation at the mudline is observed, 12.2% less than the permissible value of 0.4 . This implies the current support structure design is unlikely to experience large deflections. The buckling load multiplier in this result is 1.68 ; the limit value for this section is 1.4 . This difference shows that the present support structure design is safe under maximum buckling loads.

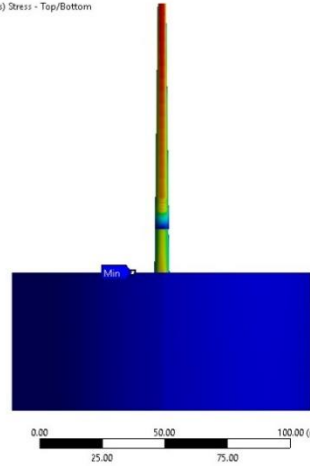
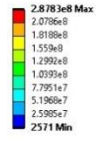
The modal analysis gives the resonance evaluation and dynamic properties of the structure. The frequency of the first mode is 0.231 Hz which is acceptable for our modal frequency limitation. However, as the frequency is one of the important drivers in the OWT design process and considering that the thicknesses of some parts and the diameter have decreased for the optimisation process, a reliability assessment must be carried out to check the structural reliability. Furthermore, in association with stress distribution, critical fatigue failure location is keen to appear at the top of the tower. Therefore, the minimum safety factor occurs on top of the tower and is equal to 1.194 , which is 5.1% higher than the minimum allowable value of 1.15 ; as a result, the current design can survive its design lifetime under fatigue-inducing loads.

E: Ultimate Limite State
 Equivalent Stress
 Type: Equivalent (von-Mises) Stress - Top/Bottom
 Unit: Pa
 Time: 1
 04/01/2021 13:44

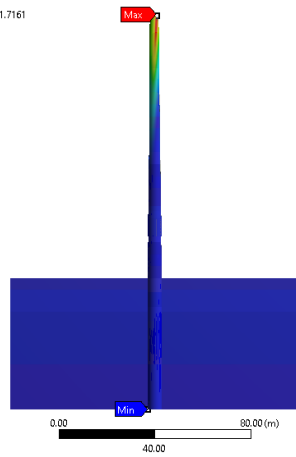
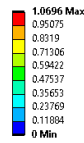


a

E: Ultimate Limite State
 Equivalent Stress
 Type: Equivalent (von-Mises) Stress - Top/Bottom
 Unit: Pa
 Time: 1
 16/09/2021 12:20

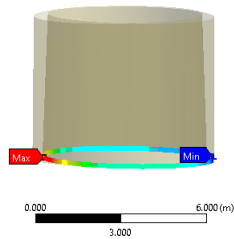
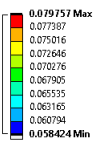


F: Eigenvalue Buckling
 Total Deformation
 Type: Total Deformation
 Load Multiplier (Nonlinear): 1.7161
 Unit: m
 04/01/2021 13:43



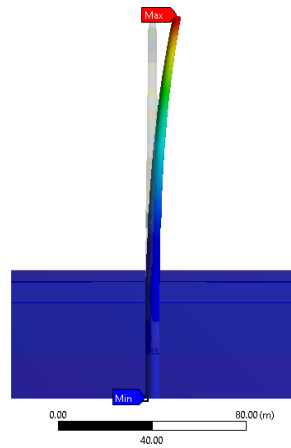
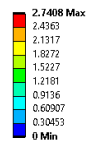
b

E: Ultimate Limite State
 Mudline Displacement
 Type: Directional Deformation(X Axis)
 Unit: m
 Global Coordinate System
 Time: 1
 04/01/2021 13:47



c

E: Ultimate Limite State
 Total Deformation
 Type: Total Deformation
 Unit: m
 Time: 1
 04/01/2021 13:40



d

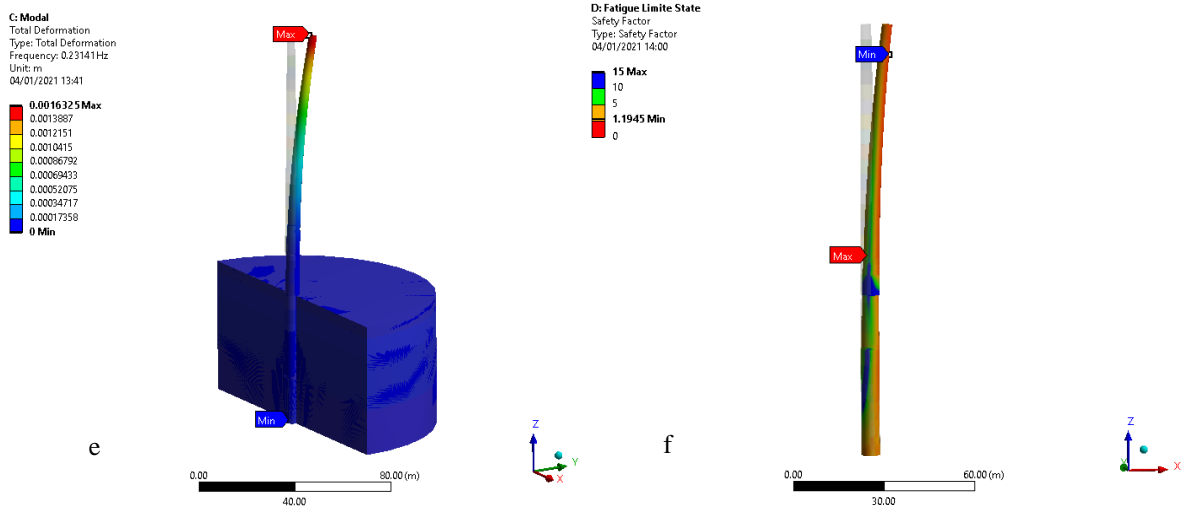


Figure 6-3 FEA results for RCO design, a) Von Mises equivalent stress, b) Buckling deformation, c) mudline displacement, d) Total deformation, e) 1st mode frequency and displacement, f) Fatigue minimum safety factor

The values of the design parameters obtained from DO and RCO designs are summarized in Table 6-2. As discussed in DO, the OWT support structure is optimised only for explicit and implicit constraints in Section 3.4.2 without implementing the reliability constraint and stochastic variables. But in the RCO framework, proposed an optimisation process by additional reliability constraints with stochastic variables. These results reveal that considering the uncertainties and adding a target reliability value as a constraint can affect the design output. Finally, the 5MW NREL OWT support structure mass can be reduced by 19.7% in the RCO framework and 19.95% in traditional deterministic optimisation (DO).

Table 6-2 The comparison of DO and RCO framework mass reduction results

Variable	Name	Unit	Lower Bound	Reference Design	Optimised Design (RCO)	Optimised Design (DO)	Upper Bound
Design Variables	Monopile base diameter	X ₁	[m]	5	6	6.10	7
	Monopile top diameter	X ₂	[m]	5	6	5.34	7
	Tower base diameter	X ₃	[m]	5	6	5.28	7
	Tower top diameter	X ₄	[m]	3	3.87	3.28	4.5
	Tower base thickness	X ₅	[mm]	20	27	30	40
	Tower Int1 thickness	X ₆	[mm]	20	25	26	40
	Tower Int2 thickness	X ₇	[mm]	15	22	21	35
	Tower top thickness	X ₈	[mm]	10	19	17	30
	Monopile substructure base thickness	X ₉	[mm]	45	60	46	70
	Monopile substructure top thickness	X ₁₀	[mm]	45	60	45	70
	Monopile foundation base thickness	X ₁₁	[mm]	40	60	45	70
	Monopile foundation top thickness	X ₁₂	[mm]	45	60	46	70

Objective function Constraints	Transition piece thickness	X_{13}	[mm]	25	30	33.54	33.43	40
	1 st Natural frequency		[Hz]	0.21	0.285	0.231	0.223	0.328
	Maximum equivalent Stress (Von Mises)		[MPa]	-	185	287	299	323
	Pile head deflection		[m]	-	0.057	0.079	0.08	0.1
	Pile head rotation		[°]	-	0.26	0.34	0.34	0.4
	Buckling load multiplier		-	1.4	2.35	1.68	1.56	-
	Minimum fatigue safety ratio		-	1.15	1.54	1.19	1.21	-
Mass Saving	Support Structure mass		[Tonnes]	-	924.5	741.4 (-19.7%)	739.1 (-19.95%)	-

In deterministic optimisation (DO), PSFs defined by DNV have been used and in reliability-constrained optimisation (RCO) the PSFs are eliminated and the stochastic variables with defined distributions are considered. The closeness of the results from DO and RCO proves the proper choice of distribution types and CoV of stochastic variables in reliability-constrained optimisation process.

Figure 6-4 presents the sensitivity analysis, showing the independent input variables' local sensitivity to the output parameters. This analysis helps designers examine which variable contributes the most to structural response and reliability performance changes. As expected, thrust and tilting moment drastically impact maximum equivalent stress in the ULS. Therefore, both tilting and torsional moments and thrust load in operational conditions influence the margin of safety calculation in the FLS. Material properties such as soil Young's Modulus depend on the deformation and displacement of the structure and pile in the mudline and the eigenfrequency of the structure as a consequence. It is evident that these material properties next to pile thickness and diameter are the modal analysis's main parameters.

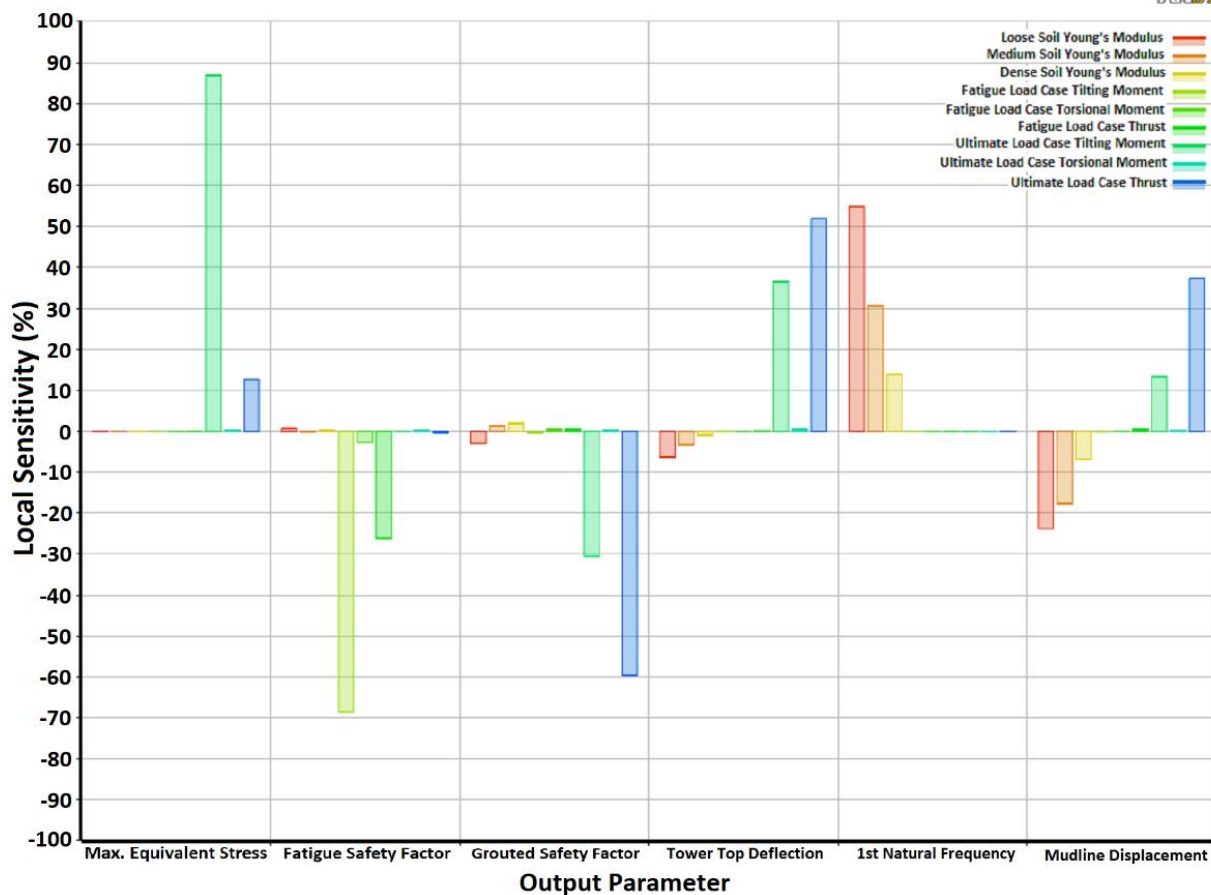


Figure 6-4 Local sensitivity analysis for each parameter

6.1.5. Fatigue assessment of RCO design using S-N curve

The fatigue life of the RCO design support structure is assessed by considering 20m water depth and having fatigue damage equivalent loads (DEL) (from the OWECs in-house software) for the FEA model. The category 'D' S-N curve has been adopted for the column circumferential welds. The results are presented in Table 6-3. Local SCFs have been considered at the conical transitions assuming no ring stiffener reinforcement. All column sections are regarded as outer diameter (OD) flush, and appropriate SCFs have been applied. No assessment has been made for the effect of local SCF due to secondary attachments or the column-to-outrigger connection. Fatigue assessment has been performed under DNVGL-RP-C203 (DNV GL, 1987), "Fatigue design of offshore structures".

Table 6-3 Fatigue life assessment for Optimised Turbine

Optimised Turbine Weld Location and Type	Elev. (m)	D (m)	Tu / Tl (mm)	SCF	Cone SCF	Life (yrs)

Tower Top of the cone	87.00	3.4	18 / 18	1.00	1.15	187
Circumferential Weld	83.50	3.5	18 / 18	1.05	1.15	169
Circumferential Weld	80.00	3.6	18 / 20	1.05	1.00	236
Circumferential Weld	76.50	3.7	20 / 20	1.05	1.00	239
Circumferential Weld	73.00	3.8	20 / 20	1.00	1.00	413
Circumferential Weld	69.50	3.9	20 / 20	1.00	1.00	457
Circumferential Weld	66.00	4.0	20 / 22	1.00	1.00	465
Circumferential Weld	62.50	4.1	22 / 22	1.00	1.00	378
Circumferential Weld	59.00	4.2	22 / 22	1.00	1.00	356
Circumferential Weld	55.50	4.3	22 / 24	1.05	1.00	246
Circumferential Weld	52.00	4.4	24 / 24	1.05	1.00	257
Circumferential Weld	48.50	4.5	24 / 24	1.05	1.00	248
Circumferential Weld	45.00	4.6	24 / 26	1.00	1.00	365
Circumferential Weld	41.50	4.7	26 / 26	1.00	1.00	379
Circumferential Weld	38.00	4.8	26 / 26	1.00	1.00	348
Circumferential Weld	34.50	4.9	26 / 28	1.05	1.00	247
Circumferential Weld	31.00	5.0	28 / 28	1.06	1.00	214
Circumferential Weld	27.50	5.1	26 / 26	1.06	1.00	234
Circumferential Weld	24.00	5.2	26 / 26	1.09	1.00	198
Circumferential Weld	20.50	5.3	26 / 28	1.10	1.00	188
Circumferential Weld	17.00	5.4	28 / 30	1.10	1.00	174
Circumferential Weld	13.50	5.5	30 / 32	1.07	1.13	148
Tower Bottom of the cone	10.00	5.6	30 / 34	1.00	1.13	136
Monopile Top of the cone	7.50	5.7	80 / 80	1.12	1.18	97
Circumferential Weld (Splash Zone)	4.00	5.8	80 / 70	1.22	1.18	88
Circumferential Weld (Splash Zone)	0.00	5.9	70 / 60	1.24	1.00	91
Circumferential Weld (Splash Zone)	-3.50	6.0	60 / 50	1.28	1.00	83
Circumferential Weld	-7.00	6.1	50 / 46	1.19	1.00	101
Circumferential Weld	-10.50	6.2	46 / 46	1.09	1.00	117
Circumferential Weld	-14.00	6.4	46 / 46	1.00	1.13	106
Monopile Bottom of the cone	-17.50	6.5	46 / 46	1.00	1.13	238
Circumferential Weld	-21.00	6.5	46 / 46	1.00	1.13	245
Circumferential Weld	-24.50	6.5	46 / 46	1.00	1.00	346
Circumferential Weld	-28.00	6.5	46 / 46	1.06	1.00	312
Circumferential Weld	-31.50	6.5	46 / 44	1.06	1.00	278
Circumferential Weld	-35.00	6.5	44 / 44	1.06	1.00	268
Circumferential Weld	-38.50	6.5	44 / 44	1.00	1.00	346
Circumferential Weld	-42.00	6.5	44 / 44	1.00	1.00	389
Circumferential Weld	-45.50	6.5	44 / 44	1.00	1.00	416
Circumferential Weld	-49.00	6.5	44 / 44	1.00	1.00	318

Circumferential Weld	-52.50	6.5	44 / 42	1.05	1.00	247
Circumferential Weld	-56.00	6.5	42 / 42	1.05	1.00	268

Fatigue assessment on the optimised model indicates that a significant impact on the wall thickness due to the conical transitions where the SCF varies between *1.05-1.28*. The cone angle primarily drives the higher SCFs. The assessment assumes all plates are OD flush, but this introduces an eccentricity at each plate thickness transition and an associated SCF. This SCF generally means that a transition in plate thickness of more than 10mm between adjacent plates is impractical. For example, a 10mm change in wall thickness will produce an SCF of *~1.15 to 1.25*. The above checks exclude other areas with local stress raisers due to attachments from secondary steel. This assessment proves that the RCO model can fulfil the fatigue criteria according to DNV regulations.

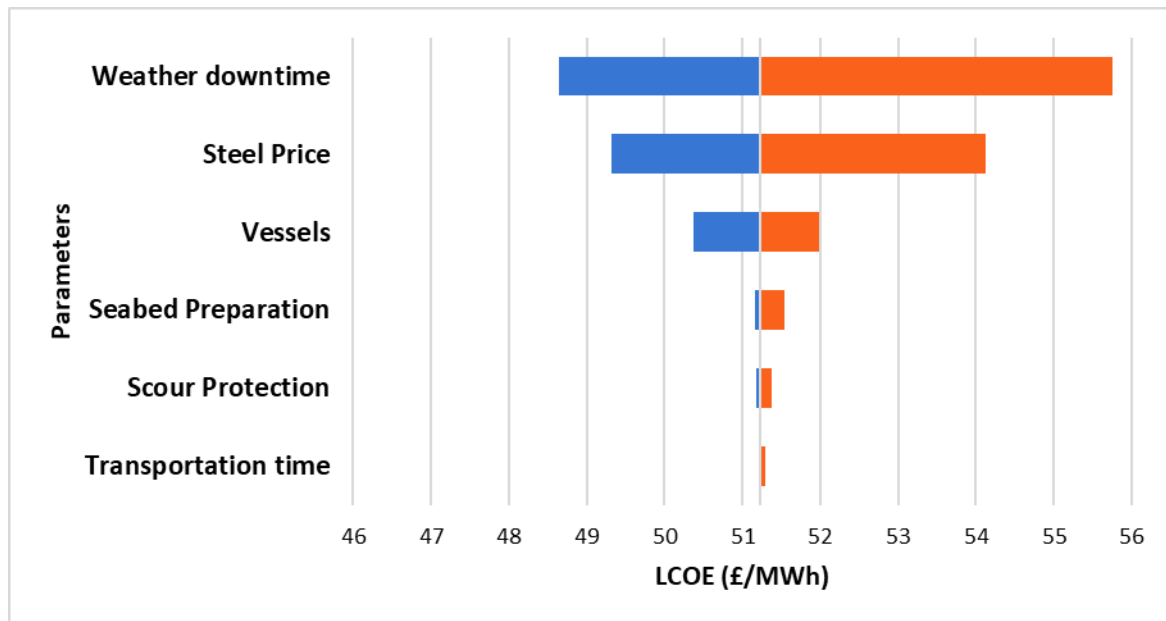
6.1.6. Cost analysis result

The 5MW NREL reference turbine was modelled, and FEA was done while loads were applied. In addition, the RCO framework was performed. As a result, the mass was reduced by 19.7%. The results of weight and volume are listed below. Considering the methodology explained in section 4.4, a rough estimation of the levelized cost of energy for reference and optimised designs can be calculated. An example of a calculation spreadsheet is provided in Appendix A.

Table 6-4 Mass and volume estimation of steel in reference and optimised design of 5MW NREL

	Reference Model		Optimised Model (RCO)	
	Volume (m ³)	Mass (Tn)	Volume (m ³)	Mass (Kg)
Tower	29.2	246.9	26	219.3
Transition Piece	7.34	62.4	7.32	62.2
Monopile	66.2	569	49.6	421
Total	105.8	878.3	83	702.6

The sensitivity analysis is done to see the most influencer in changing the cost in this analysis. Figure 6-5 shows that weather downtime and steel price are the main drivers in this matter.



Parameters	Unit	low input	high input	Spread
Transportation time	(£/MWh)	£51.21	£51.29	0.08
Scour Protection	(£/MWh)	£51.18	£51.38	0.2
Seabed Preparation	(£/MWh)	£51.16	£51.54	0.38
Vessels	(£/MWh)	£50.37	£51.98	1.61
Steel Price	(£/MWh)	£49.32	£54.12	4.8
Weather downtime	(£/MWh)	£48.65	£55.76	7.11

Initial LCOE (£/MWh)	£52.59
Optimized LCOE (£/MWh)	£51.23

Figure 6-5 Parameter sensitivity analysis in cost analysis

According to technical reports (Stehly & Duffy, 2020; UK beis, 2020) and considering cost differences in pile transportation, drilling, scouring and structure weight. We can now estimate the CapEx for Reference and Optimised models, which is 1,375,000 £/MW and 1,320,000 £/MW, respectively.

The spread value in sensitivity study is according to internal data from EPCI companies which is not publicly available but, in this study, it has been used to validate for the high level approximations. However, industry status after covid 19 pandemic and Ukraine war has been changed a lot due to increasing the costs in all sections, especially in supply chain which will cause an increase in LCOE and other estimations.

The cost analysis was performed, and a difference of 55k£/MW was estimated between the Reference model and Optimised model CapEx. The LCOE for both cases were calculated, and

the result shows that a 2.6% reduction in the final LCOE price in optimised design is expected, as presented in Table 6-5.

Table 6-5 Final LCOE results comparison

Model	LCOE/MWh	Difference
Reference	52.59	
Optimised	51.23	- 2.6%

6.2. Scaling up approach

6.2.1. FEA Analysis Results

The stability requirements set for the preliminary design of scaled-up models include the structure's eigenfrequency, buckling and stress endurance, summarised in Table 6-6.

Table 6-6 Summarized results for all developed and reference wind turbine support structures

Load Case	5MW NREL	7.5MW	12.5MW	15MW IEA
Maximum Equivalent Stress (MPa)				
ULS	185	295	233	197
Buckling Multiplier				
	2.35	20.1	11.6	4.6
Tower Head Deflection (m)				
	1.79	0.73	1.87	2.1
1st Natural Frequency (Hz)				
	0.285	0.31	0.201	0.188

For 7.5MW and 12.5MW, maximum equivalent stress equals $295MPa$ and $233MPa$, respectively, less than the allowable stress of $323MPa$. The maximum deformation of the support structure is $0.73m$ and $1.87m$, which shows the acceptable deflection experienced by the structure size. Considering the soil deformation, 0.158 and 0.259 degrees rotation at the mudline is observed, less than the allowable value of 0.4 degrees. The first natural frequency is 0.285 Hz which is acceptable for the modal frequency limitation range, as illustrated in Fig. 13. The support structure design is safe under maximum buckling loads as the buckling load

multiplier is 20.1 and 11.6, well below the limit value. Figure 6-6 (a-e) depicts the results of FE Analysis for 7.5MW presented in contour graphs.

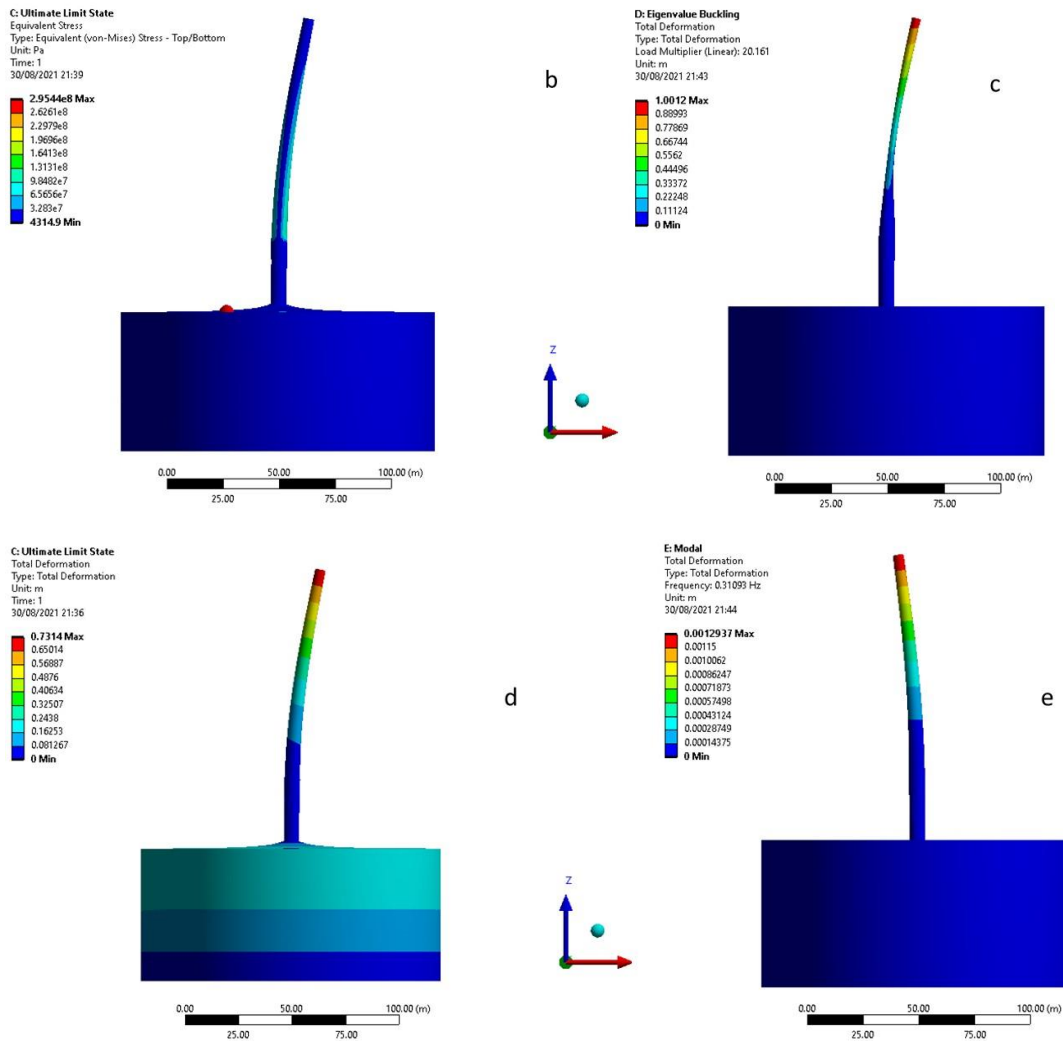


Figure 6-6 FE Analysis results for up-scaled design 7.5MW Wind Turbine b) Von Mises equivalent stress, c) Buckling deformation, d) Total deformation, e) first mode frequency and displacement

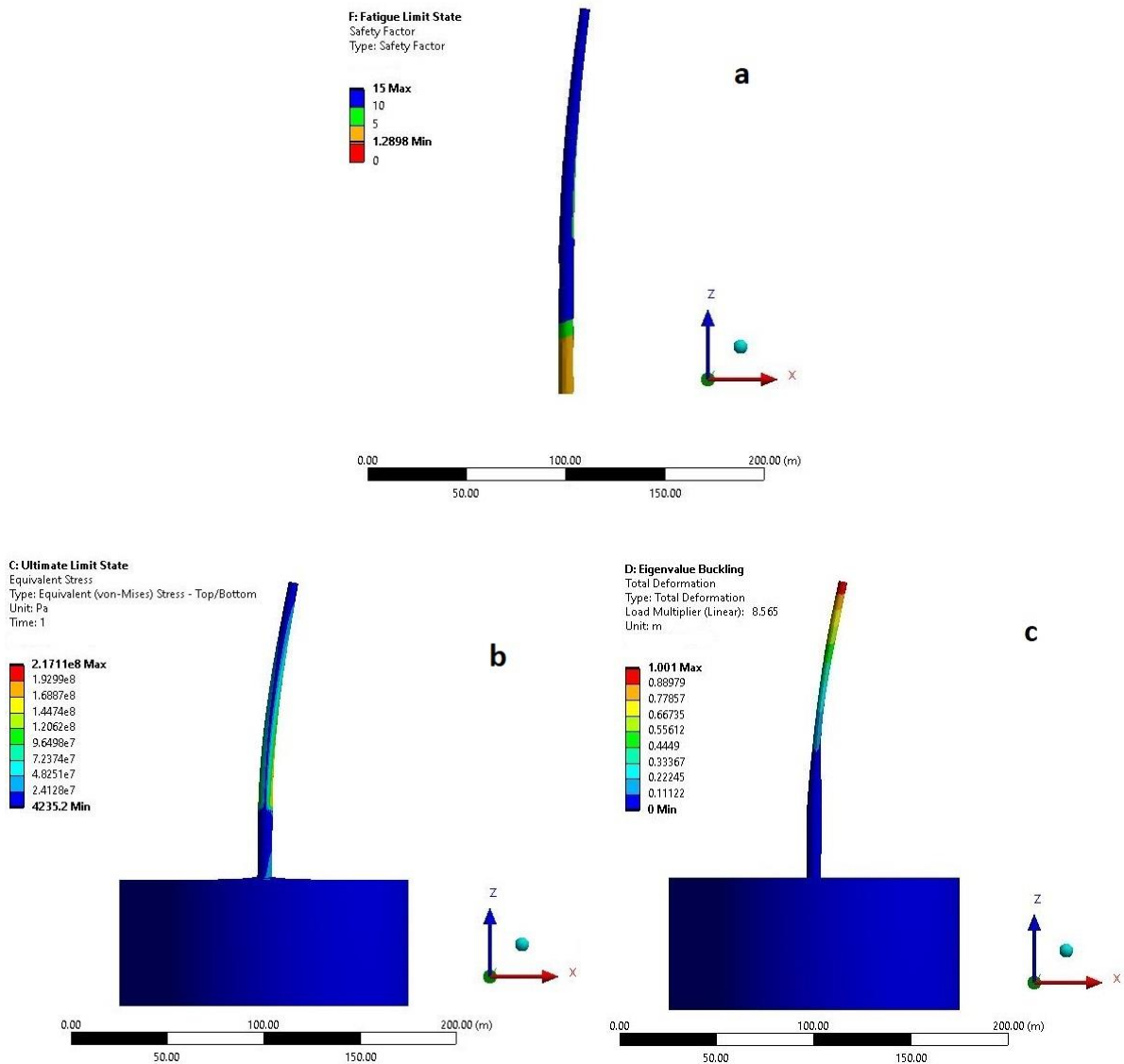
6.3. Water depth sensitivity of IEA 15MW

6.3.1. FE Analysis Results of IEA 15MW

The FEA results of the 3D model include the modal analysis, buckling, fatigue and stress endurance and total deformation of IEA 15MW in a water depth of 30m is presented in Figure 6-7 (a-e).

For the IEA 15MW wind turbine, the maximum equivalent stress equals $217MPa$, less than the allowable stress of $323MPa$. The maximum deformation of the support structure is $1.27m$,

which shows the acceptable deflection experienced by the structure size. Considering the soil deformation, a 0.146-degree rotation at the mudline is observed, less than the allowable value of 0.4 degrees. The first natural frequency is 0.171Hz , acceptable for the modal frequency limitation range. The support structure design is safe under maximum buckling loads as the buckling load multiplier is 8.56 , well above the limit value. The minimum allowable safety factor is 1.15 , and the analysis shows the current design can survive under fatigue-inducing loads by calculating 1.289 for the safety factors.



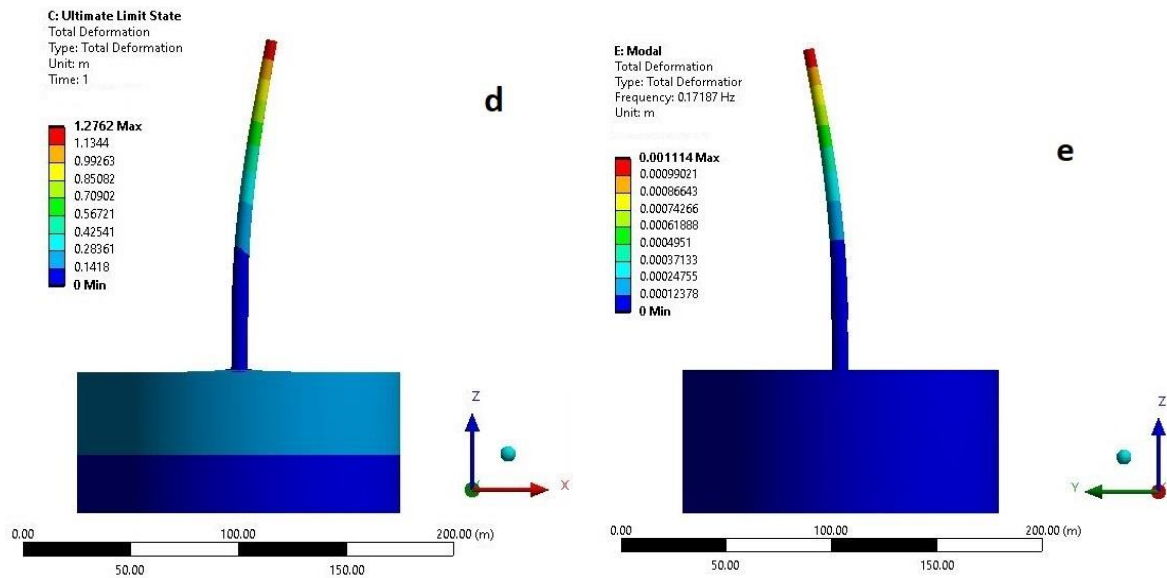


Figure 6-7 FE Analysis results for IEA 15MW a) Fatigue minimum safety factor, b) Von Mises equivalent stress, c) Buckling deformation, d) Total deformation, e) first mode frequency and displacement

6.3.2. Water-depth sensitivity results

The diagram in Figure 6-8 shows how the main design factors (global maximum equivalent stress, buckling and fatigue) change at various water depths. It can be a compact design envelope for the conceptual design of extra-large monopiles. Numerical analysis was performed for each of these points in the graphs. Fatigue analysis reveals that damage impact rises by increasing the water depth, indicating that hydrodynamic loads became more considerable at higher water depth. Fatigue prediction shows maximum damage occurs in the 60m water depth, and the increasing incline happens from shallow to deeper water depth.

The same trend happened in the stress vs water-depth chart, and the maximum equivalent stress increased by increasing water depth. Still, there is no exceeding of the allowable stress, 323MPa , obtained from analysis considering the safety factors. However, there are warnings that buckling could be an issue, as the global buckling multiplier decreased significantly, especially above 50m water depth. As a result, it exceeded the allowable value, 1.4 , mentioned in DNV (DNV GL, 2016).

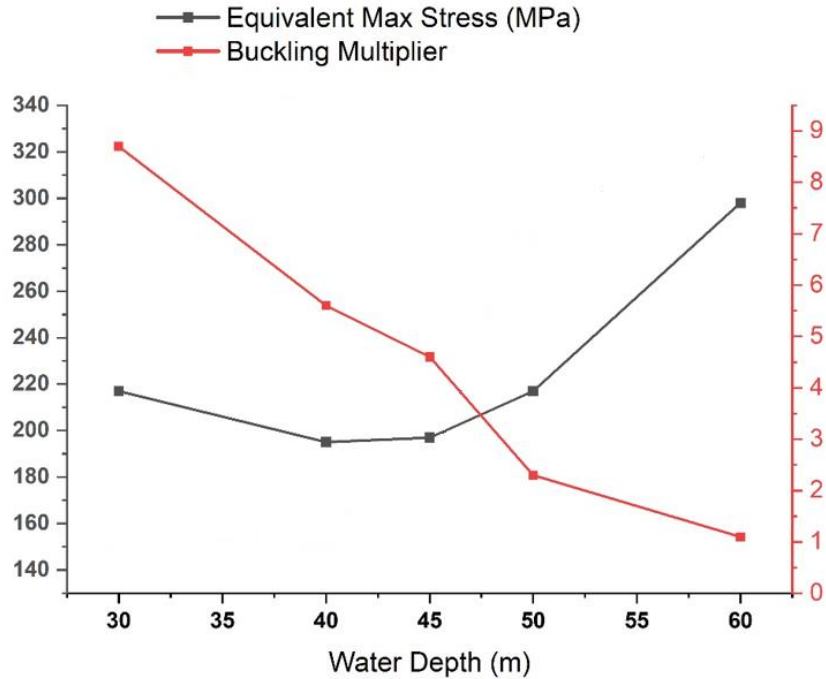


Figure 6-8 Water depth sensitivity of 15MW OWT monopile support structure in Buckling, Maximum global stress, and Global fatigue damage

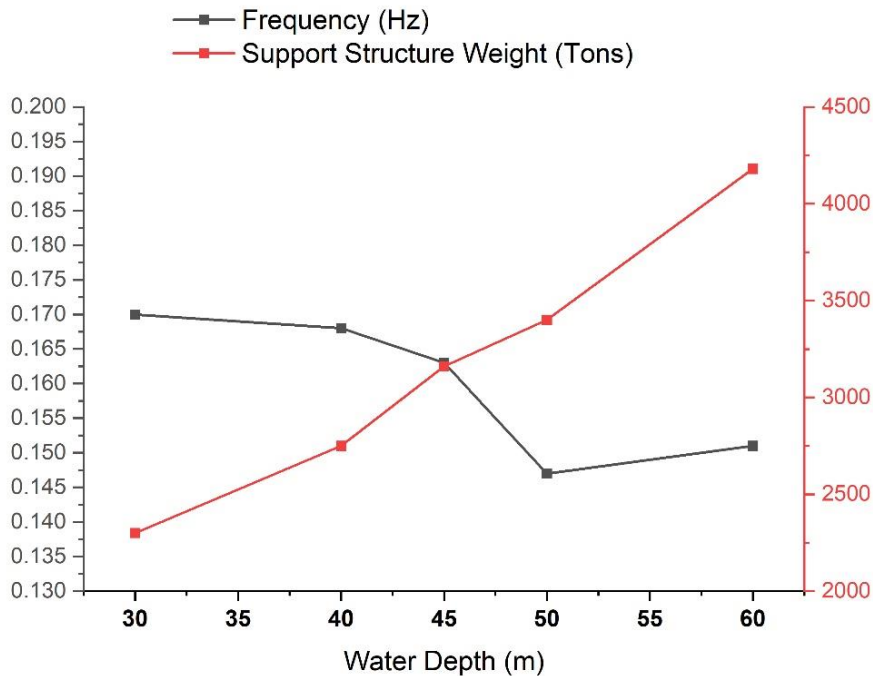


Figure 6-9 Water depth effects on first natural frequency and support structure weight of 15MW OWT

Figure 6-9 shows the predicted frequencies of different designs according to the water depth changes. In all cases, the calculated frequencies are between the respective turbine's 1P and 3P frequency constraints. Also, the trend of support structure mass can be found in the same graph.

The results are based on high fidelity detailed design that considers fatigue and stress; therefore, the mass values and trends are accountable.

Overall, if we wanted to define the maximum safe line for this diagram considering all uncertainties involved, 50m is the ultimate water depth we can imagine for a bulky monopile. However, we all know that in recent projects, even one tonne is crucial, so compared to Jacket structure capabilities and weight, in a water depth of 50m, a monopile is not the first option on paper.

6.4. Design Limitations

The extra-large monopile is approaching nine metres or more in diameter (Katsikogiannis et al., 2019). At this moment, high-capacity wind turbines are being manufactured and need next-generation XXL monopiles. The growing size of the monopile exhibits many practical obstacles (such as logistics, installation, and manufacturing) and design/analysis related. The design limitation was investigated in this study by performing a preliminary design of a support structure (from the seabed to the nacelle) for large and extra-large wind turbines from 30m to 60m water depth. The water depth sensitivity analysis for 15MW OWT was more significant than current industry standards, intending to put our present models to the test. However, several design limitations must be considered when designing extra-large monopiles for deep water depths. Some of these limitations include:

1. **Geotechnical Conditions:** The soil conditions at the wind farm site can significantly impact the design of the monopile. The soil may be more unstable or have lower bearing capacity in deep water depths, requiring more extensive or deeper foundations.
2. **Structural Integrity:** Extra large monopiles are subject to significant loads and stresses from the wind turbine, waves, and currents. Designers must ensure that the monopile can withstand these loads while maintaining its structural integrity over the wind farm's lifetime.
3. **Transportation and Installation:** As the size and weight of monopiles increase, transportation and installation become more challenging. Specialized vessels and equipment may be required to transport and install these structures, which can add significant costs to the project.
4. **Environmental Conditions:** Offshore wind farms are exposed to harsh environmental conditions, including high winds, waves, and corrosion. Designers must ensure that the

monopile and associated components are resistant to these conditions and can operate safely and efficiently over the wind farm's lifetime.

5. Manufacturing: The manufacturing process for extra-large monopiles can be complex and costly. Fabrication facilities must be able to handle the large size and weight of these structures and quality control must be carefully managed to ensure that the monopile meets the required specifications. Tolerance concerns may arise either.

The most up-to-date designs can account for soil-structure interaction. However, different physical load-bearing mechanisms are at work for big-diameter foundations. The traditional p-y curve approach is insufficient for accurate soil-structure modelling and needs some modifications (Rezaei et al., 2018). Modelling the hydrodynamic loading by diffraction slightly impacts the magnitude of the stresses for this diameter monopile. As a result, Morison's equation can be utilized without being overly conservative. The diffraction effect should be considered for monopiles larger than 10m in diameter, as preliminary load calculations indicate a 10-15% fatigue load decrease during the lifetime (Igwemezie et al., 2019). Even with the ever-increasing number of wind turbines, monopiles will be around for a long time.

7. Conclusions

7.1. Summary

In this study, an RCO framework for OWT support structures was developed. A parametric FEA model of OWT monopile support structures took into account stochastic environmental loads and material properties. The parametric FEA model was optimised in two different methods, traditional Deterministic Optimisation (DO) method and newly developed Reliability-Constrained Optimisation (RCO) framework in which Genetic Algorithm (GA) combined with the response surface and Six Sigma Analysis in order to evaluate the reliability and then optimised model considering the structural probability of failure.

Both optimised designs reduced the mass of structure 19.7% and 19.97% by RCO and DO, respectively. However, by assessing the reliability index and probability of failure of DO optimised design and compared with reliability index and probability of failure of RCO design, considering the standard target reliability ($\beta > 3.8$) as threshold, DO design failed to pass the target reliability assessment criteria in modal analysis. This shows the necessity of considering stochastic variables and reliability-based techniques in future optimisation procedures. In general, the following conclusions can also be drawn from this study:

- In the first step, good agreement is observed when comparing the deflection of the tower top section of the reference OWT and the developed ANSYS models, which confirms the validity of the initial FEA geometry.

- During the deterministic optimisation process, the whole mass of the structure was reduced by 19.97%.
- A practical response surface approach evaluates the failure function at sampling points. In addition, a Monte Carlo simulation with a Latin Hypercube reduction method technique is applied to assess the failure probability.
- The necessity for Reliability-Constrained Optimisation for a large OWT in harsh environmental conditions is evident. This optimisation framework has been proved the necessity of considering stochastic variables and reliability-based techniques in optimisation procedures.
- This study shows that not all suggested deterministic optimised design candidates fulfil structural reliability criteria. For instance, the reliability index in resonance capacity in DO design exceeds the allowable value, while the structural design fulfils all limit state function criteria in the deterministic optimisation process.
- Fatigue damage life assessment was performed on the optimised model (RCO) using the DEL approach, and designed thicknesses are acceptable according to standards and recommendations.
- LCOE Comparison was performed between the original and optimised design, which showed a 2% cost saving caused by the RCO framework.

This study also focuses on developing a parametric equation to estimate the weight and suitable water depth for future extra-large offshore wind turbines. Also, the feasibility of large bottom-fix foundations, such as monopile, in the deeper sea was examined by performing FEA (finite element analysis) simulations.

The relation between the weight of monopile structure vs turbine rating and water depth for preliminary design were extracted and utilised in functions. A dataset of several OWTs has been used from previous projects to gain this objective. The results showed that the equation has acceptable estimated values.

Furthermore, a scale-up approach is suggested for large monopile. This approach developed a support structure and tower of turbines with an estimated 7.5MW and 12.5MW. The up-scaled models can be considered preliminary designs for further studies and optimisations since the models' geometry and scale-up methodology are validated. The FE analysis results show a good agreement when comparing the design criteria by DNV. Evaluations on monopiles' static lateral load-carrying capacity in dense sand subjected to aero-hydro dynamic loads using 3D finite element analyses in fatigue and ultimate load cases were performed using the DEL

approach. The results showed that the calculated scale factors and the procedure on scaled models are satisfactory, as the computed values in maximum equivalent stress, global buckling, resonance, and fatigue capacities fulfilled the standard criteria.

In addition, the feasibility of fixed-bottom support structures in different water depths was investigated based on a high-fidelity detailed design that considered ultimate and fatigue limit states for large bottom-fix foundations.

The sensitivity analysis has been done on the IEA 15MW reference support structure using numerical calculations and 3D geometry. The maximum equivalent stress, first natural frequency, global buckling, fatigue damage and safety factor have been studied in water depths between 30-60m. The reference turbine validates the geometry and applied loads as the FEA results match the values compared to the definition report. The results show that the current design and dimension of IEA 15MW can stand up to 50m of water depth with a diameter of 10m. However, a detailed fatigue analysis needs to be done, which may decrease structure tolerance. The global buckling multiplier decreased considerably, significantly above 50m water depth, and maximum equivalent stress is on edge. Also, the support structure mass for the deeper sea was estimated and presented considering the natural frequency of designs.

In addition to these technical studies, manufacturing, transportation, lifting and installation procedures must be considered when it comes to the applicability of a structure in deep seas.

7.2. Statement of contributions

This study provides knowledge in a novel and provides value to stakeholders. Though the research is scientifically sound, all the best methods have been followed, and results have been validated against operational site reports and state-of-the-art methods. Furthermore, through an extensive literature review and working with experts in academia and industry, the research has been promised to follow the most appropriate and highest standards.

Section	Novelty	Impact
Reliability-constrained optimisation framework	Develops a framework for optimisation of an OWT support structure by contributing the target	Researchers and industry will benefit from this approach in the preliminary design step to have better

	reliability next to other typical constraints involving an iterative optimisation process using stochastic variables.	recommendations and optimised structures in early engagement meetings with their clients.
Multi-layered Validation approach	Validation of the RCO framework has been done in a multi-stage process, firstly by checking the geometry of the parametric model, secondly by assessing the fatigue life of the optimised model and then finally by comparing the LCOE of original and optimised designs.	This validation process helps other researchers or industries rely on the framework more efficiently in their future conceptual design optimisation process.
Scale-up approach and preliminary weight estimation equation	The corresponding equation in order to estimate the weight of a scaled-up support structure utilised the very recent wind farm data in the development process. Therefore, it can give the designer a good weight approximation in case of considering larger wind turbines such as 15MW or more.	Companies that want to be involved in Engineering, Procurement, Construction and Installation (EPCI) agreements with their clients need to provide feed information about that project. One of the most important sections in this feed data is the type of foundation and the estimated weight of that support structure. Here in this thesis, the developed preliminary weight approximation formula helps these companies reach that

		estimation by applying their factors in the equation. This is a time-saving opportunity.
Water depth sensitivity and feasibility of a monopile	This part of the study can be considered an envelope design for extra-large monopiles with a futuristic view in deep water depth. It felt the most relevant aspects of applicability of a monopile in water depth more than 30m.	Applicability and feasibility of a foundation type in different water depths are vital for industry. Choosing the right support structure considering cost, lifting vessels, fabrication tolerances, etc., needs preview information about that specific foundation. Monopiles, as the most common type of support structures, are usually the first alternative for most companies to install. The current sensitivity study in this thesis gives adequate information to define the limitations of monopile in the deep water of seas.

7.3. Future work

The RCO framework could be applied to other types of structures. For example, it could be valuable to be utilised in jacket structures for large wind turbines.

Considering potential future work from extra-large monopile offshore wind turbines and support structures, the installation, transportation and lifting problems in academic studies are necessary. Splitting the structure using Single slip joint or Double slip joint approaches is suggested and needs more studies in future.

Current design procedure and optimisation framework is in TRL 1, The framework can be applied in more detailed designs considering more accurate loads and time conditions for future works.

References

- Abhinav, K. A., & Saha, N. (2017). Stochastic response of jacket supported offshore wind turbines for varying soil parameters. *Renewable Energy*, *101*, 550–564. <https://doi.org/10.1016/j.renene.2016.09.019>
- Aldersey-Williams, J., Broadbent, I. D., & Strachan, P. A. (2020). Analysis of United Kingdom offshore wind farm performance using public data: Improving the evidence base for policymaking. *Utilities Policy*, *62*. <https://doi.org/10.1016/j.jup.2019.100985>
- Al-Sanad, S., Wang, L., Parol, J., & Kolios, A. (2021). Reliability-based design optimisation framework for wind turbine towers. *Renewable Energy*, *167*, 942–953. <https://doi.org/10.1016/j.renene.2020.12.022>
- Altes, J., Rackwitz, R., & Recke, H. (1990). *Reliability Analysis of Mechanical Components using the Stochastic Finite Element Code PERMAS-RA*.
- Anderson, TL. (2017). *FRACTURE MECHANICS Fourth Edition Fundamentals and Applications*.
- Arora, S., Hazan, E., & Kale, S. (2012). The Multiplicative Weights Update Method: a Meta-Algorithm and Applications. *Theory of Computing*, *8*(1), 121–164. <https://doi.org/10.4086/toc.2012.v008a006>
- Arshad, M., & O’Kelly, B. C. (2013). *Offshore wind-turbine structures : a review*. 166, 139–152.
- Ashuri, T. (2012). *Beyond Classical Upscaling : Integrated Aeroservoelastic Design and Optimisation of Large Offshore Wind Turbines*.
- Bak, C., Zahle, F., Bitsche, R., Kim, T., Yde, A., Henriksen, L. C., Hansen, M. H., Blasques, J. P. A. A., Gaunaa, M., & Natarajan, A. (2013). *The DTU 10-MW Reference Wind Turbine*.
- Banzo, M., & Ramos, A. (2011). Stochastic optimisation model for electric power system planning of offshore wind farms. *IEEE Transactions on Power Systems*, *26*(3), 1338–1348. <https://doi.org/10.1109/TPWRS.2010.2075944>

- Bezerra, M. A., Santelli, R. E., Oliveira, E. P., Villar, L. S., & Escalera, L. A. (2008). Response surface methodology (RSM) as a tool for optimisation in analytical chemistry. *Talanta*, 76(5), 965–977. <https://doi.org/10.1016/j.talanta.2008.05.019>
- Bortolotti, P., Canet Tarrés, H., Dykes, K., Merz, K., Sethuraman, L., Verelst, D., & Zahle, F. (2019). Systems Engineering in Wind Energy - WP2.1 Reference Wind Turbines. *IEA Wind TCP Task 37*, May. <https://www.osti.gov/biblio/1529216-iea-wind-tcp-task-systems-engineering-wind-energy-wp2-reference-wind-turbines>
- Box, G. E. P., & Wilson, K. B. (1951). On the Experimental Attainment of Optimum Conditions. In *Journal of the Royal Statistical Society: Series B (Methodological)* (Vol. 13, Issue 1, pp. 1–38). <https://doi.org/10.1111/j.2517-6161.1951.tb00067.x>
- Breitung, K. (1984). Asymptotic approximations for multinormal integrals. *Journal of Engineering Mechanics*, 110(3), 357–366.
- Brown, J. N., & Brown, R. C. (2012). Process optimisation of an auger pyrolyzer with heat carrier using response surface methodology. *Bioresource Technology*, 103(1), 405–414. <https://doi.org/10.1016/j.biortech.2011.09.117>
- Byrne B, & RA McAdam, H. B. G. H. C. M. W. B. (2017). *PISA: NEW DESIGN METHODS FOR OFFSHORE WIND TURBINE MONOPILES*.
- Byrne, B. W., Houlsby, G. T., Burd, H. J., Gavin, K. G., Igoe, D. J. P., Jardine, R. J., Martin, C. M., McAdam, R. A., Potts, D. M., Taborda, D. M. G., & Zdravkovic, L. (2020). PISA design model for monopiles for offshore wind turbines: Application to a stiff glacial clay till. *Geotechnique*, 70(11), 1030–1047. <https://doi.org/10.1680/jgeot.18.P.255>
- Cai, G. Q., & Elishakoff, I. (1994). Structural safety Refined second-order reliability analysis *. In *Structural Safety* (Vol. 14).
- Carswell, W., Johansson, J., Løvholt, F., Arwade, S. R., Madshus, C., DeGroot, D. J., & Myers, A. T. (2015). Foundation damping and the dynamics of offshore wind turbine monopiles. *Renewable Energy*, 80, 724–736. <https://doi.org/10.1016/j.renene.2015.02.058>

- Catapult ORE (2021) Wind farm costs – Guide to an offshore wind farm. Available at: <https://guidetoanoffshorewindfarm.com/wind-farm-costs> (Accessed: 20 February 2021).
- Chakrabarti, S. (2005). *Hand Book of Offshore Engineering*.
- Chehoury, A., Younes, R., Ilinca, A., & Perron, J. (2015). Review of performance optimisation techniques applied to wind turbines. *Applied Energy*, 142, 361–388. <https://doi.org/10.1016/j.apenergy.2014.12.043>
- Cheng, J., & Li, Q. S. (2009). Application of the response surface methods to solve inverse reliability problems with implicit response functions. *Computational Mechanics*, 43(4), 451–459. <https://doi.org/10.1007/s00466-008-0320-0>
- Clauss, G. F., & Birk, L. (1996). Hydrodynamic shape optimisation of large offshore structures. In *Applied Ocean Research* (Vol. 18). Elsevier Science Limited.
- Clauss, G. F., & Birk, L. (1997). Hydrodynamic Shape optimisation of large offshore structures. *Proceedings of the Conference on Optimisation in Industry*, 1187(96), 195–200.
- Cox, D. C., & Baybutt, P. (1981). Methods for Uncertainty Analysis: A Comparative Survey. *Risk Analysis*, 1(4), 251–258. <https://doi.org/10.1111/j.1539-6924.1981.tb01425.x>
- Damiani, R. R., Song, H., Robertson, A. N., & Jonkman, J. M. (2013). Assessing the importance of nonlinearities in the development of a substructure model for the wind turbine CAE tool fast. *Proceedings of the International Conference on Offshore Mechanics and Arctic Engineering - OMAE*, 8(March). <https://doi.org/10.1115/OMAE2013-11434>
- De Morais, D. R., Foschiera, L. C., & Gomes, H. M. (2021). Time and Frequency Domain Analysis of Wind Turbine Towers Under Spatially Correlated Wind Field. *International Journal of Steel Structures*, 21(6), 2028–2044. <https://doi.org/10.1007/s13296-021-00551-5>
- DHI. (2020). *Annual Report 2020*.
- Dirlik, T. (1985). *Application of computers in fatigue analysis*.

- Diveux, T., Sebastian, P., Bernard, D., Puiggali, J. R., & Grandidier, J. Y. (2001a). Horizontal axis wind turbine systems: optimisation using genetic algorithms. *Wind Energy*, 4(4), 151–171. <https://doi.org/10.1002/we.51>
- Diveux, T., Sebastian, P., Bernard, D., Puiggali, J. R., & Grandidier, J. Y. (2001b). Horizontal axis wind turbine systems: optimisation using genetic algorithms. *Wind Energy*, 4(4), 151–171. <https://doi.org/10.1002/we.51>
- DNV GL. (1987). RP-C203: Fatigue Design of Offshore Structures. *Welding International*, 1(12), 1155–1161. <https://doi.org/10.1080/09507118709452166>
- DNV GL. (1992). *Structural reliability analysis of marine structures Classification - DNV 1992.pdf* (p. 51).
- DNV GL. (2010a). DNV C-205: ENVIRONMENTAL CONDITIONS AND ENVIRONMENTAL LOADS. *INTELEC, International Telecommunications Energy Conference*, 2(October), 92–99. <https://doi.org/10.1109/INTLEC.1993.388591>
- DNV GL. (2010b). *DNV-RP-C201: Buckling Strength of Plated Structures*. October, 33.
- DNV GL. (2011). OS-C101: Design of Offshore Steel Structures , General - LRFD Method. *Det Norske Veritas, 2018 Ed.*(April), 49.
- DNV GL. (2014). *DNV-OS-J101 Design of Offshore Wind Turbine Structures*. May, 212–214.
- DNV GL. (2016). *DNV-ST-0126: Support Structures for Wind Turbines*. July.
- Dong, W., Moan, T., & Gao, Z. (2012). Fatigue reliability analysis of the jacket support structure for offshore wind turbine considering the effect of corrosion and inspection. *Reliability Engineering and System Safety*, 106, 11–27. <https://doi.org/10.1016/j.ress.2012.06.011>
- Drucker and Prager. (2016). *Soil Mechanics or Plastic Analysis*. 10(2), 157–165.
- Eke, G. B., & Onyewudiala, J. I. (2010). *Optimisation of Wind Turbine Blades Using Genetic Algorithm*.
- Enevoldsen, I., & Sorensen, J. D. (1994). *Structural safety ELSEVIER Reliability-based optimisation in structural engineering* *.

- Eroğlu, Y., & Seçkiner, S. U. (2012). Design of wind farm layout using ant colony algorithm. *Renewable Energy*, 44, 53–62. <https://doi.org/10.1016/j.renene.2011.12.013>
- Eurocode 3. (2005). *EN 1993-1-1: Eurocode 3: Design of steel structures - Part 1-1: General rules and rules for buildings*.
- Faravelli, L. (1989). *Response-surface approach for reliability analysis*. *Journal of Engineering Mechanics*, 115(12), 2763-2781.
- Fernandes, D. R. M., Rocha, C., Aloise, D., Ribeiro, G. M., Santos, E. M., & Silva, A. (2014). A simple and effective genetic algorithm for the two-stage capacitated facility location problem. *Computers and Industrial Engineering*, 75(1), 200–208. <https://doi.org/10.1016/j.cie.2014.05.023>
- Freebry, G., & Musial, W. (2000). Determining equivalent damage loading for full-scale wind turbine blade fatigue tests. *2000 ASME Wind Energy Symposium*, c, 287–297. <https://doi.org/10.2514/6.2000-50>
- Freudenthal, A. M., Asce, F., Garrelts, J. M., Asce, F., Shinozuka, M., & Asce, A. M. (1966). *THE ANALYSIS OF STRUCTURAL SAFETY ST 1*.
- Gaertner, E., Rinker, J., Sethuraman, L., Zahle, F., Anderson, B., Barter, G., Abbas, N., Meng, F., Bortolotti, P., Skrzypinski, W., Scott, G., Feil, R., Bredmose, H., Dykes, K., Shields, M., Allen, C., & Viselli, A. (2020). *IEA Wind - Offshore Reference Wind - 15MW*.
- Gamesa, S., Drive, D., Boost, P., Gamesa, S., Tacke, M., Gamesa, S., Energy, R., Nauen, A., Gamesa, S., Business, O., Cost, L., & Sg, T. (2020). Press release Powered by change : Siemens Gamesa launches 14 MW offshore Direct Drive turbine. *Siemens Gamesa Renewable Energy*, 1–3.
- Gao, B., Ye, G., Zhang, Q., Xie, Y., & Yan, B. (2021). Numerical simulation of suction bucket foundation response located in liquefiable sand under earthquakes. *Ocean Engineering*, 235. <https://doi.org/10.1016/j.oceaneng.2021.109394>
- Gavin, H. P., & Yau, S. C. (2008). High-order limit state functions in the response surface method for structural reliability analysis. *Structural Safety*, 30(2), 162–179. <https://doi.org/10.1016/j.strusafe.2006.10.003>

- Gentils, T., Wang, L., & Kolios, A. (2017). Integrated structural optimisation of offshore wind turbine support structures based on finite element analysis and genetic algorithm. *Applied Energy*, *199*(August), 187–204. <https://doi.org/10.1016/j.apenergy.2017.05.009>
- George, J., José Nunes de Almeida Sarmiento Eng Cyril Gilles Emile Gordreau, A., Alberto Caiado Falcão de Campos Supervisor, J., & José Nunes de Almeida Sarmiento, A. (2014). *WindFloat design for different turbine sizes Energy Engineering and Management Examination Committee*.
- Giguere, P., & Selig, M. (2000). *Blade geometry optimization for the design of wind turbine rotors*. In 2000 ASME Wind Energy Symposium (p. 45).
- Gilbert, R. B., Wang, S.-T., Senanayake, A., & Rendon, E. (2015). *Desing of Wind Turbine Monopiles for Lateral Loads Design of Wind Turbine Monopiles for Lateral Loads Design of Wind Turbine Monopiles for Lateral Loads Design of Wind Turbine Monopiles for Lateral Loads*.
- Gollwitzer, S., & Rackwitz, R. (1988). *An efficient numerical solution to the multinormal integral*.
- Grasso, F. (2012). *Hybrid optimization for wind turbine thick airfoils*. In 53rd AIAA/ASME/ASCE/AHS/ASC Structures, Structural Dynamics and Materials Conference 20th AIAA/ASME/AHS Adaptive Structures Conference 14th AIAA (p. 1354).
- Greco, A., Sheng, S., Keller, J., & Erdemir, A. (2013). Material wear and fatigue in wind turbine Systems. *Wear*, *302*(1–2), 1583–1591. <https://doi.org/10.1016/j.wear.2013.01.060>
- Gualtieri, G., Emejeamara, F. C., Tomlin, A. S., Micallef, D., van Bussel, G., Ishugah, T. F., Li, Y., Wang, R. Z., Kiplagat, J. K., Millward-Hopkins, J. T., Tomlin, A. S., Ma, L., Ingham, D. B., Pourkashanian, M., Byrne, R., Hewitt, N. J., Griffiths, P., MacArtain, P., Macdonald, R. W., ... Leuzzi, G. (2019). BSI Standards Publication Wind energy generation systems. *Boundary-Layer Meteorology*, *164*(1), 1–5.
- Guo, Y., Wang, H., & Lian, J. (2022). Review of integrated installation technologies for offshore wind turbines: Current progress and future development trends. In *Energy*

Conversion and Management (Vol. 255). Elsevier Ltd.
<https://doi.org/10.1016/j.enconman.2022.115319>

- Häfele, J. (2019). *A numerically efficient and holistic approach to design optimisation of offshore wind turbine jacket substructures*.
- Hall, M. (2012). A Cumulative Multi-Niching Genetic Algorithm for Multimodal Function Optimisation. In *IJARAI International Journal of Advanced Research in Artificial Intelligence* (Vol. 1, Issue 9). www.ijarai.thesai.org
- Harry, M. J., & Motorola University Press. (1997). *The Nature of six sigma quality* (p. 25).
- Hasofer, A. M., Lind, N. C., & Asce Iivtroouction, A. M. (1974). *EXACT AND INVARIANT SECOND-MOMENT CODE FORMAT*.
- Haupt, R. L., Haupt, S. E., & Wiley, A. J. (2004). *Algorithms Second Edition*.
- Heggen, T., Lende, R., & Løvseth, J. (1998). *Analysis of Long Time Series of Coastal Wind*.
[https://doi.org/https://doi.org/10.1175/1520-0469\(1998\)055<2907:AOLTSO>2.0.CO;2](https://doi.org/https://doi.org/10.1175/1520-0469(1998)055<2907:AOLTSO>2.0.CO;2)
- Hohenbichler, M., & Rackwitz, R. (1981). ON STRUCTURAL RELIABILITY OF PARALLEL SYSTEMS. In *Reliability Engineering* (Vol. 2, Issue 6).
- IEC. (2005). IEC 61400-1. *IEC, 61400-01(2)*, 88. <https://doi.org/10.4172/2155-9600.1000405>
- IEC. (2019). IEC 61400-3-1. *IEC*, 1–11.
- Igwemezie, V., Mehmanparast, A., & Kolios, A. (2019). Current trend in offshore wind energy sector and material requirements for fatigue resistance improvement in large wind turbine support structures – A review. *Renewable and Sustainable Energy Reviews*, *101*(March), 181–196. <https://doi.org/10.1016/j.rser.2018.11.002>
- Impollonia, N., & Sofi, A. (2003). A response surface approach for the static analysis of stochastic structures with geometrical nonlinearities. *Computer Methods in Applied Mechanics and Engineering*, *192*(37–38), 4109–4129. [https://doi.org/10.1016/S0045-7825\(03\)00379-7](https://doi.org/10.1016/S0045-7825(03)00379-7)

- Ioannou, A., Angus, A., & Brennan, F. (2017). Stochastic Prediction of Offshore Wind Farm LCOE through an Integrated Cost Model. *Energy Procedia*, 107, 383–389. <https://doi.org/10.1016/j.egypro.2016.12.180>
- Isaac Van der Hoven. (1957). *Power Spectrum Of Horizontal Wind Speed In The Frequency Range From 0.0007 To 900 Cycles Per Hour*. 160–164. [https://doi.org/https://doi.org/10.1175/1520-0469\(1957\)014<0160:PSOHWS>2.0.CO;2](https://doi.org/https://doi.org/10.1175/1520-0469(1957)014<0160:PSOHWS>2.0.CO;2)
- Ishtiyak, M., Sarkar, A., Fazeres-Ferradosa, T., Rosa-Santos, P., & Taveira-Pinto, F. (2021). Bottom-supported tension leg towers with inclined tethers for offshore wind turbines. *Proceedings of the Institution of Civil Engineers: Maritime Engineering*, 174(4), 124–133. <https://doi.org/10.1680/jmaen.2021.001>
- Ivanhoe, R. O., Wang, L., & Kolios, A. (2020). Generic framework for reliability assessment of offshore wind turbine jacket support structures under stochastic and time dependent variables. *Ocean Engineering*, 216(August 2018), 107691. <https://doi.org/10.1016/j.oceaneng.2020.107691>
- J Nocedal, & SJ Wright. (2006). *Quadratic Programming*.
- Jonkman, J., & Musial, W. (2010). *Offshore Code Comparison Collaboration (OC3) for IEA Task 23 Offshore Wind Technology and Deployment Offshore Code Comparison Collaboration (OC3) for IEA Task 23 Offshore Wind Technology and Deployment. December.*
- Jonkman, Jm., Butterfield, S., Musial, W., & Scott, G. (2009). Definition of a 5-MW reference wind turbine for offshore system development. *NREL, February*, 1–75. <https://doi.org/10.1002/ajmg.10175>
- Jung, S., Kim, S. R., Patil, A., & Hung, L. C. (2015). Effect of monopile foundation modeling on the structural response of a 5-MW offshore wind turbine tower. *Ocean Engineering*, 109, 479–488. <https://doi.org/10.1016/j.oceaneng.2015.09.033>
- Kaldellis, J. K., & Kapsali, M. (2013). Shifting towards offshore wind energy—Recent activity and future development. *Energy Policy*, 53, 136–148. <https://doi.org/10.1016/j.enpol.2012.10.032>

- Kallehave, D., Byrne, B. W., LeBlanc Thilsted, C., & Mikkelsen, K. K. (2015). Optimisation of monopiles for offshore wind turbines. *Philosophical Transactions of the Royal Society A: Mathematical, Physical and Engineering Sciences*, 373(2035). <https://doi.org/10.1098/rsta.2014.0100>
- Karimi, M., Hall, M., Buckham, B., & Crawford, C. (2017). A multi-objective design optimisation approach for floating offshore wind turbine support structures. *Journal of Ocean Engineering and Marine Energy*, 3(1), 69–87. <https://doi.org/10.1007/s40722-016-0072-4>
- Katsikogiannis, G., Bachynski, E. E., & Page, A. M. (2019). Fatigue sensitivity to foundation modelling in different operational states for the DTU 10MW monopile-based offshore wind turbine. *Journal of Physics: Conference Series*, 1356(1), 1–12. <https://doi.org/10.1088/1742-6596/1356/1/012019>
- Kharmanda, G., Ibrahim, M. H., Abo Al-kheer, A., Guerin, F., & El-Hami, A. (2014). Reliability-based design optimisation of shank chisel plough using optimum safety factor strategy. *Computers and Electronics in Agriculture*, 109, 162–171. <https://doi.org/10.1016/j.compag.2014.09.001>
- Khuri, A., & Cornell, J. (1996). *Response Surfaces: Designs and Analyses*.
- Kikuchi, Y., & Ishihara, T. (2019). Upscaling and levelized cost of energy for offshore wind turbines supported by semi-submersible floating platforms. *Journal of Physics: Conference Series*, 1356(1). <https://doi.org/10.1088/1742-6596/1356/1/012033>
- Kim, G., Kyung, D., Park, D., & Lee, J. (2015). CPT-based p-y analysis for mono-piles in sands under static and cyclic loading conditions. *Geomechanics and Engineering*, 9(3), 313–328. <https://doi.org/10.12989/gae.2015.9.3.313>
- Kim, S.-H., & Na, S.-W. (1997). *Response surface method using vector projected sampling points* (Vol. 19, Issue 1).
- Kiureghian, A. der, Asce, M., Lin, H.-Z., & Hwang, S.-J. (1987). *SECOND-ORDER RELIABILITY APPROXIMATIONS*.
- Kolios, A. (2010). A MULTI-CONFIGURATION APPROACH TO RELIABILITY BASED STRUCTURAL INTEGRITY ASSESSMENT FOR ULTIMATE STRENGTH. *PhD Thesis, 1*, 320–350. <https://doi.org/10.1558/jsrnc.v4i1.24>

- Kolios, A., & Brennan, F. (2009). *Reliability Based Design of Novel Offshore*. July, 20–24.
- Köylüoğlu, H. U.; Nielsen, S. R. K.; Cakmak, A. S., Köylüoğlu, H. U., Nielsen, S. R. K., & Cakmak, A. S. (1994). *Aalborg Universitet Perturbation Solutions for Random Linear Structural Systems subject to Random Excitation using Stochastic Differential Equations PERTURBATION SOLUTIONS FOR RANDOM LINEAR STRUCTURAL SYSTEMS SUBJECT TO RANDOM EXCITATION USING STOCHASTIC DIFFERENTIAL EQUATIONS*.
- Kuhn, M. J. (2001). *Dynamics and Design Optimisation of Offshore Wind Energy Conversion Systems* (Issue November).
- Kukul, A., David J. Earl, & Michael W. Deem. (2006). Monte Carlo Simulations. In *METHODS IN MOLECULAR BIOLOGY™* (Vol. 443).
- Labuz, J. F., & Zang, A. (2012). Mohr-Coulomb failure criterion. *Rock Mechanics and Rock Engineering*, 45(6), 975–979. <https://doi.org/10.1007/s00603-012-0281-7>
- LaNier, M. W. (2005). *Conceptual Design Study Evaluation of Design and Construction Approaches for Economical Hybrid Steel Concrete Wind Turbine Towers*. January 2005, 1–165.
- Lavassas, I., Nikolaidis, G., Zervas, P., Efthimiou, E., Doudoumis, I. N., & Baniotopoulos, C. C. (2003). Analysis and design of the prototype of a steel 1-MW wind turbine tower. *Engineering Structures*, 25(8), 1097–1106. [https://doi.org/10.1016/S0141-0296\(03\)00059-2](https://doi.org/10.1016/S0141-0296(03)00059-2)
- Lee, Y. S., Choi, B. L., Lee, J. H., Kim, S. Y., & Han, S. (2014a). Reliability-based design optimisation of monopile transition piece for offshore wind turbine system. *Renewable Energy*, 71, 729–741. <https://doi.org/10.1016/j.renene.2014.06.017>
- Lee, Y. S., Choi, B. L., Lee, J. H., Kim, S. Y., & Han, S. (2014b). Reliability-based design optimisation of monopile transition piece for offshore wind turbine system. *Renewable Energy*, 71, 729–741. <https://doi.org/10.1016/j.renene.2014.06.017>
- Leimeister, M., Bachynski, E. E., Muskulus, M., & Thomas, P. (2016). Rational Upscaling of a Semi-submersible Floating Platform Supporting a Wind Turbine. *Energy Procedia*, 94, 434–442. <https://doi.org/10.1016/j.egypro.2016.09.212>

- Leimeister, M., & Kolios, A. (2021). Reliability-based design optimisation of a spar-type floating offshore wind turbine support structure. *Reliability Engineering and System Safety*, 213(May 2020), 107666. <https://doi.org/10.1016/j.res.2021.107666>
- Liao, C. C., Zhao, X. L., & Xu, J. Z. (2012). Blade layers optimisation of wind turbines using FAST and improved PSO Algorithm. *Renewable Energy*, 42, 227–233. <https://doi.org/10.1016/j.renene.2011.08.011>
- Loh, W. L. (1996). On latin hypercube sampling. *Annals of Statistics*, 24(5), 2058–2080. <https://doi.org/10.1214/aos/1069362310>
- Long, H., & Moe, G. (2012). Preliminary design of bottom-fixed lattice offshore wind turbine towers in the fatigue limit state by the frequency domain method. *Journal of Offshore Mechanics and Arctic Engineering*, 134(3). <https://doi.org/10.1115/1.4005200>
- Mackay, & Ross. (1979). *SELF-MUTILATION*.
- Malcolm, D. J., & Hansen, A. C. (2006). *WindPACT Turbine Rotor Design Study: June 2000--June 2002 (Revised)*. April. <https://doi.org/10.2172/15000964>
- Manuel, L., Gilbert, R. B., Kinnas, S. A., Powers, E. J., Tassoulas, J. L., & Tarp-Johansen, N. J. (2008). *Structural Reliability of Offshore Wind Turbines Committee*.
- Martinez-Luengo, M., & Shafiee, M. (2019). Guidelines and cost-benefit analysis of the Structural Health Monitoring implementation in offshore wind turbine support structures. In *Energies* (Vol. 12, Issue 6). MDPI AG. <https://doi.org/10.3390/en12061176>
- Martins, J. R. R. A., & Lambe, A. B. (2013). Multidisciplinary design optimisation: A survey of architectures. *AIAA Journal*, 51(9), 2049–2075. <https://doi.org/10.2514/1.J051895>
- Maymon, G. (1993). PROBABILITY OF FAILURE OF STRUCTURES WITHOUT A CLOSED-FORM FAILURE FUNCTION. In *Computers & Structures* (Vol. 49, Issue 2).
- Mazzolani, F. M., & Piluso, V. (1997). Plastic design of seismic resistant steel frames. *Earthquake Engineering and Structural Dynamics*, 26(2), 167–191.

[https://doi.org/10.1002/\(SICI\)1096-9845\(199702\)26:2<167::AID-EQE630>3.0.CO;2-2](https://doi.org/10.1002/(SICI)1096-9845(199702)26:2<167::AID-EQE630>3.0.CO;2-2)

- Meißner, M. (2020). *Article in High Technology Letters*.
<https://doi.org/10.37896/HTL26.10/1903>
- Melchers, R. E. (2007). Structural reliability theory in the context of structural safety. *Civil Engineering and Environmental Systems*, 24(1), 55–69.
<https://doi.org/10.1080/10286600601025191>
- Melchers, R. E., & Beck, A. T. (2018). *Structural Reliability: Analysis and Prediction*. In *Structural Safety*. Wiley. [https://doi.org/10.1016/s0167-4730\(01\)00007-8](https://doi.org/10.1016/s0167-4730(01)00007-8)
- Metropolis, N., & Ulam, ; S. (1949). The Monte Carlo Method. In *Journal of the American Statistical Association* (Vol. 44, Issue 247).
- Morató, Sriramula, S., Krishnan, N., & Nichols, J. (2017). Ultimate loads and response analysis of a monopile supported offshore wind turbine using fully coupled simulation. *Renewable Energy*, 101, 126–143.
<https://doi.org/10.1016/j.renene.2016.08.056>
- Murray, C. C., Talukdar, D., & Gosavi, A. (2010). Joint Optimisation of Product Price, Display Orientation and Shelf-Space Allocation in Retail Category Management. *Journal of Retailing*, 86(2), 125–136. <https://doi.org/10.1016/j.jretai.2010.02.008>
- Muskulus, M., & Schafhirt, S. (2014). Design optimisation of wind turbine support Structures-A Review. *Journal of Ocean and Wind Energy*, 1(1), 12–22.
- Muskulus, M., & Schafhirt, S. (2015). Reliability-based design of wind turbine support structures. *Symposium on Reliability of Engineering Structures SRES'2015*, 1(1), 12–22. <https://doi.org/10.13140/RG.2.1.5125.5766>
- Nagendra, S., Haftka, R. T., Gfirdal, Z., Starnes, J. H., & Giirdal, Z. (1991). *Design of a Blade-Stiffened Composite Panel with a Hole*.
- Obayashi. (1996). *Construction of the Land Use Capability Classification Algorithm Applying the Analytic Hierarchy Process (AHP) Method*.
- Olivi, L. (1980). *Response Surface Methodology in Risk Analysis*.
- OREC. (2018). *Sparta Portfolio Review 2018/19*.

- P. Schaumann, C. Böker, A. Bechtel, S. L.-H. (2011). *Environmental 906 Wind Engineering and Design of Wind Energy Structures*. 191–253.
- Park, E. K., Jung, H. S., Yang, H. I., Yoo, M. C., Kim, C., & Kim, K. S. (2007). Optimised THP-1 differentiation is required for the detection of responses to weak stimuli. *Inflammation Research*, 56(1), 45–50. <https://doi.org/10.1007/s00011-007-6115-5>
- Parveen, N., Siddiqui, L., Sarif, M. N., Islam, M. S., Khanam, N., & Mohibul, S. (2021). Industries in Delhi: Air pollution versus respiratory morbidities. *Process Safety and Environmental Protection*, 152, 495–512. <https://doi.org/10.1016/j.psep.2021.06.027>
- Pasamontes, L., Gómez Torres, F., Zwick, D., Schafhirt, S., & Muskulus, M. (2014). *SUPPORT STRUCTURE OPTIMISATION FOR OFFSHORE WIND TURBINES WITH A GENETIC ALGORITHM*.
- Passon, P. (2015). Damage equivalent wind–wave correlations on basis of damage contour lines for the fatigue design of offshore wind turbines. *Renewable Energy*, 81, 723–736.
- Passon P, Kühn M (2007). OC3-Benchmark aeroelastischer Simulationsprogramme für Offshore Windenergieanlagen. *Gigawind 5. Symposium*, April 18, Tagungsbeiträge (Proceedings), pages 80-85. Hannover, Germany
- Passon P, Branner K (2015). Condensation of long-term wave climates for the fatigue design of hydrodynamically sensitive offshore wind turbine support structures. *Ships and Offshore Structures (in press)*. doi: 10.1080/17445302.2014.967994.
- Peeringa, J., & Bedon, G. (2017). Fully integrated load analysis included in the structural reliability assessment of a monopile supported offshore wind turbine. *Energy Procedia*, 137, 255–260. <https://doi.org/10.1016/j.egypro.2017.10.348>
- Perelmuter, A., & Yurchenko, V. (2013). Parametric optimisation of steel shell towers of high-power wind turbines. *Procedia Engineering*, 57, 895–905. <https://doi.org/10.1016/j.proeng.2013.04.114>
- Petrini, F., Manenti, S., Gkoumas, K., & Bontempi, F. (2010). Structural design and analysis of offshore wind turbines from a system point of view. *Wind Engineering*, 34(1), 85–108. <https://doi.org/10.1260/0309-524X.34.1.85>

- Pfaffel, S., Faulstich, S., & Rohrig, K. (2017). Performance and reliability of wind turbines: A review. In *Energies* (Vol. 10, Issue 11). MDPI AG. <https://doi.org/10.3390/en10111904>
- Porter, K., Simons, R., Harris, J., & Ferradosa, T. F. (2012). *Scour Development In Complex Sediment Beds*.
- Price, S. J., & Figueira, R. B. (2017). Corrosion protection systems and fatigue corrosion in offshore wind structures: Current status and future perspectives. *Coatings*, 7(2), 1–51. <https://doi.org/10.3390/coatings7020025>
- Psarropoulos, P. N., & Tsompanakis, Y. (2008). Stability of tailings dams under static and seismic loading. *Canadian Geotechnical Journal*, 45(5), 663–675. <https://doi.org/10.1139/T08-014>
- Quarton, D. C. (1998). The evolution of wind turbine design analysis—a twenty year progress review. *Wind Energy*, 1(S1), 5–24. [https://doi.org/10.1002/\(sici\)1099-1824\(199804\)1:1+<5::aid-we1>3.0.co;2-i](https://doi.org/10.1002/(sici)1099-1824(199804)1:1+<5::aid-we1>3.0.co;2-i)
- Rausand, M., Hyland, A. (1994). eds: *System Reliability Theory*. John Wiley & Sons, Inc., Hoboken, NJ, USA.
- Rezaei, R., Fromme, P., & Duffour, P. (2018). Fatigue life sensitivity of monopile-supported offshore wind turbines to damping. *Renewable Energy*, 123, 450–459. <https://doi.org/10.1016/j.renene.2018.02.086>
- Rezvanipour, M., Amirafshari, P., Wang, L., & Kolios, A. (2020). A Reliability-based optimisation framework for offshore wind turbine support structures. *30th European Safety and Reliability Conference, ESREL 2020 and 15th Probabilistic Safety Assessment and Management Conference, PSAM 2020*, 3268–3275. <https://doi.org/10.3850/981-973-0000-00-0>
- Rodon, A., Collette, Y., & Siarry, P. (2003). *A sequential multiobjective optimisation tool designed to manage on line a set of varied algorithms*.
- Rodrigues, F., Lourenco, M., Ribeiro, B., & Pereira, F. C. (2017). Learning Supervised Topic Models for Classification and Regression from Crowds. *IEEE Transactions on Pattern Analysis and Machine Intelligence*, 39(12), 2409–2422. <https://doi.org/10.1109/TPAMI.2017.2648786>

- Rychlik, I. (1987). A new definition of the rainflow cycle counting method Definition 2: rainflow cycle (RFC) counting method. In *IntJ* (Vol. 9, Issue 2).
- Saka, M. P., Hasańcebi, O., & Geem, Z. W. (2016). Metaheuristics in structural optimisation and discussions on harmony search algorithm. *Swarm and Evolutionary Computation*, 28, 88–97. <https://doi.org/10.1016/j.swevo.2016.01.005>
- Salcedo-Sanz, S., del Ser, J., Landa-Torres, I., Gil-López, S., & Portilla-Figueras, J. A. (2014). The Coral Reefs Optimisation Algorithm: A Novel Metaheuristic for Efficiently Solving Optimisation Problems. *Scientific World Journal*, 2014. <https://doi.org/10.1155/2014/739768>
- Sarkar, & Gudmestad. (2013). *Wind farm costs – Guide to an offshore wind farm*.
- Scheu, M. N., Tremps, L., Smolka, U., Kolios, A., & Brennan, F. (2019). A systematic Failure Mode Effects and Criticality Analysis for offshore wind turbine systems towards integrated condition based maintenance strategies. *Ocean Engineering*, 176, 118–133. <https://doi.org/10.1016/j.oceaneng.2019.02.048>
- Selig MS, & Coverstone-Carroll VL. (1996). *Application of a Genetic Algorithm to Wind Turbine Design*. Carolrhoda Books.
- Shahrokhi, A., & Jahangirian, A. (2007). Airfoil shape parameterization for optimum Navier-Stokes design with genetic algorithm. *Aerospace Science and Technology*, 11(6), 443–450. <https://doi.org/10.1016/j.ast.2007.04.004>
- Shinozuka, M., & Asce, M. (1983). *BASIC ANALYSIS OF STRUCTURAL SAFETY*.
- Shittu, A. A., Mehmanparast, A., Shafiee, M., Kolios, A., Hart, P., & Pilario, K. (2020). Structural reliability assessment of offshore wind turbine support structures subjected to pitting corrosion-fatigue: A damage tolerance modelling approach. *Wind Energy*, 23(11), 2004–2026. <https://doi.org/10.1002/we.2542>
- Shittu, A. A., Mehmanparast, A., Wang, L., Salonitis, K., & Kolios, A. (2020). Comparative study of structural reliability assessment methods for offshore wind turbine jacket support structures. *Applied Sciences (Switzerland)*, 10(3), 1–31. <https://doi.org/10.3390/app10030860>

- Sieros, G., Chaviaropoulos, P., Sørensen, J. D., Bulder, B. H., & Jamieson, P. (2012). Upscaling wind turbines: theoretical and practical aspects and their impact on the cost of energy. *Wind Energy*, 15(1), 3–17. <https://doi.org/10.1002/we.527>
- Sineglazov, V. M., Ziganshin, A. A., & Vasylenko, M. P. (2016). Algorithm of wind turbine combined rotor aerodynamics calculation. *Electronics and Control Systems*, 3(49). <https://doi.org/10.18372/1990-5548.49.11250>
- Stapelberg, R. F. (2009). Reliability and performance in engineering design. *Handbook of Reliability, Availability, Maintainability and Safety in Engineering Design*, 43-294.
- Stehly, T., & Duffy, P. (2020). *2020 Cost of Wind Energy Review*. www.nrel.gov/publications.
- Stieng, L. E. S., & Muskulus, M. (2020). Reliability-based design optimisation of offshore wind turbine support structures using analytical sensitivities and factorized uncertainty modeling. *Wind Energy Science*, 5(1), 171–198. <https://doi.org/10.5194/wes-5-171-2020>
- Tarp-Johansen, N. J., & Sørensen, J. D. (2006). Reliability-based optimisation and optimal reliability level of offshore wind turbines. *Advances in Reliability and Optimisation of Structural Systems - Proceedings of the 12th WG 7.5 Working Conference on Reliability and Optimisation of Structural Systems*, 15(2), 245–250.
- Theotokoglou, E. E., & Papaefthimiou, G. (2017). Computational analysis of grouted connections. *Proceedings of the International Offshore and Polar Engineering Conference*, 268–273.
- Thompson, M. K., & Thompson, J. M. (2017). *Ansys User's Guid.pdf*. Elsevier.
- Trojnar, K. (2020). Simplified design of new hybrid monopile foundations for offshore wind turbines. *Ocean Engineering*, 219(March 2020), 108046. <https://doi.org/10.1016/j.oceaneng.2020.108046>
- UK beis. (2020). *ELECTRICITY GENERATION COSTS 2020*.
- UK ETO (2024), DNV. Available at: <https://www.dnv.com/energy-transition-outlook/uk/index> (Accessed: 01 January 2024).

- Uys, P. E., Farkas, J., Jármai, K., & van Tonder, F. (2007). Optimisation of a steel tower for a wind turbine structure. *Engineering Structures*, 29(7), 1337–1342. <https://doi.org/10.1016/j.engstruct.2006.08.011>
- van der Tempel, J., Zaaier, M., & Subroto, H. (2004). *The effects of Scour on the design of Offshore Wind Turbines*.
- van Wingerde, A. M., van Delft, D. R. V., Packer, J. A., & Janssen, L. G. J. (2006). Survey of support structures for offshore wind turbines. In *Tubular Structures XI - Proceedings of the 11th International Symposium and IIW International Conference on Tubular Structures* (Issue april). <https://doi.org/10.1201/9780203734964-7>
- Velarde, J., & Bachynski, E. E. (2017). Design and fatigue analysis of monopile foundations to support the DTU 10 MW offshore wind turbine. *Energy Procedia*, 137, 3–13. <https://doi.org/10.1016/j.egypro.2017.10.330>
- Velarde, J., Kramhøft, C., Sørensen, J. D., & Zorzi, G. (2020). Fatigue reliability of large monopiles for offshore wind turbines. *International Journal of Fatigue*, 134(July 2019), 105487. <https://doi.org/10.1016/j.ijfatigue.2020.105487>
- Veldkamp, D. (2006). *Chances in Wind Energy A Probabilistic Approach to Wind Turbine Fatigue Design*.
- Vestas. (2011). *Vestas V164-8.0MW*. 8. http://homepages.ucl.ac.uk/~uceseug/Fluids2/Wind_Turbines/Turbines/V164-8MW.pdf
- Walsh, C. (2019). Offshore wind in Europe. *Refocus*, 3(2), 14–17. <https://windeurope.org/wp-content/uploads/files/about-wind/statistics/WindEurope-Annual-Offshore-Statistics-2019.pdf>
- Wang, L., & Kolios, A. (2017a). A generic framework for reliability assessment of offshore wind turbine monopiles. *Progress in the Analysis and Design of Marine Structures - Proceedings of the 6th International Conference on Marine Structures, MARSTRUCT 2017*, 931–938. <https://doi.org/10.1201/9781315157368-105>
- Wang, L., & Kolios, A. (2017b). A generic framework for reliability assessment of offshore wind turbine monopiles. *Progress in the Analysis and Design of Marine*

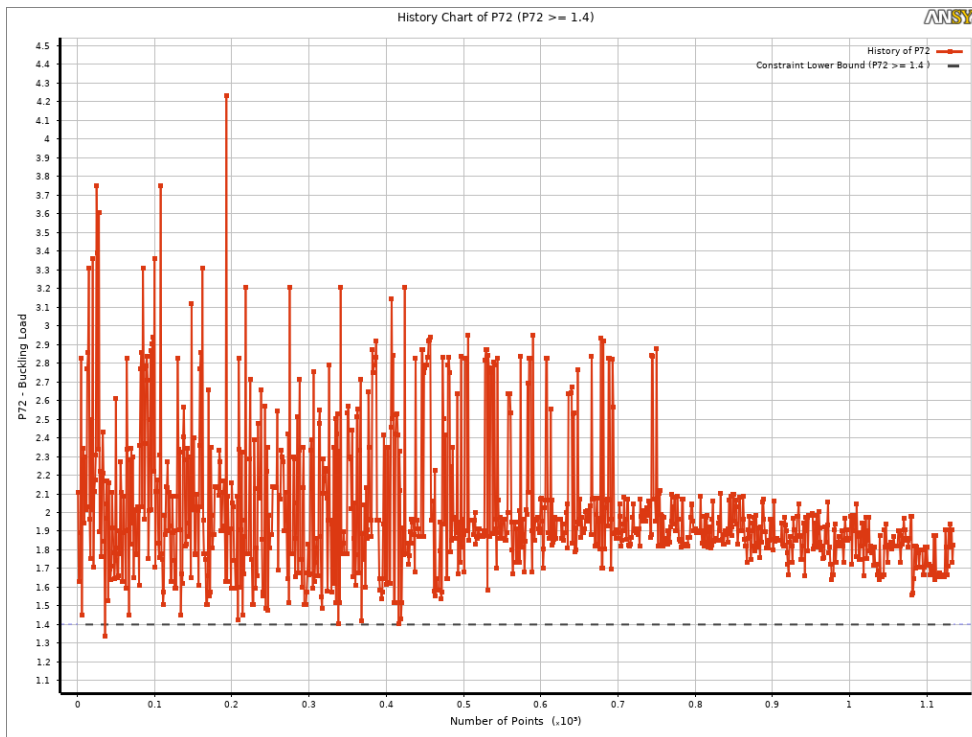
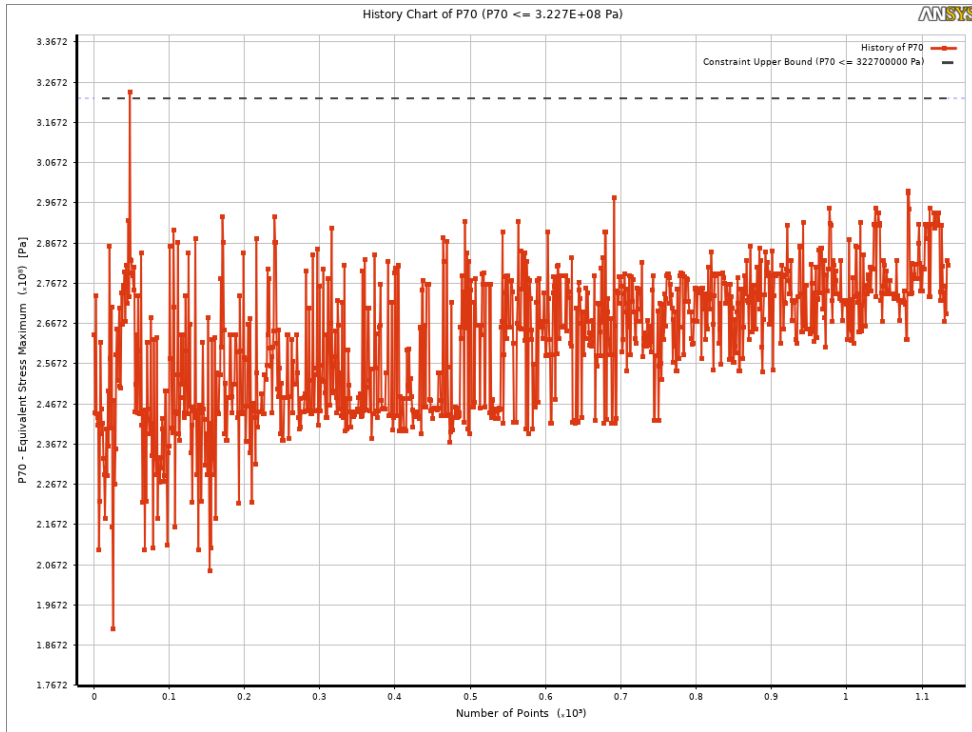
Structures - Proceedings of the 6th International Conference on Marine Structures, MARSTRUCT 2017, 931–938. <https://doi.org/10.1201/9781315157368-105>

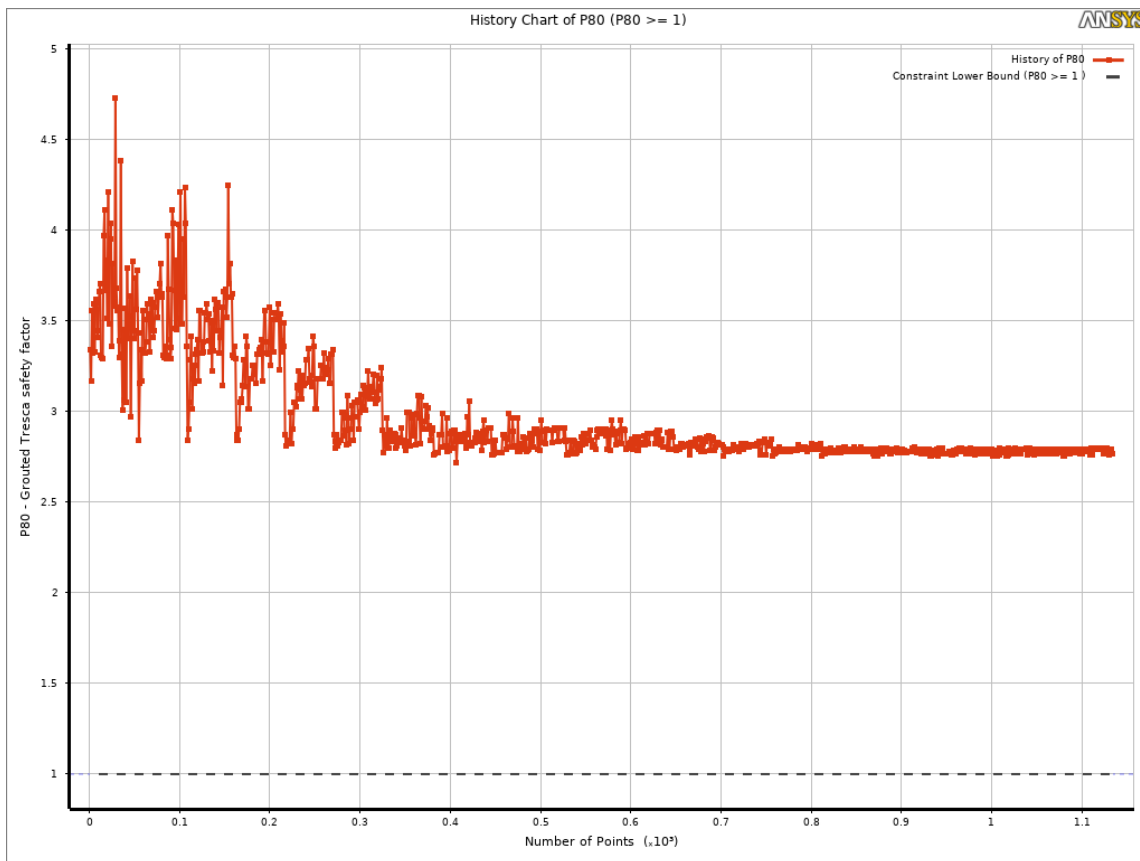
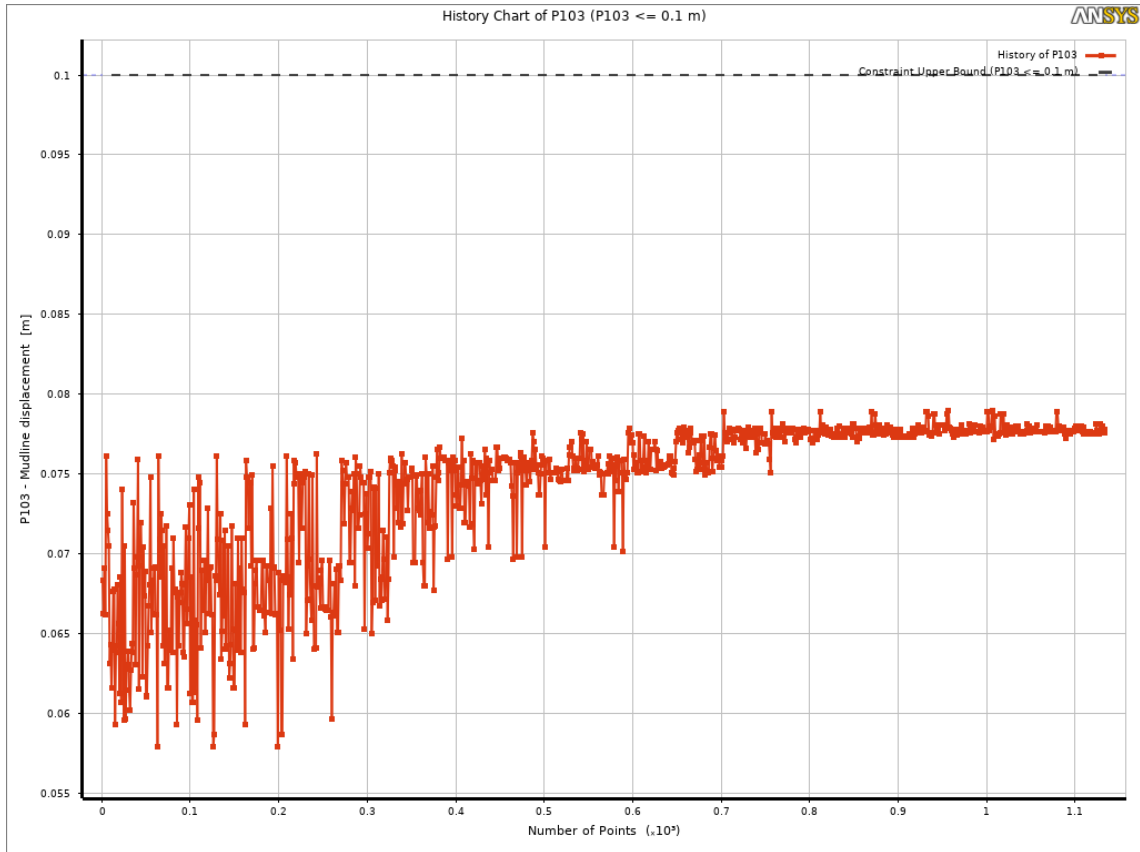
- Wang, L., & Tang, D. (2011). An Improved Adaptive Genetic Algorithm Based on Hormone Modulation Mechanism for Job-shop Scheduling Problem. *Expert Systems with Applications*. <https://doi.org/10.1016/j.eswa.2011.11.051>
- Wang, S., Larsen, T. J., & Bredmose, H. (2021). Ultimate load analysis of a 10 MW offshore monopile wind turbine incorporating fully nonlinear irregular wave kinematics. *Marine Structures*, 76, 102922.
- Weiss, C., D. C. Charmpis, & G. I. Schueller. (2006). *Precaution: the willingness to accept costs to avert uncertain danger*. <https://www.researchgate.net/publication/266019248>
- Wen, Y., AlHakeem, D., Mandal, P., Chakraborty, S., Wu, Y. K., Senjyu, T., Paudyal, S., & Tseng, T. L. (2020). Performance Evaluation of Probabilistic Methods Based on Bootstrap and Quantile Regression to Quantify PV Power Point Forecast Uncertainty. *IEEE Transactions on Neural Networks and Learning Systems*, 31(4), 1134–1144. <https://doi.org/10.1109/TNNLS.2019.2918795>
- Wilkes, E., Anderson, J., McClintic, J., & Bogard, D. (2016). An investigation of turbine film cooling effectiveness with shaped holes and internal cross-flow with varying operational parameters. *Proceedings of the ASME Turbo Expo, 5C-2016*, 1–12. <https://doi.org/10.1115/GT2016-56162>
- Wilson, R. E., Lissaman, P., & Walker, S. N. (1976). *Aerodynamic performance of wind turbines*.
- Wiser, R., & Bolinger, M. (2010). *2010 WIND TECHNOLOGIES MARKET REPORT*. <http://www.osti.gov/bridge>
- Wong, F. (1984). *First-Order, Second-Moment Methods*.
- Wu, X., Hu, Y., Li, Y., Yang, J., Duan, L., Wang, T., Adcock, T., Jiang, Z., Gao, Z., Lin, Z., Borthwick, A., & Liao, S. (2019). Foundations of offshore wind turbines: A review. *Renewable and Sustainable Energy Reviews*, 104(December 2018), 379–393. <https://doi.org/10.1016/j.rser.2019.01.012>

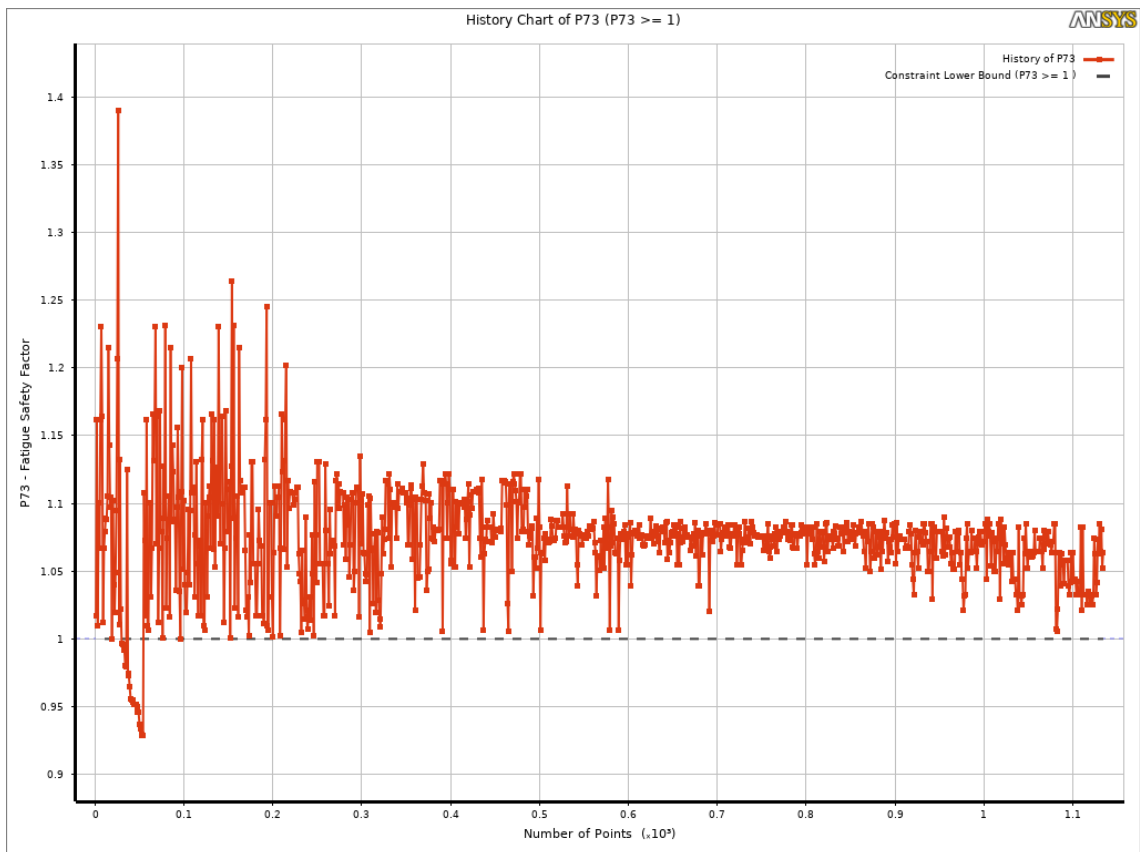
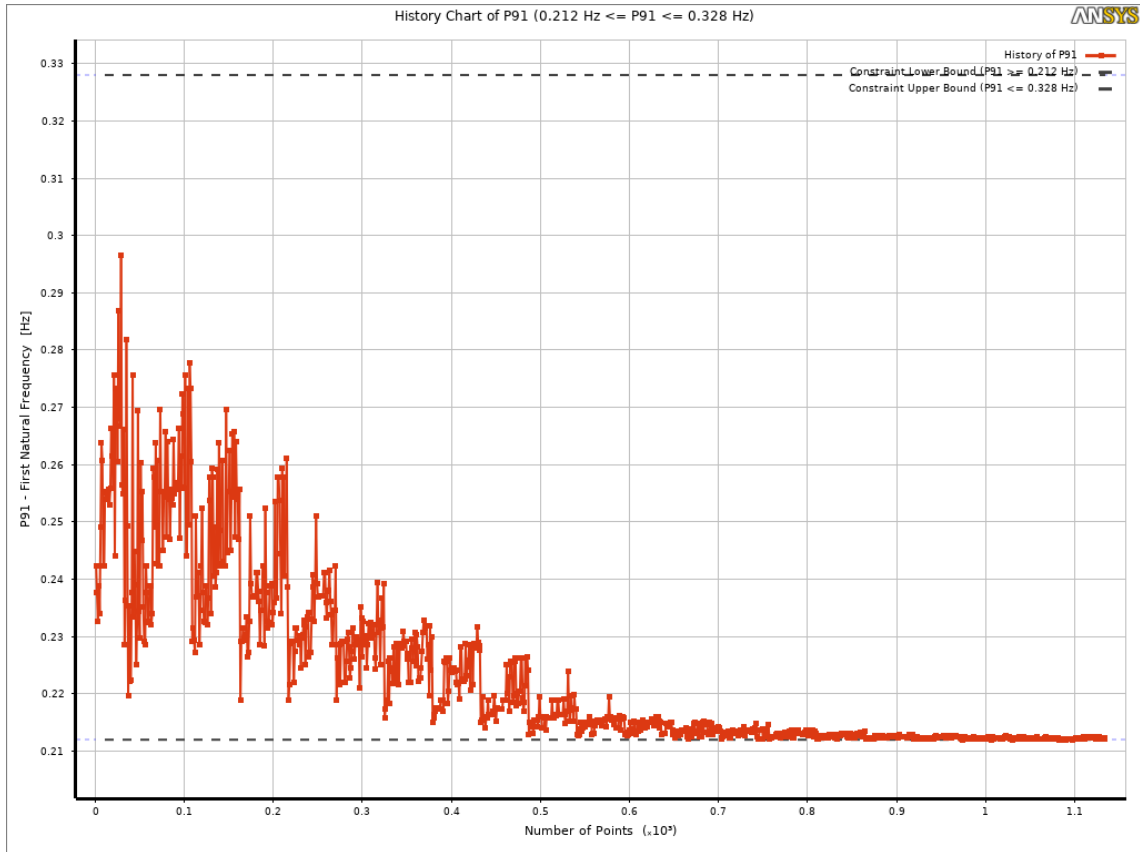
- Yeter, B., Garbatov, Y., & Guedes Soares, C. (2015). Fatigue damage assessment of fixed offshore wind turbine tripod support structures. *Engineering Structures*, *101*, 518–528. <https://doi.org/10.1016/j.engstruct.2015.07.038>
- Yoshida, S. (2006). *Wind Turbine Tower Optimisation Method Using a Genetic Algorithm* (Vol. 30, Issue 6).
- Zdravkovic, L., Jardine, R. J., Taborda, D. M. G., Abadías, D., Burd, H. J., Byrne, B. W., Gavin, K. G., Houlsby, G. T., Igoe, D. J. P., Liu, T., Martin, C. M., McAdam, R. A., Muirwood, A., Potts, D. M., Gretlund, J. S., & Ushev, E. (2020). Ground characterisation for PISA pile testing and analysis. *Geotechnique*, *70*(11), 945–960. <https://doi.org/10.1680/jgeot.18.PISA.001>

Appendix B

History of the optimisation constraint criteria, a) Von Mises equivalent stress, b) Buckling deformation, c) mudline displacement, d) Tresca SF, e) 1st mode frequency and displacement, f) Fatigue minimum safety factor.







Appendix C

Reliability assessment using FORM and regression. MATLAB Code (four variables)

```
clear
clc

er=10^-10;
% Input of dependent variables - Load patterns
xinp=[];
x_var=xinp';
%Input of independent variables - Response
yinp=[];
y_var=yinp';
[xs,ys]=size(x_var);
R=;
%Definition of Variables
x1_m=;
x2_m=;
x3_m=;
x4_m=;
x1_s=;
x2_s=;
x3_s=;
x4_s=;
% Expand x_var to X
regs=2*ys+1;
xexp=x_var;
for i=1:xs
X(i,regs)=1;
for j=1:ys
X(i,2*j-1)=xexp(i,j)^2;
X(i,2*j)=xexp(i,j)^1;
end
end
Y=y_var;
b=X\Y;
%b=inv(X'*X)*X'*Y;
% Definition of iterations
n_iter=10;
err=0.01; % Convergence criterion
% Definition of Limit State Functions
syms x1 x2 x3 x4
a1=b(1);
a2=b(2);
a3=b(3);
a4=b(4);
a5=b(5);
a6=b(6);
a7=er;
a8=er;
a9=b(regs);
g=R-(a1*x1^2+a2*x1+a3*x2^2+a4*x2+a5*x3^2+a6*x3+a7*x4^2+a8*x4+a9);

mu1=;
mu2=;
```

```

mu3=;
mu4=;

sig1=;
sig2=;
sig3=;
sig4=;

% itter=0
% % 1st iteration:
% % a)Initial point computation:
gx1=subs(g,x1,mu1);
gx1=subs(gx1,x2,mu2);
gx1=subs(gx1,x3,mu3);
gx1=subs(gx1,x4,mu4);

diffg_x1=diff(g,x1);
diffg_x2=diff(g,x2);
diffg_x3=diff(g,x3);
diffg_x4=diff(g,x4);

diffg_x1_mu1=diff(g,x1);
diffg_x2_mu2=diff(g,x2);
diffg_x3_mu3=diff(g,x3);
diffg_x4_mu4=diff(g,x4);

diffg1_6=[diffg_x1_mu1 diffg_x2_mu2 diffg_x3_mu3 diffg_x4_mu4];
diffg1_6=subs(diffg1_6,x1,mu1);
diffg1_6=subs(diffg1_6,x2,mu2);
diffg1_6=subs(diffg1_6,x3,mu3);
diffg1_6=subs(diffg1_6,x4,mu4);

diffg_x1_mu1=diffg1_6(1,1);
diffg_x2_mu2=diffg1_6(1,2);
diffg_x3_mu3=diffg1_6(1,3);
diffg_x4_mu4=diffg1_6(1,4);

p1=diffg_x1*sig1;
p2=diffg_x2*sig2;
p3=diffg_x3*sig3;
p4=diffg_x4*sig4;

beta1=gx1/(sqrt(p1^2+p2^2+p3^2+p4^2));
beta1=subs(beta1,x1,mu1);
beta1=subs(beta1,x2,mu2);
beta1=subs(beta1,x3,mu3);
beta1=subs(beta1,x4,mu4);

beta1=eval(beta1)

```

```

% =====
alpha_1_1=-diffg_x1_mu1*sig1/(sqrt(p1^2+p2^2+p3^2+p4^2));
alpha_1_1=subs(alpha_1_1, x1,mu1);
alpha_1_1=subs(alpha_1_1, x2,mu2);
alpha_1_1=subs(alpha_1_1, x3,mu3);
alpha_1_1=subs(alpha_1_1, x4,mu4);

alpha_1_1=eval(alpha_1_1)

alpha_2_1=-diffg_x2_mu2*sig2/(sqrt(p1^2+p2^2+p3^2+p4^2));
alpha_2_1=subs(alpha_2_1, x1,mu1);
alpha_2_1=subs(alpha_2_1, x2,mu2);
alpha_2_1=subs(alpha_2_1, x3,mu3);
alpha_2_1=subs(alpha_2_1, x4,mu4);

alpha_2_1=eval(alpha_2_1)

alpha_3_1=-diffg_x3_mu3*sig3/(sqrt(p1^2+p2^2+p3^2+p4^2));
alpha_3_1=subs(alpha_3_1, x1,mu1);
alpha_3_1=subs(alpha_3_1, x2,mu2);
alpha_3_1=subs(alpha_3_1, x3,mu3);
alpha_3_1=subs(alpha_3_1, x4,mu4);

alpha_3_1=eval(alpha_3_1)

alpha_4_1=-diffg_x4_mu4*sig4/(sqrt(p1^2+p2^2+p3^2+p4^2));
alpha_4_1=subs(alpha_4_1, x1,mu1);
alpha_4_1=subs(alpha_4_1, x2,mu2);
alpha_4_1=subs(alpha_4_1, x3,mu3);
alpha_4_1=subs(alpha_4_1, x4,mu4);

alpha_4_1=eval(alpha_4_1)

x1_2=mu1;
x2_2=mu2;
x3_2=mu3;
x4_2=mu4;

u1_2=0;
u2_2=0;
u3_2=0;
u4_2=0;

%% c) Now the new design point, X2, has to be computed:

x1_2=mu1+beta1*sig1*alpha_1_1;
x2_2=mu2+beta1*sig2*alpha_2_1;
x3_2=mu3+beta1*sig3*alpha_3_1;
x4_2=mu4+beta1*sig4*alpha_4_1;

u1_2=(x1_2-mu1)/sig1;

```

```

u2_2=(x2_2-mu2)/sig2;
u3_2=(x3_2-mu3)/sig3;
u4_2=(x4_2-mu4)/sig4;

fa=1.0;
u1_2=fa*u1_2;

%% 2nd iteration:
%% % a)
% while err2> err
for itter=1:n_iter

gx2=subs(g,x1,x1_2);
gx2=subs(gx2,x2,x2_2);
gx2=subs(gx2,x3,x3_2);
gx2=subs(gx2,x4,x4_2);

gx2=eval(gx2)

diff_x1_x2=eval(subs(diffg_x1_mu1,x1,x1_2));
diff_x2_x2=eval(subs(diffg_x2_mu2,x2,x2_2));
diff_x3_x2=eval(subs(diffg_x3_mu3,x3,x3_2));
diff_x4_x2=eval(subs(diffg_x4_mu4,x4,x4_2));

%% % b)

Nom=(gx2-
(diff_x1_x2*sig1*u1_2+diff_x2_x2*sig2*u2_2+diff_x3_x2*sig3*u3_2+diff_x4_x2*sig4*u4_2));
Denom=sqrt((diff_x1_x2*sig1)^2+(diff_x2_x2*sig2)^2+(diff_x3_x2*sig3)^2+(diff_x4_x2*sig4)^2);
beta2=Nom/Denom;

diffg_x1_mu=subs(diffg_x1_mu1,x1,mu1);
diffg_x2_mu=subs(diffg_x2_mu2,x2,mu2);
diffg_x3_mu=subs(diffg_x3_mu3,x3,mu3);
diffg_x4_mu=subs(diffg_x4_mu4,x4,mu4);

pp1=diffg_x1_mu*sig1;
pp2=diffg_x2_mu*sig2;
pp3=diffg_x3_mu*sig3;
pp4=diffg_x4_mu*sig4;

alpha_1_2=-diffg_x1_mu*sig1/(sqrt(pp1^2+pp2^2+pp3^2+pp4^2));
alpha_1_2=eval(alpha_1_2)
alpha_2_2=-diffg_x2_mu*sig2/(sqrt(pp1^2+pp2^2+pp3^2+pp4^2));
alpha_2_2=eval(alpha_2_2)
alpha_3_2=-diffg_x3_mu*sig3/(sqrt(pp1^2+pp2^2+pp3^2+pp4^2));
alpha_3_2=eval(alpha_3_2)
alpha_4_2=-diffg_x4_mu*sig4/(sqrt(pp1^2+pp2^2+pp3^2+pp4^2));
alpha_4_2=eval(alpha_4_2)

%% % {{{{{{}}}}}}
%% % c) Compute a new design point X3:

```

```
x1_2=mu1+beta2*sig1*alpha_1_2
x2_2=mu2+beta2*sig2*alpha_2_2
x3_2=mu3+beta2*sig3*alpha_3_2
x4_2=mu4+beta2*sig4*alpha_4_2

u1_2=(x1_2-mu1)/sig1;
u2_2=(x2_2-mu2)/sig2;
u3_2=(x3_2-mu3)/sig3;
u4_2=(x4_2-mu4)/sig4;

u1_2=fa*u1_2

%% % d) Convergence checking:

err2=(abs(beta1-beta2))/beta1

beta1=beta2;

end

Reliability_index_Betta=sprintf('%0.5e',beta2)
```